Study of degradation of polymeric filtration membranes in membrane bioreactors

Marcos Antônio Oliveira Filho

Université Fédérale
Toulouse Midi-Pyrénées

THÈSE

En vue de l'obtention du
DOCTORAT DE L'UNIVERSITÉ DE TOULOUSE

Délivré par l'Université Toulouse 3 - Paul Sabatier

Présentée et soutenue par

Marcos Antônio OLIVEIRA FILHO

Le 4 février 2022

Etude de la dégradation des membranes de filtration polymères exploitées en bioréacteurs à membranes

---

Ecole doctorale : **MEGEP - Mécanique, Energétique, Génie civil, Procédés**

Spécialité : **Génie des Procédés et de l'Environnement**

Unité de recherche :
LGC - Laboratoire de Génie Chimique

Thèse dirigée par
Christel CAUSSERAND et Yannick FAYOLLE

Jury

Mme Catherine FAUR, Rapporteure
M. Pierre BERUBE, Rapporteur
M. Christophe DAGOT, Examinateur
Mme Murielle RABILLET-BAUDRY, Examinatrice
Mme Christel CAUSSERAND, Directrice de thèse
M. Yannick FAYOLLE, Co-directeur de thèse

REMERCIEMENTS

Au terme de ces trois années de thèse, je souhaiterais adresser dans les quelques lignes qui suivent mes plus sincères remerciements à toutes les personnes qui ont contribué à rendre cette expérience extraordinairement enrichissante.

Ces travaux se sont déroulés majoritairement à la Direction Innovation du SIAAP. En premier lieu je souhaite donc remercier Vincent Rocher et Sam Azimi, directeur et directeur adjoint, respectivement, pour leur accueil et d'avoir ciblé le sujet de cette thèse de grand intérêt industriel.

Je tiens également à remercier le programme de recherche MOCOPEE qui fait partie de la programmation scientifique innEAUvation du SIAAP pour avoir financé cette thèse.

L'encadrement scientifique industriel a été assuré par Romain Mailler, à qui je voudrais remercier de m'avoir appris une méthode de travail efficace, la rigueur et la discipline que j'apporterai dans ma vie professionnelle.

Ces travaux ont été dirigés par Christel Causserand et Yannick Fayolle, directrice et co-directeur de thèse, respectivement. Je tiens à reconnaitre que leurs compétences très complémentaires, leur patience, leur gentillesse et leur disponibilité ont été primordial pour que je puisse avancer sereinement au long de ma thèse. Cette expérience n'aurait été aussi riche sans vos encadrements.

Je souhaiterais remercier à Catherine Faur, Pierre Bérubé, Murielle Rabiller-Baudry et Christophe Dagot pour avoir accepté de juger ce travail.

De plus les contributions des exploitants de Seine aval et Seine morée ont enrichit cette étude, ainsi je tiens à les remercier.

Je tiens à remercier les équipes du LGC de Toulouse, du INRAE de Anthony, en spécial, Gwenaelle Guitier, Emma Roubaud, Matthieu Dorel, Sylvain Pageot, Pierre Mauricrace, pour toute énergie dédiée à la réalisation de ces travaux.

J'adresse aussi ma reconnaissance à ceux avec qui j'ai partagé mon quotidien de la direction innovation du SIAAP, en spécial de l'équipe ME et, plus particulièrement, Céline et Capucine qui n'ont pas mesuré d'effort pour avancer sur toute question lié à la plateforme membrane.

Enfin, je terminerai par remercier ma famille qui m'a toujours tout apporté pour créer et profiter des opportunités qui la vie me pose et je tiens à remercier ma fiancée Maria Thereza qui a été toujours à mon côté tout au long de cette aventure en apportant une dose extra de bonheur.

ABSTRACT

While membrane bioreactors (MBR) have been broadly applied to wastewater treatment, a comprehensive study of the aging of membrane materials under operating conditions of MBR at full-scale is necessary in order to understand and to anticipate it. Thus, the present research aim (i) to analyse the chemical action of sodium hypochlorite to commercial polyvinylidene difluoride (PVDF)/Polyvinylpyrrolidone (PVP) hollow fibers used in MBR, (ii) to describe membrane ageing of such materials in urban wastewater full-scale MBR based on a coupled characterization of harvested membranes and full-scale process indicators. To that end, ZeeWeed® 500D membranes were aged at bench-scale by single soaking in hypochlorite solution at a concentration (1000 ppm) and pH (9.0) similar to MBR cleaning protocols. In addition, membranes were sampled between 2016 and 2021 from modules from two urban wastewater treatment plants (capacities of 50,000 m^3/d and 300,000 m^3/d, respectively). Simultaneously, process data were collected and analyzed.

Both bench-scale and full-scale aged hollow-fibers were characterized using similar analytical methods and compared considering the chlorine exposure dose (C x t). Significant differences were found between ageing mechanisms at both scales. At bench-scale, membranes presented stable mechanical properties. Three distinctive phases were observed for the changes on intrinsic permeability with an initial increasing phase up to a C x t of 78,000 ppm.h (+ 90% with respect to the initial permeability), because of hydrophilic agent degradation and the formation of small pores (diameter < 20 nm). Then, a decreasing phase is observed (from 78,000 ppm.h to 150,000 ppm.h), caused by a decline in porosity, likely due to a restructuration of PVDF chains. After 150,000 ppm.h, intrinsic permeability seemed to fluctuate around its initial values. At full-scale, a decline in mechanical properties is highlighted, probably linked to the dynamic conditions in the MBR (i.e. filtration, aeration and backwashing). Moreover, an increase in permeability is observed during the studied period (< 98,000 ppm.h) because of a more pronounced oxidation/dislodgement of PVP molecules (25% vs 40% from the initial PVP content, for full- and bench-scale respectively) leading to a higher porosity and the appearance of bigger pores (diameter > 40 nm). These changes favored irreversible fouling in contrary to bench-scale ageing.

At full-scale, permeability index (the ratio of permeate flux and transmembrane pressure during the process) after each cleaning-in-place protocol decreases to around 20% over the studied period for both facilities. This decline is well correlated to the PVP content and intrinsic permeability, allowing the determination of key indicators to monitor membrane ageing.

This study showed that understanding the mechanisms behind the action of NaOCl on supported PVDF membranes may not represent what actually occurs at full-scale operation. A non-negligible contribution of filtration conditions, mechanical stress due to aeration and backwashes, and residual fouling, specific to onsite operating conditions, may significantly change ageing mechanisms. Continuous autopsies of harvested fibers over the years and monitoring consistent full-scale operating indicators are still needed.

Key-words: membrane bioreactor, ultrafiltration, hollow-fiber, wastewater treatment, ageing, full-scale.

RESUME

Malgré le fait que les bioréacteurs à membranes (BRM) soient largement appliqués au traitement des eaux usées, l'étude approfondie du vieillissement des matériaux membranaires dans les conditions d'exploitation des BRM à l'échelle industrielle est nécessaire afin de comprendre et anticiper celui-ci. Ainsi, l'objectif de ce travail vise à (i) comprendre l'action chimique de l'hypochlorite de sodium sur les fibres creuses commerciales de polyfluorure de vinylidène (PVDF)/polyvinylpyrrolidone (PVP) utilisées dans les BRM et (ii) décrire le vieillissement dans les BRMs traitant des eaux usées urbaines, sur la base de la caractérisation de membranes prélevées sur site et des indicateurs d'exploitation à l'échelle industrielle. Pour cela, des membranes ZeeWeed® 500D ont été vieillies à l'échelle laboratoire par trempage dans une solution d'hypochlorite de sodium (1000 ppm et pH 9.0) similaires aux conditions de nettoyage à l'échelle industrielle. Par ailleurs, des prélèvements de membranes ont été effectués entre 2016 et 2021 au sein des cellules membranaires de deux stations de traitement des eaux résiduaires urbaines (de capacités respectives de 50 000 et 300 000 m^3/j). Les données d'exploitation ont été collectées et analysées en parallèle.

Les fibres creuses vieillies à l'échelle laboratoire et à l'échelle industrielle ont été caractérisées à l'aide de méthodes analytiques similaires et comparées en considérant leur dose d'exposition au chlore (C x t). De grandes différences ont été trouvées entre le vieillissement aux deux échelles. À l'échelle laboratoire, les membranes ont présenté des propriétés mécaniques stables. Trois phases distinctes ont été observées pour l'évolution de la perméabilité intrinsèque avec une augmentation jusqu'à une dose de 78 000 ppm.h (+ 90% de la perméabilité initiale) en raison de la dégradation de la PVP et de la formation de pores de petite taille (diamètre < 20 nm), suivi d'une diminution jusqu'à retourner à la perméabilité initiale (pour un 78 000 ppm.h < C x t < 150 000 ppm.h) en raison d'une décroissance de la porosité, probablement due à une restructuration des chaines de PVDF. Pour les C x t > 150 000 ppm.h, la perméabilité reste relativement constante autour de sa valeur initiale. À l'échelle industrielle, une diminution des propriétés mécaniques est observée en lien avec les conditions dynamiques des BRMs (filtration, aération, rétrolavages, etc.). De plus, une augmentation de la perméabilité est également observée (C x t < 98 000 ppm.h) en raison d'une oxydation/délogement plus prononcé des molécules de PVP en comparaison des membranes vieillies au laboratoire (25% vs 40% de la teneur initiale, respectivement), conduisant à une porosité plus élevée et à l'apparition de pores de plus grande taille (diamètre > 40 nm). Ces changements ont favorisé un

colmatage irréversible important, en comparaison des échantillons issus des vieillissements à l'échelle laboratoire.

A l'échelle industrielle, l'indice de perméabilité (représentant le rapport flux de perméat/pression transmembranaire) mesuré après chaque nettoyage intensif diminue de l'ordre de 20% sur l'ensemble de la période de suivi, pour les deux installations étudiées. Cette baisse est fortement corrélée à la teneur en PVP et à la perméabilité intrinsèque des membranes, permettant ainsi d'identifier des indicateurs clés pour la surveillance du vieillissement des membranes en BRM.

Cette étude a montré que la compréhension des mécanismes à l'origine de l'action du NaOCl sur les membranes supportées en PVDF peut ne pas représenter ce qui se produit réellement lors d'un fonctionnement en BRM. Une contribution non négligeable des conditions de filtration/rétrolavage, de l'aération et du colmatage résiduel, spécifiques aux conditions d'exploitation sur site, peuvent modifier de manière significative les mécanismes de vieillissement. Des autopsies de fibres prélevées et la surveillance d'indicateurs de fonctionnement pertinents restent donc nécessaires.

Mots-clés: Bioréacteur à membrane, Ultrafiltration, Fibre creuse, Traitement des eaux résiduaires urbaines, Vieillissement, Echelle industrielle.

SUMMARY

LIST OF ABBREVIATIONS

ADINA – Automatic Dynamic Incremental Non-Linear Analysis

AFM – Atomic force microscopy

AHL – N-acyl homoserine lactones

AI-2 – Autoinducer-2

AIPS – Autoinducer peptides

ATR-FTIR – Attenuated total reflectance Fourier transform infrared spectroscopy

BOD_5 – Biological Oxygen Demand in 5 days

BPC – Biopolymer clusters

BSA – Bovine serum albumin

CA – Cellulose acetate

CAS – Conventional Activated Sludge

CE – Cellulose ester

COD – Chemical oxygen demand

DBS – Sodium dodecylbenzene

DNA – Deoxyribonucleic acid

DOM – Dissolved organic matter

DSC – Differential scanning calorimetry

EDX – Energy dispersive X-ray spectroscopy

EPS – Extracellular polymeric substances

FEA – Finite element analysis

FESEM – Field emission scanning electron microscopy

FNA – Free nitrous acid

HRT – Hydraulic retention time

LB-EPS – Loosely bond extracellular polymeric substances

LPS – Lipopolysaccharides

MBR – Membrane Bioreactors

MFC – Microbial fuel cell

MLSS – Mixed liquor suspended solids

MS – Mass spectroscopy

NMR – Nuclear magnetic resonance

PA - Polyamide

PAN – Polyacrilonitrile

PEG – Polyethylene glycol

PES – Polyether sulfone

PET – Polyethylene terephthalate

PHB – Poly-β-hydroxybutyrate

PP - Polypropylene

PSU - Polysulfone

PVC – Polyvinylchloride

PVDF – Polyvinylidene fluoride

PVP – Polyvinyl pirrolidone

QQ – Quorum quenching

QS – Quorum sensing

RO – Reverse osmosis

SDS – Sodium dodecyl sulfate

SEC – Size exclusion chromatography

SEM – Scanning electron microscopy

SMP – Soluble microbial products

SRT – Sludge retention time

TB-EPS – Tightly bond extracellular polymeric substances

TEP – Transparent exopolymer particles

TGA – Thermogravimetric analysis

TMP – Transmembrane pressure

TOC – Total organic carbon

WHO – World Health Organization

WWT – Wastewater treatment

XPS – X-ray Photoelectron spectroscopy

XRD – X-ray diffraction

LIST OF FIGURES

LIST OF TABLES

GENERAL INTRODUCTION

Membrane bioreactors (MBR) have experienced an exponential growth during the past decade. The cumulative treatment capacity of large-scale facilities (>100,000 m^3/d), increased from 500,000 m^3/d in 2010 and is expected to reach over 14,000,000 m^3/d by 2025 [1]. The main drivers of this MBR expansion across the globe are stricter legislation concerning the reuse of the treated effluent, discharge to sensitive water bodies, space limitations, and retrofitting/upgrading wastewater treatment plants (WWTP) [2]. Membranes act as a reliable physical barrier, and thus MBR perform significantly better than classic processes. To illustrate, Bertanza et al. (2017) compared a full-scale MBR with a conventional activated sludge system (CAS) from a WWTP in Italy. Treating the same influent, MBR was able to remove 99.5% of chemical oxygen demand (COD) versus 90.6% for the CAS [3].

Despite the increasing interest in the application of MBR, its operating costs are still higher than CAS. Xiao et al. (2019) reported operating costs of MBRs in China ranging from 0.13 – 0.25 USD/m^3 compared to 0.11 USD/m^3 for the average operating costs of municipal wastewater treatment plants [4]. These costs are mainly associate to membrane fouling and the operations to overcome it. Several strategies are applied to reduce fouling such as aeration cycles, physical cleaning, i.e., relaxation or backwash, and chemical cleaning either by chemically enhanced backwash or cleaning-in-place (CIP) protocols [5]. These strategies directly affect operating costs, but may also cause unexpected changes in membrane properties, which, simultaneously to accumulation of residual fouling, decrease filtration performance.

The combined effect of residual fouling and changes in membrane properties in the long term results in membrane ageing, which ultimately leads to membrane replacement [6]. Membrane lifespan is also a decisive factor in the economic efficiency of an MBR. For instance, a 19% reduction in the total costs of an installation was reported if membranes were replaced after 10 years instead of after 5 [7].

As a result, interest in understanding the ageing process of MBR has increased. Traditionally, studies focused on comprehending the changes in membrane properties due to exposure to chemicals often used in cleaning protocols, such as oxidants, bases, and acids. Among them, sodium hypochlorite (NaOCl) is the most commonly studied and widely used reagent in ultrafiltration processes thanks to its cleaning efficiency and associated low cost; unfortunately, NaOCl is also involved in the degradation of polymeric membranes. Polyvinyl difluoride (PVDF), a chlorine-resistant polymer, has emerged as one of the most commonly used membrane materials for drinking water and wastewater treatment applications [8]. It has a high hydrophobic character and is usually mixed with hydrophilic and pore-forming additives, i.e., polyvinylpyrrolidone (PVP), polyethylene glycol (PEG), in the manufacturing of ultrafiltration membranes.

Since 2010, at least 22 studies have been published on PVDF membrane ageing. The main approach used in these studies was to accelerate ageing by single soaking in a hypochlorite solution and to observe the changes in membrane properties [9–22]. Generally, the chlorine exposure dose, which is the product (C × t) between chlorine concentration (C) and soaking time (t), is used to monitor the ageing process. This parameter allows us to compare the ageing effects between bench scale and full scale. Other approaches included filtration of model fouling solutions and backwash hypochlorite cycles to include the impact of fouling [23–25]. Finally, one study investigated PVDF membrane ageing in full-scale direct filtration facilities [26].

The main conclusions drawn from these studies are: (i) the current understanding of PVDF membrane ageing is mainly based on chemical exposure at bench scale and (ii) contradictions can be found regarding permeability, pore size, and fouling reversibility changes with ageing, probably because of the differences in ageing conditions, in analytical methods, and in membrane type. Regarding these two points, the changes in PVDF membrane properties over

time by direct filtration in drinking water production facilities were elucidated in an initial study and the findings were later compared with changes observed in ageing of the same membranes at bench scale by single soaking and by cycles of model fouling solution filtration/NaOCl backwash [25,26]. By applying the same analytical methodology, the authors were able to conclude that chemical changes were similar for both scales, but performance differed, which means that bench-scale approach can be used only when chemical changes is a concern.

However, operating conditions in direct filtration and in MBR are substantially different and a comprehensive study of changes in membrane properties over time under MBR on-site conditions is still lacking. For direct filtration units, filtration cycles may take several hours at higher fluxes, i.e., over 30 $L.m^{-2}.h^{-1}$ (LMH) before backwash, due to a low-charged influent in terms of dissolved organic carbon (DOC), i.e., approximately 3.5 mgC/L [27]. For MBR, membranes are expected to handle much more charged water (DOC over 100 mgC/L) with higher amounts of fouling agents and suspended solids, leading to smaller filtration fluxes (~25 LMH) and more frequent relaxation/backwash (every 10–90 min) [2]. In addition, there are major differences between these applications regarding: (i) membrane structure, since for MBR membranes are reinforced by other polymers, (ii) filtration is mostly performed from the outside towards inside membranes and (iii) aeration cycles are frequently performed which enables oscillation of fibers and effective control of cake formation.

The dynamics of filtration and fouling in MBR are expected to play a major role in membrane ageing compared with direct filtration facilities. Cote et al. (2012) analyzed the data set of ZeeWeed® MBRs shipped to North America over 15 years and listed five end-of-life triggers for membranes, namely, hollow-fiber breakage, mechanical module or cassette failure, upgrade to a higher performance product, weakening of the potting resin-membrane fiber bond and increasing in cleaning flow throughput. They stated that a slow increase in operating pressure and the need for more frequent cleaning are the dominant reasons for membrane replacement.

Regarding the membrane structure itself, replacement can be caused by: (i) a loss of integrity due to either pore enlargement, skin tearing or hollow-fiber breakage, which would lead to a permeate of poorer quality or (ii) an increasing transmembrane pressure (TMP) approaching to the maximum TMP that the membrane can withstand. The later would lead to more frequent cleaning and a decline in hydraulic efficiency.

Only two studies were published about membrane ageing in full-scale MBR installations. Fenu et al. (2012) confirmed that increase in operating pressure was the main end-of-life trigger assessing flowrate and pressure date from an MBR treating up to 250 m^3/h in Schilde wastewater treatment plant equipped with PVDF membranes. Authors went further into defining an end-of-life concept based on the permeability index (ratio of permeate flux and TMP) decline over time. This decline was attributed to residual fouling that accumulates in membranes even though cleaning protocols are performed. However, no membrane characterization was performed to identify changes in the physical–chemical properties and to quantify this accumulation of residual fouling [6]. Mailler et al. (2021) also determined the lifespan of membranes in an MBR equipped with polyether sulfone (PES) membranes based on the permeability index decline. Authors reported similar lifespans based on the permeability index decline and on the loss of membrane integrity [28]. They went further and correlated the decline on permeability index to the cumulated load of supernatant COD rather than the chlorine exposure, which is a new indicator to be integrated in membrane ageing studies. It is worth noting that the MBR in this study treated filtrate from sludge ultra-dewatering, which is a much more concentrated effluent (in terms of carbon and nitrogen sources) than common MBRs applied to urban wastewater treatment.

Therefore, a clear understanding of supported PVDF membrane ageing in full-scale MBR conditions is still lacking. Because of that, the representability of traditional approach of

accelerated ageing by chlorine exposure towards ageing under operating conditions is questionable. Therefore, this thesis aims to:

1) **Understand membrane ageing due to NaOCl exposure:** pristine ZeeWeed® 500D membranes will be aged by soaking in NaOCl solutions at pH and concentration similar to real operation and membrane properties will be characterized;

2) **Compare ageing due to chlorine exposure to full-scale MBR ageing to demonstrate the representability of accelerated ageing protocol at bench-scale:** ZeeWeed® 500D membranes will be harvested from a full-scale MBR in order to monitor changes in properties and compare with those samples aged by NaOCl soaking at bench-scale;

3) **Describe membrane ageing based on membrane properties and in-situ filtration performance at different full-scale MBR conditions:** Changes in membrane properties and permeability index generated from process sensors will be analyzed since the commissioning date of each MBR;

4) **Determine the effects of different operating conditions on membrane ageing in MBR based on changes in membrane properties and on in-situ filtration performance:** Changes in filtration performance obtained from full-scale data will be correlated to the changes in membrane properties and key properties will be identified.

To this aim, chapter 1, includes a bibliographic study, contextualizes the importance of understanding membrane ageing and highlights the scientific bottlenecks related to supported PVDF membrane ageing. Then, chapter 2 describes the materials and methods employed in the thesis to achieve the four objectives mentioned above. Chapter 3 describes supported PVDF membrane ageing by chlorine exposure at bench-scale and compares this accelerated ageing

protocol to ageing at full-scale MBR, answering objectives (i) and (ii). These results were published in Separation & Purification Technology [29]. Afterwards, results presented in chapter 4 characterize membrane ageing at different operating conditions at full-scale MBR and determine key indicators related to these on-site conditions to monitor ageing in MBR, elucidating objectives (iii) and (iv). Finally, a general conclusion presents the main scientific contributions and operational benefits from this research, with open perspectives.

The present thesis was developed in a partnership between *Laboratoire de Génie Chimique* (LGC) from Toulouse, *Institut national de recherche pour l'agriculture, l'alimentation et l'environnement* (INRAE) from Antony and *Service Public de l'Assainissement Francilien* (SIAAP). This partnership was built in the scientific program *Modélisation, Contrôle, Optimisation des Procédés d'Epuration des Eaux* (MOCOPEE), which brings together both scientific and operational partners in order to address actual operational difficulties and future changes in the wastewater industry

CHAPTER 1: BIBLIOGRAPHIC STUDY

1. INTRODUCTION

With population growth, climate change, emerging pollutants and poor sanitation, water scarcity already affects more than 40% of the global population and the gap between freshwater supply and demand is projected to reach 40% by 2030, according to the Water Resources Group [30]. The role of sanitation and wastewater management in public health is widely known. 280,000 deaths from diarrhea are assigned to the lack of these two factors every year, making them priority intervention areas in World Health Organization (WHO) strategic plan for 2018-2025 [31]. These facts urge for improvements in wastewater treatment (WWT), which can provide a safe disposal of the gathered effluent into the environment [32].

Wastewater treatment plants are usually composed of a preliminary treatment (physical), i.e. coarse screening, grit chambers and aeration, to get rid of heavy and larger entrained solids and protect pumping equipment. After that, a primary treatment, such as decantation, is used to remove suspended solids, phosphor based compounds and colloids in a physicochemical sedimentation, and the addition of coagulants enhances the decantation performance in this step. Then, organic matters from effluents (carbon, phosphor and nitrogen based substances) are biochemically oxidized by microorganisms in an activated sludge matrix as a secondary treatment. There are few technologies to be highlighted in this step, namely, conventional activated sludge process (CAS) followed by decantation as a clarification step, which has been optimized over more than 100 years and membrane bioreactor (MBR), which is the combination of a AS biological treatment and a membrane-assisted separation for clarification [33]. Besides these two, biofiltration is another process often used in secondary treatment, which makes possible the treatment of organic matter by passing through biologically activated filters, but this process will not be part of this report [34].

The solid fractions from the above-mentioned methods are separated in a clarification step and undergo other treatments, i.e. digestion or incineration, in order to reduce putrescibility and

pathogenic contents before their ultimate disposal, which is usually fertilization. Finally, in some wastewater treatment plants, there is also a tertiary treatment step to increase water quality by reducing micropollutants contents. These are advanced physicochemical processes, such as, adsorption on activated carbon and ozonation [33] or filtration processes, such as nanofiltration. An overview of a simplified wastewater treatment plant is shown in *Figure 1.1*.

This chapter presents a bibliographic synthesis of the biological treatment in wastewater treatment plants (section 2), including MBR, followed by a focus on the membrane technology involved in this process. Afterwards, the major drawback of this process, i.e. fouling, is presented in section 3 and the main strategies to control this phenomenon are discussed in section 4. Finally, since these operating conditions cause changes in membrane properties, membrane ageing is discussed in the following section (section 5), with a further look into PVDF membranes ageing.

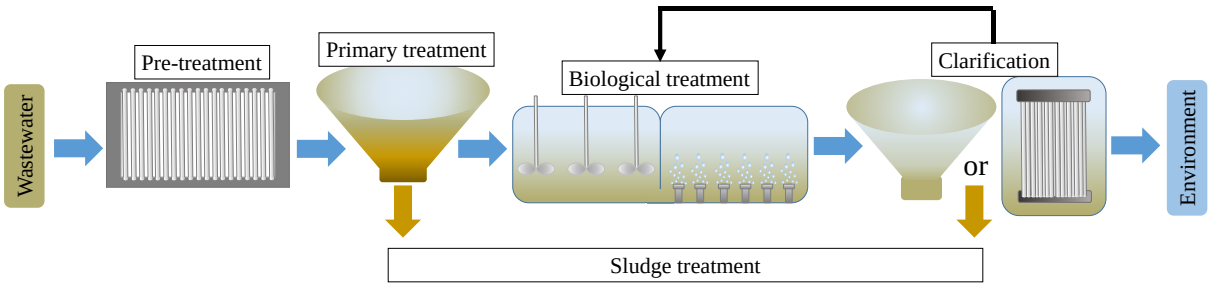

Figure 1.1: Summarized scheme of a wastewater treatment plant.

2. WASTEWATER TREATMENT

2.1. CONVENTIONAL ACTIVATED SLUDGE PROCESS (CAS)

The CAS was first developed into a full-scale plant for Manchester's sewage treatment (UK) in the beginning of the 20th century. Since then, this technology is the most widely used in wastewater treatment, because of its low energetic and capital costs, besides high efficacy in removing carbon-based pollutants [2,35]. This process consists of an aerated biological basin,

where oxygen gas is transferred into mixed liquor (composed of raw or primary treated wastewater and microbial organisms) and metabolic processes assure the stabilization of organic matter by microorganisms. Then, a secondary clarifier, where solids (biomass) are separated out from treated water and recirculated to the biological reactor in order to keep biomass concentration at levels that ensure treatment.

In the biological basin, aeration is the key parameter, because it provides oxygen to microorganisms, but also induces mixing which allows maintaining solids in suspension and improves the contact between organic matter and microorganisms. Moreover, the sludge's flocculation properties are also a key point, because it ensures the separation of the sludge and treated water. However, this property can be easily shifted by the variability in influent's content and operating parameters [36]. Some of the main parameters in CAS process are listed in the Table 1.1 along with their characteristic values.

Table 1.1: Main parameters and their characteristic values for CAS process (Based on *[33]*).

Parameters	Meaning	Characteristic values
Mixed Liquor Suspended Solids (MLSS; $\frac{g}{L}$)	Concentration of suspended solids in mixed liquor	1.5 – 7.0
Hydraulic Retention Time (HRT; h)	Time of contact between microorganisms and influent's organic matter	1 – 20
Sludge Retention Time (SRT; days)	Time that sludge remains in the reactor	4 – 20
Food to Microorganism ratio (F/M; $\frac{kg\ BOD_5}{kg\ MVSS.day}$)	Amount of substrate available to microorganism for time	0.07 – 0.5
Sludge Recirculation Factor (Q_R/Q; dimensionless)	Rate in which sludge is recirculated	0.25 – 0.8
Treatment yield (%)	Percentage of removed BOD_5	50 - >95
Kg O_2/kg BOD_5 removed	Amount of O_2 needed to remove 1 kg BOD_5	0.8 – 1.0

At the end of this process, treated water can reach often 10-15 mg BOD_5/L and solid suspension concentrations as low as 20 mg/L, which are within the limits stablished by the European Directive for wastewater of 35 mg/L of DBO_5 [37].

2.2. MEMBRANE BIOREACTORS (MBR)

MBR technology dates from late 1960s, when microfiltration membranes became commercially available. This process was introduced by the Japanese enterprise Dorr-Oliver Inc. and it was composed by a biological basin with a crossflow filtration unit operating in tangential mode with flat sheet membranes [38]. At this stage, the technology struggled to find viable applications due to energetic costs related to high crossflow velocities, aeration and loss of performance as membranes fouled. The first breakthrough came in 1989, when Yamamoto and colleagues immerged membranes into the biological basin, where the aeration had the double role of transfer oxygen to microorganisms and control fouling by increasing shear stress nearby membranes, thus decreasing costs [39]. Although important advances were achieved, it was only in 1998 that the first full-scale MBR was installed for domestic wastewater treatment in Portland, UK, capable to treat up to 1,900 m^3/day [40].

In the recent years, as a result of improvements in fouling control strategies, optimization in operating conditions and new membrane materials, treatment capacity of super-large MBRs (>100,000 m^3/day) has reached 6.0 million m^3/day and its market value has been exponentially increasing as can be seen in *Figure 1.2* [2,4]. In most of the current MBRs, membranes are immerged in a dedicated tank, after the biological basin. This strategy enables to separate aerations and optimize it for purposes of the aerobic tank and for membrane fouling in each tank.

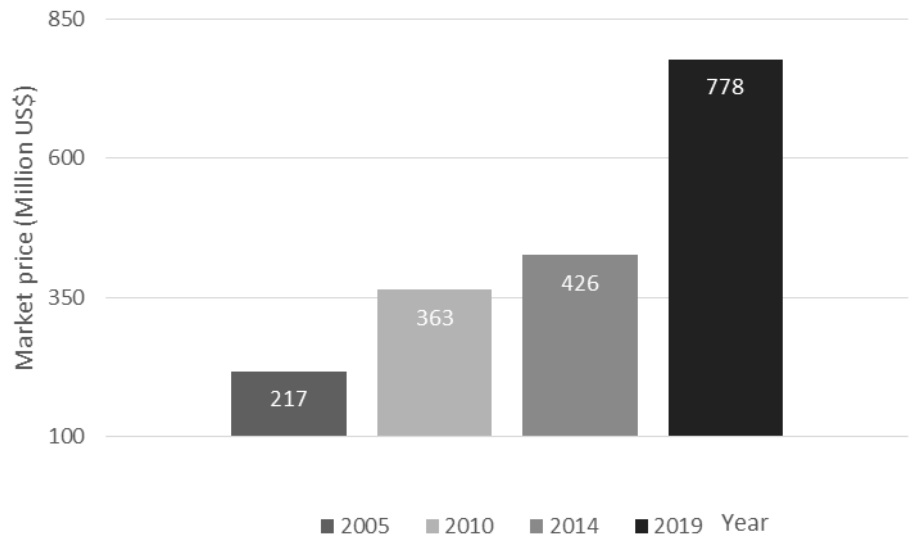

Figure 1.2: World market value of MBR technology as a function of years (Based on data from *[2,41]*).

Currently, this technology is preferred over CAS process in many cases. There are several advantages associated to MBRs, including better quality of effluents, limited sludge production and easy automation. As membranes replace clarifiers from CAS, the overall treatment footprint is considerably decreased. Indeed, with the increasing tendency in land prices, MBR technology is favored as it is a more compact technology. The use of membranes also enables better treatment performances as a result of the physical separation of the suspended solids from the

effluent and the enhanced biological process due to the higher concentration of microorganisms and related sludge retention time (SRT), increasing metabolic activity [40]. Although MBR presents better performance, capital expenses, membrane replacement and energy consumption, mainly associated to the efforts in fouling control and oxygen transport, are still the major drawback of these systems. Comparing to CAS, energy costs remains up to 30% higher in MBR applied to municipal wastewater treatment plants, but studies have presented promising results in reducing this gap [35].

2.2.1. BIOLOGICAL TREATMENT STAGE

MBR application is finding its way mainly on urban wastewater treatment as it efficiently treats ordinary pollutants, such as carbon, nitrogen and phosphor based compounds, it has an effect on less biodegradable compounds, such as endocrine disruptor chemicals, and it allows complete disinfection from bacteria and partially from viruses. The biological stages applied in large scale installations are generally composed by anoxic, anaerobic and aerobic zones [4].

2.2.1.1. ORGANIC MATTER OXIDATION

Under aerated conditions, microorganisms and pollution compose the activated sludge. These microorganisms oxidize carbon-based compounds in wastewater decreasing its biochemical oxygen demand (BOD), this reaction is generically represented in Eq. 1.

$$C_xH_yO_z + O_2 \rightarrow CO_2 + H_2O \qquad \text{Eq. 1}$$

Air is usually injected by diffusers. They are provided at the bottom of the tank, which also enable mixing of activated sludge. Air supply may be tapered along the length of the reactor in the case of a plug flow tank, reducing oxygen supply to match the quantity of oxygen demand. For this process, oxygen transfer from air to mixed liquor should be optimized for better treatment, in this case fine bubbles are preferred. Usually air is supplied in the order of 6 m^3 air/m^3 of sewage [37].

2.2.1.2. TREATMENT OF NITROGEN-BASED COMPOUND

Nitrification also takes place in the aerated tank, which is the oxidation of ammonia to nitrite (Eq. 2) by proteobacteria, such as *Nitrosomonas,* and the further oxidation of nitrite to nitrate (Eq. 3) by genera *Nitrobacter* and *Nitrococcus,* for example. The later reaction yields much less energy than the first, but both rely on slow growth bacteria which is suitable in MBRs due to the possibility of operating in longer solid retention time (SRT > 12 days).

$$2\,NH_4^+ + 3\,O_2 \rightarrow 2\,NO_2^- + 4H^+ + H_2O \qquad \text{Eq. 2}$$

$$2\,NO_2^- + O_2 \rightarrow NO_3^- \qquad \text{Eq. 3}$$

The nitrates produced in the aerobic zone will be consumed under anoxic conditions. When sludge is under anoxic conditions (absence of molecular oxygen – O_2), microorganisms use nitrate as electron acceptor by the action of enzymes such as, nitrate reductase, forming nitrogen gas or nitrous oxides (NO and N_2O). As a result, the denitrification process, described in Eq. 4, reduces concentrations of nitrogen based compounds in wastewater [42].

$$4\,NO_3^- + 5\,C_xH_yO_z + 4\,H^+ \rightarrow 2\,N_2 + 5\,CO_2 + 7\,H_2O \qquad \text{Eq. 4}$$

2.2.1.3. TREATMENT OF PHOSPHORUS-BASED COMPOUNDS

Phosphorus-based compound are mostly reduced in the primary treatment step, by coagulation with addition of metallic salts, such as ferric chloride ($FeCl_3$) or aluminum sulfate ($Al_2(SO_4)_3$). However, in the secondary treatment, biological phosphorus reduction can be achieved in the anaerobic and aerated zones.

In anaerobic conditions, low weight fatty acids and sulfate are transformed into more simple substances, such as sulfite-amide and carbon dioxide, by sulfate-reducing bacteria. In low weight fatty acid metabolism, bacteria produce poly-β-hydroxybutyrate (PHB) using polyphosphate reserves within the cells, this releases then orthophosphates in the media,

initially increasing phosphate concentration in solution to be further consumed in aerated zones [42].

In the aerated zone, PHB is used for bacteria growth and carbon dioxide and water formation. These reactions release excess energy and as a result bacteria consume great amounts of orthophosphate reducing its concentration in wastewater [40,42]. Anaerobic and aerated zones are dimensioned to yield higher consumption of phosphorus in aerated zone than its formation in anaerobic zone. Phosphorus elimination may be completed by the addition of metallic salts.

2.2.1.4. MBR X CAS: OPERATING CONDITIONS OF BIOLOGICAL TANKS

There are important operating conditions that ensure the efficient performance of these reactions. The HRT for MBRs range from 4.0 – 8.0 h, and differently from CAS, this parameter is not dependent on SRT due to the membranes, which are able to keep sludge within bioreactor for more important time (10 – 80 days). This enables operation at high MLSS (4.0 – 10.0 g/L), which reduce reactor volume making installations more compact and less sludge waste is produced. At high MLSS concentration, the ratio food to microorganism (F/M) may be as low as 0.05 – 0.15 $kg_{BOD5}.kg_{MVLSS}^{-1}.d^{-1}$, presenting efficient treatment of diluted municipal wastewater. Dissolved oxygen concentration in MBRs is also affected by the high MLSS concentration. This parameter is fundamental for carbon and nitrogen based compounds removal and it should be maintained at the minimum value of 2.0 mg/L, in order to insure aerobic conditions. However, to keep this concentration of dissolved oxygen, oxygen transfer from gas to liquid must be induced. When MLSS concentration increases, this transfer is limited by viscous and steric effect. To quantify this effect, the ratio between the rate of oxygen transfer in clean water and in mixed liquor (α-factor) is usually adopted. It is conventionally assumed that α-factor of 0.3- 0.7 is acceptable for MBRs, depending on MLSS concentration and SRT [40].

Regarding physicochemical properties of pollutants, temperature and pH present strong effects on viscosity, hydrophobicity and solubility, which can affect the performance of biological treatment, thus they must be controlled. Although temperature usually varies with weather conditions, pH remains suitable for management and it ranges from 7.0 – 8.0 in full-scale wastewater treatment plants [36].

2.2.2. MEMBRANE FILTRATION STAGE

After biochemical treatment, treated water is separated from sludge by filtration.

The membranes used in this specific application are placed mainly according to two configurations, namely side-stream and submerged. In side-stream MBRs (*Figure 1.3*.A), mixed liquor is pumped to membrane modules in a cross-flow, which are separated from biological basin. Usually, mixed liquor is pumped inside tubular membranes and this increases transmembrane pressure to permeate flow through membranes. Retentate is recirculated to the reactor. *Figure 1.3*.B presents a submerged MBR configuration, membranes are immersed into the reactor, as a result there is no need for cross-flow pumps, however, conditions around membranes cannot be separately controlled from the biological basin, thus aeration has a double role of transferring oxygen to biomass and inducing shear stress along membranes to prevent from fouling [43]. The configuration presented in *Figure 1.3*.C enables to separate the membranes in a dedicated tank. Mixed liquor is pumped in a membrane tank and usually permeate is produced by a suction pump. This configuration enables to separate aeration in the biological tank with fine bubbles for optimal oxygen transfer and coarse bubbles in the membrane tank for fouling control, in addition to air flowrate.

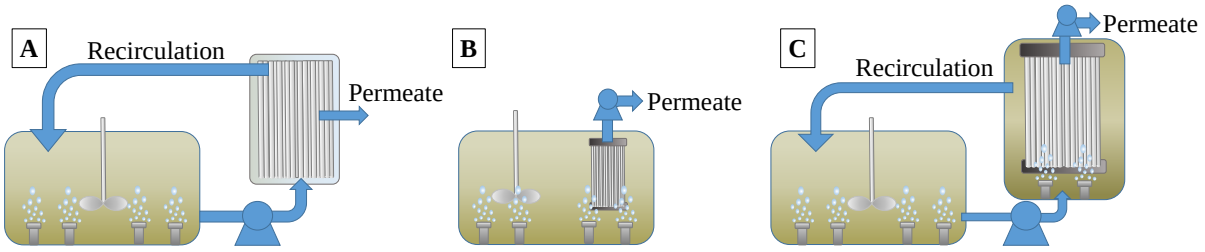

Figure 1.3: Schematic representation of (A) side-stream MBR and (B) submerged MBR and (C) membrane dedicated tank MBR.

In configurations presented in Figure 1.3.B and C, hollow fiber is the most applied membrane geometry and the filtration takes place from the outside to the inside of membranes as indicated on Figure 1.4.

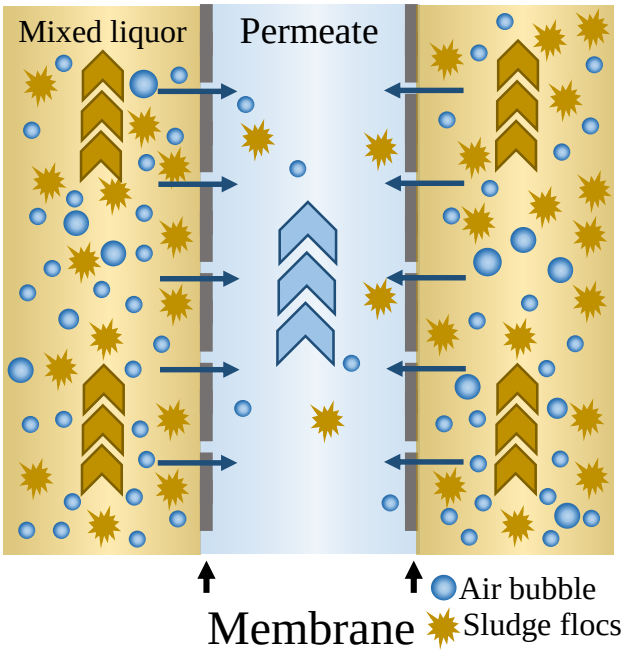

Figure 1.4: Illustration of hollow-fiber filtration from outside to inside.

Membrane processes can be classified as a function of membrane pore size, of transmembrane pressure applied, among others criteria. The classification of membrane process in relation to

the pore size is presented in *Figure 1.5*. In wastewater treatment, MBRs are usually equipped with either microfiltration or ultrafiltration membranes, so their pore size ranges from 0.01 to 0.5 µm and they are capable to reject sludge flocs, protozoa, bacteria and some viruses [43,44].

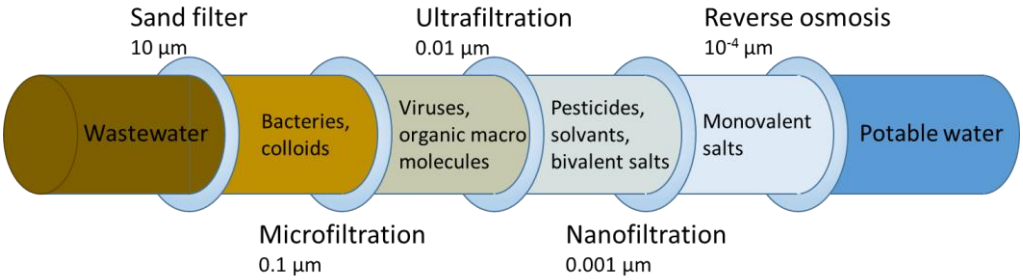

Figure 1.5: Membrane process classification based on pore size.

2.2.3. MEMBRANE MATERIAL FOR MBR APPLICATION

There are several materials that are suitable to compose membranes in MBRs, i.e. ceramic and polymers; however polymers are mostly applied as they are cheaper. Cellulose acetate, polysulfone (PSU) and polyethersulfone (PES) are the main hydrophilic polymers found in these membranes and polypropylene (PP) and polyvinylidene fluoride (PVDF) are the hydrophobic ones. The main drawbacks of these polymeric membranes include sensitivity to pH, oxidants and high temperature ranges and some of them present low mechanical resistance. To overcome the later, more resistant materials are often used as a matrix to support the selective part of membranes. In WWT, polyethylene terephthalate (PET) and polyamides (PA) are examples of those materials. Besides, hydrophilic agents are blended to membranes to decrease interactions between mixed liquor and membranes, avoiding severe fouling [44,45].

The membrane material for a given application is chosen based on several factors, such as feed stream properties, cleaning protocols and scale of process. PVDF is usually the polymer that matches the majority of these parameters and as a result it is the market leader in MBRs applications [14]. PVDF presents high thermal stability, chemical resistance, especially against halogens, oxidants, inorganic acids and aliphatic, aromatic and chlorinated solvents. Its

structure contains 59.4 wt% fluorine and 3%wt hydrogen with a degree of crystallinity from 35% to 70% and presents four semi crystalline phases, namely, α, β, γ and δ [45]. PVDF-based membranes usually undergo hydrophilic treatments to enhance their performance in WWT by blending, co-polymerization, surface-grafting and surface coating, for example. Blending is one of the most applied method and polyethylene glycol (PEG), polyethyleneimine, polyvinylpyrrolidone (PVP) and tannin are widely used as hydrophilic agents in these type of membranes [46,47]. In that case, even if the hydrophilic agent is soluble in water, which is the case for PVP, the additive will be entrapped in the membrane structure and only a small part present on the extreme surface will be washed away from the membrane structure by single water contact.

3. FOULING

3.1. THEORETICAL ASPECTS OF FILTRATION

In filtration process of pure solvents, permeate flux density (J_0, expressed in $m.s^{-1}$) is defined by Darcy's law (Eq. 5), which describes the flow of a fluid through a porous medium.

$$J_0 = \frac{Q_P}{S} = \frac{L_P}{\mu_T}\Delta P = \frac{\Delta P}{\mu_T R_m} \quad \text{Eq. 5}$$

Where, Q_P is the permeate flux ($m^3.s^{-1}$), S is the membrane surface (m^2), L_P is the hydraulic permeability of the membrane (m), ΔP is the transmembrane pressure (TMP, Pa), which is the difference between the average of feed and retentate pressures and permeate pressure, μ_T is the dynamic viscosity of permeate (in that case pure solvent, Pa.s) at temperature T and R_m is the hydraulic resistance of the membrane (m^{-1}).

When the parameters in Eq.5 are used outside the international system of the units, the permeability of a membrane is expressed in $L.h^{-1}.m^{-2}.bar^{-1}$ and corresponds to the ratio L_P/μ_T.

When fouling takes place, the fouling resistance (R_f) is added to the membrane resistance. As a result, an increase in TMP is observed in MBRs operating at constant flux or a decrease in flux for a constant TMP operation. In that last case the permeate flux (J) can be estimated by Eq. 6.

$$J = \frac{\Delta P}{\mu_T(R_m + R_f)} \quad \text{Eq. 6}$$

Indeed, when filtering different species, selectivity is another important parameter to characterize the process. The retention rate of a determined specie defines membrane selectivity and can be calculated by Eq. 7.

$$Retention\ rate = 1 - \frac{C_P}{C_0} \quad \text{Eq. 7}$$

Where:

C_P : concentration of the species in permeate;

C_0: concentration of the species in the feed.

3.2. FOULING MECHANISMS

The fouling resistance results from interactions of mixed liquor with membrane surface, following four different mechanisms, i.e. organic adsorption, mineral precipitation, pore blocking and biofouling.

Fouling process is initiated by the adsorption of organic foulants on membrane surface and inside its pores due to physical-chemical interactions. These interactions may be Van der Waals-based and electrostatic-based, but are mainly hydrogen bonds-based in MBRs. The attractive and repulsive effect of these forces create an energy barrier that foulants must overcome to adsorb on the membranes. According to Lin et al. (2014), this energy barrier is higher than the one associated to floc-to-floc interaction, which explains the first slow conditioning period of membrane surface, followed by the rapid fouling phenomena in MBRs. These interactions are affected by several parameters, including floc size, surface charge, and surface roughness [48].

Besides adsorption, inorganic fouling can occur by crystallization, when salts, such as $CaSO_4$ and $CaCO_3$, are rejected by the membrane, increasing their concentration on the surface. This accumulation in the vicinity of the membrane leads to a decrease in flux due to higher osmotic pressure, allowing the nucleation and subsequently precipitation of minerals on membrane surface [49].

Four different models , including complete, standard, intermediate blocking and cake filtration (*Figure 1.6*), can explain pore blocking. For complete blocking, each particle arriving on membrane surface blocks a pore without overlapping others. The standard blocking considers that particles will be deposit within pores decreasing the pores volume. For cake filtration, it is

assumed that particles do not block pores, they form a compressible layer on membrane surface which has its own porosity, acting as a second membrane. Lastly, intermediate blocking considers that particles either deposit over others or completely block a pore, integrating principles from cake filtration and complete blocking mechanisms [50,51].

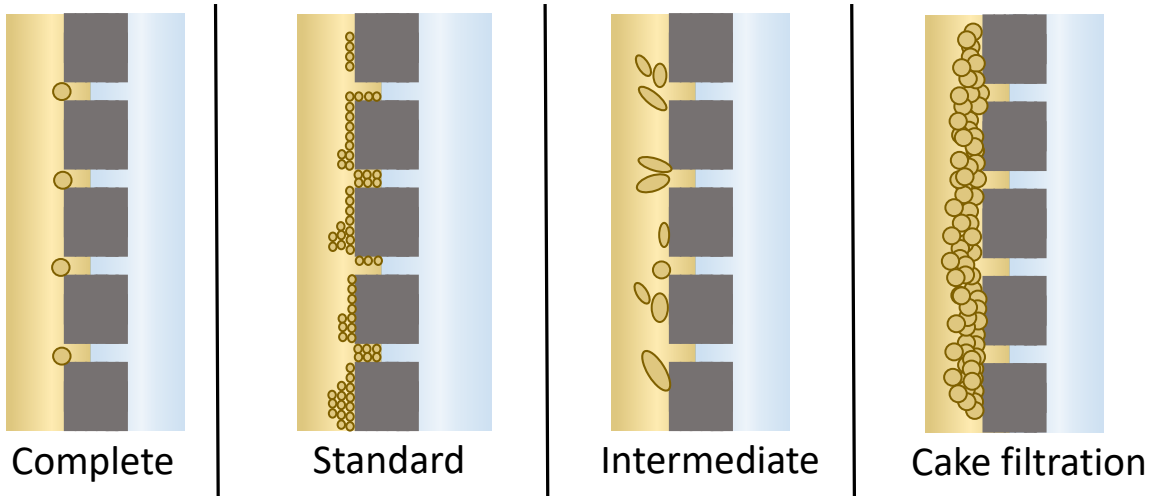

Figure 1.6: Fouling mechanisms (based on *[52]*)

Finally, biofouling occurs when membrane surface is conditioned by macromolecules, microorganisms easily attach onto it by bioadhesion and bioadsorption to form microcolonies and ultimately develop mature biofilms. Biofilms consist in layers of substrate, living and dead microorganisms and extracellular products. They strongly affect productivity of MBRs in WWT [50]. The formation of biofilms is coordinated through a signaling system known as quorum sensing (QS). Microorganisms produce signal molecules, e.g. N-acyl homoserine lactones (AHLs), autoinducer peptides (AIPS) and autoinducer-2 (AI-2), which freely diffuse through cell membranes and dictate production of specific compounds, formation of biofilms, surface motility and interspecies competition. On one hand, AHLs are mostly produced for the communication of Gram-negative bacteria. On the other hand, AIPS are used by Gram-positive bacteria. AI-2 is considered an inter-species signal molecule used by both [53].

Moreover, the higher solute/particulate concentration nearby membrane creates a gradient with the bulk solution, leading to a back diffusion into the bulk, which may trigger the formation of a gel layer and precipitation on membrane surface. This phenomenon, known as concentration polarization, is inherent in membrane process and can be described as the film theory [49,50,52].

3.3. FOULANT SPECIES IN MBR

The different components of mixed liquor are responsible for these four fouling mechanisms. The main structures that play a major role in fouling include extracellular polymeric substances (EPS), soluble microbial products (SMP), colloids and sludge flocs. These components can greatly affect permeability in MBRs in different ways that will be further discussed.

Most microorganisms on Earth live in aggregated forms within a matrix of biosynthetic polymers of biological origin, namely EPS. For a long time, they were called extracellular polysaccharides, as this is their main component, however a broader definition was established to consider the different classes of organic macromolecules, i.e. proteins, lipids, nucleic acids, humic acids, exocellular enzymes, structural components of cells and metabolites. Besides adhesion of cells in flocs and biofilms, EPS protect the cell against toxins and accumulate substrates [54]. These biopolymers exhibit complex linkage, hydrogen bonds and cation bridging interactions, and several functional groups, such as carboxyl, hydroxyl, phenolic, sulfhydryl and phosphoric groups. These groups assign a negative charge density at neutral pH, approximately, and contribute to aggregate formation, affecting therefore, hydrophobicity, adhesion, flocculation and dewatering properties of sludge. As a result EPS are highly involved in the membrane fouling process [39,48,50].

As mentioned before, EPS are mainly composed by polysaccharides and ribose, mannose, glucose and uronic acids are their predominant monomeric units [48]. Due to their high

molecular weight (>100 kDa) and low biodegradability, polysaccharides are more likely rejected in filtration and their gelling properties enable the formation of impermeable gel layer on membranes, that can increase filtration resistance and act as a support and substrate for microorganisms developing a biofilm [55].

Although proteins appear in lower content than sugars, it is also considered that they affect membrane fouling. Among the amino acids most abundant in the matrix, aspartic acid, glutamic acid, tyrosine acid and cysteine acid present negatively charged side chain responsible for major changes in EPS's hydrophobicity, surface charge and adhesion forces, thus affecting fouling as well [48].

Sludge flocs and EPS compose the solid fraction in mixed liquor. SMP are soluble products from cell metabolism, mainly soluble colloidal carbohydrates, humic acids and proteins, which freely diffuse in supernatant. They can be determined as a function of the COD in the soluble fraction of the mixed liquor (28). Shen et al. (2012) collected data of SMP from 10 full-scale MBRs and found concentrations of polysaccharides from 3-18 mg/L, humic substances from 2-10 mg/L and proteins at less than 5 mg/L with a broad molecular weight distribution from less than 1 kDa to greater than 100 kDa [56]. As SMP and EPS consist roughly of similar macromolecules, some authors found relations between them. Laspidou et al. [57] inferred that EPS can be synthesized using SMP as electron-donor or simply by adsorption on sludge flocs, but can also be hydrolyzed to form SMP. These interrelations are represented in *Figure 1.7*.

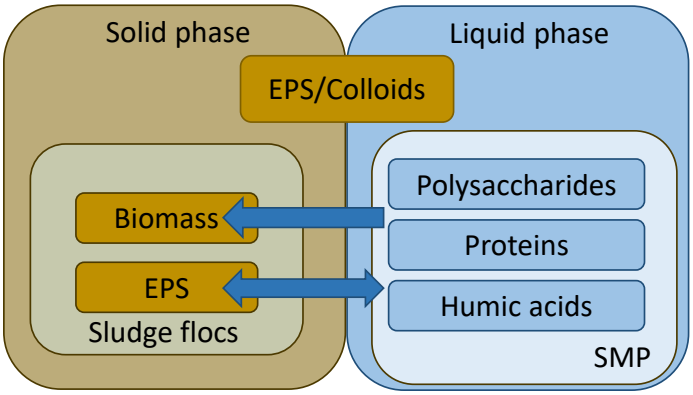

Figure 1.7: Different components in the mixed liquor.

Regarding operating conditions affecting these fouling species, although it is believed that SMP is one of the main source of membrane fouling, only the SMP concentration does not seem to correlate with fouling propensity in MBRs [41]. However, some indirect relations have been found and were assembled in Drew's review [41]. The main parameter influencing SMP concentration is SRT, these concentrations tend to drop with higher SRT, and as a result, fouling propensity decreases. Dissolved oxygen is another important parameter for SMP concentration. At limiting oxygen conditions, SMP elimination is not properly performed, hence cell hydrophobicity decreases, thereby promoting deflocculation and fouling. Shen et al. (2012) also found important relationships between fouling potential and some fractions of SMP, such as TOC, polysaccharides and humic acids contents [56]. TOC showed high impact on initial fouling, which consists of both adsorption and pore blocking. Indeed, studies suggest that SMP can increase the fouling propensity of EPS by conditioning membrane surface to the subsequent adhesion of EPS. When supernatant presented 0.03 g/L of SMP, cake resistance increased 8 times in the filtration of 13 g/L sludge floc solution [48].

The formation of the cake layer in MBRs operated at constant flux is a dynamic process decomposed in three stages according to the TMP behavior as presented in *Figure 1.8*. Firstly, the passive adsorption of high molecular weight polysaccharides (less biodegradable), proteins and colloids causes a rapid, but short increase in TMP in the early stage. After this sudden

increase, TMP builds steadily at a lower rate in the second stage with further adsorption of soluble species and biomass deposition. With the blocking of some regions on the membrane surface, flux rises in specific areas aside with fouling rate promoting a "jump" in TMP. After this stage, EPS were found to be the main foulants in the cake [55,58].

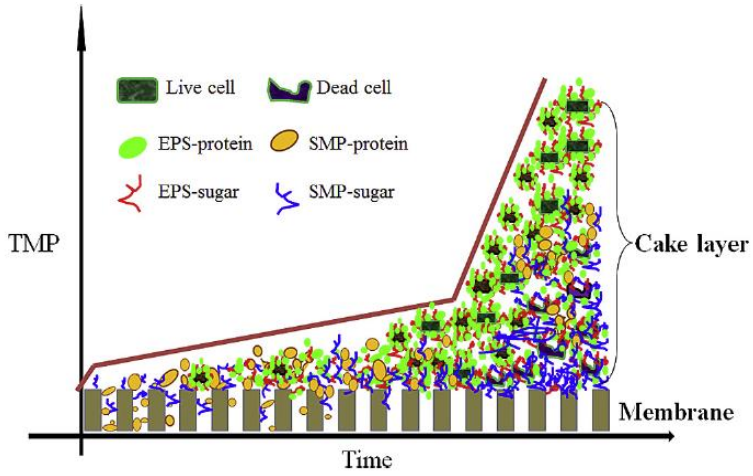

Figure 1.8: Cake formation on membrane surface and its effects on TMP over time. Figure from *[55]*.

Therefore, it seems that firstly, SMP species interact with membrane surface and pore walls, and then the insoluble species, such as EPS and sludge flocs, build up the cake layer and increase pressure as a result. Currently, efforts are still needed into identifying the main causes of fouling and on developing strategies to better control it in order to reduce energetic costs of MBRs. Regarding these strategies, fouling can be classified as reversible, when the fouling layer can be removed by pressure release or specific physical cleaning, and as irreversible, otherwise [49].

4. FOULING CONTROL

Fouling is the major challenge in MBRs because it leads to a decline on productivity and a rise on energy consumption, thus on operating costs. That is the reason why researches have focused

on antifouling strategies in the recent years [5]. As a result, the progress achieved with these strategies have gradually reduced energy consumption. In China, MBRs commissioned from 2006 to 2014 presented energy consumption of about 0.5-0.7 kWh/m^3, against 0.35-0.65 kWh/m^3 for MBRs built thereafter [4].

There are several approaches to prevent extensive clogging and fouling of membranes. Table 1.2 summarizes these techniques and principle involved in each one. Some of them are widely applied on full-scale operation and others are still been developed, this is indicated in Table 1.2. These strategies are further discussed on the following sections.

Table 1.2: Fouling control strategies applied in MBRs treating wastewater. Based on *[5]*.

Method	Strategy	Application (Lab. vs. Industrial scale)	Principle	Examples
Mechanical	Aeration	Industrial scale	Increase shear stress on membrane surface	Upwards, turbulence fluctuations
	Backwashing	Industrial scale	Reduction of gel polarization layer, prevent layer compaction and remove deposited layer	Air, clean water, permeate
	Biofilm carriers	Lab scale	Affect physiochemical characteristics of mixed liquor and mechanical effects on membrane surface	Granular activated carbon, PU, PEG, PVDF
	Vibration	Lab scale	Increase shear stress on membrane surface	-
	Ultrasonic waves	Lab scale	Dissolve and displace soluble and insoluble to prevent polarization layer and biofilm layer	-
Chemical cleaning	Acids	Industrial scale	Remove inorganic foulants	Oxalic, citric, sulfuric acids
	Bases	Industrial scale	Remove organic foulants	NaOH and KOH
	Oxidants	Industrial scale	Oxidation of organic foulants and desinfection of biological foulants	NaOCl, H2O2, PVP-iodine
	Surfactants	Industrial scale	Solubilize foulants based on fat, oil and proteins	SDS
	Chelating chemicals	Lab scale	Affect intermolecular bridges within foulants releasing them to their original losen conformation	diamine tetraacetic acid, sodium tripolyphosphate
	Emerging chemicals	Industrial scale	Affect biofilm properties	Rhamnolipids, free nitrous acid
Fouling release membranes	Active approach		Antimicrobial agents to eliminate proliferative fouling	Acrylic acid, cellulose, graphene NMs
	Passive approach	Industrial scale	Prevent the adsorption of foulants on membrane surface without any impacts on the intrinsic features of the foulants	PEG, zwitterionic polymers, PVP and metals and carbon-based NMs

Cell immobilization	Passive immobilization	Lab scale	Use of surface to prevent accumulation of bound EPSs and SMPs	Granular activated carbon, PU, PEG, PVDF
	Cell entrapment	Lab scale	Artificially entraps cells in a porous polymeric matrix to prevent accumulation of bound EPSs and SMPs on membrane surface	Agar, alginate, carrageenan, polyvinyl alcohol, xanthan gum
Biological	Quorum quenching	Lab scale	Disruption of QS by blockage of production, interference with the signal receptor or inactivation of signal molecules.	Lactonase and acylase or *E. coli* and *Rhodococcus* to degrade AHLs
	Enzymatic disruption of EPS	Lab scale	Enzymes destroy the physical integrity of EPSs through degradation process and facilitate detachment of biofilm	Proteinase K, trypsin and subtilisin
Electrical	Electrocoagulation	Lab scale	An anode and a cathode powered with direct current. Metal cations are generated from the electrodissolution of anodes in the MBR reducing fouling by charge neutralization.	Aluminum or iron as anodes
	Microbial Fuel Cell (MFC)	Lab scale	It promotes fouling mitigation through electrostatic repulsion and by in situ generation of H2O2 and OH radicals	-

4.1. MECHANICAL APPROACH

Among the mechanical approaches, aeration, relaxation and backwashing are the most applied on full-scale MBRs. They contribute to the turbulence on membrane surface, which limits cake formation. Aeration can be performed in continuous at a fixed air flowrate, but it was observed that same results to limit cake formation could be achieved with cyclic aeration with 10s/10s intervals of aeration on and off achieving up to 50% of saving related to aeration consumption [55]. Besides air flowrate is beneficial for permeability of membranes up to an optimal value, higher values may damage sludge flocs leading to EPS and colloids release, being detrimental for permeability [5].

Along with aeration, operating MBRs in intermittent cycles of filtration and relaxation, i.e. when permeate flowrate is set to zero, have shown great results to overcome fouling. Relaxation could decrease by half the fouling rate [59]. The same study showed that relaxation time is a key parameter: cycles of 10 min of filtration and 1.5 min of relaxation presented the lowest fouling rates, whereas applying 2 min of relaxation increased fouling rate as high as operating with no relaxation.

Since aeration and relaxation cannot deal with internal fouling, backwashing is also employed in the majority of wastewater treatment plants with the purpose of reducing internal fouling. It can be achieved by pushing clean water or permeate on the other sense of filtration and it is efficient on removing deposited layer, reducing gel polarization layer and preventing compaction of gel layer. In a pilot-scale study, using cycles of 250 s filtration/50 s relaxation and 30 s of backwashing each ten cycles, membranes operated for 2 years kept permeability above 100.0 $L.h^{-1}.m^{-2}.bar^{-1}$ filtering up to 25 g/L of suspended solids at fluxes between 9 and 13.3 $L.h^{-1}.m^{-2}$ and air scouring at 0.3 $Nm^3/(h.m^2)$ [60]. Indeed, the flowrate (10-25 $L.h^{-1}.m^{-2}$) and duration (10 – 30 s) of backwash was verified and authors concluded that higher intensities were more effective than long duration [61].

Other mechanical approaches are being developed mostly at lab and pilot scale MBRs and presenting promising results, which is the case for biofilm carriers, vibrating membranes and ultrasonic waves. Biofilm carriers can reduce fouling by both affecting physicochemical properties of sludge and scouring the deposit on membrane surface. It was shown that biofilm carriers could affect the content of EPS and SMP and increased filtration time up to 8 times, however there are few information about the impact of configuration and type of biofilm carriers on MBR operation. Besides, vibrating membranes can act only enhancing shear stress on membrane surface, but it can also homogenate mixed liquor in submerged MBRs. Applying vibration or rotation allowed membranes to achieve higher levels of fouling mitigation than air scouring. Although promising, the major drawback of this technology is still the elevated energy cost. Ultrasonic waves are also being studied as they can act dissolving and displacing soluble and insoluble particles. Employing sonication can form cavitation bubbles that can remove biofilm and prevent cake deposition. Nevertheless, cleaning efficiency is reduced at high TMP levels and membrane damage is a frequent issue on practical applications [5].

4.2. CHEMICAL CLEANING

The use of chemical reagents is also a widely spread practice on MBRs. Chemical cleaning of fouled membranes follows six main steps. When reagents are injected, they can (i) react in the bulk solution, followed by their (ii) transportation to the interface between bulk solution and fouling layer. Cleaning reagents (iii) penetrate into fouling layer, (iv) the oxidization of foulants and/or (v) their solubilization and detachment take place. After that, oxidized/detached foulants and the waste cleaning agents are (vi) transported back to the interface and (vii) finally to the bulk solution [5].

Several species are employed as chemical cleaning agents of fouled membranes including acids, bases, oxidants and surfactants. In traditional cleaning protocols, each of those solutions can be

directly injected by backwashing into the membranes or membranes can simply be soaked into cleaning solutions for a determined time.

Among the acids, oxalic, citric, nitric, hydrochloric and phosphoric acids are the most used and they are effective in removal of mineral fouling by neutralization and double decomposition reactions with the precipitated salts on membrane surface. On one hand, mineral acids are low cost and effective on foulants removal but they can damage membranes and easily change pH of medium, affecting microbial activity in the activated sludge. On the other hand, oxalic and citric acids have buffering properties decreasing pH shock and membrane damage and they are able to remove metal cations by forming complexes with them [55].

Bases, such as sodium and potassium hydroxides, are preferred to remove organic fouling. They are applied at pH ranging from 11.0 to 12.0 to hydrolyze and solubilize proteins and carbohydrates. They also react with fats and oils through saponification forming water-soluble micelles. These reagents present high permeability recovery in a short period of cleaning [62,63].

Organic fouling can also be removed by oxidants. These agents oxidize functional groups of foulants to ketone, aldehyde and carboxylic groups, making them more hydrophilic, thus less attracted to membrane surface. Besides oxidation, they also disinfect membranes from biological fouling [5]. Sodium hypochlorite and hydrogen peroxide are examples of oxidants used in cleaning protocols. At full-scale, sodium hypochlorite is preferred due to its efficiency and low cost. The study of Brepols et al. (2008) showed that at lab-scale, both oxidants presented same cleaning efficiency, but when applied to full-scale, hydrogen peroxide was not able to maintain permeability over a period of several weeks even at concentrations as high as 2000 ppm [64]. Moreover, when compared to NaOH, NaOCl was more efficient in cleaning a membrane fouled by a solution of 0.3 g/L bovine serum albumin (BSA) [16].

Studies presented in the Wang et al. (2014) suggested that the use, either jointly or sequentially of reagents have a positive effect on membrane recovery [65]. It was shown that a solution composed of NaOCl and NaOH could increase relative flux, i.e. flux of cleaned membrane related to flux of fouled membrane, up to 150%, whereas the increase using the isolated solutions was only 60% for NaOCl and 10% for NaOH. Furthermore, the long-term cleaning with hypochlorite and acids is widely used in wastewater treatment plants as they affect inorganic and organic fouling.

Surfactants are other class of chemicals often used in MBRs to clean organic foulants, mainly from specific effluents rich in fats, oils and proteins. These amphiphilic compounds reduce surface tension between liquids and solids and are able to solubilize macromolecules. Their hydrophobic tail adsorbs organic foulants, while their hydrophilic moiety interferes with the ion bridges [5]. Levitsky et al. (2012) found that Tween-20 presented the highest cleaning efficiency on polyether sulfone (PES) membranes and when filtering a solution of BSA, membranes previously cleaned by the surfactant presented less protein adsorbed than the ones cleaned by NaOCl [63]. However, a cocktail of both was the most effective cleaning solution. Electrostatic repulsions and surfactant hydrophobicity help to loosen bonds between proteins and membrane surface. As a result, mass transfer of oxidants through the fouling layer is facilitated and the detached foulants are enclosed in surfactant micelles, avoiding repeatable attachment.

Recently, laboratory studies have demonstrated the efficiency of some emerging chemicals as cleaning reagents of fouled membranes. Rhamnolipids are a class of low cost and low toxicity surfactants that have been successfully applied for fouling prevention and cleaning with high degree of biofilm detachment. They enhance surface hydrophobicity of foulants by release of lipopolysaccharides (LPS) and EPS, mitigating fouling on hydrophilic membranes. However,

in long-term operation, membranes are expected to become more hydrophobic and the performance of these reagents has never been accessed [5].

Another promising chemical is free nitrous acid (FNA), which is formed at low pH nitrite solutions, and is able to inactivate microorganisms responsible for biofouling by damaging lipids, proteins and deoxyribonucleic acid (DNA). It has been studied as cleaning reagent since 2015 and has shown to be more effective than NaOH on cleaning of heavily and moderately fouled membranes and could also descale membrane surfaces. Some of the drawbacks of this compound that must be overcame include possible membrane damage at very low pH (~2.0) and possible increase of NO_2 concentration in effluent impairing treatment performance [55].

Next to their performance in cleaning protocols, most of these chemical agents have been reported to change membrane properties, such as, mechanical strength, hydraulic resistance, pore size and hydrophilicity. Moreover, they negatively affect microbial process in MBRs by inactivating important enzymes for organic matter biodegradation, nitrification and denitrification, increasing EPS production or producing toxic intermediates. With these changes, interactions between foulants and aged membranes may differ, resulting in different cleaning efficiency for the same protocols over time. For this reason, researchers are still developing other methods to avoid consume of harmful chemicals.

4.3. ALTERNATIVE METHODS

The development of antifouling membranes has emerged in literature as a promising way to avoid all those down times from physical and chemical cleaning. Several hydrophilic agents, such as PEG and polyvinyl alcohol based polymers compose commercial membranes used in ultrafiltration. These agents decrease interactions between foulants and membrane surface and are very effective in the early stages of full-scale operations. Nanomaterials including silver nanoparticles, titanium and zinc oxides and all carbon-based nanomaterials have been tested as

components of ultrafiltration membranes. These species present photocatalytic activity, antimicrobial ability and hydrophilic characteristics that can act in synergy to alleviate membrane fouling. These membranes can be classified as active or passive approaches for fouling control. For example, silver nanoparticles and graphene-based nanomaterials can actively affect microbial cells undermining cell growth on membrane surface, whereas titanium dioxide nanoparticles passively retard bacterial adhesion and growth by the development of a thin layer of water on membrane surface, due to hydrophilic interactions [5,55].

Besides changing membrane properties to reduce interaction with foulants, researchers have proposed to reduce the amount of foulants that reaches membranes by cell immobilization. On one hand, biofilm carriers, previously discussed, are a passive way to immobilize cells onto a surface to avoid contact between foulants and membrane surface. On the other hand, cell entrapment, i.e. immobilized inside a porous polymer matrix, enables to prevent fouling and protects cells from toxins, prolongs SRT and has a simple design for MBR application. MBRs relying on entrapped cells are similar to a hybrid system of biofilters with membranes. The membranes enable overcoming the removal of pathogens and large particles, one of the major drawbacks of process based only on entrapped cells. Agar, alginate, Carrageenan as well as polyvinyl alcohol and xanthan gum have been introduced as matrix. The successful application of these materials depends on their durability and size, cell to matrix ratio and cell viability [5].

Quorum quenching (QQ) is another strategy to mitigate fouling. It consists on avoiding the intercellular communication among bacteria (Quorum sensing). Bacteria produce autoinducers in proportion to the cell density that are identified by receptor proteins. When a threshold level is reached, the transcription of specific genes is activated and actions such as secretion of EPS and biofilm formation are promoted. AI-2 and AHL are two important autoinducers targeted by QQ. AI-2 is considered a universal autoinducer secreted by both Gram-positive and Gram-negative bacteria, but, as Gram-negative bacteria are predominant in MBRs, controlling AHL

is also effective to prevent fouling [5,55]. QQ is often based on either avoiding autoinducers synthesis, deactivating signal molecules or interfering transport and reception.

Among the novel approaches, electrical methods, such as electrocoagulation, electrophoresis and microbial fuel cell (MFC), have been proposed to control fouling in recent years. In electrocoagulation process, two electrodes in the MBR are powered with direct current, where the metal composing the anode is electrically dissolved forming a positively charged coagulant that neutralizes the negative organic matter, reducing its accumulation on membrane surface. As barriers, this process exhibits high-energy costs due to electricity consumption. The electrophoresis consists in the application of a uniform electrical field to generate an electric repulsive force between foulants and membrane surface. This process share the same drawbacks as electrocoagulation, however, some membranes can be used as cathodes, such as polypyrrole-based membranes, decreasing energetic costs of this process [5]. Some studies have coupled MBRs with MFCs in order to generate the electrical repulsion between foulants and membranes, by microorganisms' electrochemical reactions. Besides the electrical repulsion, generation of hydrogen peroxide on the cathode can enhance the degradation of biopolymers and the detachment of foulants from membrane surface [55].

All these methods to mitigate fouling coupled with the operating conditions promote changes on membrane properties over time. These changes alter the treatment productivity, increasing process costs. Therefore, the study of changes on membrane properties over time, i.e. membrane ageing, is a subject of great interest in the wastewater treatment field and will be further discussed in the next section.

5. MEMBRANE AGEING

The mechanical stress and chemical exposure of the strategies to control fouling may alter physical/chemical properties of the materials composing membranes with time. These changes

define the process of ageing. Membrane ageing leads to a loss of productivity, an increase of operating costs and, ultimately, the membrane replacement, which accounts for 25-40% of the total membrane plant costs. That is the reason why researchers have been focusing on this particular subject lately and publications related to ageing have been multiplied by a factor of 10 from 2000 to 2010 [66].

It is worth noting that ageing is a comparative study between used and pristine membranes, consequently, it is impossible to quantify it without a reference. Ageing generally leads to membrane failure, but they must not be confused. Membrane failure is linked to the loss of removal efficiency and can be determined by integrity tests, such as pressure decay tests or particle monitoring [67]. It is a concept often applied to the production of potable water, which uses non-supported membranes. In wastewater treatment, productivity is the key important, therefore, it is usually prioritized over loss of permeate quality.

Since the process efficiency is closely related to ageing and failure, anticipating and scheduling activities for the membrane replacement is vital for operators of full-scale plants. Currently, the membrane lifespan is estimated based on membrane manufacturers' warranty, which can range from 3 to 10 years. However, there are cases reporting membrane lifespan of less than 6 months and others showing that membranes could withstand their operating conditions and filtration efficiency for up to 13 years [68]. Therefore, there is a clear need for membrane ageing assessment tools based on reliable properties that describe ageing correctly.

5.1. PROPERTIES AFFECTED BY AGEING

Soaking membranes into cleaning agent solutions is the most used method to age membranes in laboratory and to predict what could happen in full-scale operation. This way membrane ageing can be described by monitoring the behavior of physical/chemical properties and filtration performance characteristics, such as pore size distribution, tensile strength,

hydrophobicity, retention, permeability and fouling rate [66]. As already discussed, ageing is based on the evolution of several properties followed by different techniques in published studies. In Robinson et al. (2016), authors presented the *Figure 1.9* below, which correlates performance factors with membrane properties and the possible analytical methods to determine these values established from the membrane literature [8].

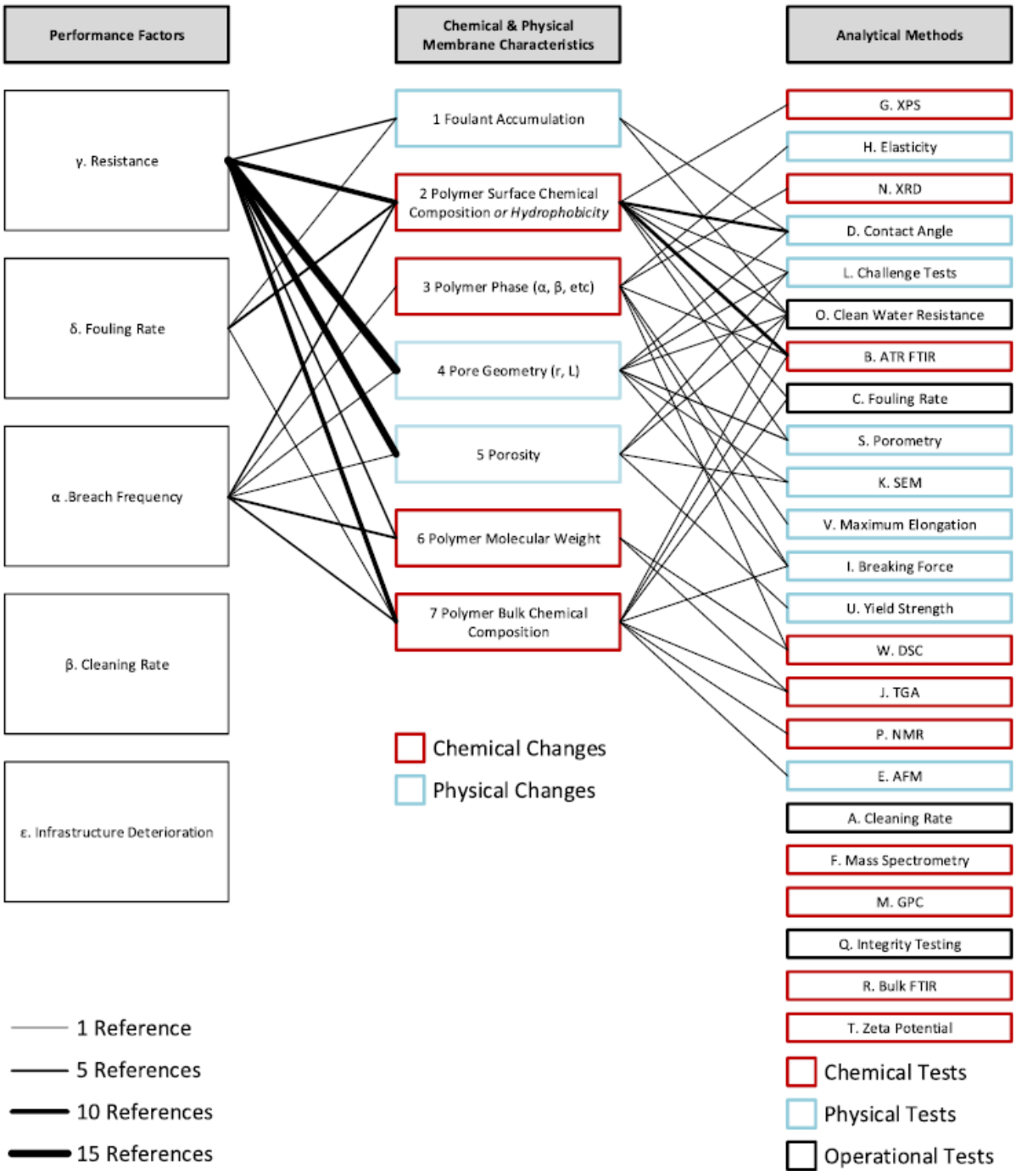

Figure 1.9: Correlation between performance factors, membrane characteristics and analytical techniques established in the literature. The line thickness corresponds to the number of references that suggest the particular relation (from *[8]*).

5.1.1. PHYSICAL PROPERTIES

Among the existing techniques to assess mechanical characteristics of membranes, traction tests are the most frequently applied and parameters such as ultimate elongation and ultimate tensile strength can determine the ageing process. The first quantifies the deformation of membranes at break and provides information about the elasticity of membranes, whereas the latter is the uniaxial stress that can be applied prior to fracture. Aged membranes tend to become stiffer and more brittle, however, contrastive results were already reported for PVDF membranes soaked in hypochlorite [8,67].

The morphology of membranes are often evaluated by visualization techniques, such as atomic force microscopy (AFM), scanning electron microscopy (SEM) and field emission scanning electron microscopy (FESEM). AFM measures surface morphology and roughness by the force to drag a precision tip along the membrane surface [67]. In membrane ageing, this assay mainly provides comparative studies of topography, which trends to increase over time. When comparing different materials of aged membranes, this increase was more pronounced on PVDF-based than on PES-based membranes [66]. The other two techniques (SEM and FESEM) can provide further information on pore size, thickness, symmetry and physical damage via high-resolution images [67]. For example, enlargement of the pore size of PVC hollow fibers aged with NaOCl was already found by FESEM [66]. However, the control of imaging variables is primordial to avoid bias when applying these techniques, indeed pore distribution can be overestimated as they cannot differentiate surface pits and true pores [69].

Compared to these imaging techniques, bubble pressure measurement is a more reliable tool to determine pore size. It provides the size of the largest pore in a sample. This method correlates the pore size with the pressure needed for a wetting fluid (mainly water) to be displaced by another or by air. Narrow pores exhibit higher capillary forces, thus higher pressures are

expected for these pores. This behavior is described in the equation of Young-Laplace (Eq. 8), which correlates the size of the largest pore (r_{max}) and the capillary pressure in a tube (P_b).

$$r_{max} = \frac{2\,\gamma\,cos(\theta)}{P_b} \qquad \text{Eq. 8}$$

With:

γ: Water superficial tension,

θ: contact angle of water on membrane surface.

5.1.2. CHEMICAL PROPERTIES

To assess chemical properties of aged membranes, there are a wide range of techniques available that can be as simple as contact angle measurement, or highly sophisticated, such as mass spectroscopy (MS). Contact angle is widely used to determine hydrophobicity of membrane surfaces as they age. It is based on the angle between the membrane surface and the droplet of a probe liquid, generally hydrophilic. Similarly, the captive bubble method can be applied by immersing the sample in a liquid and place an air bubble on the membrane surface, this way porosity plays a less important role in the measurement. Thus, a high angle indicates a more hydrophobic surface, which is generally attributed for aged membrane to reactions between cleaning agents and membrane polymers or accumulation of irreversible foulants, as example [8,70]. Attenuated Total Reflectance Fourier Transform Infrared Spectroscopy (ATR-FTIR) is another widely used technique that evaluates chemistry surface of membranes by identification of functional groups. By this technique, many studies have concluded the PVP leach out in hydrophilic membranes or the degradation mechanism of PES membranes in contact with hypochlorite [66].

To evaluate macromolecular changes in the main polymer of membranes during ageing, thermogravimetric analysis (TGA) and size exclusion chromatography (SEC) were already reported. TGA is based on the thermal degradation of polymers: as the temperature increases,

components are removed from the membrane matrix and the material is continuously weighted. In polymers, shorter chains are volatilized at lower temperatures, so the TGA profile of an aged membrane can highlight the predominance of cross-linking or chain scission among the polymers molecules with ageing and the degradation of co-polymers. Whereas, SEC provides detailed information about the molecular mass distribution of polymers. It consists of dissolving the membrane material into a solvent and passing through a column that separate larger molecules from smaller ones, giving a quantitative measure of polymeric chain scission and crosslinking of aged samples [8].

Less frequently, Nuclear magnetic resonance (NMR) spectroscopy, MS, differential scanning calorimetry (DSC) and X-ray diffraction (XRD) are employed in membrane ageing studies. NMR and MS are techniques that are more sophisticated. They, respectively, identify chemicals and determine the molecular masses of substances present in samples. NMR is also able to quantify the species in the membrane, which gives an advantage over ATR-FTIR. DSC and XRD assess the crystallinity of polymers. The first is based on measurements of melting enthalpy by the melting temperature, and the latter allows the examination of the crystal structure by measuring angles and intensities of diffracted X-ray beam of a sample [8].

Assessing the elemental composition of a material surface can be useful in ageing, as reactions of elimination or irreversible fouling can be evidenced. X-ray Photoelectron Spectroscopy (XPS) is an interesting tool as changes in common atoms in polymer membranes, such as C, F, O, N and S, can be observed. This method also gives information about the oxidation state of these elements, whereas, a simpler way to assess just the elemental composition of samples is the combination of SEM with energy dispersive X-ray spectroscopy (EDX) [8,67].

5.1.3. FILTRATION PERFORMANCE

Membrane filtration properties, such as intrinsic permeability, fouling rate and selectivity are useful macro-scale properties to monitor membrane ageing, since they are impacted by most of the other physical-chemical properties.

Intrinsic permeability is measured by filtration of clean water, either distilled, ultra-pure or potable, at different flowrates. For instance, changes in intrinsic permeability of membranes during ageing are often related to changes in pore size and hydrophobicity. Intrinsic permeability may be measured in-situ for application such as evaluating cleaning efficiency with a standard liquid (clean water), but also to monitor membrane ageing.

Fouling rate may be determined by filtration of fouling agents and tracking the changes of permeate flux, if TMP is constant, or changes in TMP, if permeate flux constant. These changes are also related to hydrophobicity: as membranes aged, they usually become more hydrophobic, thus more susceptible for interactions with organic matter. Analysis of fouling rate can also be performed in-situ, to determine whether fouling potential of the matrix has changed in the short-term, but also to give information about membrane ageing in the long-term.

Challenge tests are also useful tools to estimate pore size evolution by the measurement of the retention of polymeric probes, such as dextran, or of the rejection capability by filtering bacteria, such as *Escherichia coli*, or viruses [8,71]. These are also interesting indicators of integrity loss for in-situ measurements of permeate, if the presence of these species increase overtime in permeate, it may be a sign of membrane degradation or fiber breakage.

Membrane ageing studies consist in the comparison of a number of properties between aged and pristine membranes. Changes in these properties affect each other during ageing. Thus, ageing can be demonstrated by correlating changes in elemental, molecular, microscopic and macroscopic properties. According to the literature, the direct correlation among these properties for PVDF membranes, either supported or not, is illustrated in the *Figure 1.10* below.

Several studies related filtration performance to pore size and hydrophobicity of membranes. The changes in hydrophobicity were linked to additive or PVDF degradation, which also affected pore size. In addition, membrane mechanical resistance was mostly influenced by PVDF chain reactions. The relationship between these modifications will be further discussed in section 5.3.

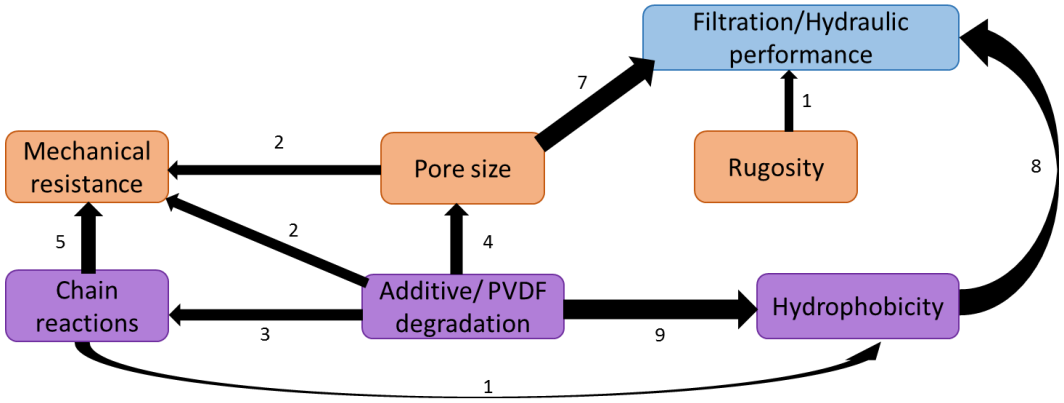

Figure 1.10: Interactions among chemical properties (purple), physical and structural characteristics (orange) and filtration performance (blue) used to explain results in literature. Numbers and thickness of arrows represent the amount of publications that discuss the relation between these properties.

Membrane properties evolve differently depending on its composition, operating conditions and cleaning agents. As the most used cleaning agent is sodium hypochlorite, its impacts on membranes are the most explored in the literature. Thus, the chemistry of sodium hypochlorite in solution and its effects on membranes properties will be hereby summarized.

5.2. CHEMICAL AGEING BY SODIUM HYPOCHLORITE SOLUTION

5.2.1. CHEMISTRY OF SODIUM HYPOCHLORITE SOLUTION

Sodium hypochlorite can dissociate into different oxidant species depending on pH, which will determine its action on membrane properties. These species present different oxidation-reduction potentials that make NaOCl generally more effective on disinfecting membranes at around pH 9.0 when it can act as a detergent at pH 11.5, for example. Typically, chlorine (Cl_2), hypochlorous acid (HClO) and hypochlorite ion (ClO^-), which are predominant at acid (pH<3.0), neutral (4.0<pH<7.0) and basic (pH>9.0) solutions, respectively, are the species that contribute to total chlorine concentration. However, these are not the only species involved on the ageing of polymeric membranes. As can be seen in equations 9 - 11, ClO• and OH• radicals are two reactional intermediates likely to be present in solution and believed to have an effect on polymeric membranes degradation [66].

$$HOCl + ClO^- \rightarrow ClO\bullet + Cl^- + OH\bullet \quad \text{Eq. 9}$$

$$OH\bullet + ClO^- \rightarrow ClO\bullet + OH^- \quad \text{Eq. 10}$$

$$ClO\bullet + ClO^- \rightarrow 2Cl^- + O_2 + OH\bullet \quad \text{Eq. 11}$$

5.2.2. EFFECTS OF NAOCL EXPOSURE ON DIFFERENT MEMBRANES

Some of the most used polymers in water and wastewater treatment plants, i.e. cellulose-derived, polyvinylchloride (PVC), PSU, PES and PVDF based membranes, were reviewed regarding the ageing effects of sodium hypochlorite by Regula et al. (2014) [66]. In this review, the authors observed that cellulose-based membranes, i.e. cellulose acetate (CA) and cellulose ester (CE), and PVC membranes are less used membranes for water treatments and one of the reasons is that they are highly sensitive to hypochlorite. CA and CE membranes presented

integrity faults even at small hypochlorite exposure concentrations. Besides, changes in pore size distribution, decrease in breaking force (from 240 to 80 MPa), formation of carboxyl, aldehydes and ketones end groups due to cellulose oxidation and departure of additives, such as PVP, were confirmed by ATR-FTIR spectra and SEM images. CE membranes also increased intrinsic permeability when cleaned by NaOCl (40 ppm) or NaOH (300 ppm) for 72h, probably due to pore enlargement. For PVC membranes, pristine and fouled membranes exhibited NaOCl sensitivity. Enlargement of pore size during exposure to hypochlorite solutions of concentrations as low as 1% was observed. For higher concentrations, permeability first increased followed by a decline caused by twists and wrinkles.

PSU membranes are the most used membranes in drinking water production along with PES and PVDF membranes, but they are also applied in hemodialyzers. In both applications, they must be cleaned and bleach is the most used agent. Although these are more NaOCl resistant membranes, Regula et al. (2014) mentioned several studies reporting increasing permeability after NaOCl exposure for these membranes [66]. These changes were attributed to PSU degradation, which led to chain scission and contributed for loss in mechanical properties [72]. In another study, Regula et al. (2013) showed that this increase in permeability and the decline in elongation at break were underlined as temperature, contact time and concentration increased [73]. Decline in elongation at break reached 80% at 40 °C and pH 11.7. Moreover, they observed that the breaking force also decreased continuously, making membranes rigid and fragile, which increased chances of early breakage.

The impact of NaOCl on PES membranes is one of the most developed subjects in membrane ageing recently. Chlorine tends to increase permeability because of an increase in pore size at pH 6.0 – 9.0. These changes in pore size were related to changes in PES chemical structure observed on ATR-FTIR spectra. The proposed ageing mechanism of PES membranes evolved over time [74] and actually the most recent results consider two mechanisms occurring at the

range of pH 6.0 – 8.0. HClO predominance (pH 6.0) and its coexistence with OCl^- (pH 8.0) promotes: (1) the formation of phenol groups in the PES chain by radical oxidation (OH•) (*Figure 1.11*.A) confirmed by measurements of tangential streaming current measurements; (2) PES chain scission forming sulfonic acid groups (*Figure 1.11*.B) confirmed by the presence of a C-Cl covalent bond in XPS spectra [75].

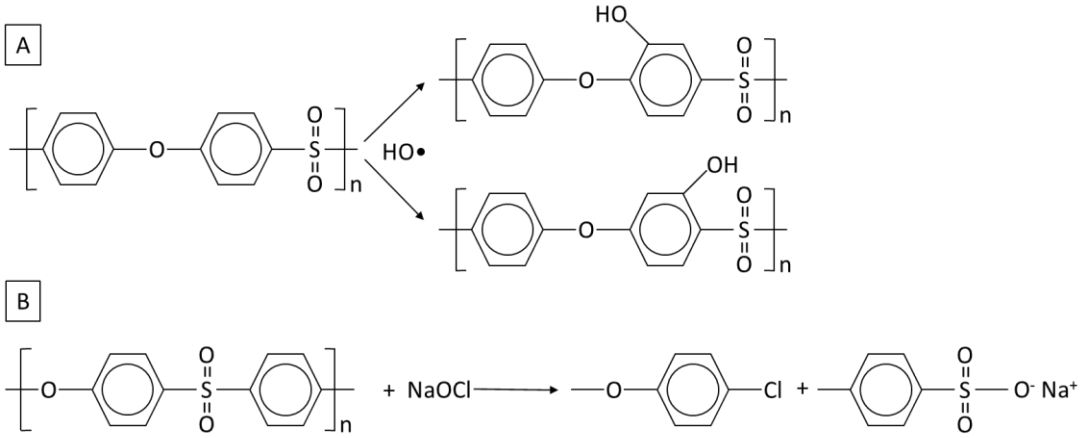

Figure 1.11: Formation of phenol groups in the PES chain and PES chain scission to form sulfonic acid groups and chlorinated phenols. Based on *[74,75]*.

5.2.3. INTERACTIONS BETWEEN HYDROPHILIC AGENT AND NAOCL

Most of the selectivity skins of membranes used in water treatment processes are composed of a secondary material (additive) that is responsible to increase hydrophilicity of membrane surface in order to decrease fouling and increase permeability. In the case of hydrophilic treatment by membrane coating, this additive is present only on the membrane surface. In the case of hydrophilic agent addition by blending in membrane material, even if the additive is supposed to be present all over the membrane thickness, it is significantly detected only within the first 30 µm of the membrane thickness [71]. However, most of these additives are highly reactive with some of hypochlorite dissolution products and these reactions can greatly affect overall membrane properties.

Different characteristics in PES/PVP membranes ageing in contact with hypochlorite at pH 8.0 were assessed by [70,71]. Both studies observed PVP dislodgement and degradation, which resulted in an increase in pore size. In Hanafi et al. (2016), the authors aged membranes by single soaking and showed that membrane surface was more negatively charged with ageing as a result of a slight increase in oxygen atoms due to ring opening of PVP and formation of carboxylic acid and carboxylate groups ($COOH/COO^-$) [75]. With the PVP dislodgement, they expected a decline in hydrophilicity, however contact angle measurements remained constant after ageing, possibly due to the partial ionization of the membrane surface previously explained that counterbalances the loss in hydrophilic agent in the overall hydrophilicity of the surface. These modifications contributed to the loss of permeability after filtration of a dextran solution, which evolved from 12% to 45% for pristine and 144 h aged membranes (200 ppm chlorine), respectively. Authors attributed this decline to the loss of membrane hydrophilicity, which favored its fouling, and to structural modifications of membrane.

In Causserand et al. (2015), the authors investigated the impact of different ageing conditions and procedures for PES/PVP membranes applied to the drinking water industry in contact with NaOCl solutions. The parameters investigated were NaOCl concentration, soaking duration and the exposure mode, i.e. static by soaking, under stirring and dynamic by filtration/backwashing cycles of NaOCl solution [70]. Similarly to others studies, the authors observed an increase in permeability, which correlated well with the PVP content decline as membranes are exposed to NaOCl. Regarding concentration and exposure duration, authors reported that NaOCl concentration contributed the most for the membrane degradation, monitored via the elongation at break and PVP degradation. This implies that, for a same exposure dose, results may vary if concentrations or exposure time (t) are different, therefore, a correction factor (n) was proposed in the calculation of the exposure dose, resulting in Eq. 12. Since exposure time contributed the least, “n” was found to be usually below 1.0. Regarding exposure mode, static or dynamic, aged

membranes exhibited a similar increase in permeability. However, the dynamic exposure by filtration and backwashing of NaOCl solution promoted a slightly greater degradation of PVP and decline in elongation at break. It is worth noting that authors considered that the number of experiments carried out with filtration/backwashing cycles was not enough to conclude an effect of these exposure modes on membrane ageing.

$$\text{Exposure dose} = [\text{Total free chlorine}] \times t^{n} \qquad \text{Eq. 12}$$

In PVDF membranes with hydrophilic additive, Marbelia et al. (2019) observed the same effect of pore enlargement and increasing water permeability as the hydrophilic agent leached out [76]. Contrastively, Ravereau et al. (2016) found a slight decrease in pore size for PVDF/PVP membranes. This study compared PVDF membranes with and without PVP exposed to hypochlorite at several pH (6 – 11.5) [17]. The authors observed PVP degradation regardless the pH of exposure. Concerning the decline in pore size, they hypothesized that this structure modification is linked to the presence of additive but the mechanism is yet to be established. Besides, in the same study, the authors found that the presence of PVP changed the way that PVDF reacted with hypochlorite. These results will be further discussed in the next section along with ageing of PVDF-based membranes.

5.3. POLYVINYLIDENE DIFLUORIDE-BASED MEMBRANES

PVDF is the market leader for membranes applied on wastewater treatment [77]. Its tolerance to chlorine is the primary reason that this material is often chosen for full-scale applications [66]. Although this polymer is resistant to chlorine, several studies have demonstrated changes on physical/chemical structure and filtration performance for these types of membranes in contact with NaOCl [8].

The results of 24 scientific papers about ageing of PVDF membranes will be discussed in this section regarding membrane characteristics and ageing methods. Among these studies, 16 of

them assess ageing by soaking membranes in hypochlorite solutions to simulate exposure. Only four of them aged membranes by cycles of filtration of model solutions and cleaning with hypochlorite solutions [16,23,25,78]. The other four studies evaluated different aspects of ageing in membranes from either pilot or full-scale operation [6,26,35,79]. Firstly, results from the 20 scientific papers that used artificially aged membranes (by soaking or filtration cycles at lab scale) will be discussed, interestingly only three of those papers aged supported membranes, which are often used in wastewater treatment plants.

5.3.1. PHYSICAL AND STRUCTURAL PROPERTIES

Regarding physical properties, PVDF membranes tend to decrease their elongation at break and tensile strength with NaOCl contact (40,42,59–61). However, Ravereau et al. (2016) obtained little or no impact of NaOCl on mechanical properties for non-supported PVDF membranes either with or without hydrophilic agent at pH ranging from 6.0 to 11.5 [17]. Li et al. (2021) aged non-supported PVDF membranes in NaOCl solutions ranging from pH 3 to 11 and only observed weakening of fibers at pH 11 [13]. This decline in tensile strength was comparable to the weakening of membranes exposed to NaOH at pH 11, which is known to cause defluorination in the PVDF matrix [80]. Thus, they attributed this effect to defluorination of PVDF molecules rather than any changes in additives. Both studies aged their membranes at similar NaOCl concentrations (4000 and 5000 ppm, respectively), but Li et al. (2021) used NaOH to adjust pH at 11 in their research, whereas Ravereau et al. (2016) only mentioned the use of NaOCl [13,17].

Regarding MBR applications, hollow-fibers are reinforced with other polymers to withstand the high shear-stress conditions, i.e. supported membranes. Thus, the mechanical resistance of these membranes is less related to PVDF properties and is expected not to change under chlorine exposure. However, Wang et al. (2018) characterized NaOCl aged membranes reinforced with a PET nonwoven fabric and found a slight decline of 10% in ultimate tensile

strength [20]. With only one study dealing with reinforced fibers, there is a clear lack of investigation on these type of membranes.

Under the range of physical characteristics, roughness of membrane surface was evaluated by three studies [11,12,20]. All of them remarked rougher membranes as they aged, which could facilitate adsorption of foulants onto surface.

The most controversial parameter among the physical/structural aspects of membranes is the evolution of pore size with ageing. This parameter was evaluated in 11 publications. In 6 researches, pore size tends to increase, most likely due to the degradation of additives, leading to the appearance of bigger pores. Contrastively, Li et al. (2021) obtained no changes in pore size in SEM images, although, a degradation of additives was observed [13]. Only one study presented a decline of pore size [17]. Authors hypothesized that changes in porosity involve modifications at a dimension scale not directly linked to molar mass of PVDF or additive degradation. They speculated an indirect mechanism between change in porosity and degradation of the additive that is yet to be established. In the same study, no changes in pore size were observed for PVDF membranes without additive. Puspitasari et al. (2010) and Levitsky et al. (2011) obtained contrastive tendencies for this parameter [12,14]. The first observed by capillary flow porometer smaller pores at first, followed by higher pores as exposure doses increased. The authors linked the initial decrease of pore size to the additive leach out, which produced smaller pores and decreased mean pore size on the membrane structure, but as exposure increased, more additive was degraded and bigger pores were formed [14]. The later found an increase followed by decrease of mean pore size by challenge tests using PEG and Dextran solutions. They discussed that these tests do not exclude the contribution of membrane hydrophobicity, which could be misleading these conclusions [12].

Some differences might be influencing these contrastive conclusions:

i) **Ageing conditions variability**: the values of NaOCl concentration, pH and temperature was not always mentioned, and the range of dose studied varied (from 5,000 – 120,000 ppm.h to 1.680,000 – 3,528,000 ppm.h). Some studies exposed the membranes to NaOH in combination to NaOCl, or used acids to control pH.

ii) **Analytical method**: pore size was determined in some studies by SEM imagery, which is sensible to the analyzed zone and topography. Solute transport tests were also used, which are influenced by chemical interactions between solutes and membrane surface. Additionally, capillary flow porometry and nitrogen adsorption methods were employed, in which measure of small pores sizes can be challenging since these technics apply high pressures which can be detrimental to membrane structure;

iii) **Membrane type**: even though these studies used PVDF-based membranes, they are often from different manufacturers. This means that production method and compositions may vary, affecting the overall changes as membranes age.

5.3.2. CHEMICAL PROPERTIES

Membrane chemical properties are assessed by interpretation of ATR-FTIR spectra in most of the times. To follow the hydrophilic agent degradation, authors usually refer to peaks appearing at 1660 – 1675 cm^{-1} attributed to amide bond of PVP, for example, and peaks appearing at 1730 – 1750 cm^{-1} assigned to carbonyl bond originated from both PEG and PVP as examples [70,73]. By following the evolution of bands at the range of 760 – 1403 cm^{-1} alterations in PVDF fingerprint can be identified. Moreover, dehydrofluorination can be indicated by the presence of peaks at a range of 1590 – 1650 cm^{-1} ascribed to carbon double bond and 2100 cm^{-1}, which represents carbon triple bond [16]. Table 1.3 presents recurrent bands followed by ATR-FTIR

spectra for the ageing of PVDF/PVP membranes. Besides ATR-FTIR, XPS and thermogravimetric analysis are widely used to determine hydrophilic agent and PVDF degradations.

Table 1.3: Characteristic peaks in an ATR-FTIR spectra, evaluated in PVDF/PVP membrane ageing studies.

Group	Characteristic band	Reference
C-F (PVDF)	3025; 1200; 471	[76]
PVDF α-phase	762; 796; 875; 974; 1070; 1181	[14,16]
PVDF β-phase	841; 1274; 1403	[14,16]
C=C (Dehydrofluorination)	1590 – 1650	[16]
C≡C (Dehydrofluorination)	2100	[16]
C=O (Hydrophilic agent)	1670 - 1800	[16,76]
C-O (PVP amide)	1663; 1674	[70,73,81]
Succinimide (Degradation product from PVP)	1700/1770	[81]
Secondary amide	1540	[81]
Carboxilic acid	1730/1720	[82]
Carboxylate ($-COO^-$)	1590	[13,82]

For all the studies that followed the evolution of hydrophilic agent content, a decline was observed after extensive exposition to hypochlorite. Depending on pH, the PVP degradation rate and degradation products would change. Li et al. (2021) aged PVDF/PVP membranes for 500,000 ppm.h at pH from 3 to 11 and found higher PVP degradation in the pH zone of 7.0 – 9.0 [13]. At pH > 9.0, PVP underwent ring opening, forming carboxylic acids, whereas at lower pH, the formation of succinimide was preferred.

Ren et al. (2021) exposed membranes to 200 ppm NaOCl at pH 11 at doses ranging from 4,800 to 96,000 ppm.h and obtained PVP degradation, but no changes in the PVDF fingerprint were observed [18]. At higher doses (240,000 – 1,920,000 ppm.h), Gao et al. (2016) found the complete elimination of the hydrophilic agent after 480,000 ppm.h (1665 cm^{-1}), whereas C-F peak (1000-1100 cm^{-1}) at first increased, but after the total departure of PVP, this peak

decreased [24]. The first increase was assigned to internal crosslinking among PVDF structure, which was possible as PVP leached out. After 480,000 ppm.h, authors hypothesized that defluorination and oxygenation reaction due to high pH could be the reason to C-F peak decline as already seen for sodium hydroxide exposure. Indeed, these results were supported by thermogravimetric analysis. Complementarily, Li et al. (2021) aged membranes for 500,000 ppm.h at different pH and only observed defluorination at pH 11 [13]. Thus, it seems that for chlorine exposure lower than around 500,000 ppm.h PVDF molecules are stable, but these membranes undergo defluorination at higher doses and pH> 9.0.

Another widely discussed chemical parameter is membrane hydrophobicity, usually determined by contact angle measurements. As already seen, with the hydrophilic agent degradation, membranes are expected to become more hydrophobic (increasing contact angle), this is true for seven out of eleven studies using hydrophilised membranes. Among the other four, Vanysacker et al. (2014) found no changes in contact angle measured on aged membranes for 300,000 ppm.h [19]. Hajibabania et al. (2012) attributed the decreasing contact angle they observed to the impact of roughness and pore size on the analytical method [23]. Puspitasari et al. (2010) and Zhang et al. (2017) obtained increasing contact angle at first, followed by a decline (19, 65). The first attributed this decline to partial ionization of membrane surface analogously to PES aged membrane, whereas the later assigned it to the presence of carbonyl on membrane surface confirmed by XPS. These groups are originated from the defluorination process of PVDF that forms firstly carbon double bonds, then carbonyl groups as presented in *Figure 1.12*.

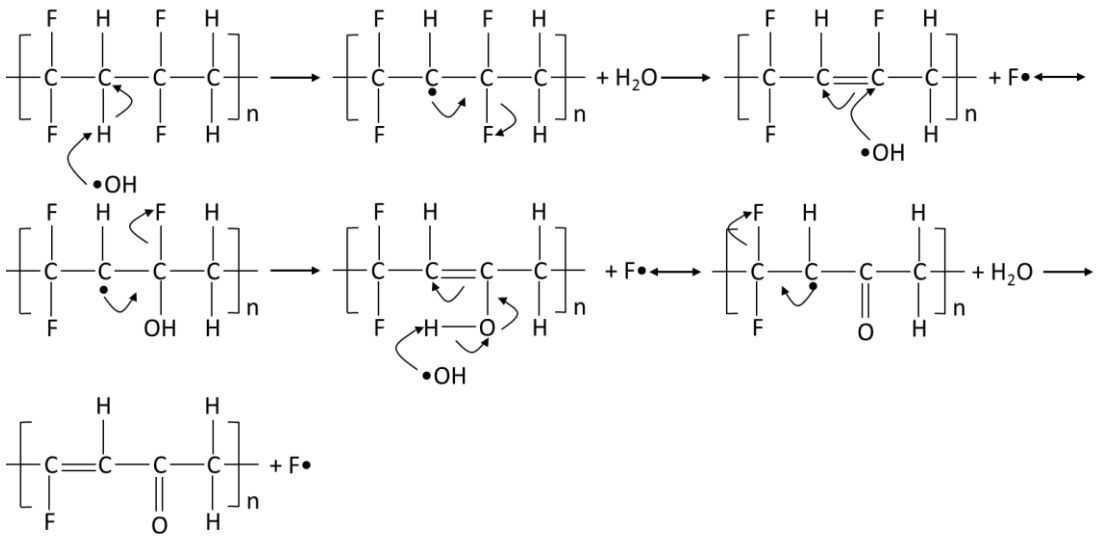

Figure 1.12: Defluorination mechanism of PVDF in alkali condition Based on *[80]*.

Additionally, Gao et al. (2017) used the extended Derjaguin-Landau-Verwery-Overbeek (XDLVO) theory to quantify surface energy of PVDF membranes aged with NaOCl from 240,000 ppm.h up to 1,920,000 ppm.h [11]. According to this theory, the total interaction energy in an interface is the sum of Van der Waals, Lewis acid-base and electrostatic double layer energies. These energies are determined by contact angle measurements with probe liquids of known surface tension. Authors found that aged membranes presented more apolar characteristics and high electron donor components. The sum of Van der Waals and acid-base interactions when a solid is immersed in water provides a quantitative information about the hydrophilicity/hydrophobicity of the given surface. In this case, membranes became more hydrophobic as they aged due to hydrophilic agent degradation. Nevertheless, after 576,000 ppm.h, membranes presented a decline in hydrophobicity, that authors ascribed to defluorination and oxygenation of PVDF.

Besides these reactions in the PVDF molecules, crosslinking and chain scission are often part of discussion in ageing of PVDF membranes, but they are hardly ever directly assessed. Ravereau et al. (2016) dissolved aged membranes and analyzed obtained samples by SEC [17].

Authors observed the predominance of chain scissions over crosslinking for membranes with or without hydrophilic agent and aged at pH of 6.0 and 7.5. Furthermore, the presence of additive significantly favored chain scission. For higher pH (11.5), chain scissions were less extensively favored. The authors speculated that non-random reactions can be superposing the random ones, thus selective attack of short chains might be changing macromolecular structure of these membranes [17].

A fewer studies evaluated the effects of NaOCl on the electrical charges of PVDF membranes by zeta potential [11,13]. For membranes aged at pH 7.5, Gao et al. (2017) firstly found an increase in negative charge on aged membranes at 240,000 ppm.h due to the ionization of weak acids formed from the ring opening of PVP molecules. Then these charges are reduced at 576,000 ppm.h probably due to the elimination of these PVP degradation products. Finally, after 960,000 ppm.h negative charge increased again, which was probably related to dehydrofluorination and oxygenation with formation of carbonyl and carboxylate groups in PVDF molecules [11]. Li et al. (2021) exposed PVDF membranes to 500;000 ppm.h of NaOCl at pH ranging from 3 to 11 using HCl or NaOH for adjustment [13]. Ageing increased the negatively charged character of these membranes for all tested pH. At higher pH (9 and 11), this increase was higher and authors attributed this result to the formation of carboxylic groups from the opening of PVP ring.

Therefore, ageing seemed to increase membrane hydrophobicity because of PVP degradation. Additionally, membranes are likely to become more negatively charged, especially at higher pH and higher doses due to PVP ring opening and defluorination and oxygenation of PVDF. These changes along with membrane structural changes will highly interfere in filtration properties. These changes are reviewed in the following section.

5.3.3. FILTRATION PERFORMANCES

Besides understanding physical/chemical characteristics of membranes in ageing studies, they are also tested for their filtration parameters, aiming to understand the way ageing could affect membranes performance on operating conditions.

The most frequent parameter assessed is pure water flux or permeability, i.e. fifteen studies presented results on this topic. Even if the pure water permeability of MF/UF membranes is expected to be impacted by membrane degradation, its monitoring in the frame of membrane ageing studies is quite tricky. Indeed, this parameter is simultaneously modified by (i) the decrease in hydrophilicity due to the additive degradation, (ii) the increase in hydrophilicity due to partial material ionization and (iii) the increase in porosity due to pore enlargement following hydrophilic agent dislodgment.

Water permeability tends to grow with ageing in most of the works as a result of pore enlargement ~~or higher hydrophilicity~~ for doses ranging from 7,000 – 2,000,000 ppm.h at different pHs [13,18,20,22,23,25,63,78]. In addition, Wang et al. (2018) observed a connection between the permeability increase and the pore enlargement due to PVDF chain breakage as a result of dehydrofluorination in alkali conditions [20]. Ren et al. (2021) found a greater correlation between water permeability and the maximum pore size for membranes aged up to 960,000 ppm.h at pH 11 [18], while the correlations are poorer with the mean pore size and hydrophilicity. This suggests that the formation of macro voids is the dominant factor on permeability increase. Conversely, Vanysacker et al. (2014) and Ravereau et al. (2016) obtained no changes or a slight decrease in water permeability, which remained of the order of experimental errors, for PVDF membranes with and without hydrophilic additive [17,19]. Vanysacker et al. (2014) exposed membranes up to 336,000 ppm.h of NaOCl and Ravereau et al. (2016) exposed membranes up to 12,960,000 ppm.h at pH 6 – 11.5. Puspitasari et al. (2010) and Wu et al. (2018) found a decline followed by an increase of permeability for extensively

aged membranes (over 1,200,000 ppm.h) [14,21]. Puspitasari et al. (2010) correlated this behavior mainly to a decrease in hydrophilicity because of hydrophilic agent degradation, and then membrane surface experienced partial ionization increasing hydrophilicity [14]. Whereas, Wu et al. (2018) also stated that the decline in hydrophilicity was responsible to the decline in permeability, but the following increase was due to pore enlargement linked to hydrophilic agent degradation [21].

Filtration with pure water is unavoidable to characterize the effect of membrane structure evolution on filtration capability but this parameter is far from real conditions applied on these membranes, that is the reason some studies evaluate filtration of activated sludge or model solutions simulating foulants from full-scale process. To evaluate filtration performance of membranes under real conditions, the critical flux is one of the important parameters. Critical flux concept was firstly defined as the flux below which a decline of flux with time does not occur; above it fouling is observed [83]. With a methodology point of view, different protocols can be followed to determine this parameter. Robles et al. (2012) focused on MBR membranes [84], the filtration is performed at a defined flux for a certain duration before physical cleaning and then increased by a constant flux-step size, TMP evolution is followed, the critical flux can be defined as the threshold flux which TMP build up exponentially. Wang et al. (2018) arbitrarily defined critical flux when TMP increased above 0.3 kPa within 15 min of filtration of activated sludge (HRT 4h; SRT 30 d; MLSS 6 g/L) [20]. They observed that critical flux decreased slowly as membranes aged and they assigned this behavior to increasing hydrophobicity and roughness, and more electron acceptor components on membrane surface, which was defined by the XDLVO theory in their work. Unlike the concept of critical flux, Abdullah and Bérubé (2018) evaluated the filtration capacity of their membranes as being the filtered volume (HRT 10 h; SRT 12d; MLSS 4 g/L; at 25 LMH) before permeability decreased by 10% [9]. A slight decline in filtration capacity was observed for membranes exposed up to

1,000,000 ppm.h of sodium hypochlorite (≈ 18% of decrease) but for samples exposed to 2,000,000 ppm.h, filtration capacity sharply fell from 5,600 $L.m^{-2}$ (pristine membranes) to values as low as 600 $L.m^{-2}$.

All these different parameters can give information about the fouling propensity of membranes over ageing. The majority of studies that evaluated fouling propensity found increasing trends for higher doses which means that as they age, membranes become more likely to interact with foulants, decreasing cleaning efficiency and increasing the down time of installations for maintenance [9,12,20,22–24]. Moreover, Vanysacker et al. (2014) found that membrane ageing not only increased protein-fouling fraction in EPS, but also influenced EPS production in biofoulant in the three filtration cases, namely, monospecies feed (*P. aeruginosa* culture) or duospecies (*P. aeruginosa* + *E. coli* culture) or spiked activated sludge (*P. aeruginosa* + activated sludge) [19]. Authors suggested the growth behavior or metabolism of these species on the surface of aged membranes were changed in comparison to pristine ones, since cell density was not affected by membrane aging.

Instead of filtering real activated sludge, a way to decrease variability to assess these interactions is to filter specific compounds that mimic components present in raw wastewater or activated sludge. Specific interactions between membrane surface and these compounds and retention of these last as membranes age are then evaluated. The most tested compounds in these situations are BSA, humic acids, sodium alginate, polysaccharides, bacteria, such as *Escherichia coli*, and viruses.

Eight publications tested filtration performance and retention of aged membranes to some of these compounds. Hajibabania et al. (2012) filtered a model solution composed of 20 $mg.L^{-1}$ humic acid sodium salt, 10 $mg.L^{-1}$ alginic acid sodium salt and 10 $mg.L^{-1}$ BSA and observed a decrease in retention analyzing permeate by TOC [23]. They attributed this effect to possible pore enlargement or changes in membrane surface, accordingly to Li et al. (2021) [13].

Interestingly, they observed that this decline in retention was less extensive when they aged membranes by filtration/cleaning cycles of model solution and sodium hypochlorite solution than when membranes were only soaked in the reactive agent at the same doses.

Gao et al. (2017) also filtered these compounds with aged PVDF membranes and decomposed interactions between these foulants and membranes [11]. They observed that interactions between foulants and membranes were largely determined by hydrophilicity and electrical charges. New membranes were apolar and presented higher electron donor characteristics and negative charges resulting, globally, in a hydrophobic material. Because of this high hydrophobicity, membranes were repulsive to humic acid, the only hydrophilic foulant, causing low fouling potential. Regarding BSA and sodium alginate, they both presented hydrophobic interactions with membranes, but due to the high electron donor character, they were more repulsive to sodium alginate and more attractive for BSA. When these foulants were mixed, BSA acted as a bridge interacting directly with membrane surface and improving sodium alginate fouling. All aged membranes presented a hydrophobicity even higher than the pristine one, having higher interactions with foulants, but at 960,000 ppm.h hydrophobicity started to slightly decrease, decreasing also fouling propensity. Authors argued that these changes are due to a decline in the C-F peak and the appearance of a carbonyl peak. They associated these changes to the formation of sodium carboxylate between the PVDF and NaOCl in these aged membranes [11].

Wu et al. (2018) confirmed the decline in retention with ageing for raw water instead of model solutions as the case for Gao et al. (2017) [11,21]. Moreover, they observed that pristine membranes present higher hydrophilicity, increasing repulsion between membrane-foulants. This promotes the formation of a cake layer denser than membrane pore structure. As membranes aged, hydrophilicity decreased and foulants are able to flow through the pores, decreasing retention.

Three other studies tested rejection of BSA by aged membranes (43, 63, 64). Levitsky et al. (2011) observed that membranes became more hydrophilic with ageing and BSA retention increased, although pore size increased. These changes in pore size did not correlate to BSA retention. Thus they proposed that hydrophilicity is governing BSA retention by adsorption, since BSA is often used as model of hydrophilic protein [12]. These results were corroborated by Zhang et al. (2017) more recently, indeed they proposed that electrostatic repulsion is probably another reason for the increased BSA retention, since membranes became more negatively charged as they aged and BSA is negatively charged in aqueous solutions at neutral pH [22]. On the other hand, Rabuni et al. (2015) obtained poorer BSA retention within aged membranes of bigger pores [16]. Thus, they proposed that BSA retention was not only governed by membrane hydrophilicity, but size exclusion mechanism might have an effect on protein filtration.

Retention of polysaccharides is expected to follow a different path from that of proteins. Polysaccharides, such as dextran, are often uncharged, thus a separation governed by size exclusion mechanism is expected [81]. However, since Zhang et al. (2017) obtained higher retention and hydrophilicity as membranes aged, they proposed that a hydration layer would tightly bound to the membrane surface as its hydrophilicity increased, which could prevent dextran to pass through the membrane even if pore size increase during ageing [22]. Contrarily, Ren et al. (2021) observed a decrease in hydrophilicity aging PVDF membranes. They tested aged membranes for polymer flooding, which are effluents rich in polymers that promote a much quicker fouling. In this environment, authors found that aged membranes presented greater flux decline during filtration and this loss was more related to irreversible fouling rather than physically reversible fouling. They stated that the increase in hydrophobicity increased interactions between membrane surface and polymers present in their effluent [18].

5.3.4. SYNTHESIS OF CHANGES IN PVDF MEMBRANE PROPERTIES DUE TO AGEING

Table 1.4 presents the major changes in membrane properties found in PVDF membrane ageing studies during exposure to hypochlorite. All studies that analyzed additives content observed a decline, mainly due to the high reactivity of these agents in alkali conditions or with chlorine radicals. Hydrophilic agents are oxidized and can form secondary products or be dislodged from membrane structure generating mostly an increase in hydrophobicity, but other changes were not rare. This may lead to pore enlargement, which caused intrinsic water permeability to increase in most cases, but the combined effect of simultaneous increase in hydrophobicity and pore size in some studies have led to different conclusions. These two properties presented the most controversial results, partly due to a lack of reliable analytical method.

Mechanical properties were often tested and changes in the ultimate tensile strength are highlighted in this table. The most part of the studies observed decreasing ultimate tensile strength as membranes aged, however, two studies did not observe changes in this property. Between these two studies, Ravereau et al. (2016) observed stable ultimate tensile strength for non-supported membranes without hydrophilic agents, whereas a decline was observed for membranes presenting these agents [17]. In the second study, Ren et al. (2021) used supported membranes with PET, which explains the higher resistance and stability over chlorine exposure [18]. However, Wang et al. (2018), using similar membranes and ageing conditions than Ren et al., claimed to have observed a decline in ultimate tensile strength of these supported membranes [20]. Actually both studies observed variations of less than 10%, however these variations were within experimental error for Ren et al. (2021), but not for Wang et al. (2018) [18,20].

The chemical resistance of PVDF against NaOCl was observed in several studies, three of them observed stable PVDF fingerprint as membranes aged whereas ten observed signs of

degradation. Ravereau et al. (2016) reported higher degradation rates at acidified conditions of NaOCl solutions (6.0 < pH < 7.5) than for solutions at pH of 11.5 [17]. Furthermore, the presence of hydrophilic agent favored PVDF chain scission. The differences observed in PVDF fingerprint changes may not only come from ageing conditions or membrane compositions, but also from analytical methods employed to characterize this polymer. For instance, Gao et al. (2017) suggested PVDF degradation based on changes in zeta potential results, whereas Ren et al. (2021) claimed PVDF stability applying ATR-FTIR and XPS measurements [11,18]. In addition, Ravereau et al. (2016) observe low variations in PVDF matrix in ATR-FTIR results that they confirmed thanks to a thoroughly characterization based on nuclear magnetic resonance, size exclusion chromatography and differential scanning calorimetry [17].

Rejection and fouling propensity to specific molecules were also controversial among these researches. When facing foulants, aged membranes mostly increased their fouling propensity due to increasing roughness or hydrophobicity, with higher interactions towards proteins. These increasing interactions resulted in some cases increasing retentions due to adsorption on membrane surface and formation of a denser cake layer, but in some studies pore enlargement allowed more molecules to flow through membranes, decreasing retention.

These papers evaluated ageing of PVDF membranes by either i) soaking in NaOCl solutions or ii) cycles of filtration/cleaning with foulants and chemicals, respectively. These conditions are far from the real conditions that these membranes are operated. Four other publications directly assessed the concept of ageing in membranes operating at full or pilot scale and these results are presented in the following section.

Table 1.4: Results of studies on PVDF ageing in contact with hypochlorite from scientific literature.

Ageing effects	Membrane properties							
	HA Content	**Ultimate Tensile strength**	**PVDF fingerprint**	**Rejection**	**Fouling propensity**	**Permeability**	**Hydrophobicity**	**Pore size**
+ (increase)				[12,17,21,22]	[9,11,12,18,20, 22–26]	[11–13,18,20,22,23,25,63,78]	[10,13,16–18,20,21,24,25]	[14,16,18,20,21,23–25,78,80]
= (stable)		[17,18]	[17–19,21]		[19]	[17]	[19]	[13,17]
- (decrease)	[10,13,14, 16–18,20,21,23–26,80]	[10,13,16,17, 20,21,23,26,78]	[11,13,16,17,20,22,24,78,80]	[11,13,16,23]		[9,14,21,26]	[12,14,17,22,23,63,78]	[12,17]

The last review about PVDF membrane ageing was performed in 2016 [8]. Since then, one of the major findings was the effect of ageing on membrane surface electrical charges. Gao et al. (2017) and Li et al. (2021) reported that membranes become more negatively charged with ageing [11,13]. Moreover, the first study reporting results of membrane ageing in full-scale installations was published, which confirmed the degradation of hydrophilic agent at the chemical level, but highlighted differences in permeability and fouling propensity behavior with ageing compared to accelerated ageing [26].

5.3.5. MEMBRANE AGEING UNDER OPERATING CONDITIONS

Ageing in pilot or full-scale operating conditions was investigated by a few studies, mainly for the drinking water industry.

Despite Childress et al. (2005) didn't study ageing, they investigated the evolution of integrity of four different hollow fiber membranes under pilot scale operation (Asymmetric: PSU, and polyacrilonitrile – PAN; symmetric: PP, and PVDF) [85]. These four membranes were operated over a 10-month period in a drinking water plant and physical integrity was evaluated by the probability of trace occurrence of total and fecal coliforms in permeate. The symmetric membranes presented nearly total removal, whereas probability of measuring total coliforms reached 50 and 90% for asymmetric PAN and PS membranes. Authors concluded that symmetric fibers were less prone to failure; however, no tests with asymmetric and symmetric fibers of same material were analyzed. Interestingly, they modeled the loads on the structure of membranes and potting juncture due to fluid flow by Automatic Dynamic Incremental Non-linear Analysis (ADINA) using finite element analysis (FEA). With these results, they observed that water hits the interface between membrane and potting structure adding extra stress at the juncture that may lead to fractures over time. Although they simulated fluid as water, this

analysis provided insights on the importance of the potting material for real operations and not only the membranes themselves.

In another study at pilot-scale with membranes filtering real municipal wastewater, Marbelia et al. (2019) evaluated accelerated fouling filtration of hollow fiber PVDF/PVP membranes in a magnetically induced membrane vibration system [76]. In accelerated fouling filtration, i.e. operating at higher filtration fluxes and more frequent backwashing with NaOCl, they obtained unexpected results. Instead of a systemic decline in permeability after each cycle of filtration and cleaning due to irreversible fouling, permeability actually increased reaching up to 300% of its initial. They attributed this behavior to the leaching of PVP, which promoted increasing membrane porosity, however when membranes were merely soaked in NaOCl solutions, release of PVP occurred much slowly. Thus, they proposed that during a short exposure to NaOCl, long chains of PVP undergo chain scission turning into smaller ones that require a convective flow to be released in the bulk.

Regarding full-scale studies, Yu et al. (2020) evaluated the performance of PVC membranes operated for 7 years in an ultrafiltration drinking water treatment plant. Over this period, flux declined from 28.4 to 16.5 LMH due to increasing frequency of cleaning approaches. In addition, costs increased by 55% mostly related to increasing TMP (energy), waste water related to backwashing and chemicals. Besides, membrane fouling was also increased over the long-term as cations, metabolites and organic matter in the cake layer increased [27].

Focusing on membrane ageing, Robinson and Bérubé (2021) studied the changes in PVDF membrane properties in drinking water facilities. For the first five years, the properties of the membranes remains stable. After 5 years, mechanical resistance started to decrease, along with increasing clean membrane resistance (or decrease in intrinsic permeability) and fouling rate. These changes were related to the decline in hydrophilic agent concentration. Authors stated that for samples that were more exposed to hypochlorite, these indicators changed faster and

limiting chlorine exposure was advised. Additionally, clean membrane resistance (or intrinsic permeability) measurements seemed to be a good benchmark in determining the state of membranes during operation [26].

Regarding full-scale MBR operation, van Bentem et al. (2010) summarized five years of operational experience in the first MBR from Netherlands [35]. The MBR was equipped with Zenon ZW500d modules, composed of supported PVDF hollow fiber membranes. By looking at changes of permeability index (ratio of flux and TMP during mixed liquor filtration) over the 5 years operation at logarithmic scale, they concluded that permeability remained high, but a decline was observed as a slow but steady process. These data highlight the importance of developing and/or adapting characterization techniques to monitor membranes physical/chemical properties at full-scale.

In contrary, Fenu et al. (2012) stated that the increase in operating pressure (decrease in permeability) is the main end-of-life trigger for membrane replacement [6]. They evaluated membrane life-time concept by five different ways: (i) maintaining permeate flow throughput, (ii) permeability index decline, (iii) oxidative aging, (iv) increase in energy costs and (v) mechanical ageing. Firstly, they found that maintaining permeate flow throughput is detrimental as an end-life trigger, because seasonal changes, such as temperature and fouling propensity of the matrix, can mislead to a premature replacement. A decline in permeability index was assessed by looking (i) at top permeability points as a result of successful cleaning; these points provide information about irreversible fouling, (ii) and bottom permeability points, which represent the minimum permeability levels that can be reached due to excess TMP operation (Figure 1.13). These two series of points tend to converge at a theoretical lifetime, which was estimated around 10 years also considering hydraulic capacity for the installation studied.

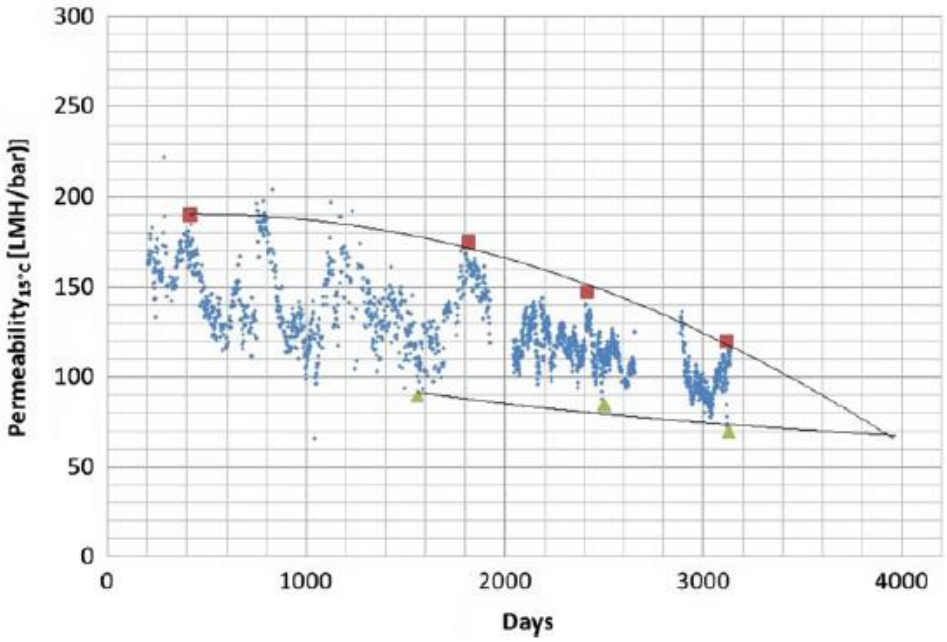

Figure 1.13: Determination of end-point of operation in MBR. Red squares represent maximum permeability index after cleaning and green triangles represent minimum permeability index before cleaning. From: [6].

Regarding chlorine contact, they estimated a life span of 15 – 16 years considering the maximum exposition recommended by the manufacturer of 500,000 ppm.h. As life-time estimated using the permeability decay was shorter than this one, authors considered more convenient to increase frequency of cleaning than excessively foul membranes from an investment cost perspective. With a financial point of view, authors concluded that energy costs could not be considered a trigger for membrane replacement as operations close to the end of life are still economically feasible, even though energy consumption doubled. Finally, a life span concept based on membrane mechanical resistance was not advised, since episodes of increasing turbidity of permeate were related to punctual breakage in potting resin. Reparation and partial substitution of these parts solved the problem. Replacing whole membrane lanes because of punctual breakages would not be economically viable.

The same conclusions about permeability decay were draw by Cote et al. (2012) in a study using the data set of ZeeWeed® membranes shipped across North America in plants bigger than 200 $m^3.d^{-1}$ over 15 years [79]. These data revealed that fiber breakage was never an issue thanks to a resistant support layer that composes these membranes. The frequency of failure of surrounding structures such as connections, pipes and resin decreases with time as these membrane cassettes/modules aged. The origins of these failures were virtually eliminated from the most recent cassettes. Weakening of the potting resin at the juncture was not a concern within the first 12 years of operation, when the advised maximum chlorine exposure (40,000 ppm.h/year) was respected. They concluded that the constant TMP rise and the necessity of more frequent chemical cleanings were the triggers for membrane end of life. Thus, planned replacements were proposed over 2 – 4 years of the entire inventory in sub-sets representing 10 – 25% of the plant membrane surface in a way to avoid operation of aged and new membranes by the same pumping system. By following this methodology, membranes could operate for an average of 10 years.

6. CONCLUSION

Although several studies have been published about ageing of PVDF membranes, many of them are focused in membranes applied in drinking water plants. Knowledge about membrane ageing in MBRs treating urban wastewater is still scarce. From the scientific literature, ageing is highly dependent on operating conditions besides chemicals and materials used. Moreover, the contradictory results from chemical ageing, especially pore size, hydrophobicity and permeability, show that this process is not completely understood and the strategies used to accelerate ageing in lab can mislead those results. The representability of these assays regarding real complex operation was only assessed in drinking water applications and the characterization of membrane ageing in full-scale MBRs with respect to (i) membrane properties and (ii) in-situ filtration performance is still lacking. In MBRs, membranes are loosely attached, filtration cycles are usually shorter, biological activity is higher leading to higher concentrations of foulants and other metabolites that may interact with membranes and alter their ageing.

CHAPTER 2: MATERIAL AND EXPERIMENTAL METHODS

1. INTRODUCTION

This chapter aims to present the membranes studied in the present thesis. Furthermore, ageing procedure at bench-scale is presented. For full-scale ageing, a detailed description of each wastewater treatment plant and their respective membrane bioreactor is provided. Finally, the various methods used to characterize membranes are described.

2. MATERIALS AND AGEING PROCEDURE

2.1. ZEEWEED® MEMBRANES

This study was performed with hollow-fibers harvested from ZeeWeed® 500D modules (SUEZ Water Treatment Solutions, France). These are ultrafiltration membranes with a mean pore size of 0.04 µm. Table 2.1 presents detailed information about these membranes.

Table 2.1: Nominal characteristics of ZeeWeed® membranes provided by the manufacturer.

Reference	ZeeWeed® 500D
Material	PVDF
Type	Supported hollow fiber
Filtration orientation	Outside-inside
Nominal Pore size	0.04 µm
Fiber diameters	1.9 mm Outer/ 0.8 mm Inner
TMP range	-55 to 55 kPa
pH	5.0 – 9.5 (operation) 2.0 – 10.5 (cleaning)
Maximum Temperature	40 °C
Maximum Cl_2 Concentration	1000 ppm

Since their primary application is MBRs in which they encounter important mechanical stresses, these membranes present an internal support to ensure their mechanical resistance. The material of this support is not provided by the membrane manufacturer, but according to the comparison of its infrared spectrum to the ones of species in the HR Nicolet sampler library with OMNIC software (Thermo fischer, USA), the support material signature presented 64% similarity to polyethylene terephthalate (PET) spectrum (Figure 2.1).

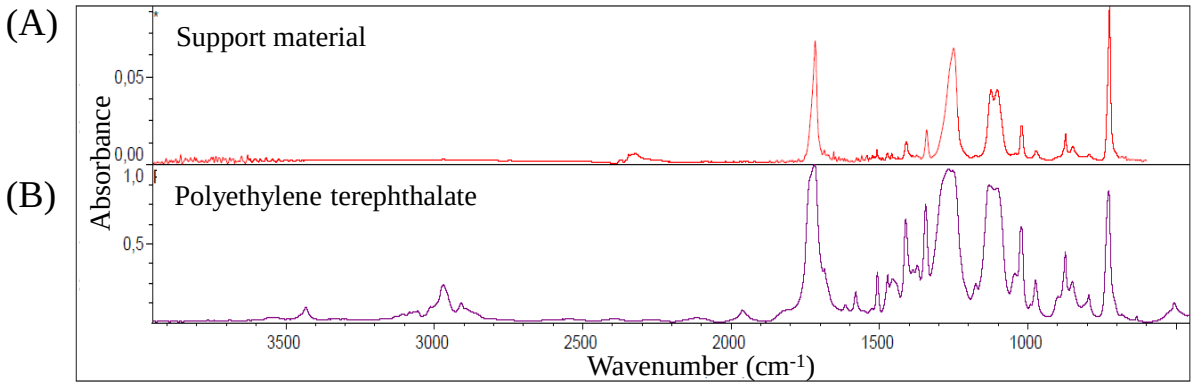

Figure 2.1: Infrared spectra for the ZeeWeed® support membrane material (A) and Polyethylene terephthalate (B) sample from HR Nicolet sampler library extracted from OMNIC software (Thermo fischer, USA).

A skin of polyvinyl difluoride (PVDF) covers the outer surface of this support; this is the main layer responsible for filtration characteristics. Other agents are incorporated to PVDF in the skin to increase hydrophilicity and pore formation. Infra-red analysis suggest polyvinyl pirrolidone (PVP) as a hydrophilic agent in these membranes. An image of these membranes is presented in Figure 2.2.

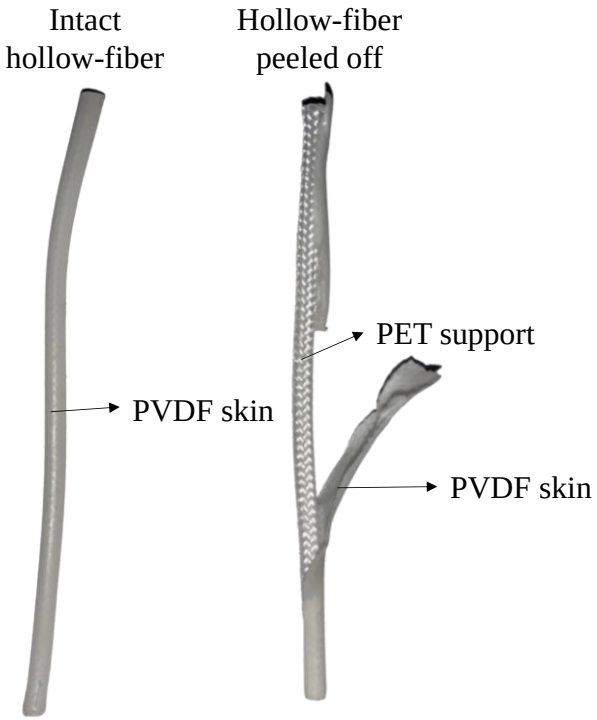

Figure 2.2: Pictures taken of intact ZeeWeed® hollow-fiber (left) and a hollow-fiber peeled off with its PET support material visible (right).

2.2. CHEMICAL AGEING AT BENCH-SCALE

For this study, virgin ZeeWeed® 500D (SUEZ Water Technologies, France) membranes were sampled from virgin ultrafiltration modules produced in 2018 equivalent to those installed in both WWTP considered in the study (Figure 2.3) (cf. section 2.3). Membranes were harvested by cutting in both potted ends, resulting in fibers of around 2.0 m. Membranes were stored in 1 g/L sodium bisulfite solution at room temperature (21 ± 2 °C) before use.

Figure 2.3: ZeeWeed® 500D membrane module.

The chemical cleanings performed in-situ for these membranes include usually acids (citric acid, hydrochloric acids, etc) and bases/oxidants (sodium hydroxide, sodium hypochlorite, etc). PVDF membranes are not sensible to acid exposure as shown elsewhere [13]. Since several researches confirmed changes in PVDF membrane properties after exposure to oxidants and

sodium hypochlorite is the most used in MBR, this study focused on the effects of sodium hypochlorite on these membranes. Hypochlorite solutions used for the bench-scale ageing experiments were obtained by dilution of commercial sodium hypochlorite at 14-wt% (VWR chemicals, USA). In addition, concentrated sulfuric acid (analytical grade 95%, VWR chemicals, USA) used for pH adjustment and sodium bisulfite (Honeywell Research Chemicals, USA) used for membrane storage were of analytical grade. Aqueous solutions were all prepared using pure water from Milli-Q^{TM} equipment (Thermo Fisher Scientific, USA).

After rinsing in a large volume of pure water, laboratory ageing was performed by single soaking the pristine membranes in NaOCl solution at a total free chlorine concentration of 1000 ppm at room temperature. The intensity of ageing is presented as C × t ranging from 0 to 750,000 ppm.h, which is higher than the maximum exposure dose advised by membrane manufacturers (500,000 ppm.h). The volume of fibers did not exceed 1% of the soaking solution volume in order to avoid significant consumption of chlorine. Total chlorine concentration was checked three times a week via silver nitrate titration (Hach, USA). When a deviation of more than 10% from the target concentration was measured, the concentration was corrected by adding NaOCl. Concentrated sulfuric acid was added to adjust the pH to 9.0 that was corrected whenever changes greater than 5% were observed over time. These chlorine concentration and pH are similar to the ones found in cleaning in place (CIP) protocols for MBRs applied to municipal wastewater treatment. These are precisely the conditions applied to the membranes in the MBR from Seine aval WWTP as described in section 2.3. The actual free chlorine concentrations and pH measured during the bench-scale ageing ranged from 950 to 1060 mg Cl/L (ppm) and from 8.98 to 9.09, respectively. Temperature for these expositions was kept at 21 ± 2 °C. Therefore, the conditions were considered very stable.

After harvesting from single soaking expositions, membrane samples were stored in 1 g/L sodium bisulfite at room temperature (21 ± 2 °C) prior characterization.

2.3. FULL-SCALE AGEING

Membranes in the full-scale operation were sampled from the Seine-Morée (SEM) and Seine aval (SAV) WWTP in France (SIAAP). In parallel, data from MBRs installed in both WWTP were collected in order to analyze the evolution of membrane performances. The list of the collected parameters is presented in Table 2.2 and each MBR is presented in details in the following sections.

Table 2.2: Process data collected for both SEM and SAV's MBRs.

Parameter	Units	Frequency
TSS inlet	(mg / L)	Daily
MLSS in recirculation channel	(mg / L)	Daily
COD influent and permeate	(mg O_2 / L)	Daily
BOD_5 influent and permeate	(mg O_2 / L)	Daily
TKN influent and permeate	(mg N / L)	Daily
NH_4 influent and permeate	(mg N / L)	Daily
Total phosphorus (TP) influent and permeate	(mg P / L)	Daily
PO_4^{3-} influent and permeate	(mg P / L)	Daily
Influent flowrate	(m^3 / day)	Averaged from instantaneous data
Recirculation flowrate	(m^3 / day)	Averaged from instantaneous data
Permeate flowrate	(m^3 / day) or (m^3/h)	Averaged from instantaneous data
Permeate temperature	(°C)	Averaged from instantaneous data
pH of influent	-	Averaged from instantaneous data
Supernatant COD in recirculation channel	(g_{O2}/L)	Daily
Aeration flowrate in membranes	(Nm^3 / d~~h~~)	Averaged from instantaneous data
Indicator of sodium hypochlorite maintenance cleaning	-	Daily

2.3.1. SEINE MORÉE WWTP

This facility was commissioned in 2014 and designed to treat up to 50,000 m^3/d wastewater (300,000-population equivalent) from the northern Paris urban area. This WWTP is composed of screening, grit and grease removal in its pretreatment unit, followed by a primary lamellar settler. The biological treatment and post-clarification are performed by MBR (Ultrafor®, Suez, France). Pretreated wastewater is divided equally into three biological basins (total volume of 39,500 m^3) composed of anaerobic, anoxic, and aerated zones. Then, the mixed liquor is sent to eight membrane tanks of 300 m^3 each (SEM-UF1 to SEM-UF8). Each membrane tank contains 10 immerged cassettes composed of ZeeWeed® 500D membrane modules. The total filtering surface of this MBR is 106,000 m^2 (13,250 m^2 per tank). A schematic representation of this WWTP is presented in Figure 2.4. This WWTP was supposed to be coupled with a biogas unit for the sludge treatment, but the project was not approved by all institutions involved. To avoid the high costs and flow of truck evacuation of sludge produced, the WWTP is operated at 30% of its designed capacity. This choice implied a discontinuous way to operate membranes. Due to this choice, the average daily filtration time for each membrane tank was 5.4 ± 1.9 h.

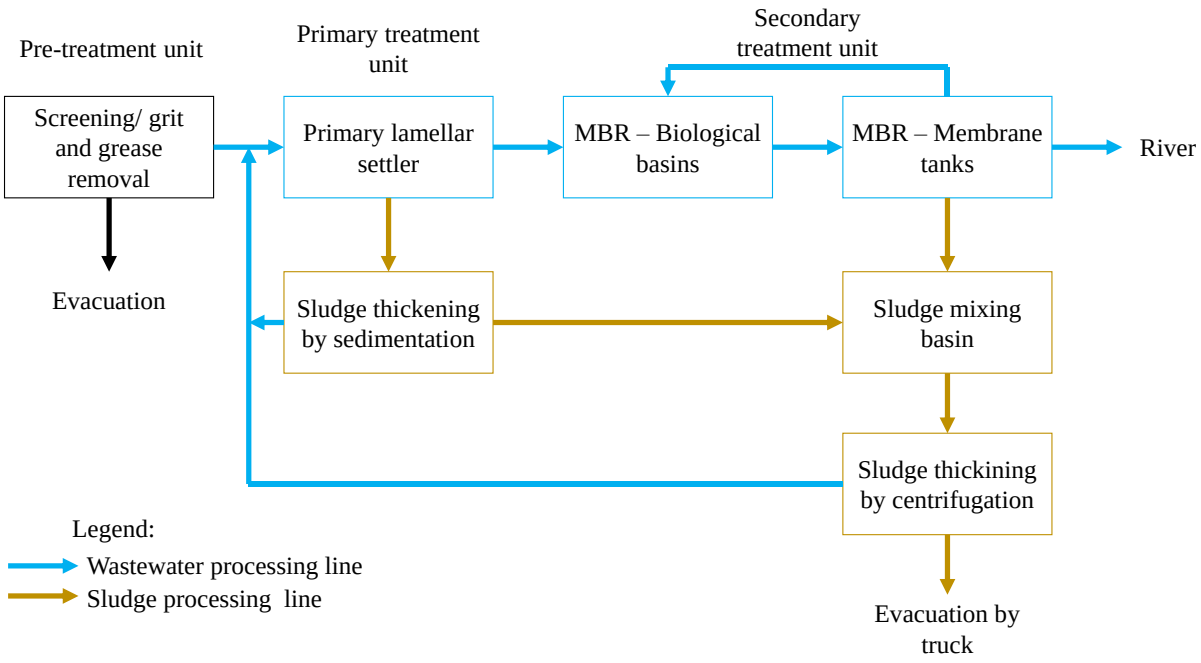

Figure 2.4: Schematic representation of Seine Morée WWTP.

Membranes are operated under coarse bubble aeration during 10-s on/off intervals. Filtration cycles occur for 15 min followed by physical cleaning, i.e., 30 s relaxation and 30 s of backwashing with permeate (25 LMH). Mixed liquor suspended solids concentration (MLSS) is recirculated from the membrane tanks to the biological basin and sludge extraction is performed periodically.

Chemical cleaning events

Chemically enhanced backwashes (CEB) are performed once a week with NaOCl solution (200 ppm) and once every 2 weeks with citric acid solution (1000 ppm). These solutions are injected in 10 cycles of 30 s at 25 LMH and 4.5 min of relaxation. The annual NaOCl exposure dose (C × t) related to CEB is estimated at 500 ppm.h, but since these data only would account for 3% of the annual chlorine exposure and data of their execution were not available, the calculation of the exposure dose of membranes related to CEB are not considered for this MBR.

Cleaning-in-place (CIP) is performed once a year. Ideally, membranes are submerged in a solution of 800 ppm NaOCl, and after rinsing they are then submerged in a solution of citric acid at a pH around 2.7. Each soaking is performed for 20 h with cyclic aeration every hour; giving a theoretical annual NaOCl C × t of 16,000 ppm.h related to CIP protocols. The soaking solution is collected at the beginning of soaking and analyzed in laboratory for chlorine concentration as described in section 2.1.2. In addition, SEM-MBR presented variations in soaking times for each CIP protocol, since the start and end of these protocols are controlled manually (Figure 2.5). Soaking time could vary between 17 h and 28 h for SEM-MBR.

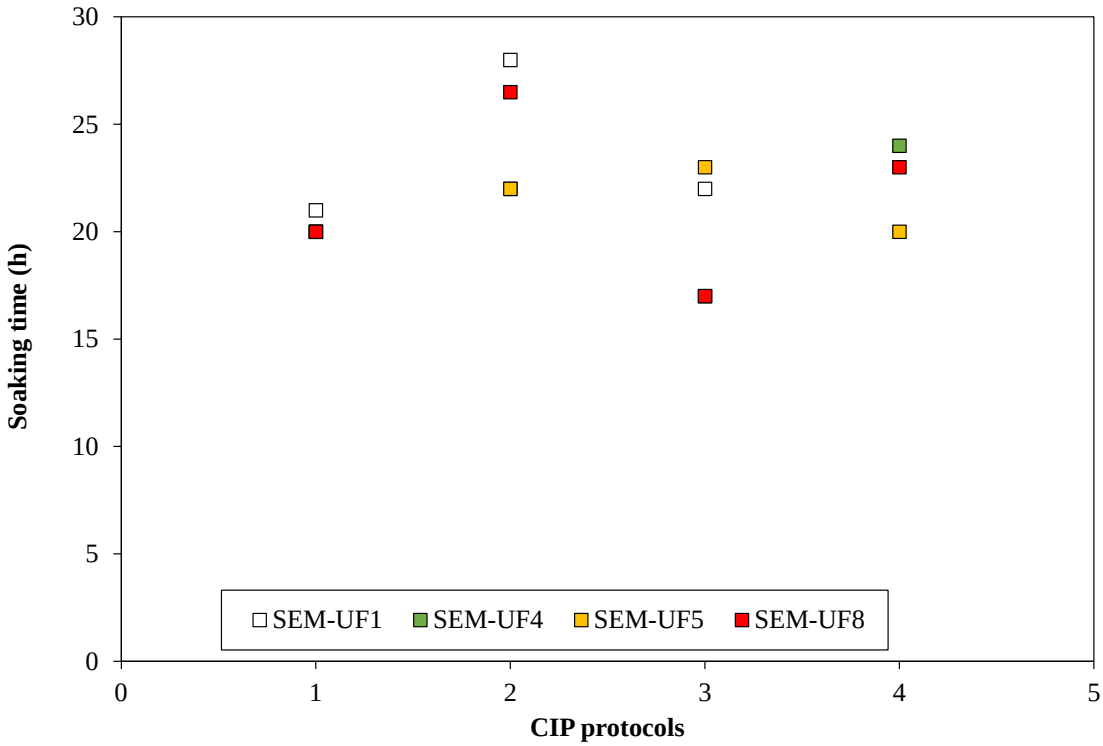

Figure 2.5: Soaking time during CIP protocols for SEM-MBR.

2.3.2. SEINE AVAL'S WWTP

The Seine aval's (SAV) WWTP is the oldest one in Paris region treating wastewater since 1940 with a treatment capacity of 200,000 m^3/d, increasing to 2,100,000 m^3/d by 1980 with a biological treatment, i.e., classic activated sludge, and anaerobic digestion for the produced

sludge. Since then, Paris' wastewater treatment was decentralized and SAV decreased its capacity to 1,500,000 m^3/d. Its pretreatment unit is composed of screening, grit and grease removal. Then, the effluent is sent to primary decantation before biological treatment. Since 2013, the biological treatment was largely modernized with 80% of this wastewater being treated by biofiltration and 20% by MBR. The schematic representation of this WWTP is shown in Figure 2.6.

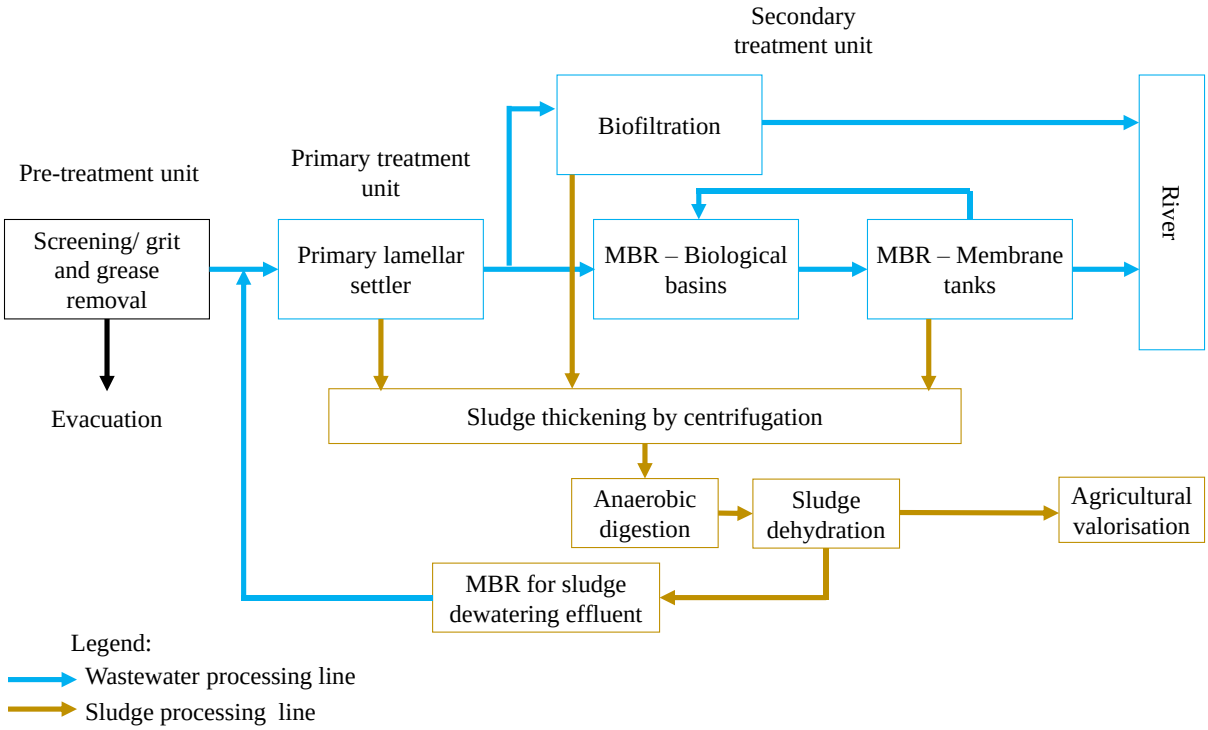

Figure 2.6: Schematic representation of SAV WWTP.

SAV's MBR is composed of two rows (A and B) of three biological tanks (total volume of one basin is 19,600 m^3). These biological tanks present: a preanoxic zone (373 m^3) for residual nitrate removal, an anaerobic zone (4,400 m^3) for biological phosphorus removal, an anoxic zone (6000 m^3) for denitrification and an aerobic zone (8,800 m^3) for BOD removal and nitrification. After the aerobic zone, mixed liquor is sent to the membrane tanks (14 per row, for row A, SAV-A1 to SAV-A14 and for row B, SAV-B1 to SAV-B14), where treated water is separated from sludge by ultrafiltration using ZeeWeed® 500D hollow-fibers. This MBR

operated at its designed capacity, thus the average daily filtration time was 20.7 ± 1.7 h. The representative scheme of one of these two rows is presented in Figure 2.7.

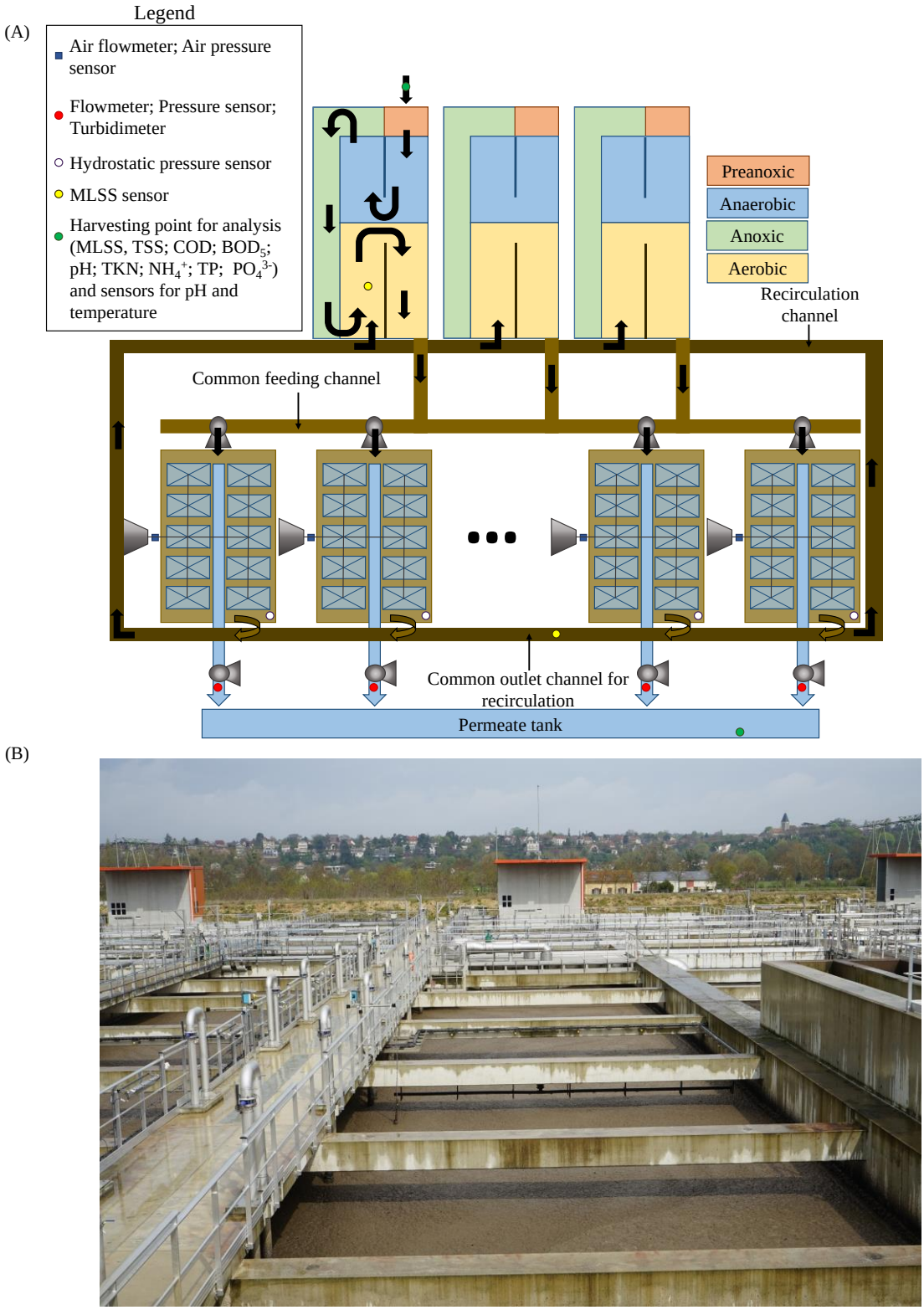

Figure 2.7: Schematic representation of SAV-MBR (A) and photo of anoxic zone from one of the biological basins (B).

Each membrane tank has 300 m^3 capacity and is equipped with 10 cassettes, composed of 48 membrane modules of 34.4 m^2 of filtration surface (total filtration surface of a membrane tank is 16,512 m^2) (Figure 2.8). In addition, mixed liquor is recirculated from membrane tanks to aerated zone.

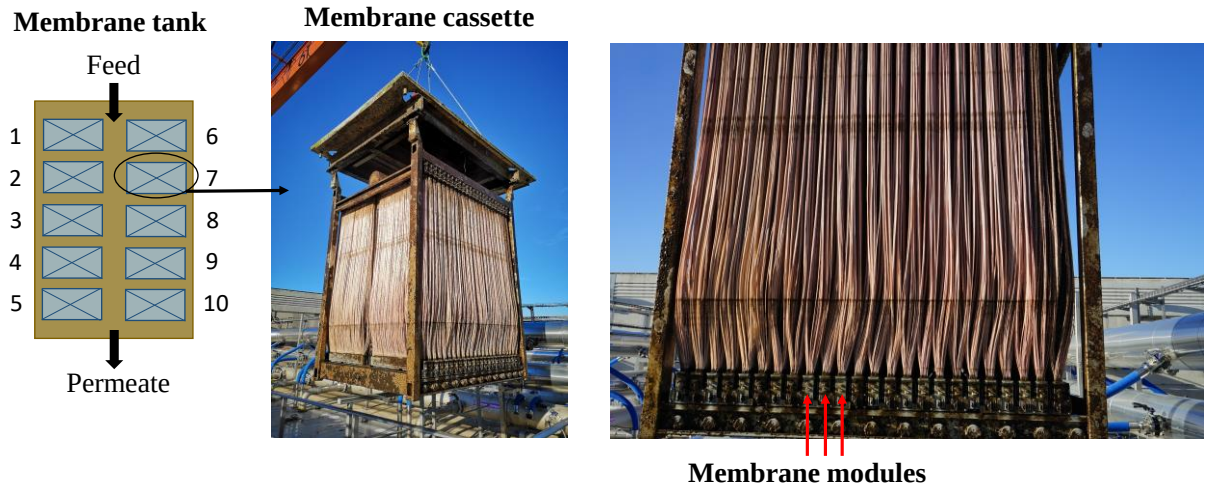

Figure 2.8: Schematic representation of a membrane tank, cassette and module of ZeeWeed® 500D hollow-fibers.

These membranes are aerated by coarse bubbles in 10 s on/ 10 s off intervals at a specific aeration demand (SADm) of 0.18 – 0.30 $m^3.h^{-1}.m^{-2}$ of membrane. Each filtration cycle takes 11 min with permeate flux varying from 18 to 40 LMH as a function of the influent flowrate, followed by 45 s of relaxation; after 8 filtration/relaxation cycles, a permeate backwash is performed for 35 s at 34 LMH.

Chemical cleaning events

Chemically enhanced backwashes (CEB) are performed three times a week, two of them at 200 ppm of NaOCl and once a week at 1100 ppm of citric acid. For these CEB, filtration stops, and 9 cycles of injection of chemically enhanced permeate for 0.5 min at 20 LMH and 4.5 min of aeration are performed. The annual NaOCl C × t related to CEB is estimated at 1000 ppm.h.

Cleaning in-place (CIP) is usually performed twice a year. Firstly, membranes are submerged in a NaOCl solution at 1000 ppm for 6 h, then they are rinsed before being soaked in a citric acid solution at pH around 2.7. The annual NaOCl C x t related to CIP is estimated to 12,000 ppm.h. Therefore, the total annual theoretical chlorine exposure (CEB + CIP) is estimated at 13,000 ppm.h.

Specific conditions for membrane tanks in SAV-MBR

Concerning the filtration and aeration cycles among membrane tanks in SAV-MBR, this MBR is composed of 28 membrane tanks, thus data treatment and graphical representations are challenging and time consuming. All membrane tanks presented similar permeate flux (Table 2.3) and similar specific aeration demand (SADm) (Table 2.4) over time. Thus, these parameters were not able to differentiate them in order to reduce the number of analyzed tanks.

Table 2.3: Permeate instantaneous flux at 20°C for the 28 membrane tanks from SAV-MBR calculated between November/2017 and June/2021.

Permeate instantaneous flux 20°C (LMH)							
Membrane tanks	**A1**	**A2**	**A3**	**A4**	**A5**	**A6**	**A7**
Average	26.6	27.1	26.6	26.6	26.9	26.0	25.7
SD	6.3	6.0	6.4	6.4	6.5	6.2	6.4
Membrane tanks	**A8**	**A9**	**A10**	**A11**	**A12**	**A13**	**A14**
Average	26.8	27.1	26.8	27.0	27.2	27.0	26.5
SD	6.3	6.4	6.3	6.4	6.4	6.4	6.5
Membrane tanks	**B1**	**B2**	**B3**	**B4**	**B5**	**B6**	**B7**
Average	27.0	26.6	27.0	26.8	26.1	26.6	26.4
SD	6.4	6.4	6.9	6.6	6.1	6.5	6.6
Membrane tanks	**B8**	**B9**	**B10**	**B11**	**B12**	**B13**	**B14**
Average	26.8	26.3	25.2	26.6	26.2	25.9	26.3
SD	6.7	6.4	6.2	6.3	6.2	6.3	6.4

Table 2.4: SADm for the 28 membrane tanks from SAV-MBR calculated between November/2017 and June/2021.

	SAD ($m^3/m^2/h$)						
Membrane tanks	**A1**	**A2**	**A3**	**A4**	**A5**	**A6**	**A7**
Average	0.22	0.21	0.22	0.21	0.22	0.20	0.21
SD	0.06	0.05	0.06	0.06	0.05	0.05	0.06
Membrane tanks	**A8**	**A9**	**A10**	**A11**	**A12**	**A13**	**A14**
Average	0.22	0.21	0.22	0.21	0.22	0.22	0.19
SD	0.06	0.05	0.05	0.05	0.05	0.05	0.06
Membrane tanks	**B1**	**B2**	**B3**	**B4**	**B5**	**B6**	**B7**
Average	0.20	0.21	0.22	0.22	0.21	0.21	0.22
SD	0.05	0.05	0.05	0.05	0.05	0.05	0.05
Membrane tanks	**B8**	**B9**	**B10**	**B11**	**B12**	**B13**	**B14**
Average	0.23	0.23	0.22	0.20	0.22	0.20	0.22
SD	0.05	0.05	0.05	0.05	0.05	0.05	0.05

Membrane tanks from SAV-MBR presented some particularities whenever they had to be shut down due to different reasons, e.g. unavailability of cleaning-in-place line, pump issues, maintenance, etc. During these non-operating days, these membrane tanks were stocked in low NaOCl concentration solutions (3 – 15 ppm). Some of these membrane tanks were stocked this way more often than others, thus the ratio of these non-operating days since the commissioning date (November/2017 to June/2021) were calculated and presented in Table 2.5. Based on this ratio, two groups of membrane tanks were observed, group 1 of membrane tanks presenting under 10% of non-operating days since the commissioning date and group 2 of membrane tanks presenting between 13% and 36% of non-operating days. Therefore, this is a parameter able to differentiate membrane tanks. Based on this ratio and in order to choose membrane tanks in

different locations with respect to the feed, 14 membrane tanks were chosen and are highlighted in Table 2.5 to further analysis of process data.

Table 2.5: Ratio of non-operating days since the commissioning date (in %) for each membrane tank from SAV. Bold membrane tanks are further analyzed.

Membrane tank	Operating days	Non-operating days	%Non-operating days since commissioning date
Group 1			
A13	**1451**	**41**	**3%**
A5	**1457**	**68**	**4%**
A12	**1399**	**70**	**5%**
B2	1373	69	5%
B8	**1362**	**80**	**6%**
B13	**1166**	**72**	**6%**
A11	1401	90	6%
A8	**1400**	**112**	**7%**
B4	1334	108	7%
A1	**1410**	**115**	**8%**
A10	1393	132	9%
B14	**1316**	**126**	**9%**
B6	1297	130	9%
B7	1295	146	10%
Group 2			
B12	1249	192	13%
A14	1252	238	16%
A4	1266	259	17%
B1	**1201**	**250**	**17%**
B3	1169	268	19%
B9	1164	276	19%
A6	1187	338	22%
B5	**1083**	**367**	**25%**
A2	**1127**	**398**	**26%**
A3	**1127**	**398**	**26%**
A9	1104	421	28%
A7	1050	475	31%
B10	**928**	**423**	**31%**
B11	**928**	**514**	**36%**

2.3.3. COMPARISON OF CHEMICAL CLEANING PARAMETERS

To illustrate the potential variations of the doses and pH that membranes are exposed for each CIP, Figure 2.9 presents the chlorine concentration (Figure 2.9.A) and pH (Figure 2.9.B) measured in laboratory for the soaking solutions harvested during CIP for SAV-MBR row A and B and SEM-MBR, except pH for SEM-MBR (data not available). In addition, plant operators from SAV-MBR only started tracking chlorine concentration and pH after the third CIP. Chlorine concentration during CIP for SEM-MBR varied from 610 to 1030 ppm, whereas for SAV-MBR, it presented a higher dispersion varying within the range of 532 – 1136 ppm. As a result pH during CIP for SAV-MBR varied between 8.3 and 9.7.

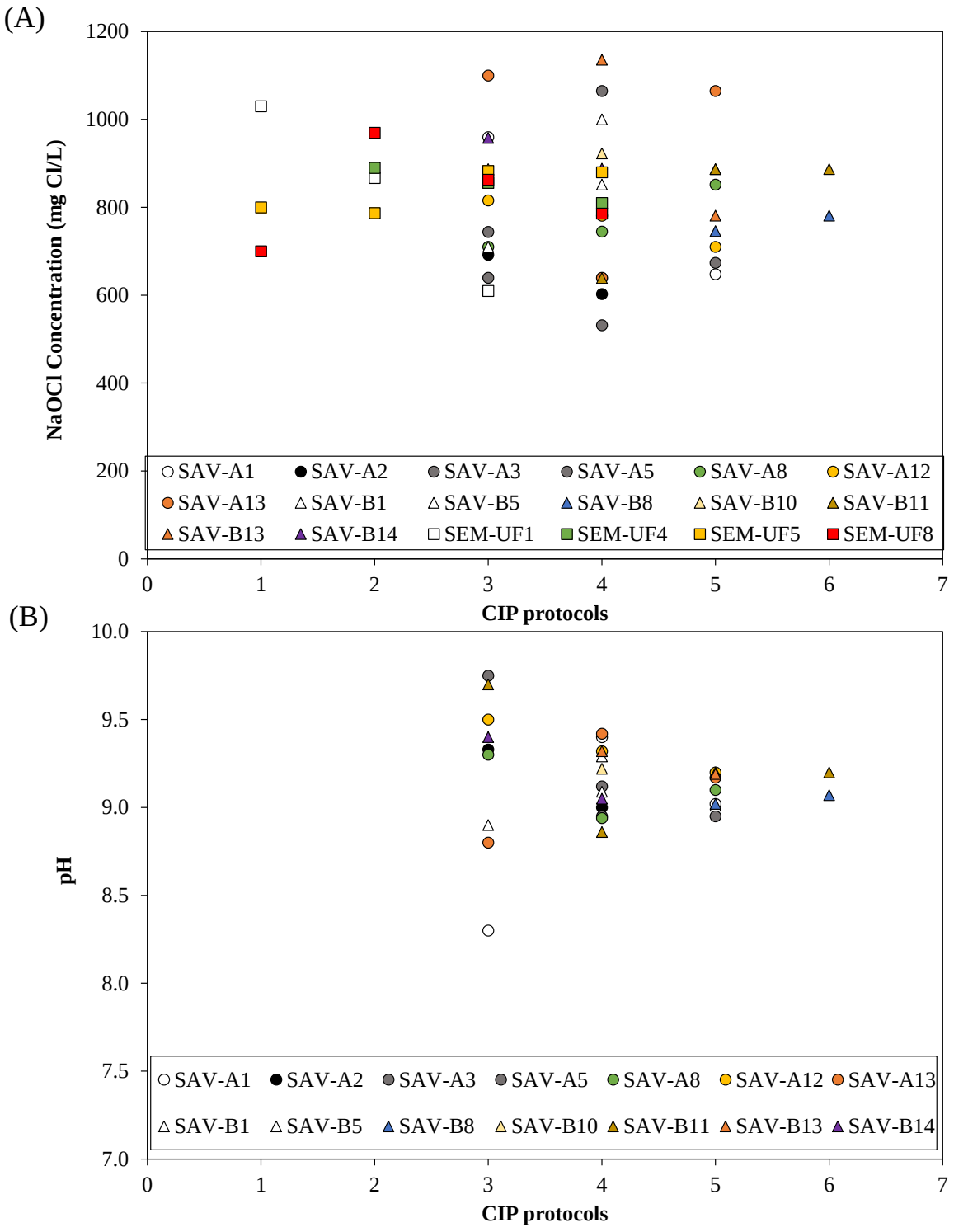

Figure 2.9: Chlorine concentrations of soaking solutions harvested at the beginning of CIP protocols for SAV-MBR and SEM-MBR (A) and pH of these solutions for SAV-MBR (B).

2.3.4. MEMBRANE HARVESTING AND PREPARATION

Fibers were harvested by cutting in both potted ends and stocked in a sodium bisulfite solution at 1 g/L. For SEM-MBR, Membranes were sampled from the same center cassette with respect to feed and in the extremity of a module from membrane tanks SEM-UF1, SEM-UF3, SEM-UF4, SEM-UF5, SEM-UF7 and SEM-UF8 from 2016 to 2021 before CIP (from 2 to 7 years in operation). For SAV, hollow-fibers were harvested from central cassettes of tanks A1, A5, A8, B1, B5, B8, B10, B11 and B14 from 2018 to 2021 before CIP. The place of these harvesting are represented with a red cross in Figure 2.10. Besides membrane tanks chosen based on their location for the process data collection and analysis are represented in this figure with red squares.

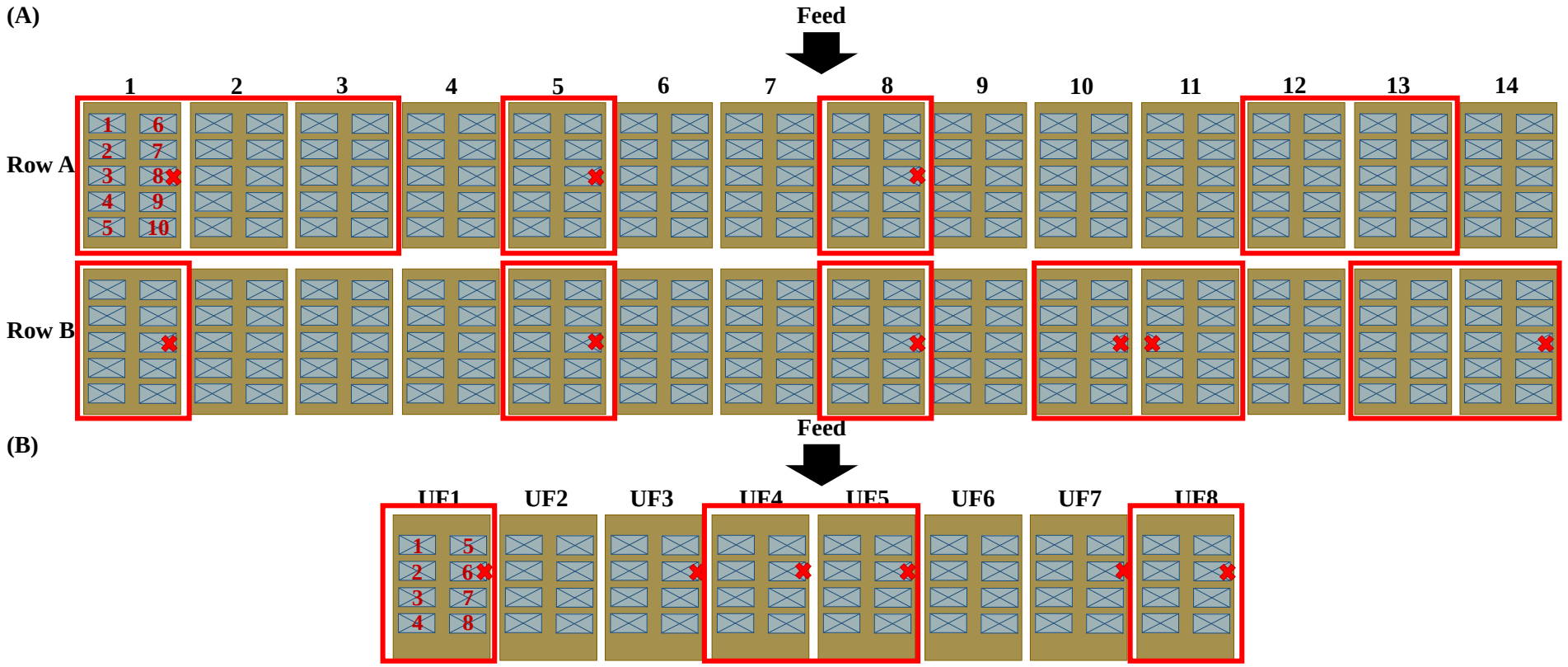

Figure 2.10: Schematic representation of membrane harvesting place for SAV-MBR (A) and SEM-MBR (B).

Red squares indicate which membrane tanks were considered in the analysis based on operating data and red crosses represent harvesting cassettes inside each membrane tank.

Before characterization, membranes were cleaned at bench-scale according to the CIP protocol applied at full-scale. The NaOCl C × t undergone by each sample is calculated using the concentration and exposure time given by the operators for each CIP and CEB. The C × t ascertained in the laboratory before measurements was also added to these values. The total C × t values to which each sample is exposed are presented in Table 2.6 for bench-scale and 2.7 for full-scale.

For full-scale samples, other cumulative indicators than the C × t that may characterize the chronological data from membranes were determined for each sample. The cumulative indicators calculated were: operating days, exposure dose, specific permeate volume (V_p), specific aeration demand and filtered MLSS mass, filtered supernatant COD mass and filtered supernatant ΔCOD mass, which are calculated as ascribed in Eq. 2.1 – 2.3. COD measurements were not available for the full operation of SEM-MBR, therefore, the associated indicators were not calculated.

$$MLSS\ mass = \frac{MLSS_{recirculation\ channel} \times V_p}{S} \quad \text{Eq. 2.1}$$

$$COD\ mass = \frac{COD_{mixed\ liquor\ supernatant} \times V_p}{S} \quad \text{Eq. 2.2}$$

$$\Delta COD\ mass = \frac{\left(COD_{mixed\ liquor\ supernatant} - COD_{permeate}\right) \times V_p}{S} \quad \text{Eq. 2.3}$$

Permeate volume, aeration demand, MLSS, COD and ΔCOD masses were divided by S the filtration surface of each membrane tank, since membrane tanks from SAV-MBR and SEM-MBR do not present the same filtration surface.

As already mentioned, the membrane tanks from SAV-MBR are divided in two rows (A and B) of 14 tanks. Regarding these process indicators, operating days, permeate volume, exposure dose and aeration volume are individually measured for each membrane tank, whereas filtered MLSS, COD and ΔCOD are measured by row in the recirculation channel, which implies that

we consider homogeneous concentrations among tanks from the same row. Similarly, to SAV-MBR, SEM-MBR membrane tanks presented the same individualized parameters, whereas only one MLSS value is available for all eight membrane tanks, implying the same hypothesis. The operating time is calculated based on the number of days each membrane tank filtered more than 5th percentile of the daily permeate volume.

Table 2.6: Exposure doses of membrane samples aged at bench-scale.

	Bench-scale single soaking							
C x t (ppm.h)	0	12,000	24,000	36,000	48,000	60,000	72,000	78,000
	84,000	100,000	125,000	148,000	170,000	249,000	500,000	750,000

Table 2.7: Process indicators to monitor ageing for membrane samples harvested at full-scale.

Time since commissioning date (days)	**C × t (ppm.h)**	**Specific permeate volume (m^3/m^2)**	**Specific filtered Supernatant COD (kg O_2/m^2)**	**Specific filtered ΔCOD (kg O_2/m^2)**	**Specific filtered MLSS mass (kg MLSS/m^2)**	**SADm (m^3/m^2)**	**Non-filtration time (days)**
			SAV-A1				
314	6,600	144	6.2	3.5	404	1569	76
667	13,500	314	14.2	8.7	1357	3548	89
1053	26,500	494	18.0	9.6	2319	5794	104
			SAV-B1				
239	6,900	117	4.1	0.8	433	1340	95
836	19,900	401	14.2	3.9	1983	4185	126
1090	26,700	517	16.9	4.2	2583	5358	237
			SAV-A5				
349	6,800	173	7.1	3.9	460	2079	21
743	13,700	364	15.7	9.2	1542	4151	40
1086	14,600	520	18.9	10.0	2380	5881	54
1270	21,100	595	20.5	10.4	2737	6681	68

Time since commissioning date (days)	C × t (ppm.h)	Specific permeate volume (m^3/m^2)	Specific filtered Supernatant COD (kg O_2/m^2)	Specific filtered ΔCOD (kg O_2/m^2)	Specific filtered MLSS mass (kg MLSS/m^2)	SADm (m^3/m^2)	Non-filtration time (days)
SAV-B5							
515	7,500	320	10.2	6.3	1002	2849	104
802	13,900	405	13.5	7.3	1765	4190	350
SAV-A8							
344	6,800	170	6.9	3.8	443	1904	24
1017	20,400	488	17.7	9.3	2203	5536	88
1199	26,800	560	19.3	9.7	2547	6416	101
SAV-B8							
304	6,800	141	5.1	2.7	484	1900	15
755	25,700	356	13.4	7.5	1667	4289	53
1081	26,600	495	16.2	8.2	2381	5948	61
SAV-B10							
433	13,100	209	8.0	4.5	964	2860	148
756	13,900	345	10.8	5.1	1683	4298	293

Time since commissioning date (days)	**C × t (ppm.h)**	**Specific permeate volume (m^3/m^2)**	**Specific filtered Supernatant COD (kg O_2/m^2)**	**Specific filtered ΔCOD (kg O_2/m^2)**	**Specific filtered MLSS mass (kg MLSS/m^2)**	**SADm (m^3/m^2)**	**Non-filtration time (days)**
			SAV-B11				
606	20,100	289	14.6	8.0	1887	4609	383
			SAV-B14				
303	6,800	138	4.7	2.5	464	1743	18
939	20,300	443	15.6	7.8	2328	5018	30
			SEM-UF1				
991	22,900	165	-	-	953	597	113
1293	47,700	206	-	-	1203	1041	288
1606	59,300	266	-	-	1579	1453	339
			SEM-UF3				
816	33,000	140	-	-	717	718	65
1079	42,400	185	-	-	1028	1064	158
1282	61,600	218	-	-	1206	1344	362
1552	72,200	268	-	-	1519	1638	399
1864	98,200	294	-	-	1943	1969	409

Time since commissioning date (days)	**C × t (ppm.h)**	**Specific permeate volume (m^3/m^2)**	**Specific filtered Supernatant COD (kg O_2/m^2)**	**Specific filtered ΔCOD (kg O_2/m^2)**	**Specific filtered MLSS mass (kg MLSS/m^2)**	**SADm (m^3/m^2)**	**Non-filtration time (days)**
			SEM-UF4				
1084	26,000	181	-	-	1015	1027	141
1511	32,900	244	-	-	1401	1621	338
			SEM-UF5				
1359	45,900	234	-	-	1389	2074	244
1525	63,800	266	-	-	1588	2328	275
			SEM-UF8				
988	41,000	157	-	-	911	845	124
1127	56,000	178	-	-	1038	1089	288
1449	74,500	226	-	-	1336	1416	353

2.4. HIGH FREQUENCY DATA TREATMENT

Besides, high frequency (15 min) data related to filtration (permeate flowrate, transmembrane pressure and temperature) were obtained for key periods between 15 days before and 15 days after a CIP protocol for these same membrane tanks. TMP is calculated thanks to pressure sensor in the permeate collector pipe after membranes and level sensors in the membrane tank. This way, TMP is automatically determined in mbar according to Eq. 2.4. Additionally, permeate flux at 20 °C (J_{20}) was calculated based on temperature (T) and permeate flowrate (Q_p) by Eq. 2.5 [86].

$$\text{TMP} = h_i * \frac{1000}{10.13} - \text{P}_{perméat_i} \times 1000 \qquad \text{Eq. 2.4}$$

$$\text{J}_{20} = \frac{Q_p}{S\, e^{-0.0239(T-20)}} \qquad \text{Eq. 2.5}$$

Where:

h_i: mixed liquor level in the membrane tank i (m), measured by a pressure sensor Vegabar 82 (Vega Technique, France);

$P_{perméat_i}$: permeate pressure (bar), measured by pressure sensor Cerabar PMP71 (Endress+Hauser, Switzerland);

S: filtering membrane surface (m^2).

After determination of permeate flux at 20°C and transmembrane pressure, in order to monitor membrane ageing of these membrane tanks, the permeability index was determined. This is the ratio between permeate flux at 20°C and transmembrane pressure when membrane tanks are filtering mixed liquor. Since this indicator can be used to monitor long-term changes in membrane behavior when filtering mixed liquor, factors other than the membrane properties can affect this measure, i.e. filtration conditions, fouling state and mixed liquor characteristics. To minimize such impacts, the method to calculate permeability index in the long-term is presented in the following section.

2.4.1. DETERMINATION METHOD OF PERMEABILITY INDEX FOR LONG-TERM ANALYSIS

Permeability index, similarly to membranes intrinsic permeability, represents the inverse of the hydraulic resistance of membranes in filtration. This indicator can be determined after a Cleaning-In-Place (CIP), when membranes are at their cleaned stage. On site, permeability index is currently used to monitor whether CIP are successful, but it can also be used to observe membrane ageing, since a continuous decline in this index is expected due to residual irreversible fouling accumulation [6].

Before calculating these permeabilities for the studied MBRs, high frequency data (5 s) of Q_p and TMP were collected to evaluate the dynamics of permeability before and after CIP. These data were recovered for the three initial cleaning in-place events for membrane tank A1 from SAV, since this membrane tank was representative of a regular operation, with only 8% of non-filtration days since commissioning, an average permeate net flux of 26.6 ± 6.3 LMH and SADm of 0.22 ± 0.06 $m^3/m^2/h$. These data were firstly cleaned following two simple steps: (i) All zeros (non-filtration periods) were deleted and (ii) values of flowrate below the first percentile (value below which 1% of values in its frequency distribution falls) were also deleted.

These values mostly represented times of transition between filtration and relaxation/backwash. The cleaned data for the first period (16/04/2018 – 30/04/2018) is presented in Figure 2.11.

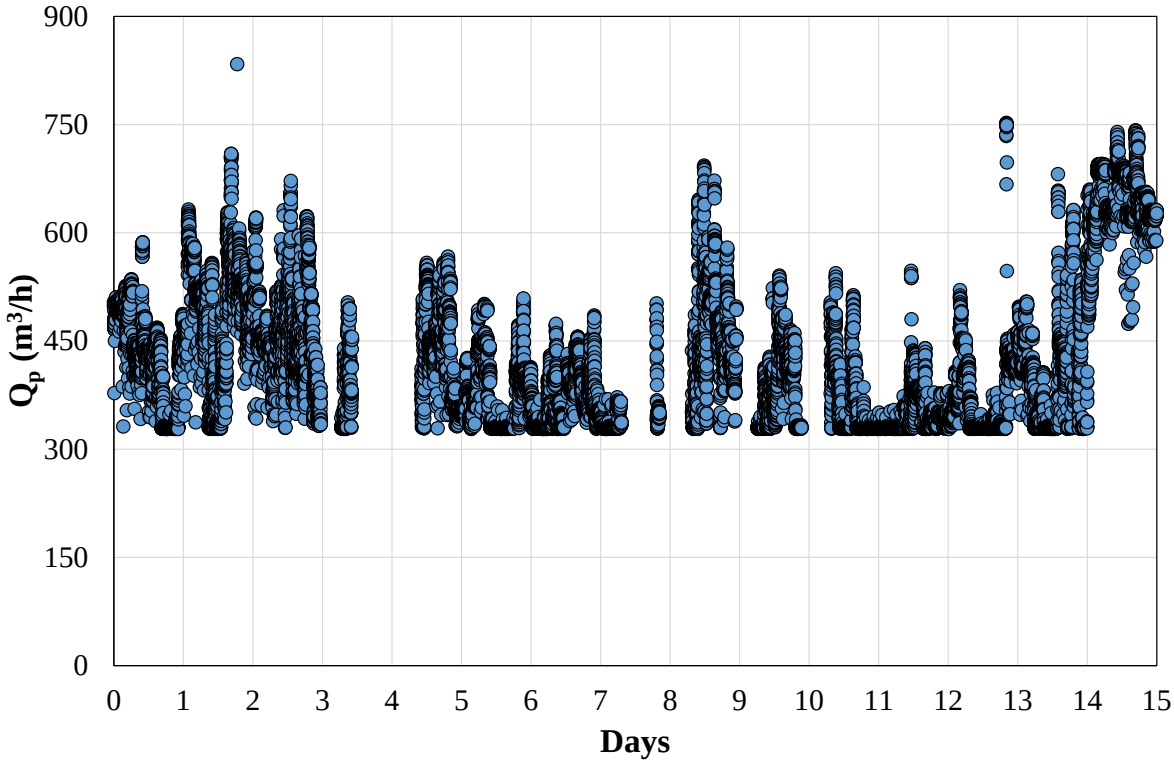

Figure 2.11: Cleaned permeate flowrates from membranes tank SAV-A1 from 16/04/2018 to 30/04/2018.

Then, permeate flux (J) adjusted to 20°C is calculated according to Eq. 2.5 and divided by TMP, to obtain the permeability index (Eq. 2.11).

$$Permeability\ index = \frac{J_{20}}{TMP} \qquad \text{Eq. 2.11}$$

These values were smoothed by the median of values during 2 min to obtain the chronic presented in Figure 2.12 for this first period.

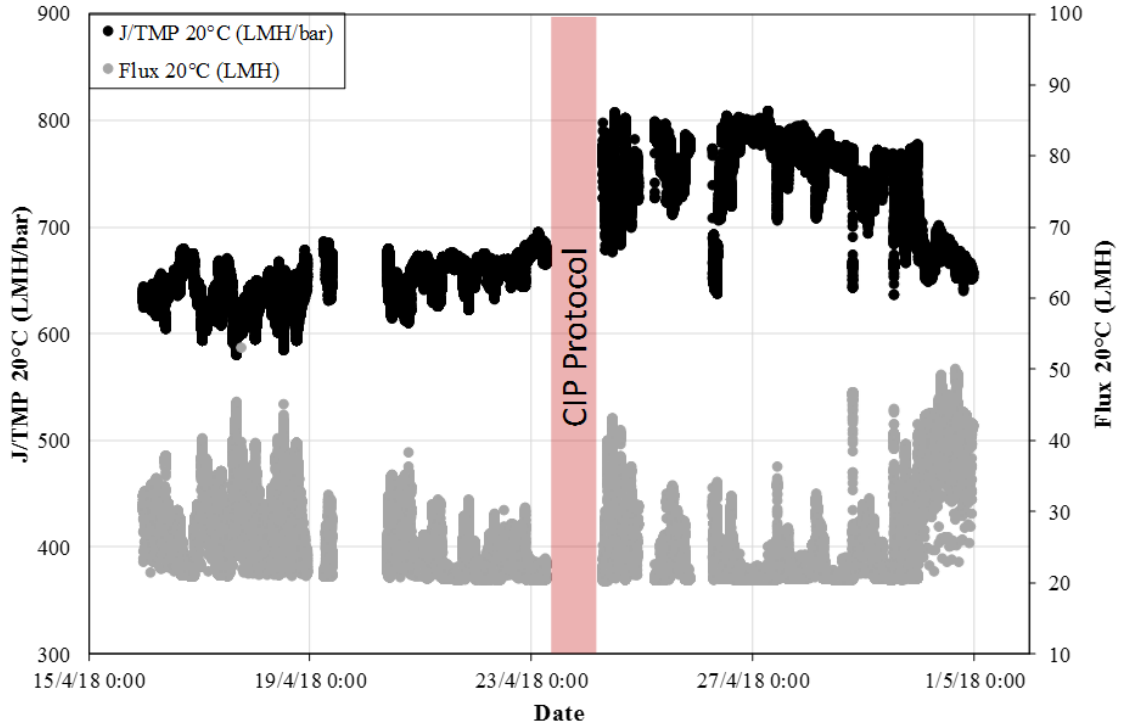

Figure 2.12: Permeability index and flux at 20°C for membranes tank SAV-A1 from 16/04/2018 to 30/04/2018.

From these data, large variations of J_{20} are observed between 20 and 50 LMH, which is due to the variable volume of influent sent to the station during the day and the availability of membrane tanks. These oscillations in J_{20} seemed to affect permeability index even in short filtration periods (~10 min). Permeability index is supposed to be independent of the J_{20} for short periods of filtration according to Darcy's law, assuming that fouling does not take place. Therefore, these changes were investigated. Some of these periods are extracted from Figure 2.12 and highlighted in blue in Figure 2.13.

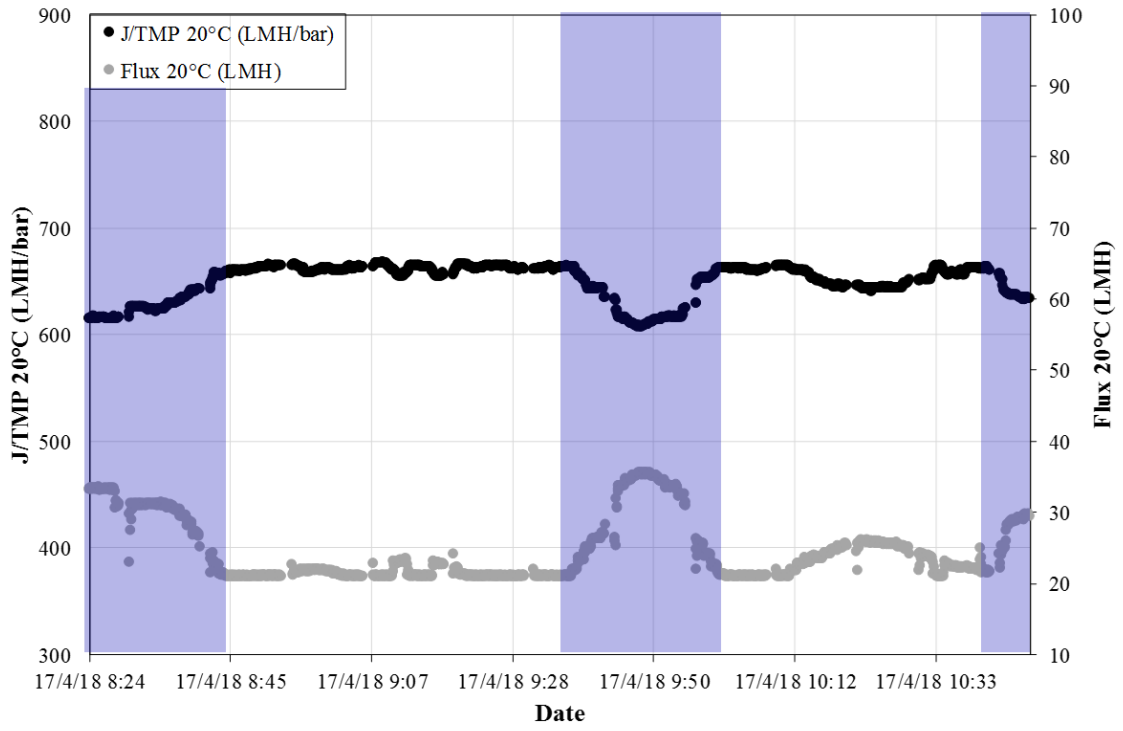

Figure 2. 13: Permeability index and permeate fluxes for membranes tank SAV-A1 as a function of time with periods of flux variations highlighted in violet.

This sensitivity of permeability index was evaluated for membranes tank A1 at different stages of fouling and ageing. For instance, short periods were extracted in 2018 and 2019 before and after CIP protocols for fouled and cleaned membranes. The permeability index and TMP as a function of flowrate are presented in Figure 2.14, confirming the impact of flowrate on this indicator at different fouling stages.

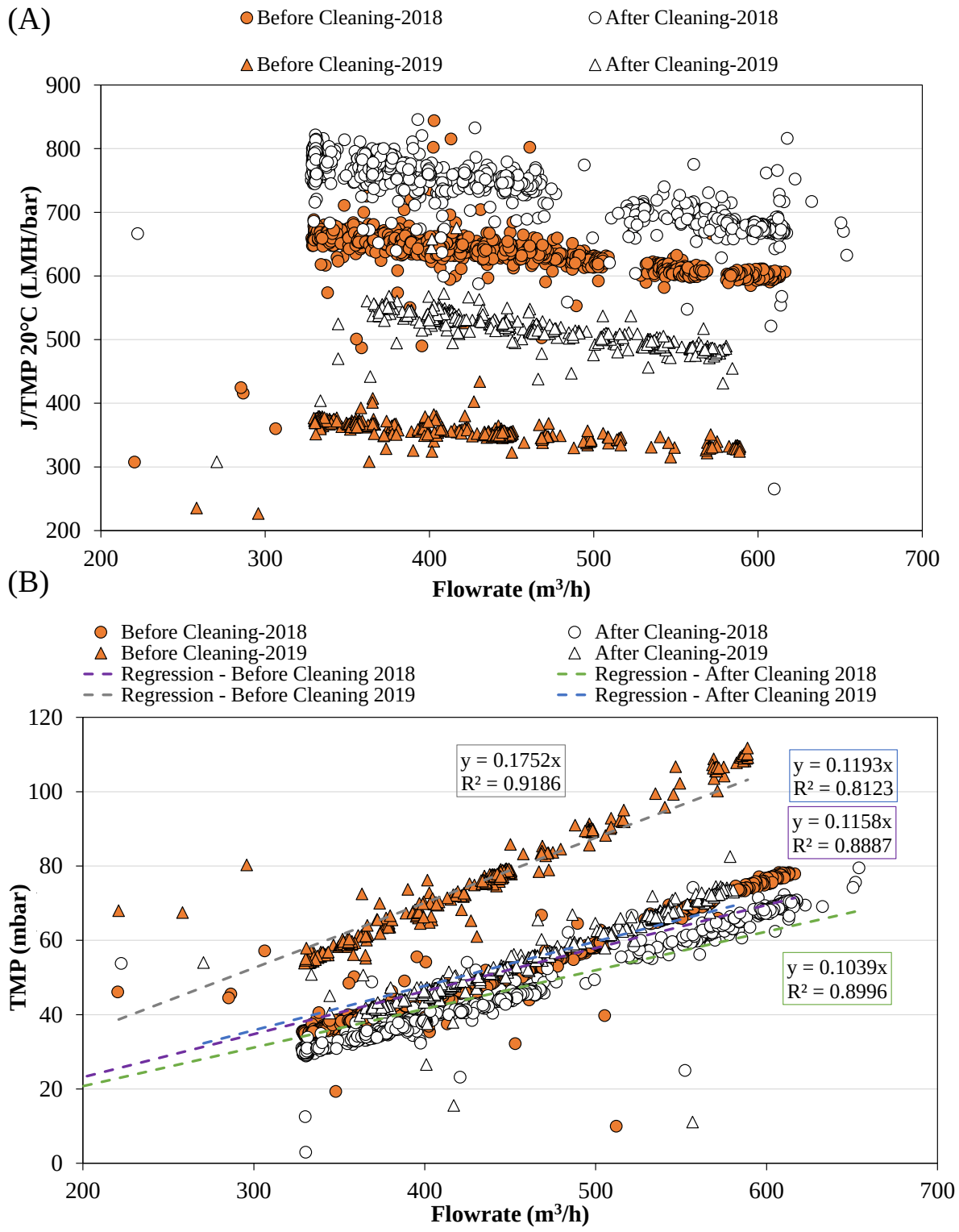

Figure 2.14: Variations of permeability index (A) and TMP (B) as a function of flowrate for membranes tank SAV-A1 before and after CIP protocols in 2018 and 2019.

From the blue zones in Figure 2.13 it is possible to validate the reversible characteristic of these evolutions. Thus, two phenomena may be involved in this behavior:

(i) At higher flowrates, the cake is compressed, overly increasing TMP (Figure 2.14.B), or reducing drastically permeability index (Figure 2.14.A). Most points of TMP above 500 m^3/h are placed above the linear regression in Figure 2.14.B;

(ii) The geometry of pipes and hydraulic flow between membranes and pressure sensors cause friction and local losses in pressure resulting in an overestimation of TMP at higher fluxes [87]. Nicolas Philippe (2014) proposed a method to estimate a pressure drop coefficient to adjust these variations in the calculation of TMP and permeability index as a result. This method is based on determining the nature of flow by the Reynolds number, followed by the calculation of the pressure drop, based on the Moody's or Darcy's method, which involve specific information about material and geometry of permeate line.

In order to reduce variations on the permeability index not linked to long-term operation, two points will be taken into consideration in the following sections:

1. The effect of permeate flux: a simple approach is proposed to calculate permeability index as a function of the permeate flux;
2. The duration of filtration period: to calculate the permeability index after CIP to be representative.

2.4.1.1. EFFECT OF PERMEATE FLUX

To control the impact of flux variation, instead of fixing a given permeate flux and limiting the analysis to this only flux, 9 flux intervals were established between 18 and 36 $L.h^{-1}.m^{-2}$, covering

the range of values between the 10th and 90th percentile of permeate flux observed in this study, and their corresponding permeability indexes were calculated, whenever the installation was operated at such fluxes. To illustrate this procedure, the permeability indexes are presented for the first (Figure 2.15.A) and third (Figure 2.15.B) CIP of membrane tank A1 in April 2018 and October 2019, respectively.

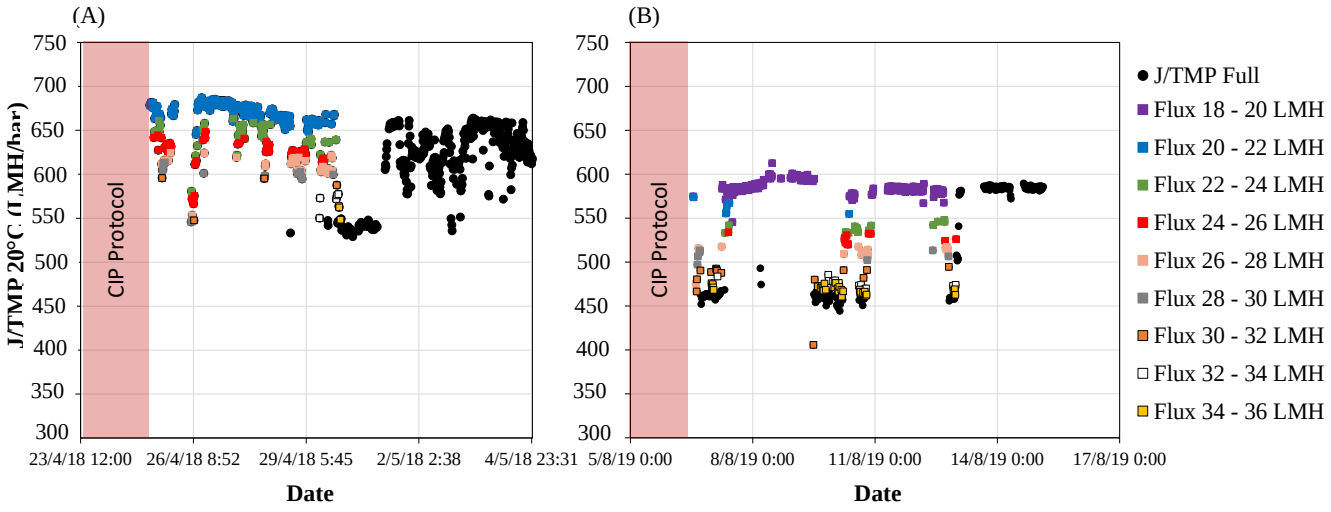

Figure 2.15: Permeability indexes after the first CIP protocol in April 2018 (A) and the third one in October 2019 (B) for membranes tank SAV-A1.

This categorization successfully reduced the variability of values taken into consideration to represent the permeability index after CIP as shown in the boxplots from Figure 2.16, when comparing the box from J/TMP for all fluxes (black) against the ones separated by flux intervals.

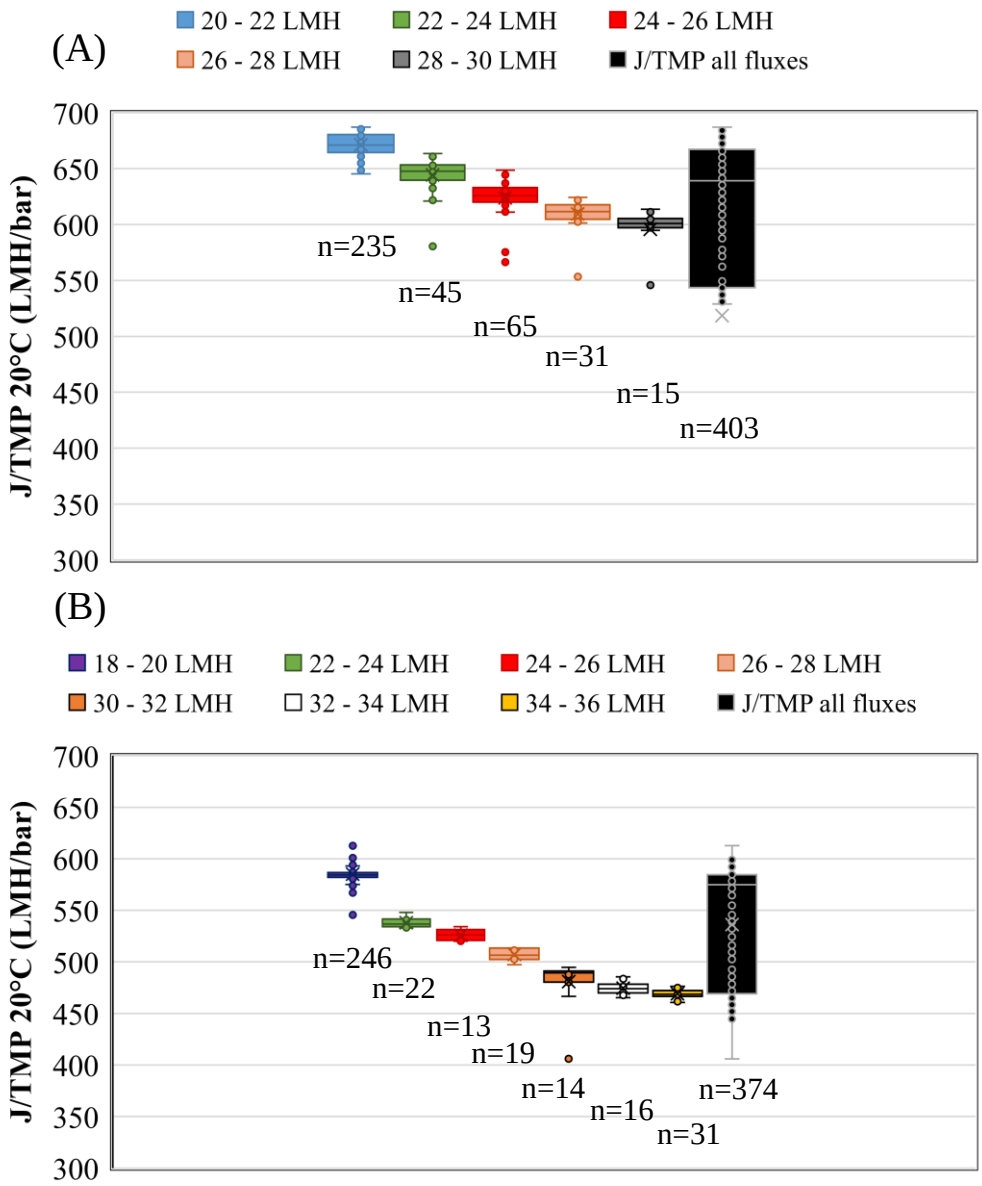

Figure 2.16: Boxplot of permeability indexes according to their range of flux for short period just after the first CIP protocol in April 2018 (A) and the third one in October 2019 (B) from membranes tank SAV-A1.

In order to follow the long-term evolutions of this indicator, values of J/TMP 20°C for each range were normalized by a referential state in the beginning of operation, which is November/2017 for SAV-MBR and May/2014 for SEM-MBR ($\left(\frac{J}{TMP}\right)_{0,i}$) when membranes started filtration in mixed liquor following Eq. 2.6. The graphical examples of referential stage

for the membrane tank A1 for SAV-MBR and membrane tank UF1 for SEM-MBR are presented in Figure 2.17.

$$(Normalized\ permeability\ index)_{t,i} = \frac{\left(\frac{J}{TMP}\right)_{t,i}}{\left(\frac{J}{TMP}\right)_{0,i}} \quad \text{Eq. 2.6}$$

Where:

t: indicates the corresponding CIP involved;

i: identify the range of flux;

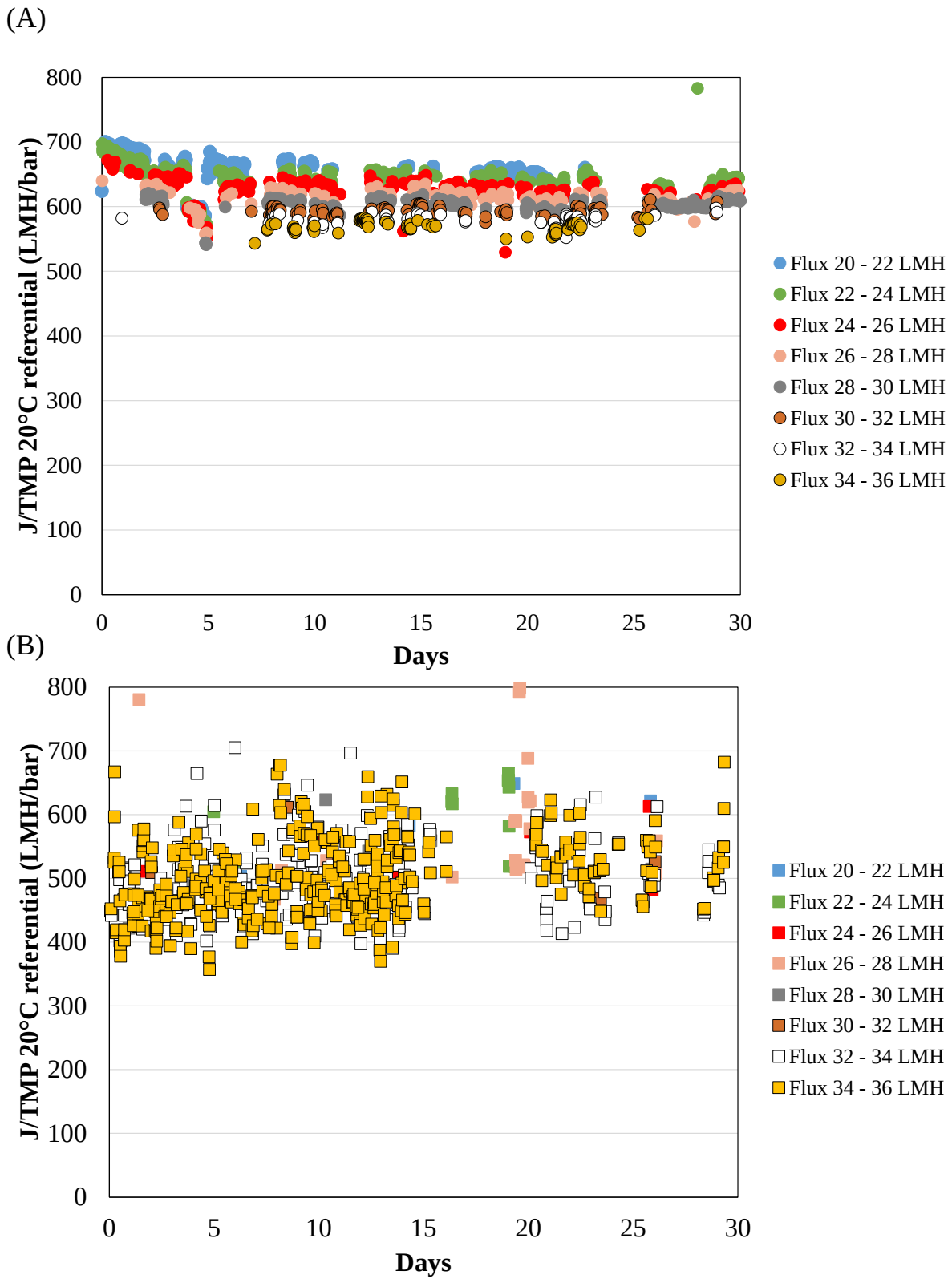

Figure 2.17: Referential J/TMP for membranes tank SAV-A1 (A) and membranes tank SEM-UF1 (B).

Once the normalization is performed, the normalized permeability indexes are in a common scale. For instance, these values for each CIP can be plotted as a function of the operating days, as shown in Figure 2.18 for membrane tanks SAV-A1 and SEM-UF1.

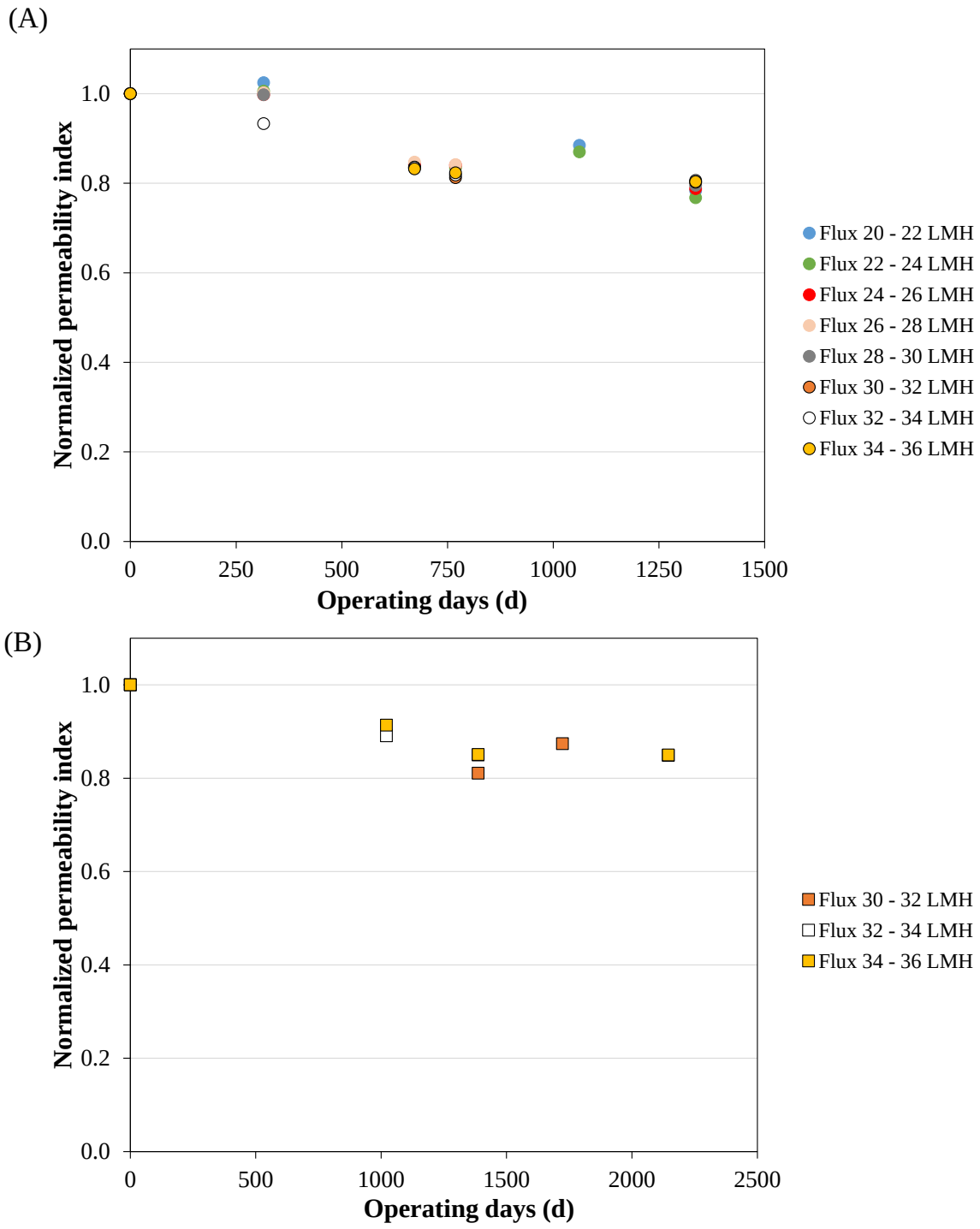

Figure 2.18: Normalized permeability index for different permeate fluxes as a function of the operating days for membranes tank SAV-A1 (A) and SEM-UF1 (B).

Then these normalized permeability indexes can be averaged for each CIP to be used as an indicator of membrane ageing, resulting in Figure 2.19. As membranes age, mixed liquor filtration is hampered by residual fouling and changes in membrane properties, translating in a decline of permeability index over time. Thus, this parameter measures the ability of membranes to filter mixed liquor with respect to its referential state.

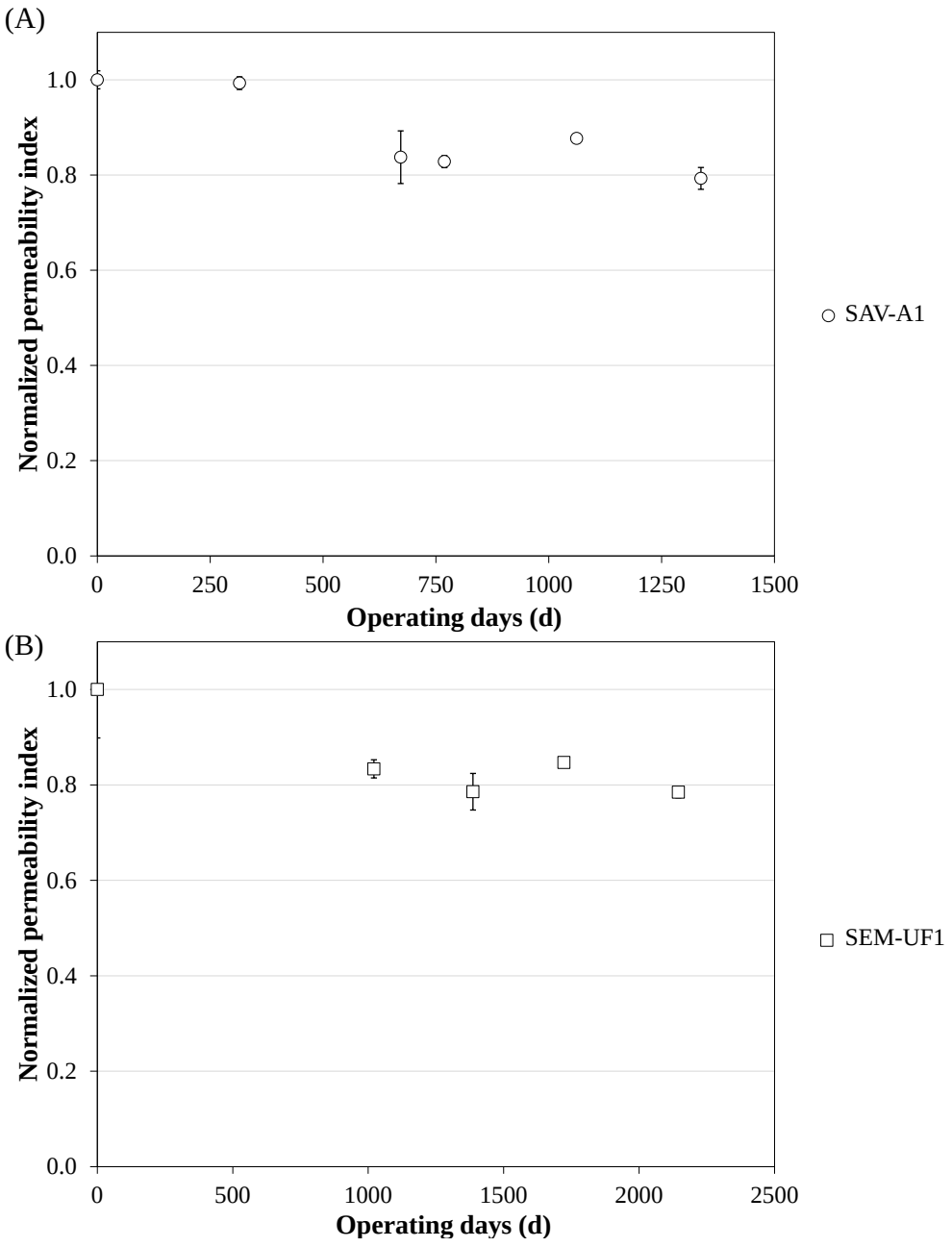

Figure 2.19: Averages of normalized permeability index for membrane tanks SAV-A1 (A) and SEM-UF1 (B).

2.4.1.2. EFFECT OF DURATION

Although the categorization of permeability index by permeate flux decreases variability related to other factors than the membrane stage, after CIP protocols the first values of permeability index may be influenced by the mixed liquor quality, residual chemical cleaning agents, among other. For instance, these dynamics after CIP can be observed in Figure 2.15 in the previous section and a zoom in the first CIP of membrane tank SAV-A1 is illustrated in Figure 2.20.

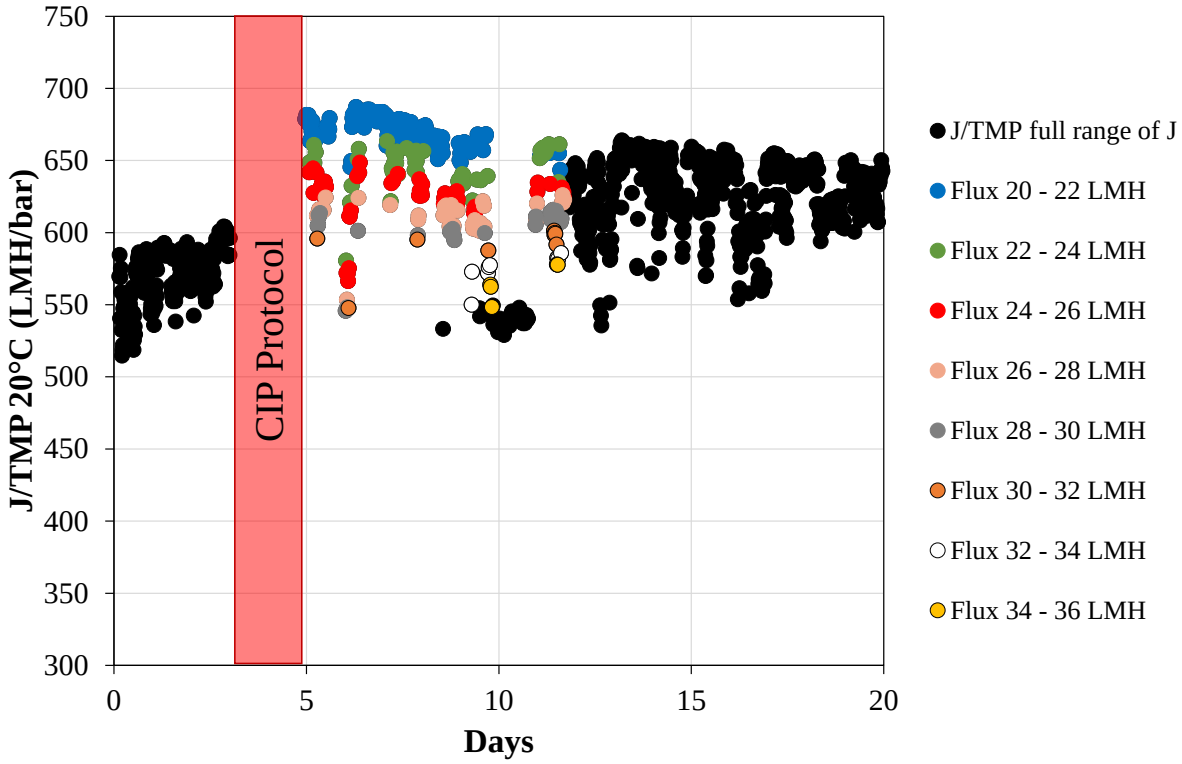

Figure 2.20: Permeability index of membrane tank SAV-A1 around the first CIP protocol.

Thus, a sensitivity study was carried out to determine the impact of the number of days after a CIP to be considered in the permeability index calculation. The tested length ranged from 1 to 7 days after CIP (CIP+1 up to CIP+7), as a complete cycle of filtration and chemical enhanced backwash takes 7 days. Besides, tests were performed considering the 7 following days of a CIP, but excluding the first (CIP +1 to +7) and second (CIP +2 to +7) days just after CIP.

The results of average J/TMP calculated, standard deviations and number of observations (filtration cycles) are presented in Tables 2.8 and 2.9 for each condition of the CIPs of April/2018 and October/2019, respectively, for membrane tank SAV-A1 and Tables 2.10 and 2.11 for membranes SEM-UF4. From these tables, we seek the conditions with simultaneously, a relevant number of observations, so that values are representative, and the minimization of absolute standard deviations to limit variability. Firstly, J/TMP were only calculated when they presented 10 or more filtration cycles. As expected, the total number of cycles increased with increasing number of days considered between CIP+6 and CIP+7. Standard deviation was low in CIP+1, because of the low number of filtration cycles, then increased and fluctuated between CIP+2 and CIP+6. After CIP+7 standard deviation decreased over most of the range of permeate fluxes. Thus, CIP+7, CIP+1 to +7 and CIP+2 to +7 seemed to satisfy these conditions. Therefore, to consider the whole filtration cycle of each tank and avoid strong dynamics in the beginning of a cycle due to sludge conditions, CIP+1 to +7 is chosen to the general determination of permeability indexes.

Table 2.8: Impact of period length on J/TMP (CIP: April/2018, SAV-A1). Averages and standard deviations calculated with "n" filtration cycles. J/TMP averages were only calculated if n ≥ 10.

Length	J/TMP_{20-22} (LMH/bar)	J/TMP_{22-24} (LMH/bar)	J/TMP_{24-26} (LMH/bar)	J/TMP_{26-28} (LMH/bar)	J/TMP_{28-30} (LMH/bar)	J/TMP_{30-32} (LMH/bar)	J/TMP_{32-34} (LMH/bar)	Filtration cycles (∑n)
CIP+1	n = 5	n = 5	634,8 ± 6,4 n =14	625,3 ± 5,64 n =10	n = 9	n = 6	n = 2	51
CIP+2	671,6 ± 20,5 n =32	647,5 ± 23,4 n =11	634,3 ± 25,1 n =30	622,3 ± 26,9 n =15	608,7 ± 28,8 n =14	n = 6	n = 2	110
CIP+3	651,7 ± 37,3 n =66	638,2 ± 23,8 n =11	627,1 ± 20,5 n =26	n = 7	n = 8	n = 0	n = 0	118
CIP+4	661,8 ± 30,9 n =143	643,0 ± 19,0 n =26	627,8 ± 19,9 n =29	n = 8	n = 8	n = 0	n = 0	214
CIP+5	662,8 ± 26,9 n =202	644,7 ± 17,3 n =35	627,0 ± 16,6 n =49	615,1 ± 18,9 n =13	n = 9	n = 0	n = 1	309
CIP+6	662,4 ± 25,3 n =235	643,1 ± 16,1 n =44	625,8 ± 15,2 n =65	612,2 ± 15,1 n =31	600,4 ± 17,4 n =15	n = 2	n = 3	395
CIP+7	671,0 ± 9,4 n =240	644,2 ± 13,7 n =50	625,8 ± 15,2 n =79	613,4 ± 13,1 n =41	600,4 ± 17,4 n =24	568,6 ± 13,3 n =14	541,1 ± 6,9 n = 27	475
CIP+1 to +7	671,2 ± 9,2 n =235	644,4 ± 14,0 n =45	623,9 ± 15,8 n =65	609,5 ± 12,5 n =31	595,7 ± 20,5 n =15	n = 8	539,8 ± 5,3 n = 25	424
CIP+2 to +7	670,9 ± 9,5 n =208	643,3 ± 14,6 n =39	620,6 ± 16,8 n =49	608,2 ± 13,1 n =26	588,9 ± 22,2 n =10	n = 8	539,8 ± 5,3 n = 25	365

Table 2.9: Impact of period length on J/TMP (CIP: October/2019, SAV-A1). Averages and standard deviations calculated with "n" filtration cycles. J/TMP averages were only calculated if n ≥ 10.

Length	J/TMP_{18-20} (LMH/bar)	J/TMP_{20-22} (LMH/bar)	J/TMP_{22-24} (LMH/bar)	J/TMP_{24-26} (LMH/bar)	J/TMP_{26-28} (LMH/bar)	J/TMP_{30-32} (LMH/bar)	J/TMP_{32-34} (LMH/bar)	Filtration cycles (∑n)
CIP+1							461,4 ± 2,5 n = 24	24
CIP+2	583,0 ± 5,9 n =59						462,1 ± 2,8 n = 38	97
CIP+3	586,5 ± 7,4 n =96						462,1 ± 2,8 n = 38	134
CIP+4	588,4 ± 7,8 n =118					462,6 ± 4,9 n = 18	462,6 ± 3,1 n = 70	206
CIP+5	586,78 ± 8,4 n =136		536,5 ± 2,9 n =18	526,2 ± 5,5 n =11	506,6 ± 14,9 n =12	471,1 ± 5,4 n =42	461,6 ± 4,2 n = 83	302
CIP+6	585,8 ± 7,07 n =202		536,5 ± 2,9 n =18	526,2 ± 5,5 n =11	506,6 ± 14,9 n =12	471,1 ± 5,4 n =42	461,6 ± 4,2 n = 83	368
CIP+7	585,0 ± 6,8 n =246		538,1 ± 4,5 n =22	526,1 ± 5,1 n =11	509,7 ± 12,5 n =19	471,0 ± 5,3 n =47	461,2 ± 4,0 n = 94	441
CIP+1 to +7	585,1 ± 6,8 n =245		538,1 ± 4,5 n =22	526,1 ± 5,1 n =13	513,8 ± 3,6 n =14	470,8 ± 5,3 n =45	461,2 ± 4,5 n = 70	409
CIP+2 to +7	585,7 ± 7,0 n =186		538,2 ± 4,6 n =20	525,4 ± 4,7 n =12	513,5 ± 3,5 n =13	470,4 ± 5,2 n =40	460,7 ± 4,6 n = 56	327

Table 2.10: Impact of period length on J/TMP (CIP: October/2017, SEM-UF4). Averages and standard deviations calculated with "n" filtration cycles. J/TMP averages were only calculated if n ≥ 10.

Length	**J/TMP_{32-34} (LMH/bar)**	**J/TMP_{34-36} (LMH/bar)**	**Filtration cycles (∑n)**
CIP+1	n = 3	n = 2	5
CIP+2	402.2 ± 59.1 n =10	398.0 ± 49,5 n =12	24
CIP+3	399.0 ± 48.8 n =21	398.6 ± 45.7 n =20	44
CIP+4	396.7 ± 43.5 n =30	394.7 ± 39.3 n = 31	65
CIP+5	395.4 ± 40.3 n =39	401.2 ± 42.1 n =43	87
CIP+6	395.7 ± 37.4 n =51	400.7 ± 39.5 n =53	109
CIP+7	395.0 ± 37.2 n =62	401.2 ± 40.7 n =62	130
CIP+1 to +7	395.0 ± 37.2 n =62	401.2 ± 40.7 n =62	130
CIP+2 to +7	392.2 ± 37.2 n =59	399.5 ± 39.3 n =60	125

Table 2.11: Impact of period length on J/TMP (CIP: June/2019, SEM-UF4). Averages and standard deviations calculated with "n" filtration cycles. J/TMP averages were only calculated if n ≥ 10.

Length	J/TMP_{28-30} (LMH/bar)	J/TMP_{30-32} (LMH/bar)	Filtration cycles (∑n)
CIP+1	n = 2	n = 5	7
CIP+2	n =9	498.3 ± 44.4 n =24	33
CIP+3	483.1 ± 45.5 n =19	503.5 ± 44.2 n =39	58
CIP+4	485.3 ± 43.3 n =23	491.4 ± 46.1 n =56	79
CIP+5	488.0 ± 50.0 n =30	489.6 ± 46.0 n =69	99
CIP+6	488.7 ± 46.6 n = 37	492.8 ± 46.5 n =78	115
CIP+7	485.0 ± 45.2 n =42	497.8 ± 47.8 n =95	139
CIP+1 to +7	483.2 ± 44.6 n =40	498.0 ± 48.4 n =90	132
CIP+2 to +7	482.7 ± 46.1 n =33	497.7 ± 49.1 n =71	106

3. CHARACTERIZATION OF MEMBRANE PERFORMANCE FACTORS

The performance factors of aged membranes were measured to identify the impact of NaOCl exposure at bench-scale and the impact of operating conditions at full-scale.

3.1. MECHANICAL PROPERTIES

To evaluate mechanical resistance of membrane samples, uniaxial tensile tests were performed on an INSTRON 3340 series apparatus (INSTRON®, USA). The initial distance between grips was fixed at 100 mm and samples of wet membranes were extended at a constant elongation rate of 110 $mm.min^{-1}$. Maximum tensile strength, elongation at break, and Young's modulus were calculated from the experimental stress–strain curves using Bluehill 3 software. Experimental error of the maximum tensile strength indicators are under 5% and elongation at break and Young's modulus are both around 10%. For each sample, two measures were performed. An example of stress-strain curve of the pristine ZeeWeed® membrane is presented in Figure 2.21.

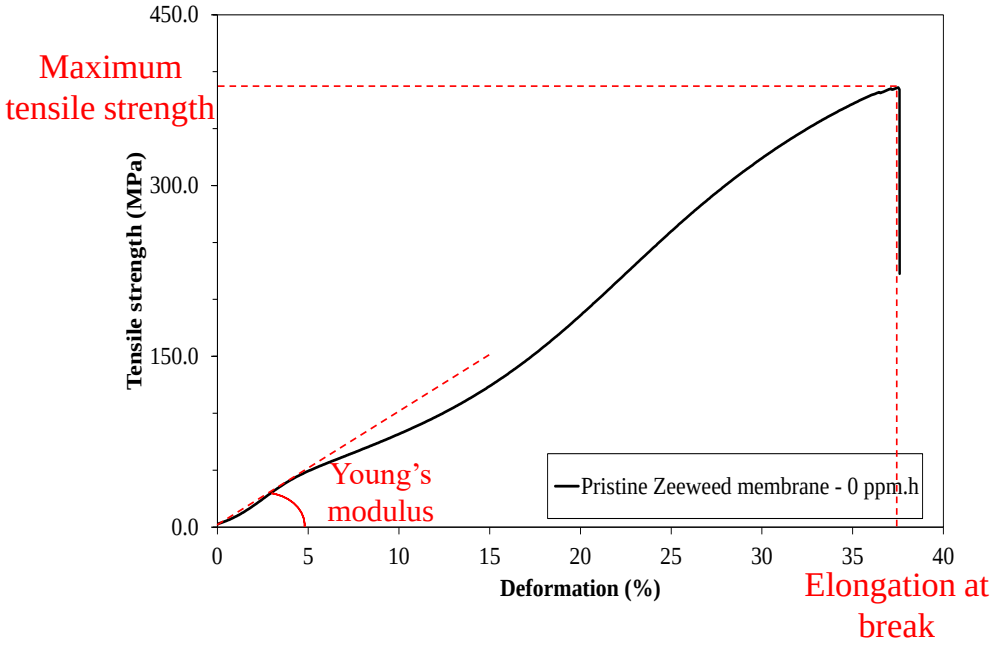

Figure 2. 21: Stress-strain curve of pristine ZeeWeed® membrane.

3.2. FILTRATION PROPERTIES

3.2.1. WATER PERMEABILITY

Intrinsic membrane permeability was measured by frontal filtration of pure water at different permeate flowrates (Q_p) in KrosFlo Research apparatus (SpectrumLab, USA). Temperature (T) is measured during the essay and permeate flux is corrected to 20°C according to Eq. 2.5 [86]. Pressures of inlet and outlet (P_{in} and P_{out}, respectively) were measured for each J_{20} to determine TMP (Eq. 2.8) and permeability (Lp/μ_{20}) was then calculated by the slope of the curve (J_{20} versus TMP) according to the Darcy's law (Eq. 2.9).

$$TMP = P_{in} - P_{out} \quad \text{Eq. 2.8}$$

$$\frac{Lp}{\mu_{20}} = \frac{J_{20}}{TMP} \quad \text{Eq. 2.9}$$

The Lp/μ_{20} values obtained for each sample were then normalized with respect to the value Lp_0/μ_{20} of a pristine membrane as the ratio Lp/Lp_0. Error propagation was calculated based on each physical quantity and precision of Lp/μ_{20} was around 11%. Experiments for each samples were performed in duplicates.

3.2.2. FOULING REVERSIBILITY

Evaluating how aged membranes would act when facing real fouling matrices is a key indicator to understand the impact of ageing in a practical way. Some studies assessed these behaviors by using model solutions for filtration tests, usually composed of bovine serum albumin (BSA), sodium alginate, and/or polysaccharides to mimic real effluents [23,24]. Only one study performed tests with real mixed liquor, and although these matrices are not standardized, these protocols are expected to be more transposable to full-scale applications [9]. In the present study, both sets of samples (bench-scale- and full-scale-aged membranes) were submitted to hydraulic cleaning recovery tests against foulants (mainly colloidal) from a real MBR mixed liquor in order to assess fouling reversibility.

To this aim, 11-cm-long modules composed of three fibers were constructed and submitted to three successive cycles of filtration and backwash of mixed liquor sample. The mixed liquor was collected from SAV-MBR recirculation channel and filtered at 1.2 µm on the same day. This colloidal suspension was stored at 4°C for a maximum of 2 weeks before use. The procedure was performed to avoid high variations in the mixed liquor characteristics over the storage time and to focus on colloidal fouling. The resulting matrix is mainly composed of the colloidal fraction typically present in an MBR mixed liquor (COD: 15.6 ± 0.8 mg O_2/L; DOC: 7.3 ± 2.4 mg C/L; KTN: 1 ± 0.1 mg N/L; NO_2: 0.07 ± 0.01 mg N/L; NO_3: 9.2 ± 1.9 mg N/L; PO_4^-: 0.17 ± 0.04 mg P/L). These experiments were conducted with a Convergence Inspector Hydra device (Convergence Industry, The Netherlands).

In order to determine the fouling reversibility, filtration was performed at 0.55 bar of TMP for 60 min, which is the maximal advised TMP for filtration by membrane manufacturer, until the permeate flux reached the pseudo-stable condition (change of flux less than 5% over a 5 min period of filtration). These conditions ensure effective fouling. Then, conditions of permeate backwash to ensure full physical cleaning recovery were tested to establish an adapted protocol. For this, backwash was performed at 0.8 bar for 15, 30 and 60 min with permeate. Backwash TMP was chosen based on the ratio between backwash and filtration TMP at full-scale MBR, which is 1.7. This ratio for the assay only reached 1.5, due to limitations of the apparatus. Permeate flowrate, pressure and temperature were continuously measured. Permeate flowrate was adjusted to flux at 20 °C. The standard filtration behavior for these tests are presented in Figure 2.22.

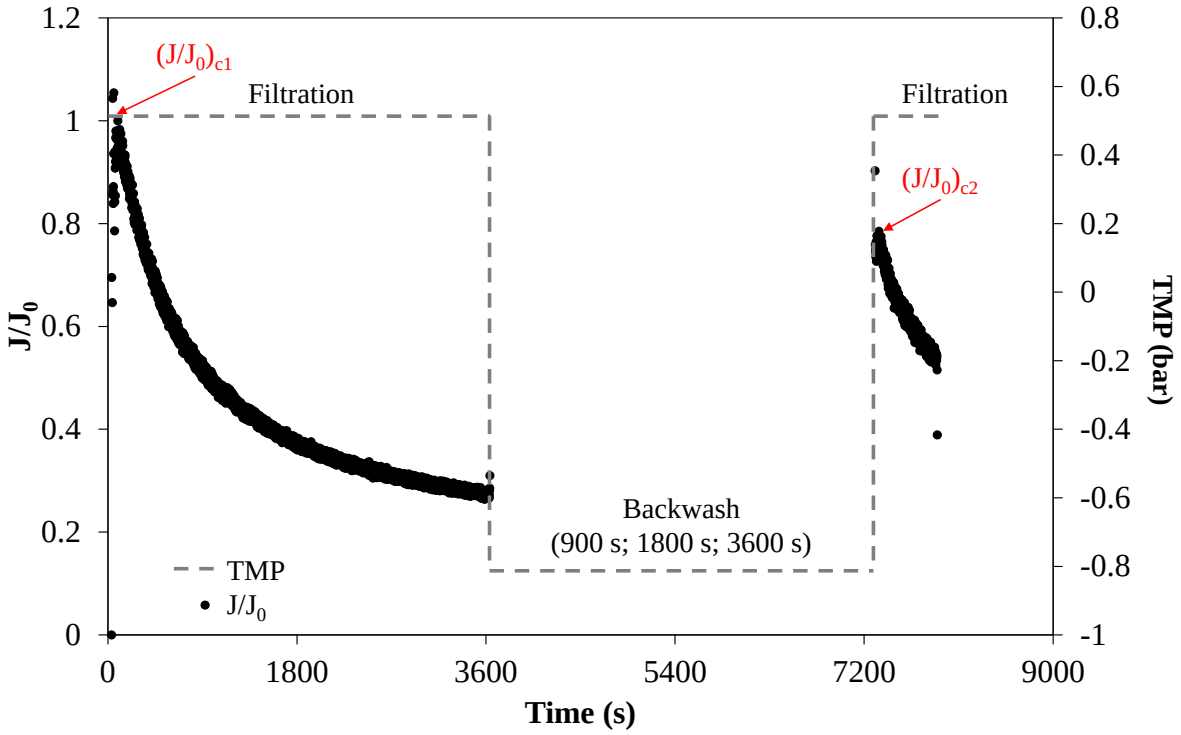

Figure 2.22: Standard behavior of the fouling reversibility test.

To evaluate the efficiency of backwashes at different duration, the cleaning recovery was calculated as Eq. 2.10, in which J_0 is the pure water permeate flux measured at a TMP of 0.55 bar. Results of cleaning recovery for each backwash duration are presented in Table 2.12. These results indicated that a 30 min backwash was the optimum duration to maximize physical recovery among the tested conditions. Thus, the protocol to determine cleaning recovery for membrane samples in this research was established with a backwashing duration of 30 min.

$$\text{Cleaning recovery (\%)} = \frac{(J/J_0)_{c2}}{(J/J_0)_{c1}} \times 100\% \qquad \text{Eq. 2.10}$$

Table 2.12: Cleaning recovery for different backwash duration.

Backwash duration (min)	Cleaning recovery
15	77 %
30	82 %
60	69%

For the determination of fouling reversibility, membrane modules of each sample were submitted to two cycles of 60-min filtration with this matrix at a fixed TMP of 0.55 bar and 30 min of permeate backwash at TMP 0.8 bar. The third filtration cycle was performed for 10 min prior to a final backwash of 30 min for practical reasons. Flowrate, pressure and temperature were automatically monitored every 2 s. Prior to these measures, membrane samples aged at bench-scale, which did not filter before, were compressed by filtration of pure water at 0.55 bar of TMP for 2 h (sufficient duration to reach a stabilized permeate flowrate).

Membranes filtered pure water for 10 min prior to the mixed liquor filtration/backwash cycles at the same TMP, and pure water permeate flux (J_0) was measured. The permeate fluxes in

mixed liquor (J) during filtration were then normalized by J_0, giving the curve J/J_0 presented in Figure 2.23.

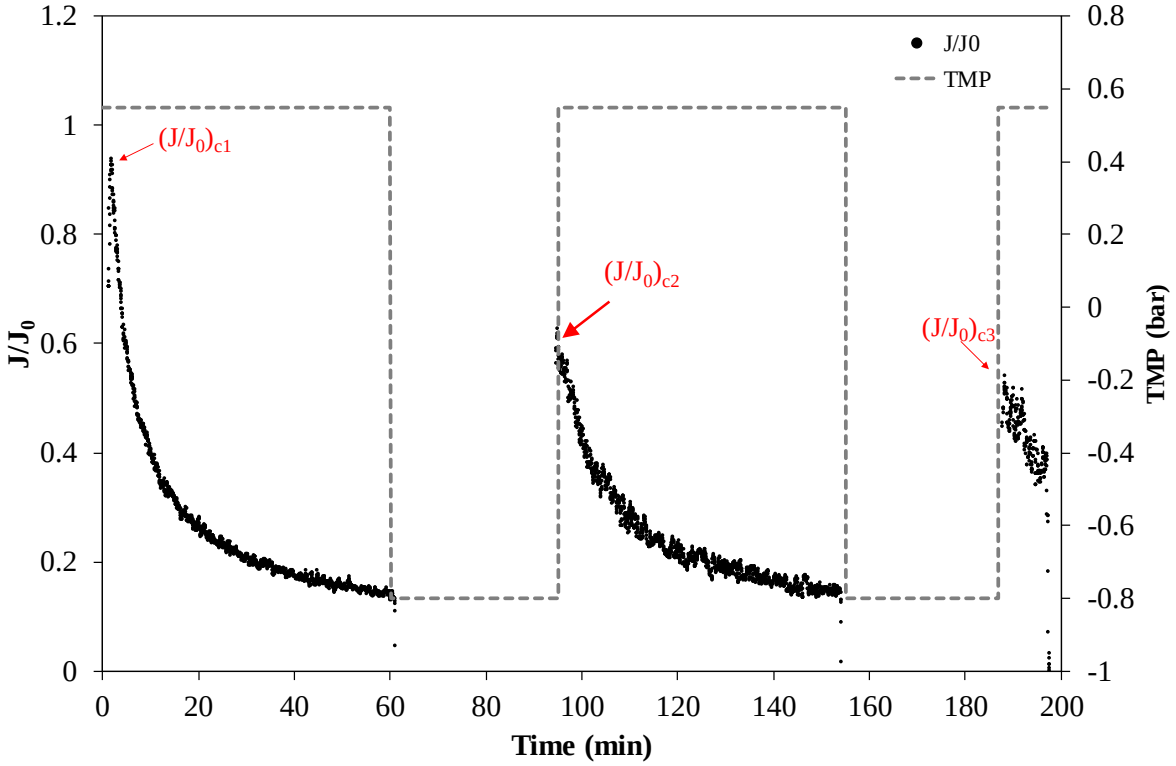

Figure 2.23: Filtration and backwash cycles in the cleaning recovery assay.

Cleaning recovery after a backwash could then be expressed as a percentage of the initial normalized flux $(J/J_0)_{c1}$. Cleaning recovery presented in this study was obtained for third filtration cycle $(J/J_0)_{c3}$ (Eq. 2.11). The experimental error of these two measures were estimated at 9 and 13%, respectively.

$$\text{Cleaning recovery c3 (\%)} = \frac{(J/J_0)_{c3}}{(J/J_0)_{c1}} \times 100\% = \frac{J_{c3}}{J_{c1}} \times 100\% \qquad \text{Eq. 2.11}$$

The cleaning recovery results allow us to estimate reversible fouling in terms of recovered filtration flux after backwash. The remaining non-recovered flux is related to the physically

irreversible fouling fraction. Cleaning recovery c3 takes into account the interactions between membrane surface and foulants, but also residual foulants and additional foulants during the second cycle of filtration, which is a more realistic approach to the behavior expected at full-scale.

4. CHARACTERIZATION OF MEMBRANE PHYSICAL–CHEMICAL PROPERTIES

In the same way as for performance factors, physical–chemical properties of aged membranes were measured to identify the impact of NaOCl exposure at bench-scale and the impact of operating conditions at full-scale.

4.1. CHEMICAL COMPOSITION BY INFRARED SPECTROMETRY

Functional chemical groups present on the material at the membrane surface were analyzed via attenuated total reflection-Fourier transform infrared (ATR-FTIR) using a Nicolet iS5 spectrometer with a germanium cell (Thermo Fisher Scientific, USA). Infrared (IR) spectra were recorded at wavelengths from 600 cm^{-1} to 4000 cm^{-1} (128 scans at 4.0 cm^{-1}). Spectral analyses were performed with OMNIC® software. For each sample, 5 spectra were performed.

These membranes are mainly composed of PVDF, which is relatively stable over chlorine exposure; besides hydrophilic agents and pore formers are added to their composition to enhance membrane filtration ability. The FTIR spectrum of a pristine ZeeWeed® membrane is presented in Figure 2.24. The PVDF fingerprint is observed by the bands at wavelengths of 1403, 1277, 1178, 1072, 880, and 841 cm^{-1}. In addition, the band around 1674 cm^{-1} is usually related to carbonyl stretches bonded to an amide group. This is a characteristic band associated with PVP used as hydrophilic agent and pore former by polymeric membrane manufacturers [82]. It is known that PVP is reactive in alkali conditions and in the presence of chlorine radicals [82]. Therefore, changes in the 1674 cm^{-1} band were studied among other changes. Since the

absorbance of the band at 1403 cm^{-1}, related to C-F bonds in PVDF is supposed to be stable over chlorine exposure, it is used to normalize changes on the absorbance of the peak at 1674 cm^{-1} to a common scale [25]. In the present study, the PVP content of each aged sample is then expressed as a percentage of the value obtained for pristine membranes. Peaks at 1590 cm^{-1} (Carboxylate), 1700/1770 cm^{-1} (succinimide) and 1720/1730 cm^{-1} (carboxylic acid) were also observed, since they are supposed to be either related to PVP degradation products or residual fouling [12].

In case of full-scale aged membranes, the residual fouling agents are different compounds in mixed liquor that may present peaks in the range between 1600 – 1700 cm^{-1}. However, since membranes are thoroughly cleaned before analysis, the effects of these compounds are supposed to be minimized in the spectra.

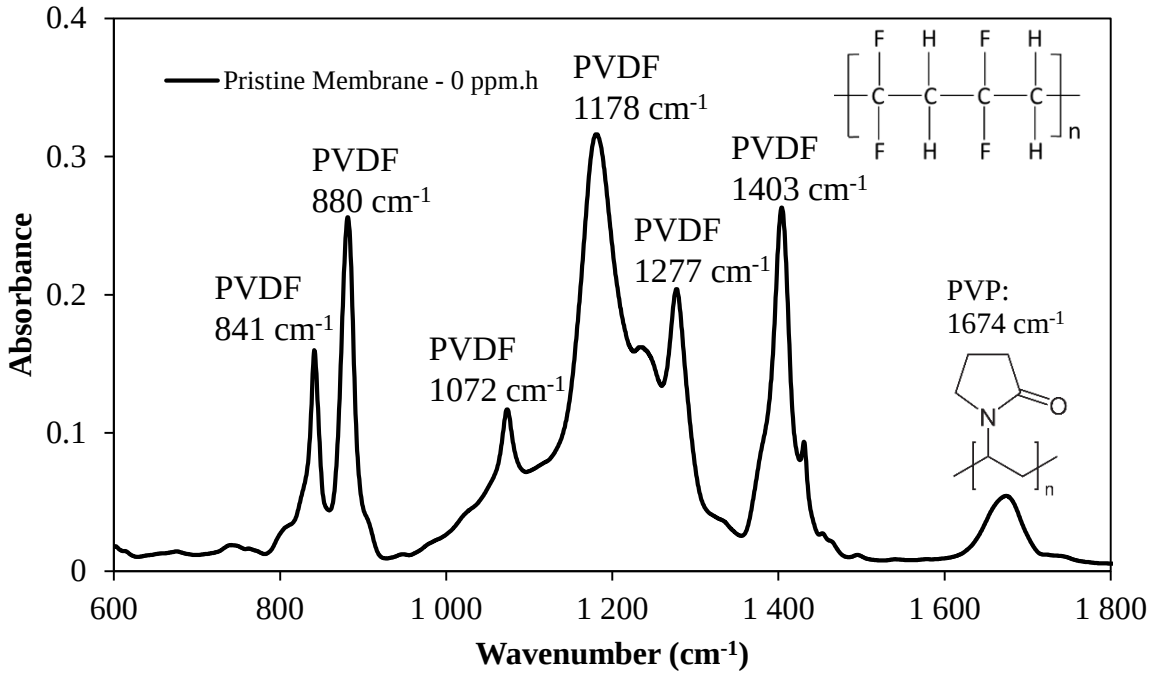

Figure 2.24: FTIR spectra of a pristine ZeeWeed® membrane.

4.2. SURFACE WETTABILITY

Membrane surface wettability was characterized indirectly by contact angle measurements using the captive bubble method, which was previously described by Pellegrin et al. (2013) [81]. This method is used instead of the sessile drop technique in the case of porous materials to avoid capillarity effects and it provides a more realistic measure as the membrane surface is kept in wet conditions [81]. For these measurements, PVDF surface skin from samples was first peeled off from the support material and fixed on a microscope slide, then immersed in the measuring cell filled with water. 10 measures were performed by sample and the experimental error is around 13%. This method was only applied to bench-scale samples as peeling off did not allow us to recover a piece of intact skin from the full-scale samples, and measurements on the whole hollow fiber led to large errors due to their concave surface.

4.3. PORE SIZE AND VOLUME

Porous volume and pore size distributions were measured by nitrogen adsorption for both bench-scale- and full-scale-aged samples. Membrane samples of 0.2 g were oven dried at 40 °C for 72 h and placed in the measurement chamber. Measurements were carried out once for each sample at 77 K in a Belsorp apparatus (Microtrac MRN, Germany). The sorption isotherms can be used to determine porous volume and pore size distribution by the BJH model [88].

4.4. SURFACE MORPHOLOGY BY SCANNING ELECTRON MICROSCOPY

Scanning electron microscopy (SEM) was performed using a Hitachi TM3030. Firstly, random pieces of membranes from each sample were dried for 48h at 40°C then coated with 5 nm of gold. Then, images with an optical magnification of 60× and 500× were acquired in order to qualitatively evaluate the topographic aspects of the membranes.

5. STATISTICAL ANALYSIS

All statistical analyses were conducted in R software and XLStat (Microsoft Office, USA) [89]. Normality tests (Shapiro-Wilk), principal compound analysis and correlation tests presented in Chapter 3 were performed in R software for membrane autopsies. The normality tests (Shapiro-Wilk), PCA and correlation tests for the relationships among process data and autopsies presented in Chapter 4 were performed in XLStat.

6. CONCLUSIONS

This chapter detailed the experimental tools used to quantify the evolution of PVDF membrane properties over ageing process.

The following chapter applies most of these methods to characterize membrane samples aged at bench-scale by chemical action (NaOCl) and full-scale in MBRs to establish how ageing changes membrane properties in these two scales.

CHAPTER 3: COMPREHENSIVE STUDY OF SUPPORTED PVDF MEMBRANE AGEING IN MBR: A DIRECT COMPARISON BETWEEN CHANGES AT BENCH-SCALE AND FULL-SCALE

1. INTRODUCTION

Studies usually simplify membrane ageing by accelerating it by single soaking in a hypochlorite solution and by observing the changes in membrane properties [9–22]. Recently, some studies quantified the representativeness of accelerated ageing at bench-scale towards ageing in drinking water facilities [25,26]. With regard to membranes used in MBR, the evaluation of the representability of single soaking accelerated ageing is still lacking. In MBR, parameters such as more frequent cycles of filtration/backwashing, aeration, mixed liquor more charged in foulants, could have a greater impact on membrane ageing than the solely chemical action of sodium hypochlorite. Therefore, this chapter aims to establish the representativeness of accelerated membrane ageing by single soaking of pristine membrane at bench-scale (1000 ppm; pH 9.0) with respect to full-scale MBR operation. In parallel, membrane samples were harvested from the membrane tank UF3 of SEM-MBR from 2016 to 2021, corresponding to 7 years of operation since the date of commissioning (2014). In terms of hypochlorite exposure dose, these samples ranged from 33,000 ppm.h to 100,000 ppm.h.

For that, the following approach was carried out:

- Quantifying and understanding membrane ageing, i.e. changes in membrane properties, by sole sodium hypochlorite contact and under operating conditions at full-scale MBR;
- Highlighting the differences between these two processes and discussing explicative hypothesis.

Data presented in this chapter were published in the journal Separation and Purification Technology [29].

2. RESULTS

First, the changes in performance factors, namely, mechanical and filtration properties, are presented for both ageing at bench scale and at full scale (section 2.1). Then, the physical–chemical properties are evaluated in order to establish cause–effect relationships (section 2.2). Finally, these changes due to sodium hypochlorite contact and MBR operating conditions are discussed further in sections 3.1 and 3.2, respectively.

2.1. IMPACT OF AGEING ON MEMBRANE PERFORMANCE FACTORS AT BENCH SCALE AND FULL SCALE

2.1.1. MECHANICAL PROPERTIES

Regarding mechanical resistance, pristine ZeeWeed® 500D membranes presented an ultimate tensile strength of 395.8 ± 13.7 MPa, ultimate elongation of 40.5 ± 4.2 % and Young's modulus of 1075.2 ± 114.5 MPa.

At bench scale, membranes were single soaked in sodium hypochlorite between 0 and 750,000 ppm.h of exposure dose. This exposition did not cause statistically significant changes in the ultimate tensile strength as seen in Figure 3.1.A (Kruskal test, p = 0.468). This stability was also observed in percent ultimate elongation (Figure 3.1.B). Moreover, Young's modulus slightly increased between 0 and 60,000 ppm.h, then stabilized around 1200 MPa (Figure 3.1.C).

Regarding membranes aged at full scale, the ultimate tensile strength and Young's modulus showed a 45% and a 33% decline, respectively, over the study time that corresponds to a cumulative exposure dose to hypochlorite of 100,000 ppm.h (Figure 3.1.A and C). Nevertheless, operators did not report significant fiber breakage during the whole operation

period. Ultimate elongation was stable for all samples, but lower than samples aged at bench-scale (Figure 3.1.B).

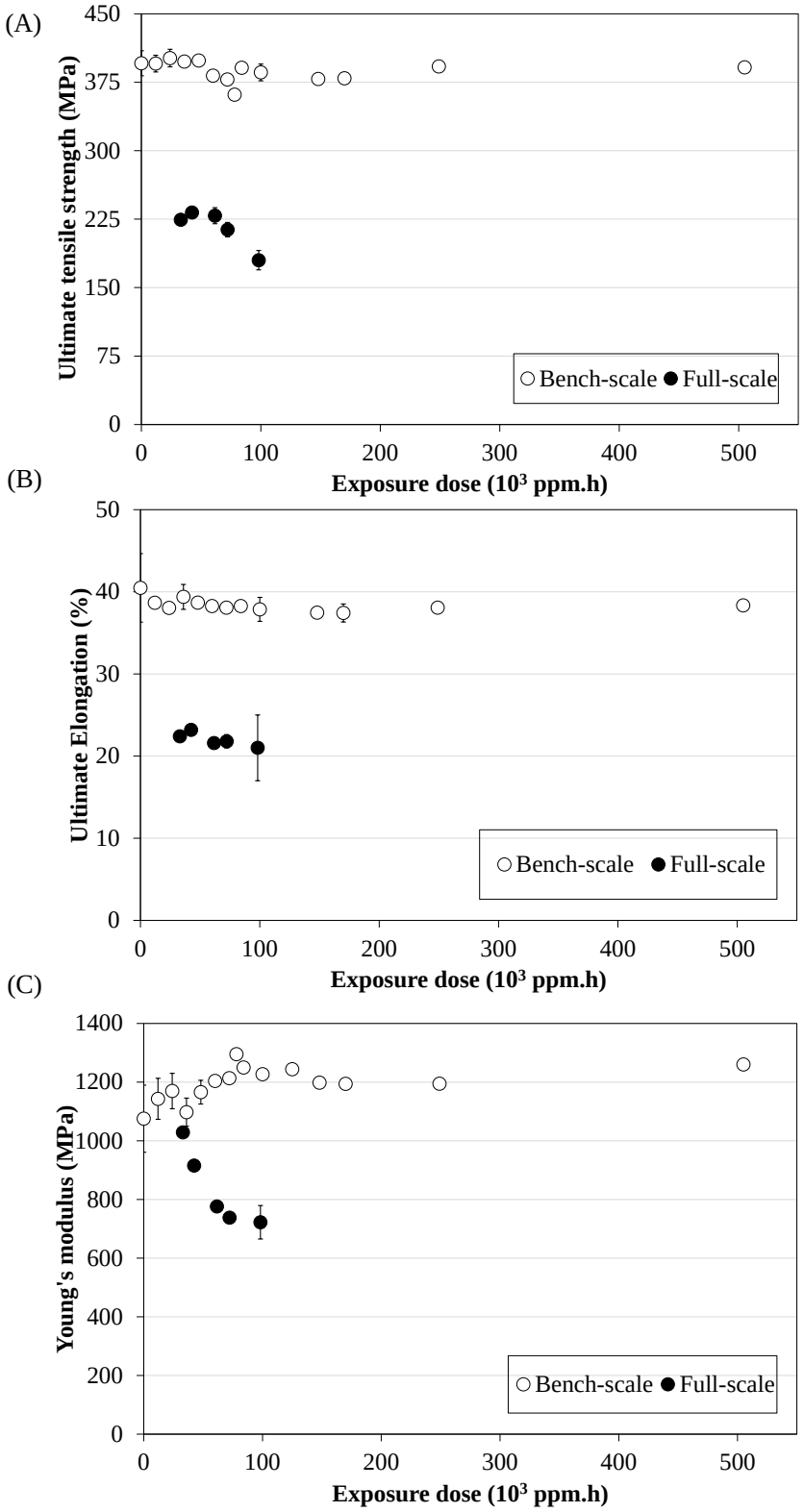

Figure 3.1: Ultimate tensile strength (A), Ultimate elongation (B) and Young's modulus (C) for bench-scale- and full-scale-aged membranes as a function of the cumulative exposure dose to hypochlorite.

2.1.2. FILTRATION PROPERTIES

Intrinsic membrane permeability

Pristine membranes presented an intrinsic permeability of 1222.1 ± 156.0 LMH/bar. Thus, intrinsic membrane permeability of aged membranes is presented in Figure 3.2 as a ratio between the values obtained on aged and pristine membranes (Lp/Lp_0) with respect to the exposure dose to hypochlorite. Error bars represent experimental error.

For ageing at bench scale, these results can be divided into three phases. The first phase, corresponding to membranes exposed to a dose C × t of up to 78,000 ppm.h, showed an increasing trend until reaching 1.9 times the initial permeability. The second phase (C × t = 78,000 – 150,000 ppm.h) presented a decreasing Lp/Lp_0 ratio; and in the third phase, after 150,000 ppm.h, samples' intrinsic permeability reached a plateau at a value comparable to the one of the pristine membrane.

Moreover, the Lp/Lp_0 ratio of membranes at full scale showed an increasing trend with C × t (and the associated time of operation), although to a lesser intensity than bench-scale-aged samples, at least during the 7 years of data collection in the present research.

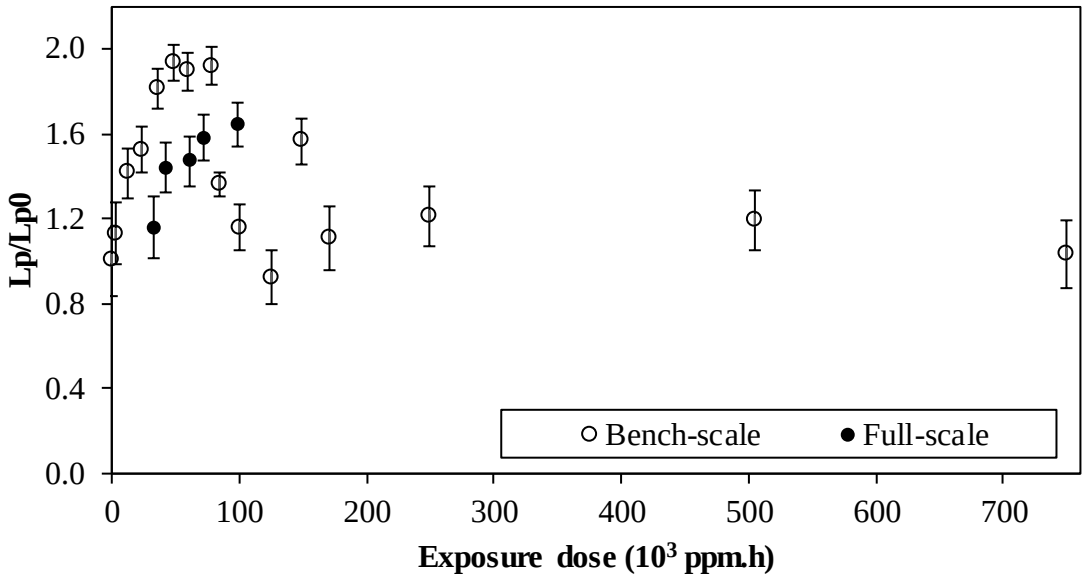

Figure 3.2: Changes in intrinsic permeability of samples aged at bench-scale and full-scale with respect to virgin membrane permeability (Lp/Lp0 ratio) as a function of the cumulative exposure dose to hypochlorite.

Cleaning recovery

Mixed liquor fouling reversibility was performed using a pre-filtered mixed liquor (at 1.2 µm) to focus mainly on the colloidal fouling. However, salts can also be present. Three cycles of filtration and backwashing were performed and cleaning recovery was defined as the recovered flux in the beginning of the third cycle with respect to the first one (as detailed in Chapter 2).

Pristine membrane recovered 56% of its flux. Samples aged at bench-scale reached 65% at 24,000 ppm.h and remained stable up to 125,000 ppm.h; subsequently, samples exposed to 500,000 ppm.h experienced a decline to a value of 51% (Figure 3.3). When comparing these values with those obtained for full-scale aged samples (Figure 3.3), we found that cleaning recovery was always higher in samples aged at bench-scale, regardless of the exposure dose

value. In addition, full-scale harvested membranes showed a decline from 39% to 32% in cleaning recovery when the C × t increased from 33,000 to 100,000 ppm.h.

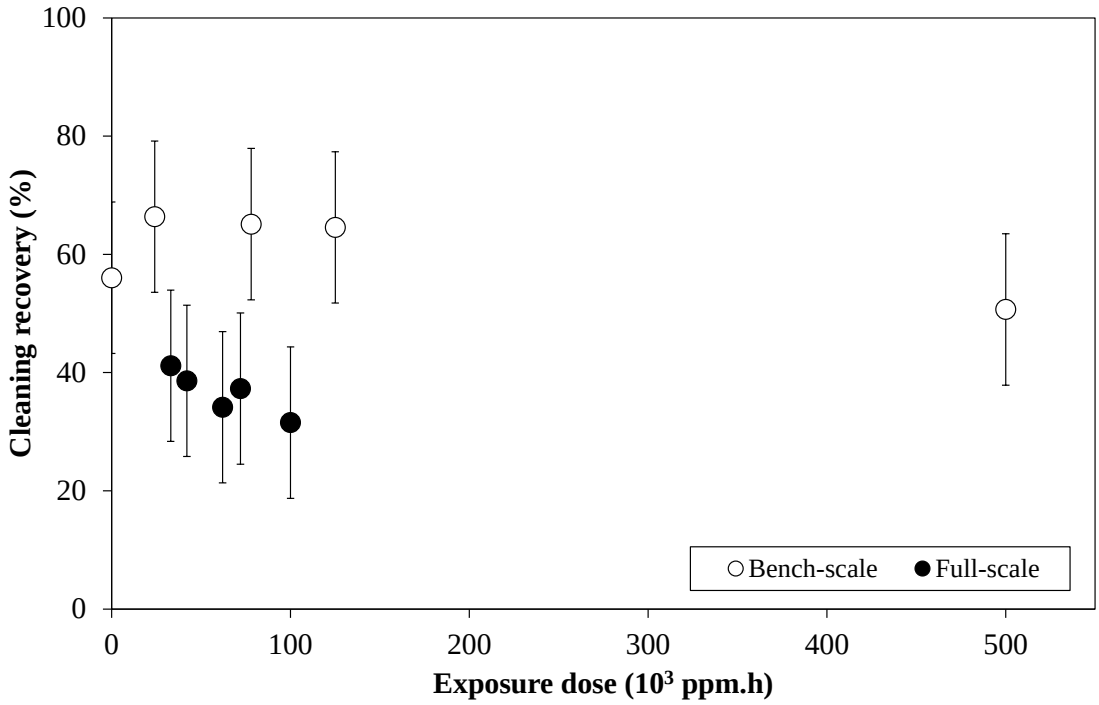

Figure 3.3: Cleaning recovery (%) after two cycles of filtration and hydraulic backwash on membranes aged at bench scale and at full scale as a function of the cumulative exposure dose to hypochlorite. Error bars represent experimental error.

2.2. IMPACT OF AGEING ON MEMBRANE PHYSICAL–CHEMICAL PROPERTIES AT BENCH SCALE AND FULL SCALE

2.2.1. MEMBRANE SURFACE CHEMISTRY

Surface functional groups by ATR-FTIR

The external skin of the pristine ZeeWeed® membrane was analyzed by ATR-FTIR and the IR spectrum is presented in Figure 3.4. The spectrum presented confirmed the PVDF fingerprint, with characteristic peaks of alpha-phase PVDF (875, 1070 and 1181 cm^{-1}) and beta-phase PVDF (841, 1274 and 1403 cm^{-1}) [16]. Moreover, it presented a band at around 1674 cm^{-1}, which may be related to carbonyl stretches bonded to the amide group in the PVP chain, which is used in these membranes to increase hydrophilicity.

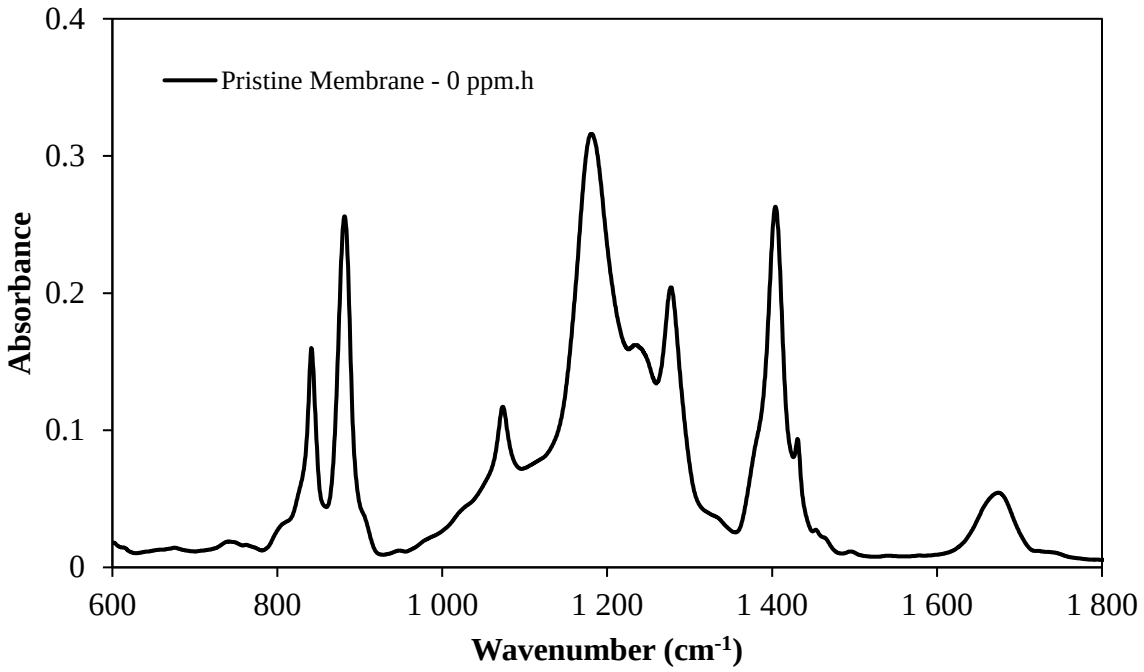

Figure 3.4: IR spectrum of a pristine ZeeWeed® membrane.

The same analysis was performed on membranes aged at bench-scale and at full-scale (Figure 3.5.A). An enlarged view of the characteristic region of PVDF is presented in Figure 3.5.B. The IR spectra in this figure confirmed, during NaOCl exposure in the dose range investigated in the present study from 33,000 to 500,000 ppm.h, a relatively good stability of the peaks at 841, 875, 1070, 1181, 1274 and 1403 cm^{-1} which characterize PVDF. However some variations may

be observed. Considering Figure 3.5.C, which presents a zoom in the 1500-1800 cm^{-1} interval for bench-scale aged membranes, we can observe the growth of a band at 1650 cm^{-1}. PVDF is well-known for its chemical stability. However, in alkali media, an alteration in chemical composition of PVDF can be observed, associated with the dehydrofluorination reaction. The dehydrofluorination process, an ionic mechanism, is mainly indicated by the occurrence of the peaks at 1650 cm^{-1} assigned for carbon-carbon double bond and 2100 cm^{-1} for the carbon-carbon triple bond [66]. In the case under study the band at 1650 cm^{-1} can then be attributed to carbon-carbon double bonds formation in PVDF structure. Similar results were obtained by Ravereau et al. (2016), study in which the modifications in FTIR spectra at 1650 cm^{-1} were low but visible even if the hypochlorite solution pH studied were around the neutrality (6.0 and 7.5). The authors confirmed some crosslinking and chain scissions using size exclusion chromatography and nuclear magnetic resonance analyses [17]. Rabuni et al. (2015) also observed the appearance of a peak at 1650 cm^{-1} on PVDF membranes exposed to NaOCl 0.01 M for 60 min or 0.1 M for 20 min, but the authors underlined a low peak signal [8]. If now we consider Figure 3.5.D presenting a zoom in the 1500-1800 cm^{-1} interval for full-scale aged membranes, no peak appeared at 1650 cm^{-1}, indicating that at full-scale, on the range of exposure dose studied, PVDF chemical alteration is not observed.

By contrast, PVP is generally highly reactive in alkali conditions or in the presence of oxidative radicals. Moreover, it is known that the wave numbers between 1500 and 1800 cm^{-1} concentrate most of the signals related to PVP degradation products [82]. Therefore, this zone is enlarged in Figure 3.5.C and D for both bench-scale and full-scale ageing, respectively. The PVP content, quantified through the intensity of the band at 1674 cm^{-1}, on bench-scale- and full-scale-aged membranes is presented with respect to the one on pristine membrane in Figure 3.6 as a function of C × t. It is worth noting that, although full-scale samples may present residual fouling (1730

cm^{-1}) [12], measurements of PVP and degradation product peaks, except for by-products presenting carboxylic acids (1730 cm^{-1}), were still possible. Both sets of membranes (bench and full-scale) showed a decline in PVP content that can be associated with either its removal from the membrane structure and/or to its degradation into other by-products. Pellegrin et al. (2013) among others also observed decreasing PVP content in PES/PVP membranes during exposure to hypochlorite solution (pH 6, 8 and 11; NaOCl concentration 350 ppm) [74,81]. In addition, Ravereau et al. (2016) aged PVDF membranes with and without hydrophilic agent in sodium hypochlorite (pH 6 – 11.5 concentration of 4000 ppm NaOCl) and also obtained a decline in the 1674 cm^{-1} band for membranes that contained hydrophilic agent [17]. However, Figure 3.6 shows that for bench-scale samples after 78,000 ppm.h exposition, PVP content seemed to reach a plateau at around 50% of the initial value on pristine membrane.

The decline in PVP content for full-scale-aged membranes seemed to follow the same trend observed at bench scale for C × t values lower than 78,000 ppm.h, except for the first sample at 33,000 ppm.h, which presented higher PVP content. For higher C × t values, the PVP content continued to decrease reaching 25% of the initial content (Figure 3.6).

(A)

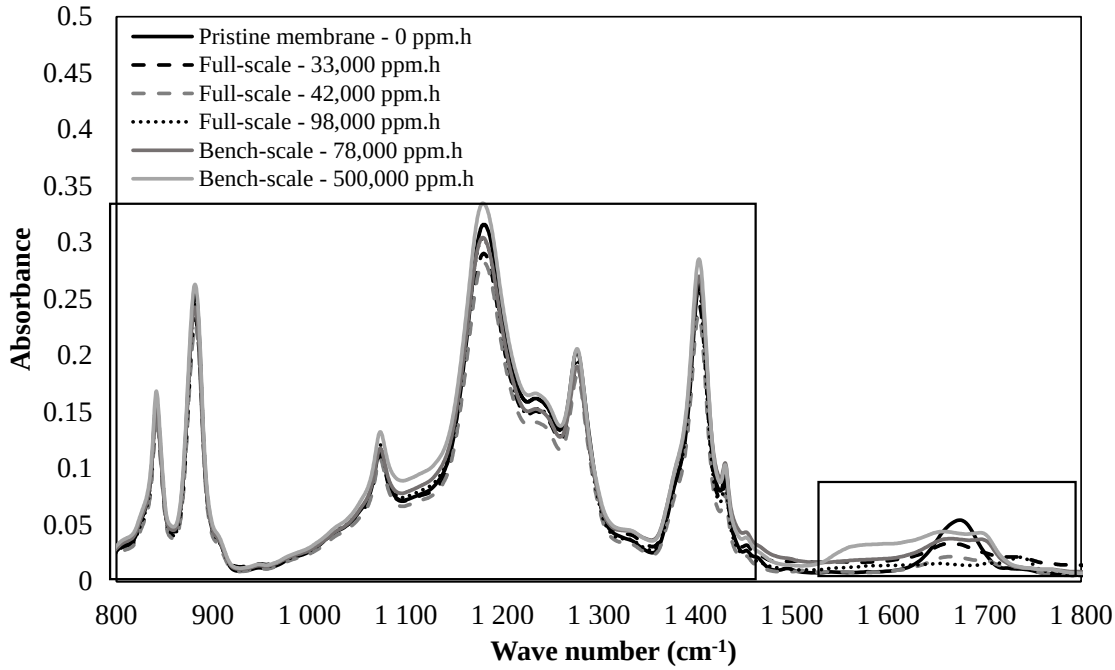
Pristine membrane - 0 ppm.h
Full-scale - 33,000 ppm.h
Full-scale - 42,000 ppm.h
Full-scale - 98,000 ppm.h
Bench-scale - 78,000 ppm.h
Bench-scale - 500,000 ppm.h
Absorbance
0.5
0.45
0.4
0.35
0.3
0.25
0.2
0.15
0.1
0.05
0
800
900
1 000
1 100
1 200
1 300
1 400
1 500
1 600
1 700
1 800
Wave number (cm-1)

(B)

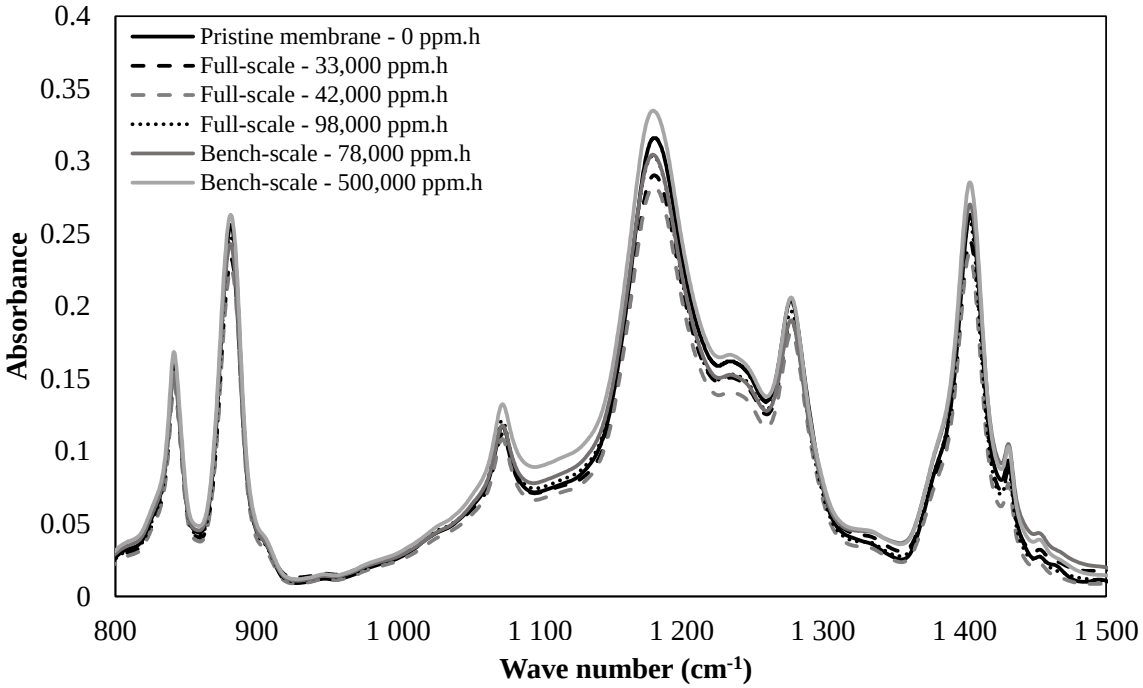
Pristine membrane - 0 ppm.h
Full-scale - 33,000 ppm.h
Full-scale - 42,000 ppm.h
Full-scale - 98,000 ppm.h
Bench-scale - 78,000 ppm.h
Bench-scale - 500,000 ppm.h
Absorbance
0.4
0.35
0.3
0.25
0.2
0.15
0.1
0.05
0
800
900
1 000
1 100
1 200
1 300
1 400
1 500
Wave number (cm-1)

(C)

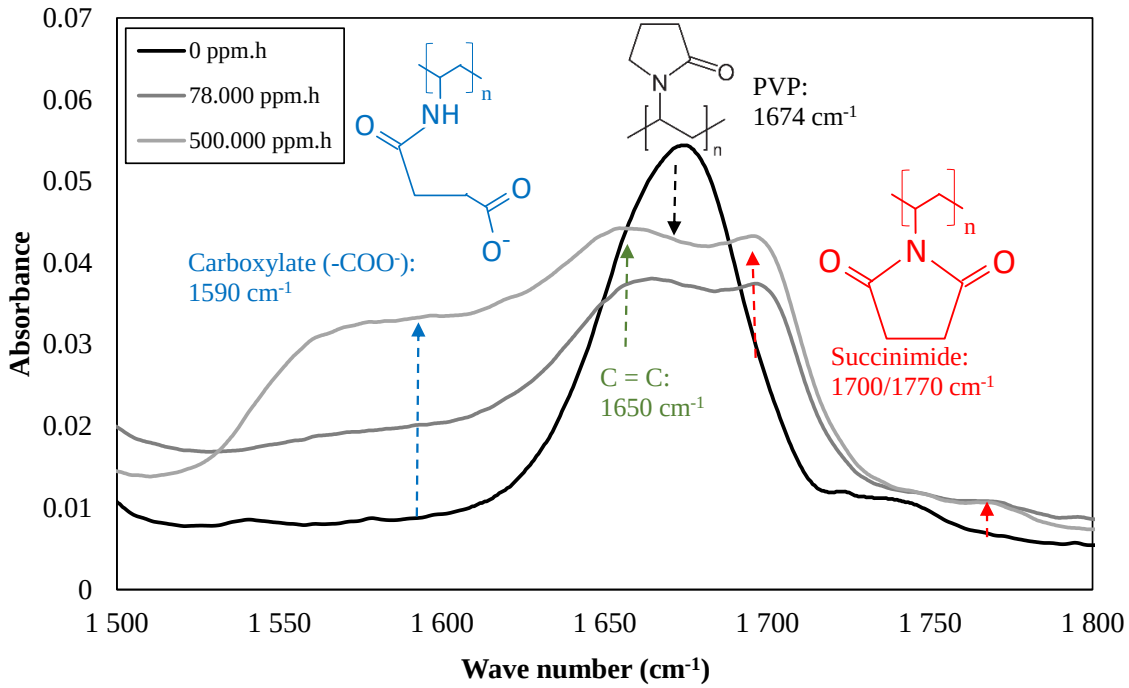

(D)

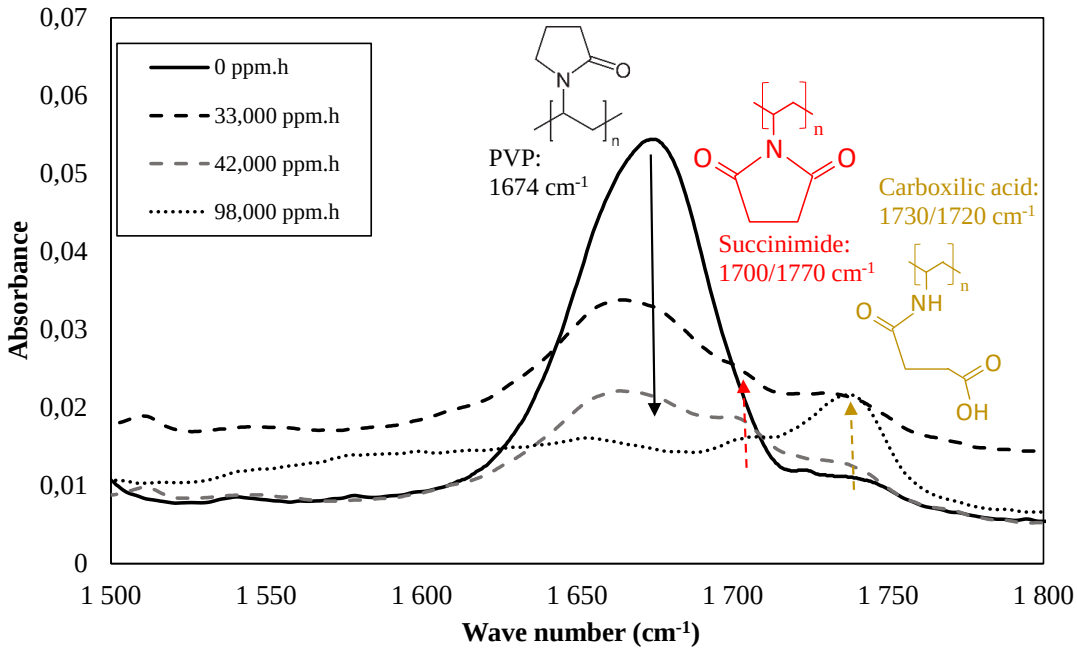

Figure 3.5: Full-range FTIR spectra (600–1800 cm-1) of membranes aged at bench-scale and full-scale (A) and enlarged view of the characteristic region of PVDF (B) and PVP and its degradation products (1500–1800 cm-1) for samples aged at bench-scale (C) and at full-scale (D).

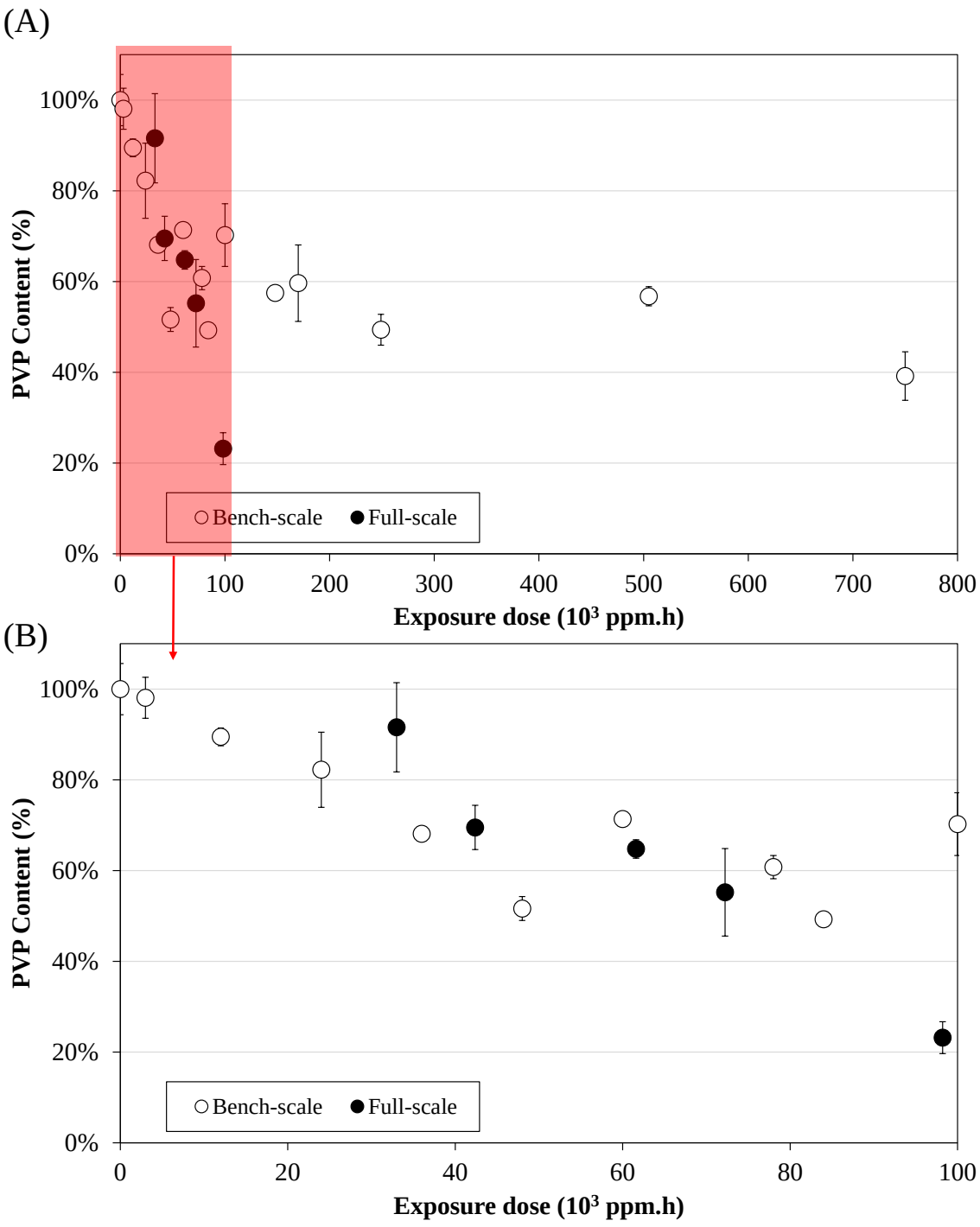

Figure 3.6: Change in PVP content in bench-scale and full-scale-aged membranes as a function of the full range of exposure dose (A) and a zoom in the zone between 0 and 100,000 ppm.h (B).

Wettability

Contact angle measurements using the captive bubble method were performed to evaluate the effects of hypochlorite exposure on wettability of pristine and bench-scale aged membranes. The obtained value of contact angle is an average of ten measurements taken in different locations on the membrane skin peeled off from the support material. The pristine membrane presented a contact angle of 39 ± 4°. This value increased to 45 ± 4° at 12,000 ppm.h, then decreased to 40 ± 5 at 24,000 ppm.h and remained stable for higher doses. Statistical analysis showed that sodium hypochlorite exposure at bench-scale had no significant influence on the contact angle (Kruskal–Wallis test, $p = 0.1041$).

Contact angle measurements on full-scale samples were not performed as these analyses at macroscopic scale would not only characterize intrinsic wettability of membrane material, but would be also influenced by residual fouling. In addition, skin peeling off was not possible for membranes harvested from full-scale.

2.2.2. MORPHOLOGICAL PROPERTIES

Pore volume and pore size distribution

Regarding morphological properties, results of pore volume and pore size distribution measurements by nitrogen adsorption are presented in this section. The results of pore volume as a function of pore diameter (dp) are presented in Figure 3.7 for membranes aged at bench-scale (A) and at full-scale (B). Regarding the pore volume of bench-scale aged membranes (Figure 3.7.A), an increase in porosity is first noted up to 78,000 ppm.h. For higher exposure doses to hypochlorite 125,000 and 500,000 ppm.h, it seems that a collapse or a reorganization in the membrane material structure promoted a decline in pore volume which takes a value lower than the one of the pristine membrane. Moreover, these changes in total pore volume

seem to be governed by an initial increase followed by a decline in the zone of small pores (dp < 20 nm, gray zone). Measurements are performed by nitrogen adsorption, which takes into consideration membrane surface and bulk material, so overestimation of these values are possible, however these overestimations are applied for all samples.

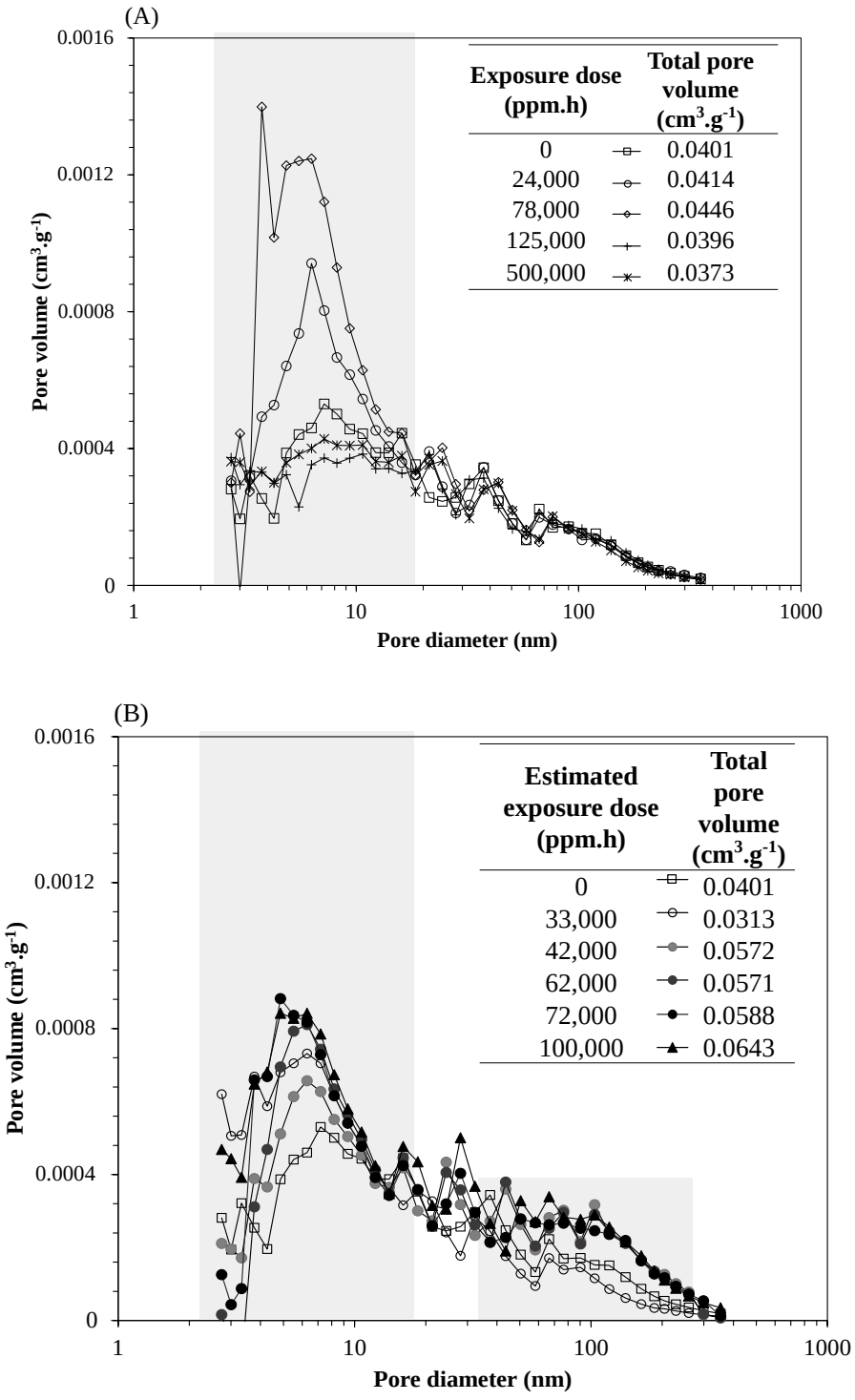

Figure 3.7: Pore volume and size distribution of aged membranes at bench-scale (A) and at full-scale (B) as a function of the exposure dose to hypochlorite.

For membranes ageing at full-scale (Figure 3.7.B), although samples harvested in the early phase of ageing (33,000 ppm.h) have a slightly lower total porous volume compared to pristine membrane, a huge increase in pore volume was observed in the whole range of exposure dose investigated. In parallel, similarly to bench-scale aged membrane in the exposure range 0-78,000 ppm.h, an increase in the number of small pores was observed. In addition, samples aged for 42,000 ppm.h showed an increasing number of larger pores (dp > 40 nm). These two zones are highlighted in gray in Figure 3.7.B.

SEM images

SEM images were performed for both sets of samples, which might provide some qualitative information about surface morphology of these membranes. It is worth noting that image analysis are not able to differentiate surface pits from true pores. Comparing SEM images of the pristine membrane (Figure 3.8.A) to the bench-scale aged sample at 78,000 ppm.h (Figure 3.8.B), an increase in the number of pores is noticeable. For the sample aged at 500,000 ppm.h the number of pores seemed to decrease. Roughness does not seem to change for bench-scale aged membranes. On the other hand, images from full-scale aged samples qualitatively confirmed the appearance of the larger pores (Figure 3.9.C). In addition, an increase in surface roughness can be observed when comparing full-scale aged samples to bench-scale-aged ones or to the pristine membrane.

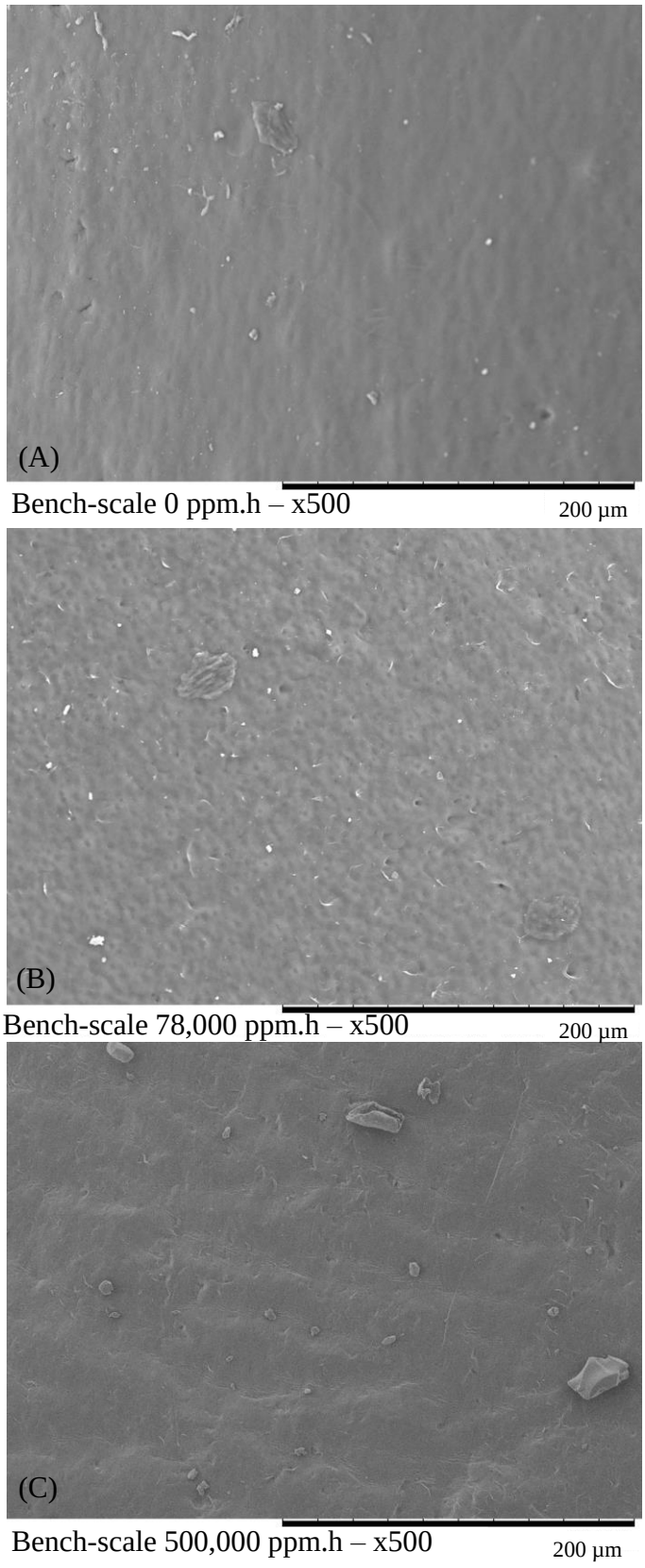

Bench-scale 0 ppm.h – x500

Bench-scale 78,000 ppm.h – x500

Bench-scale 500,000 ppm.h – x500

Figure 3.8: SEM images zoomed at x500 for pristine membranes (A), bench-scale aged membranes at 78,000 ppm.h (B), and 500,000 ppm.h (C).

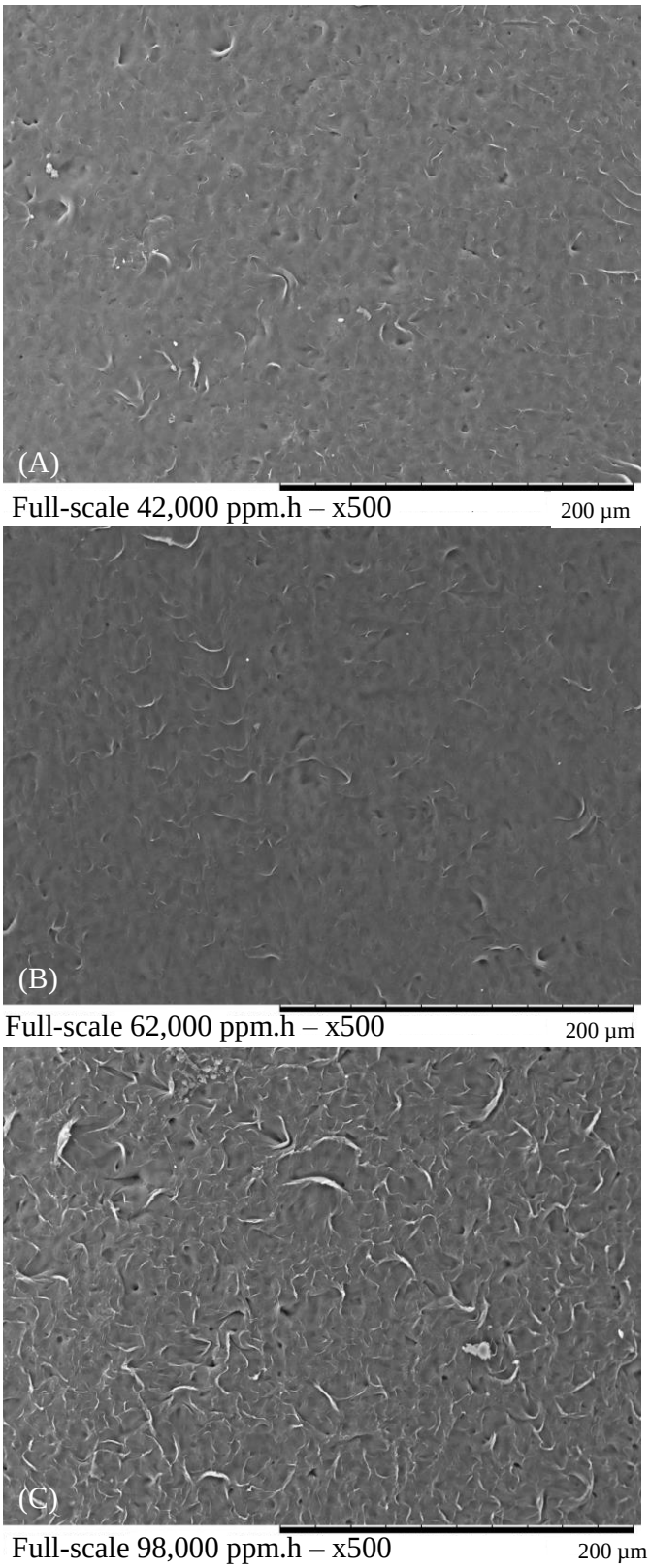

Figure 3.9: SEM images of full-scale aged samples harvested after 42,000 ppm.h (A), 62,000 ppm.h (B) and 98,000 ppm.h (C) chlorine exposure doses.

3. DISCUSSION

3.1. SODIUM HYPOCHLORITE IMPACT ON MEMBRANE PERFORMANCE

FACTORS AT BENCH-SCALE

Impact of NaOCl chemical ageing on mechanical resistance

In the case of supported membranes, mechanical resistance is mainly linked to the material used to support PVDF. By ATR-FTIR analysis, it was found that the supporting material of these membranes had 68% accordance with PET. PET is often used as a support material for ultrafiltration membranes. However, only few studies of membrane ageing characterized its mechanical resistance. Pulido et al. (2019) evaluated the properties of recycled PET-based membranes and concluded that the material was chlorine resistant after a 2-h exposure to a 5000 ppm hypochlorite solution [90]. However, the effects of long-term exposure were not determined. The results of bench-scale-aged samples in the present research indicate that the long-term exposure to NaOCl (static soaking of 20 days in 1000 ppm NaOCl) does not impact the mechanical properties at break (ultimate tensile strength and ultimate elongation) of these supported hollow fibers, but fibers became a slightly more rigid with chlorine exposure. Conversely, Wang et al. (2018) characterized hypochlorite aging of membranes reinforced with PET nonwoven fabric and found a slight decline in ultimate tensile strength. It is worth noting that these membranes when pristine exhibited ultimate tensile strength in the range of 40 MPa, which is around 10 times less resistant than the fibers used in the present study (395.8 ± 13.7 MPa). Therefore, the support used in ZeeWeed® membranes presents a mechanical resistance capable to withstand long exposure to hypochlorite.

Impact of NaOCl chemical ageing on intrinsic permeability

Changes in water permeability of bench-scale-aged membranes can be associated mainly with: (i) changes in the surface physical–chemical characteristics, especially hydrophobicity and electrical charges and (ii) modifications in skin porosity (pore size and number).

The first phase of increasing permeability between 0 and 78,000 ppm.h presented in Figure 3.2 was found to be linked to the decline in PVP content observed in Figure 3.6. Statistical analysis confirmed a significant correlation in this dose range between both parameters, giving a correlation coefficient (r) of -0.951 (p = 0.0003, Pearson correlation test). Despite the decline in PVP content, the contact angle values did not change significantly. In fact, this parameter is not only influenced by hydrophilic agent content, but also by electrical charges on the membrane surface and by morphological aspects such as surface roughness. When in contact with NaOCl, the PVP cyclic group, pyrrolidone, is opened forming carboxylates. As a result, membranes may increase their negative charges as they age. Recently, Li et al. (2021) confirmed the increase in negative charges on PVDF/PVP membranes during exposure to NaOCl [13]. Thus, changes in membrane wettability due to an increase in hydrophobicity may be counter-balanced by an increase in electrical surface charges. This was observed by Pellegrin et al. (2015) on hypochlorite aged PES/PVP membrane [71]. As a consequence of this combined effect, membrane permeability is not expected to be significantly impacted by changes in surface physical–chemical properties, which oblige to look after another source of evolution in permeability observed in the present study.

Morphological properties were thus evaluated. Regarding the change in membrane skin porosity for exposure dose up to 78,000 ppm.h, a formation of small pores (d_p < 20 nm) is observed in Figure 3.7.A, enhancing overall membrane porosity. In fact, FTIR spectra (Figure 3.5.C) showed that PVP molecules are not fully dislodged from the membrane structure. They are instead oxidized into succinimide (at 1700/1770 cm^{-1}) and carboxylates (1590 cm^{-1})

following the PVP degradation mechanism proposed by Prulho et al. (2013) [82]. These molecules remained (totally or partially) in the membrane structure, possibly leading only to the formation of small pores, whereas a full PVP dislodgement would lead to the formation of macro-voids. By contrast, some works in the literature concluded that NaOCl exposure causes PVDF membrane permeability to increase as a result of a pore enlargement due to the oxidation and dislodgement of PVP from the fiber structure for exposure doses ranging from 10,000 ppm.h to 2,000,000 ppm.h [20,23]. These observations were found based on rejection tests and SEM images, which may be impacted by chemical interactions between probe molecules and membranes and characterize surface pits as true pores, respectively. However, Ravereau et al. (2016) similarly to us reported an increasing volume of pores smaller than 10 nm, only for PVDF commercial membranes containing PVP when exposed to sodium hypochlorite at doses as high as 13,000,000 ppm.h, whereas PVDF membranes with no additive did not show any changes in pore size distribution [17]. Hence, our results demonstrated that in the range of exposure dose up to 78,000 ppm.h, ZeeWeed® membranes permeability increase is controlled by the appearance of small pores due to partial dislodgment of PVP and of its by-products.

After the exposure threshold of 78,000 ppm.h, the decline in Lp/Lp_0 was no longer correlated with PVP content. It is then assumed that the degradation and dislodgment of the PVP within PVDF matrix increases not only the free volume of the membrane structure but also the molecular mobility [24]. PVDF chemical alteration being observed on these bench–scale aged membranes (Figure 3.5.C), we then conclude that at a certain exposure dose (here 78 000 ppm.h) the membrane structure changed possibly due to a reorganization of the polymeric chains in membrane skin, decreasing pore volume and Lp/Lp0 as a result. A statistically significant correlation was found between Lp/Lp_0 and the volume of smaller pores for the whole range of C × t studied (r= 0.966, p = 0.008, Pearson correlation test).

Impact of NaOCl chemical ageing on cleaning recovery

Similarly to water permeability, cleaning recovery is also impacted by the physical–chemical properties of the membrane surface and by its porosity.

Pore volume did not correlate well with cleaning recovery ($p > 0.05$). This indicates that the increase in number of small pores observed up to 78,000 ppm.h of exposure dose did not change the fouling mechanisms. This make sense as these new pores are added to the main pore population around 10 nm in size present on pristine membrane, maintaining the same foulants size to pore size ratio.

Cleaning recovery can also be related to the interactions between foulants and membrane surface. Firstly, cleaning recovery slightly increased from 0 to 24,000 ppm.h of ageing at bench-scale then became stable after 24,000 ppm.h, indicating that foulants became less attached to the membrane surface, i.e., increasing fouling reversibility. Irreversible fouling is mainly related to organic matter adsorption on the membrane surface, which is explained by the extended Derjaquin–Landau–Verwey–Overbeek (DLVO) theory as a synergic work of Van der Waals force, polar force, and electrostatic interactions. Foulants in mixed liquor are mostly organic matter that are hydrophobic and negatively charged at neutral pH [91]. As previously mentioned, aged membranes hydrophobicity may increase due to PVP content decrease. This should contribute to higher adsorption of organic matter. However, at the same time, negative charges on aged membranes may increase, leading to higher electrostatic repulsions between the membrane surface and foulants and weakening the membrane-foulants interactions. The initial slight increase in cleaning recovery observed in the present study on samples aged at bench-scale (from 0 to 25,000 ppm.h) seems to show that the effect of electrostatic interactions is predominant by comparison to hydrophobic interaction one.

For samples exposed to higher exposure dose (500,000 ppm.h), cleaning recovery dropped to 51%. Although they are less apparent on bench-scale samples than on full-scale one (Figures 3.8 and 3.9 respectively), we hypothesize that topographic changes (potential increase in roughness) may be playing a bigger role favoring foulant adsorption, as reported by Levitsky et al. (2011). These authors observed that this increase in roughness correlated well with an increase in protein adsorption onto the membrane surface [12].

3.2. MEMBRANE AGEING UNDER MBR OPERATING CONDITIONS AT FULL SCALE

Impact of full-scale operation on mechanical resistance

Regarding mechanical resistance, membranes aged by single soaking in hypochlorite solutions did not experience the weakening observed for the membranes under full-scale operation (Figure 3.1). These findings suggest that an effect of mechanical stress (under aeration and/or filtration conditions) in MBR may be the reason for the decline in ultimate tensile strength. However, the precise mechanism behind these changes could not be assessed and further studies are needed.

Concerning the membrane skin, we remind here that although other studies reported embrittlement of PVDF due to dehydrofluorination and chain scission after exposure to NaOCl (70,000 – 12,000,000 ppm.h) [16,17,23], in the present study FTIR spectra failed to confirm changes in the PVDF functional groups at full-scale (0 ppm.h – 750,000 ppm.h, Figure 3.5.B and D) while PVDF chemical changes were visible at bench-scale (Figure 3.5.C).

Concerning the membrane support, which is the main responsible for membrane mechanical resistance, the functional groups showed no changes on the PET fingerprint (1124 and 1240 cm^{-1}) in the IR spectra (Figure 3.10).

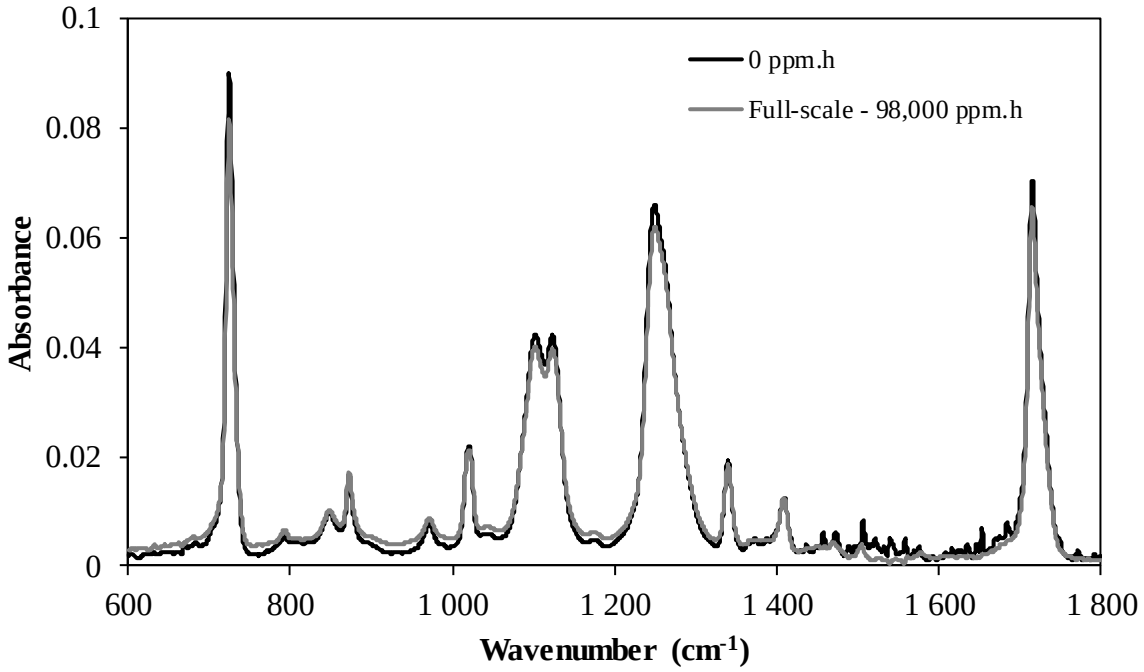

Figure 3.10: Infrared spectra of support material of pristine and full-scale aged ZeeWeed® membranes after peeling off PVDF skin.

However, alterations in the support polymer crystalline structure, crosslinking/chain breakage, and material fatigue could be the reasons for mechanical resistance decline without significant modification of the polymer fingerprint on its IR spectra. Techniques such as, size exclusion chromatography, thermogravimetric analysis and differential scanning calorimetry were already reported as effective tools to measure these kind of changes [17,24] and would have to be considered for go further in the analysis.

The membrane weakening observed on samples aged at full-scale could lead to fiber breakage, which could degrade the filtration quality. Nevertheless, operators reported no changes in the

permeate quality (no suspended solids measured in permeate) over 7 years of operation despite the decline in mechanical resistance.

Impact of full-scale operation on PVP degradation

The mechanisms of PVP degradation are also different between bench-scale and full-scale ageing (Figure 3.5.C and D, respectively). At bench scale (Figure 3.5.C), the sole effect of hypochlorite (pH 9.0) induced the production of carboxylate and succinimide from the chemical attacks to PVP molecules. At exposure doses between 100,000 and 500,000 ppm.h, these degradation products remained in the membrane structure while the non-oxidized PVP was maintained around 40 – 50% of the pristine membrane PVP content (Figure 3.6). At full scale (Figure 3.5.D), the PVP peak (1674 cm^{-1}) was strongly suppressed, reaching 20% of the initial content at an exposure dose of 98,000 ppm.h (Figure 3.6.B). Additionally, the typical peaks associated with by-products did not seem to increase to the same extent, with only a slight appearance of the succinimide peak (1700 cm^{-1}) being observed, suggesting that part of the PVP was oxidized into succinimide and then removed from the membrane structure by leaching. In addition, a peak at 1730 cm^{-1} (carboxylic acids) was formed, which can be assigned either to a PVP degradation product or to residual fouling. For the former, Prulho et al. (2013) reported that carboxylates (1590 cm^{-1}) are favored under alkali conditions [82], which is the case in the present study for the whole ageing process at bench-scale. At full-scale, membranes are cleaned by sodium hypochlorite followed by citric acid solutions at a pH between 2.5 and 3.0, which might favor the formation of carboxylic acids versus carboxylates in the PVP degradation process. In addition, the remarkable increase of the peak at 1730 cm^{-1} for samples aged at 98,000 ppm.h at full-scale might be associated to the extensive PVP degradation and formation of carboxylic acids. For the latter, it is worth noting that this carboxylic acid peak may be assigned

to residual proteins, which are present in the mixed liquor and contribute to the irreversible membrane fouling, as reported by Levitsky et al. (2011) [12].

Several studies compared PVP degradation in different ageing protocols. For instance, Causserand et al. (2015) found no significant differences in PVP content decline between single-soaked membranes and membranes submitted to filtration/backwash cycles using NaOCl solution at bench scale [70]. In addition, Robinson and Bérubé (2021) investigated the hydrophilic agent content of (i) membranes single-soaked, (ii) membranes submitted to cyclic NaOCl filtration at bench-scale and to (iii) full-scale ageing in drinking water facilities. These authors also reported no significant differences in the decrease of hydrophilic agent content whatever the ageing procedure [25]. However, the impacts related to specific MBR operating conditions were not assessed in such ageing studies. In direct filtration facilities for drinking water production, membranes are usually trapped inside their housing. In comparison, ZeeWeed® fibers in MBR modules are potted on both ends but not stretched under tension, thus being able to oscillate when aeration cycles are performed. These cycles usually occur for 10 s with aeration and between 10 – 30 s with no aeration to remove foulants during filtration and cleaning protocols, by increasing shear stress at the membrane surface and convective forces. These operating conditions might also enhance dislodgement of hydrophilic agent and its degradation products from the membrane structure.

Impact of full-scale operation on intrinsic permeability

Fibers harvested from a full-scale MBR seemed to experience an increasing Lp/Lp_0 for the whole study period (Figure 3.2), highlighting two main differences when compared to the sole hypochlorite action at bench scale: (i) permeability increased to a lesser extent and (ii) no

decline in Lp/Lp_0 was experienced in the exposure dose range studied. Both residual fouling and the differences in porosity changes can be related to these results.

(i) For the first point, membranes operating at full scale still showed high amounts of PVP in the early stages (up to exposure dose 33 000 ppm.h), which was considered the main driver for permeability changes. Moreover, these membranes experience fouling, which is partially removed by chemical cleanings. However, the later appearance of bigger pores may enhance residual fouling in the long term as more organic matter is able to flow through and be adsorbed into the membranes (Figure 3.7). This may increase membrane hydrophobicity [23] and despite the increasing porosity, water is hampered to flow through membranes, whereas membranes aged by single-soaking in NaOCl solution did not experience fouling, which enables the permeability to increase to higher values. By comparing the changes in permeability of membranes exposed only to sodium hypochlorite with membranes that went through cycles of a model fouling solution filtration and sodium hypochlorite cleaning at bench scale, Hajibabania et al. (2012) confirmed the smaller increases among the latter samples, assigning this difference to residual fouling [23].

In addition to the previous discussion, the C × t value is used as a reference for comparison between bench-scale and full-scale ageing, but it is worth noting that at full-scale, NaOCl species are reacting not only with membrane polymers but also with the organic matter. In addition, plant operators reported declines in free chlorine concentrations of up to 30% over CIP soaking time. As in this study the C × t was calculated considering a stable free chlorine concentration over the CIP soaking time, this may have led to an overestimation of the actual C × t to which the membranes are really exposed at full-scale. To avoid this probable overestimation in C × t for full-scale samples, the relationship between PVP content and Lp/Lp_0 is plotted in Figure 3.11 for both sets. For the same PVP removal, the increase in Lp/Lp_0 in

samples aged at bench scale is higher than for full-scale-aged membranes. This illustrates the role of the different pore size distributions and residual fouling, which impairs the increase in Lp/Lp_0.

It is worth noting that the lack of decline in permeability at full-scale should be confirmed by additional samples in the later phases of membrane's lifetime.

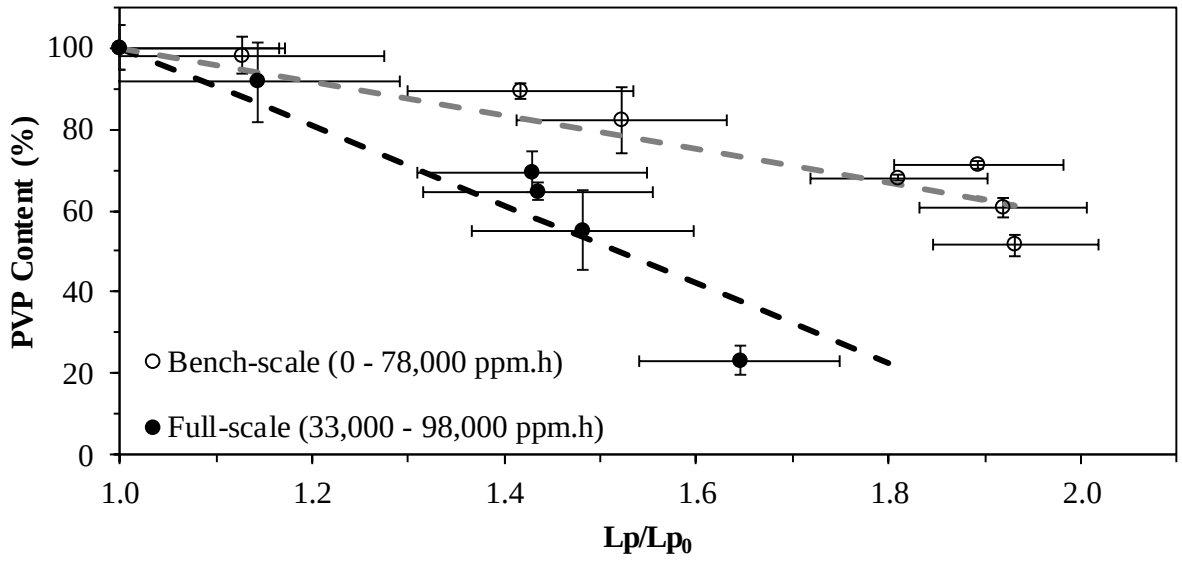

Figure 3.11: Relationship between PVP content removal and the changes in Lp/Lp0 for membranes aged at bench-scale and at full-scale.

(ii) For the second point, the lack, at full-scale, of a permeability-declining phase for higher exposure dose might be linked to the difference in the ageing process. Concerning the PVP, at bench scale, it was degraded until its content reached approximately 40% of the pristine fibers (Figure 3.6), and the PVP by-products seemed not to be fully dislodged from the polymer structure (Figure 3.5.C), leading to the appearance of only smaller pores (Figure 3.7). On the other hand, samples of full-scale-aged membranes continued to lose PVP, reaching 25% of the

pristine membrane (Figure 3.6). This change along with the FTIR spectra in the PVP and its degradation product region (Figure 3.5.D) might indicate that PVP is not only degraded but also dislodged from the membrane structure, leading to the appearance of bigger pores as presented in Figure 3.7.B. The operating conditions in MBR such as cyclical aeration and backwashes certainly contribute to the dislodgement enhancement at full-scale of hydrophilic agent and its by-products from the membrane structure. A study of Akhondi et al. (2017) has also shown that cyclical backwashes induce mechanical stresses to the membrane material that contribute to the increase in pore size and as a consequence to an increase in permeability [92]. Another difference in the ageing process in the range of exposure dose investigated, is the absence of PVDF chemical changes at full-scale. Therefore, despite the noticeable increase in the free volume due to the degradation and dislodgment of the PVP within PVDF matrix, no reorganization of the polymeric chains in membrane skin occurred. This reorganization was supposed to be responsible for the decrease in permeability at bench-scale. This difference in PVDF stability between bench-scale and full-scale requires further analysis to determine the actual mechanisms involved.

The relationships between (i) PVP content and total pore volume (r = -0.864, p = 0.026, Pearson's test), (ii) total pore volume and Lp/Lp_0 (r = 0.904, p = 0.014, Pearson's test), and (iii) PVP content and Lp/Lp_0 (r = -0.930, p = 0.007, Pearson's test) were confirmed to be statistically significant. These results highlight the importance of the hydrophilic agent content in preserving the membrane filtration properties. Moreover, they illustrate that changes in Lp/Lp_0 are mostly governed by changes in pore size for either bench-scale or full-scale ageing.

Impacts of full-scale operation on cleaning recovery

The lower overall values of cleaning recovery for full-scale-aged membranes and its declining trend (Figure 3.3) can be ascribed to: (i) stronger interactions between foulants in mixed liquor and with residual fouling remaining on the membrane surface; (ii) much rougher surface as shown on SEM images (Figure 3.9), which enhances fouling especially by adsorption [12]; (iii) and the appearance of larger pores that can lead to higher amounts of matter inside the membrane structure causing more severe pore clogging, which is a less reversible form of fouling than floc adhesion or cake formation [48].

Statistical analysis were performed for changes in bigger pore volumes (>40 nm) and smaller pore volumes (<20 nm), separately, with respect to cleaning recovery and no significant linear correlations were found ($p > 0.05$). Ultimately, changes in cleaning recovery correlated well with the loss of hydrophilic agent and with the increase in Lp/Lp_0 ($r = 0.819$, $p = 0.046$ and $r = -0.897$, $p = 0.015$, Pearson's test, respectively).

Since permeability correlated well with all other parameters, MBR operators should apply the measurement of Lp after CIP as an in situ diagnostic tool for membrane ageing. For increasing values, operators should expect a build-up of hydraulic irreversible fouling, which would lead to an increasing requirement for chemical cleanings. In addition, hydrophilic agent degradation seems to be the primary cause for all the other changes and as in situ FTIR measurements are becoming available, it could also provide important information on membrane ageing in MBR operation.

Figure 3.12, below, illustrates the changes in membrane properties during ageing at bench-scale and at full-scale found in this research. In addition, the conclusions that could be drawn from this chapter are presented afterwards.

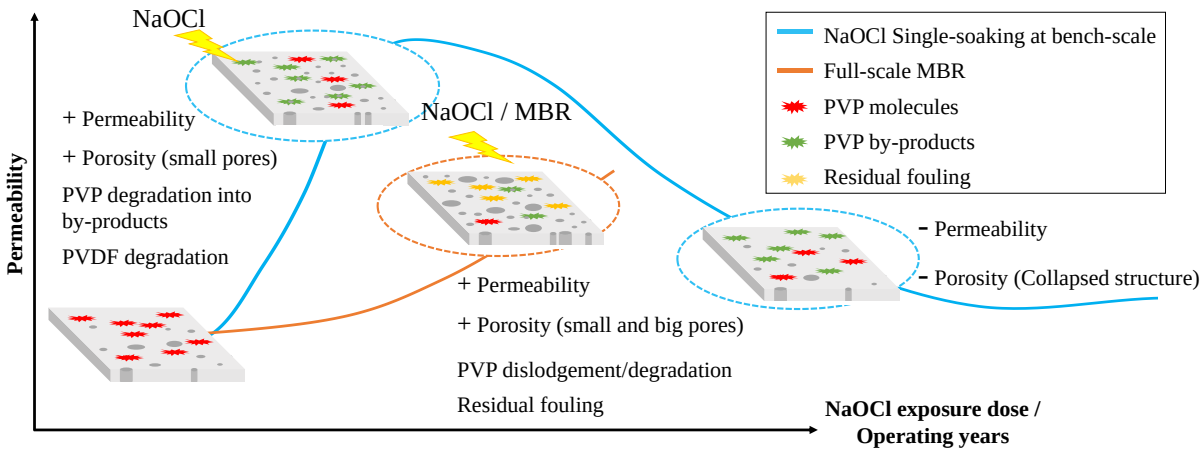

Figure 3. 12: Illustration of changes in membrane properties during ageing at bench-scale by NaOCl single soaking and at full-scale MBR.

4. CONCLUSIONS

The main conclusions deduced from the results obtained and discussed in this chapter can be summarized as:

- Differences in the membrane ageing process for membranes aged by single soaking in NaOCl solution and during a 7-year period in an MBR treating municipal wastewater are highlighted by applying the same methodological protocol. A non-negligible contribution of filtration conditions, mechanical stress due to aeration and backwashes, and residual fouling, specific to full-scale operating conditions, may significantly change ageing mechanisms. This study showed that understanding the mechanisms behind the action of NaOCl on PVDF membranes may not represent what actually occurs at full-scale operation and does not replace continuous autopsies of harvested fibers over the years or monitoring of consistent full-scale operation indicators.
- At bench scale, NaOCl species caused PVP oxidation, which led to the formation of small pores causing an increase in Lp/Lp_0 in contrast to the generally accepted

hypothesis of pore enlargement reported in the literature. For exposure doses higher than 78,000 ppm.h, the membrane material seems to submit a re-arrangement, which is made possible by PVDF chemical alteration, leading to a decrease in Lp/Lp_0.

- In contrast to bench-scale ageing, full-scale-aged membranes experienced a decline in mechanical resistance due to MBR operating conditions, i.e., aeration, filtration and backwash. In addition, bigger pores are formed as a result of a more pronounced degradation of PVP when compared to bench-scale ageing, which ultimately led to an increasing Lp/Lp_0 during the study period. At the same time, in the range of exposure dose investigated, no PVDF chemical alteration was observed.
- The increase in Lp/Lp_0 with age in full-scale samples is less intense than in bench-scale samples for the same PVP removal as a result of residual fouling on the membrane surface that also led to a decline in hydraulic cleaning recovery. Thus, the presence of organic matter at the membrane surface would play a protection role when the membrane is exposed to hypochlorite.
- Lp/Lp_0 and PVP content correlated well with all ageing changes among full-scale samples and can be applied for full-scale MBR operators as nondestructive in situ tools to monitor membrane ageing.
- Since the major changes seemed to be related to PVP oxidation, efforts are needed to change membrane formulations in order to achieve a stronger bond between PVP or other hydrophilic agents and the main polymer.
- Since bench-scale ageing protocols are not fully representative of full-scale MBR ageing, an accelerated ageing protocol at pilot-scale would be useful for validating long-term membrane performance.

- Changes in membrane properties from full-scale MBR are becoming available. Thus, efforts into membrane ageing modelling are needed to perform predictive calculations of the long-term ageing effects in MBR operation.
- The correlation between membrane properties changes and filtration performance data directly from process sensors would be useful to monitor ageing from an operational standpoint.

CHAPTER 4: IMPACT OF FULL-SCALE MBR OPERATING CONDITIONS ON MEMBRANE AGEING AND MONITORING TOOLS

1. INTRODUCTION

Monitoring membrane ageing is crucial for plant operators, in order to schedule WWTP's downtime due to membrane replacement. Depending on the operating conditions in MBRs, we expect that the changes in membrane properties may differ, but results are lacking in the scientific literature. Studies about membrane ageing hardly ever consider the chronological operating conditions that membranes experience during their lifetime. Therefore, the aim of this chapter was to evaluate the impacts of operating conditions on membrane properties and create oriented process indicators to monitor membrane ageing. Samples of membranes were harvested from two similar MBRs in the wastewater treatment facilities of Seine Aval (SAV), designed to treat 200 000 m^3/d since November/2017, and Seine Morée (SEM), designed to treat 50 000 m^3/d since May/2014, and operated by SIAAP.

Firstly, chronological data regarding operating conditions are presented for both MBRs, then cumulative indicators regarding membrane operation are calculated. This is followed by the analysis of the changes in membrane properties for membranes harvested during the period of this research. Finally, the filtration performance in the long-term is assessed directly by process data (mainly permeate flux and transmembrane pressure) to establish process oriented indicators to monitor membrane ageing.

2. MBR CHARACTERISTICS AND OPERATING CONDITIONS

2.1. CHARACTERISTICS OF INFLUENTS

The quality characteristics of influents and effluents and performances of the studied MBRs are compared in this section. Chronological data was collected from May/2014 to January/2021 for SEM-MBR and from November/2017 to June/2021 for SAV-MBR. The main characteristics of influents for both MBRs considered in this study are presented in Table 4.1.

Table 4.1 Quality characteristics of influents (after pre-treatment) from SEM-MBR (data from May/2014 to January/2021) and SAV-MBR (data from November/2017 to June/2021).

		Influent's characteristics	
Parameter	**Units**	**SEM-MBR**	**SAV-MBR**
TSS	(mg / L)	332.9 ± 107.5	123.0 ± 43.2
COD	(mg O_2 / L)	694 ± 166	311 ± 92
BOD_5	(mg O_2 / L)	299.3 ± 74.6	123.0 ± 37.8
Total Kjeldahl Nitrogen (TKN)	(mg N / L)	68.3 ± 14.0	46.0 ± 9.8
NH_4	(mg N / L)	49.8 ± 12.2	33.4 ± 8.5
Total Nitrogen (TN)	(mg N / L)	69.3 ± 14.0	47.0 ± 9.7
Total phosphorus (TP)	(mg P / L)	7.5 ± 1.6	4.5 ± 1.1
PO_4^{3-}	(mg P / L)	4.2 ± 1.2	2.2 ± 0.9
pH	-	7.8 ± 0.2	7.7 ± 0.2
Temperature	(°C)	-	19.1 ± 3.3
TAC	(mg CO3/L)	-	216.2 ± 42.3

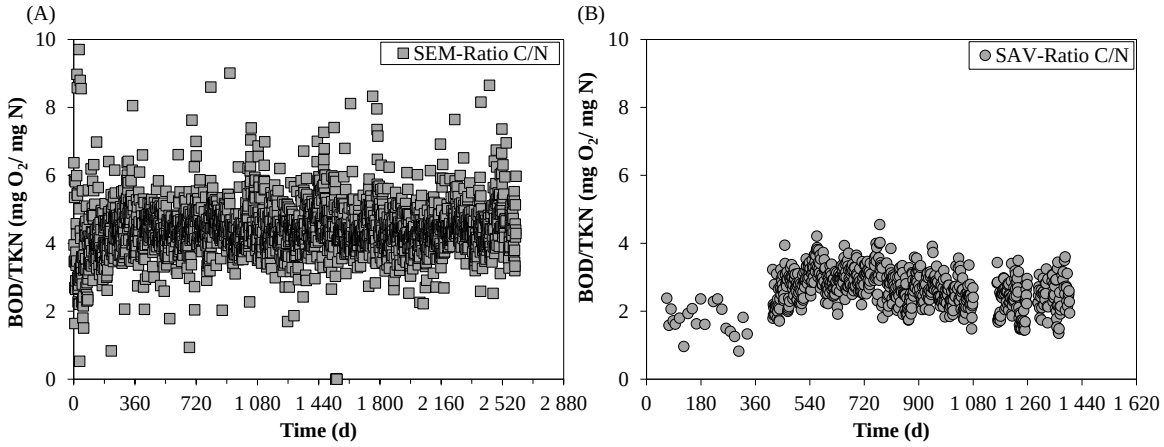

Figure 4.1 Ratio BOD_5/TKN for SEM (A) and SAV (B) MBR.

SEM presented a more concentrated influent, in terms of carbon and nitrogen. The BOD/TKN ratio (Figure 4.1) from SEM is also higher than SAV (4.4 ± 0.9 and 2.6 ± 0.6, respectively). These differences are mainly linked to the differences in pre-treatment processes applied on each WWTP, since SAV WWTP is composed of a higher performance (in terms of solid/liquid

separation) settling tank based on the injection of microsand and coagulants (Actiflo®, Veolia water technologies, France), compared to a lamellar settling tank.

2.2. MBR OPERATING CONDITIONS

MBR's operating conditions are also important in membrane ageing studies, since they are related to the characteristics of fouling, which triggers chemical cleanings and the combination of all these events lead to membrane ageing. The chronological behavior of the main operating conditions for both MBRs related to biological basin are presented in Figure 4.2 and Figure 4.3. The averages and standard deviations of these parameters for the whole period are summarized in Table 4.2.

COD organic rate (Figure 4.2.A and D) was slightly lower for SEM, mainly because of higher MLSS concentrations in this MBR (Figure 4.2.C and F). However, the BOD loading rate is quite equivalent for both WWTPs (0.05 and 0.04 $kg_{BOD5}.kg_{MLSS}^{-1}.d^{-1}$ for SEM and SAV respectively). Similarly, SEM-MBR is operated at lower N-NH_4 to sludge ratio (Figure 4.2.B and E).

Besides, SEM presents a lower SRT than SAV (Figure 4.3.A and C), varying between 10 and 30 days (with an average value of 16 d during the studied period), whereas SAV presented a first period of narrow SRT between 25 – 30 days and after the day 800, SRT variations were wider between 25 – 40 days (with an average value of 29 days during the studied period). Variation in SRT are common since solid extraction was usually performed 4-5 times a week. Temperatures were similar for both MBRs over the whole period (Figure 4.3.B and D).

Finally, the influent flowrate normalized by the total membrane surface of each MBR is highly different between the two WWTPs (0.15 and 0.40 $m^3.m_{membrane}^{-2}.d^{-1}$ for SEM and SAV respectively), since SEM-MBR operated at around 30% of its designed flowrate.

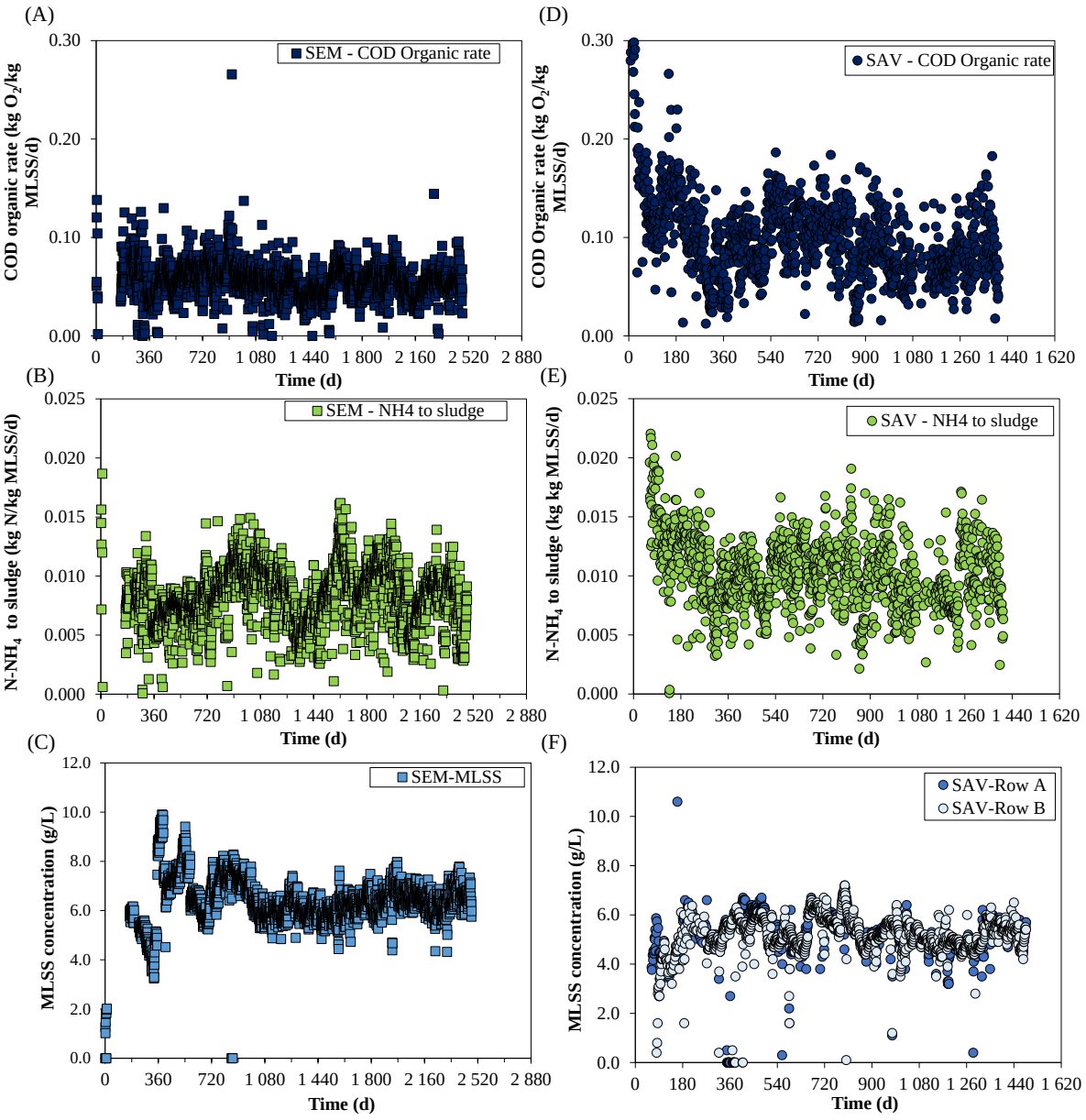

Figure 4.2 Chronological data of COD organic rate (A for SEM and D for SAV), N-NH4 to sludge ratio (B for SEM and E for SAV) and MLSS concentration in the aerated zone (C for SEM and F for SAV) since commissioning of both MBRs.

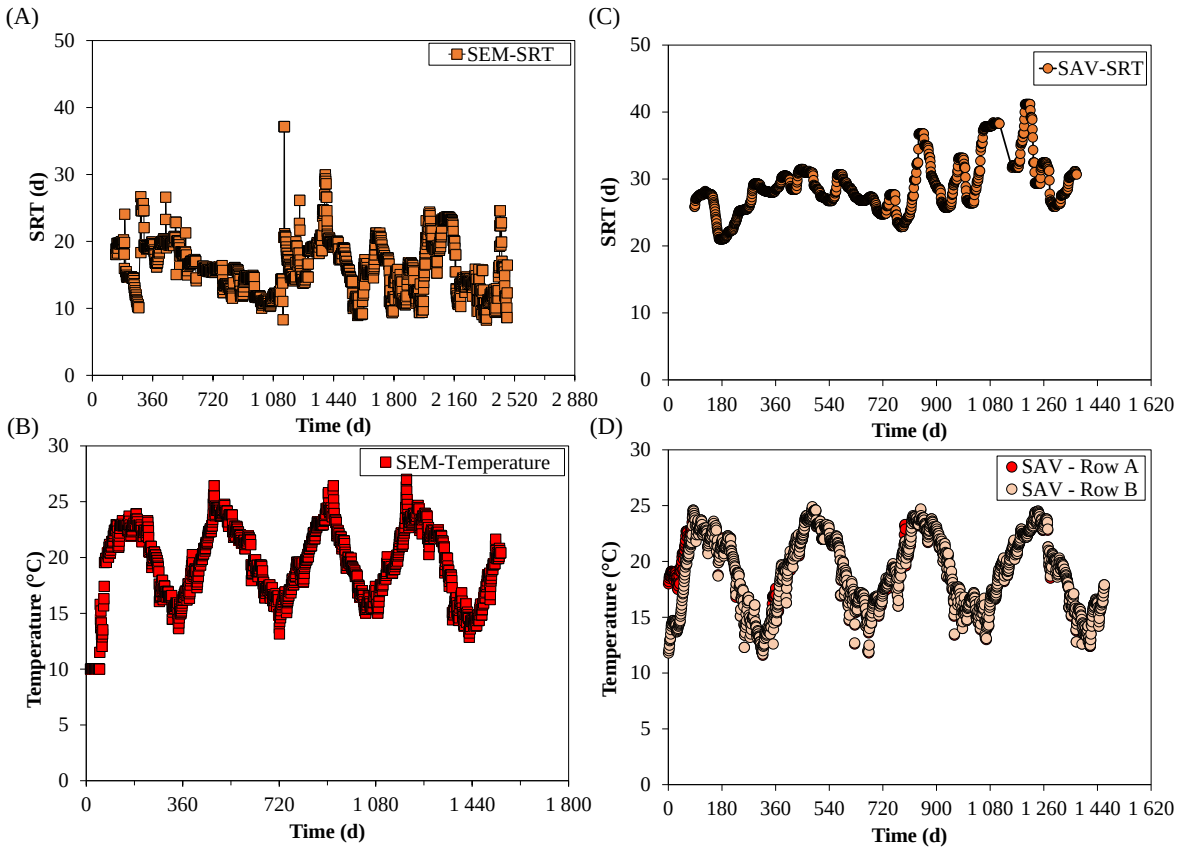

Figure 4.3: Chronological data of SRT (A for SEM and C for SAV), and Temperature (B for SEM and D for SAV).

Table 4.2 : Averages and standard deviations of the main operating conditions of SAV and SEM MBRs. * means differences between these values are not statistically significant.

		SEM	SAV
Operating conditions - Biological Basin			
Influent flow rate	(m^3/total m^2 of membrane/day)	0.15 ± 0.03	0.40 ± 0.02
COD organic rate	(kg COD / kg MLSS / d)	0.06 ± 0.02	0.10 ± 0.05
BOD_5 organic rate	(kg BOD_5 / kg MLSS / d)	0.05 ± 0.01	0.04 ± 0.01
Organic loading rate	(kgCOD / m^3 / day)	0.75 ± 0.19	0.48 ± 0.19
N-NH_4 to sludge	(kg N-NH_4 / kg MLSS / d)	0.008 ± 0.002	0.010 ± 0.003
N-NH_4 loading rate	(kgN-NH_4 /m^3 aerated / d)	0.114 ± 0.04*	0.117 ± 0.034*
MLSS in aerated zone	(g/L)	6.4 ± 0.9	5.0 ± 1.0
HRT	(h)	4.3 ± 0.9	4.6 ± 0.9
SRT	(d)	16 ± 4	29 ± 5
Recirculation factor	(-)	4.7 ± 0.3	4.5 ± 0.5
Temperature	(°C)	19.7 ± 3.1	19.1 ± 3.3

2.3. MBR BIOLOGICAL PERFORMANCES AND EFFLUENT QUALITY

Regarding performances, MBR are known to be an efficient, reliable and robust process. The results in terms of performances and effluent quality are presented for each studied WWTP in the following.

- SAV's MBR

The performances of SAV-MBR were determined in terms of TSS, COD, BOD, TN, NH_4, TP and PO_4 during the studied period (Figure 4.4). Averages and standard deviations for all these removals are presented in Table 4.3. TSS and BOD removals were kept stable and around 98 ± 1%, which is expected for an MBR (Figure 4.4.A). Moreover, COD elimination presented a

slightly higher dispersion fluctuating around 85 ± 7% for this MBR. Regarding nitrogen-based compounds, this MBR achieved eliminations of 98 ± 3% and 70 ± 10%, respectively, for NH_4 and TN (Figure 4.4.B). Moreover, PO_4 and TP removal were at 68 ± 26% and 76 ± 22%, respectively (Figure 4.4.C). TP presented a more inconsistent trend and a higher variability due to recurrent issues in the ferric chloride injection, which enhances the physical-chemical precipitation of phosphate and the flocculation/coagulation of sludge flocs. During periods without $FeCl_3$ injection, P-PO_4 removal solely lays on biological dephosphatation.

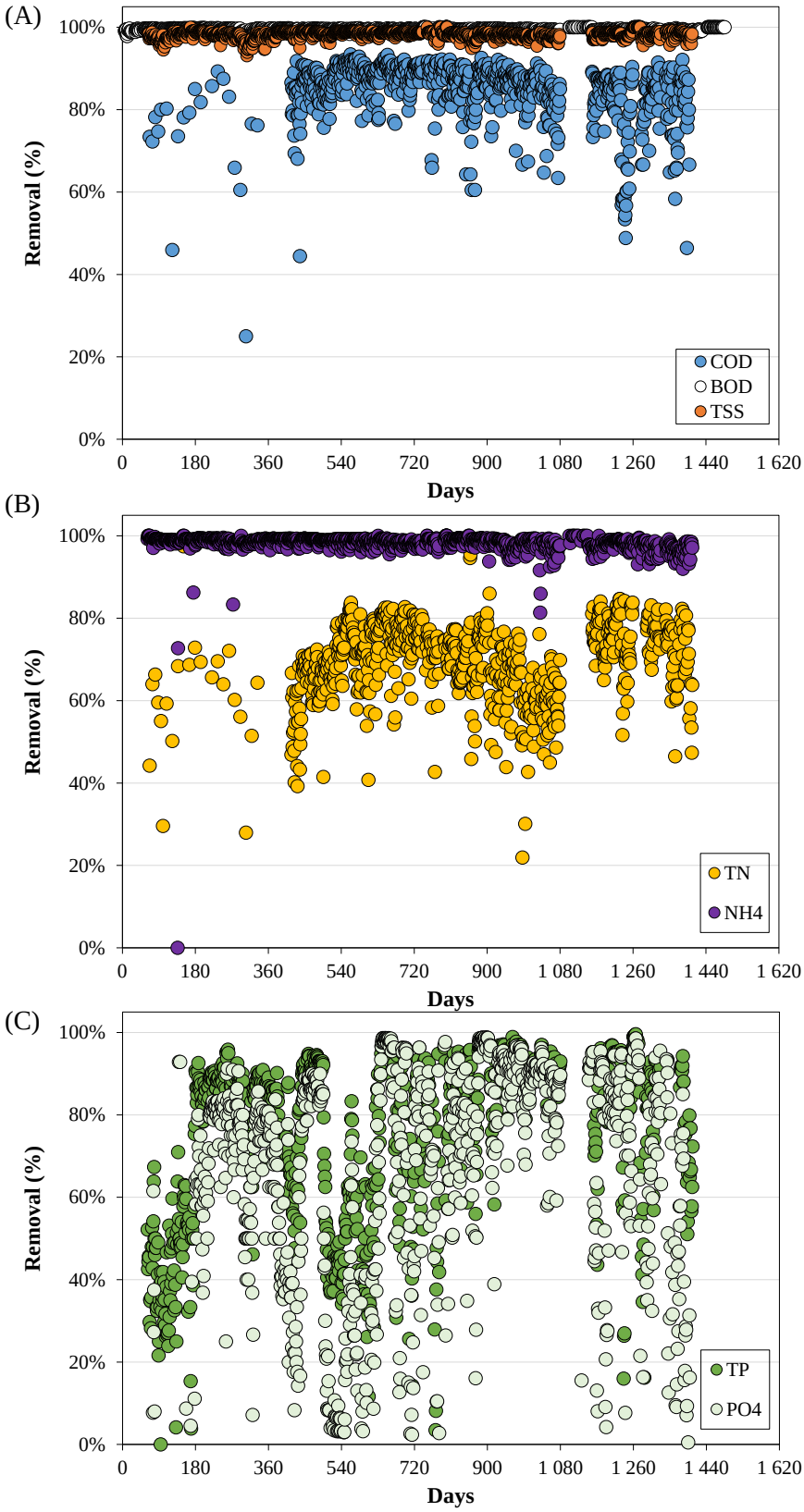

Figure 4.4 : SAV-MBR removal in terms of COD, BOD and TSS (A), TN and NH_4 (B) and TP and PO_4 (C).

- SEM's MBR

SEM's MBR presented overall greater performances than SAV (Table 4.3). TSS and BOD were comparable to SAV and above 99% (Figure 4.5.A). COD removal also remained highly efficient at 97 ± 4% (Figure 4.5.A). Considering nitrogen treatment, NH_4 removal was at 98 ± 12% and TN removal was kept at 84 ± 10 % due to the ratio BOD/TKN more optimal for denitrification process than for SAV-MBR. Regarding phosphorus-based compounds, TP and PO_4 removals were at 97 ± 9% and 95 ± 11%, respectively. These eliminations were mostly stable over time. While SAV's plant operators reported inconsistent injection of ferric chloride throughout this period, SEM's plant operators reported over injection in comparison to the required dose. Since SEM-MBR operates at a lower flowrate than the designed one, the minimal flowrate of the pumps used to inject ferric chloride is still too high, resulting in ferric chloride overdoses.

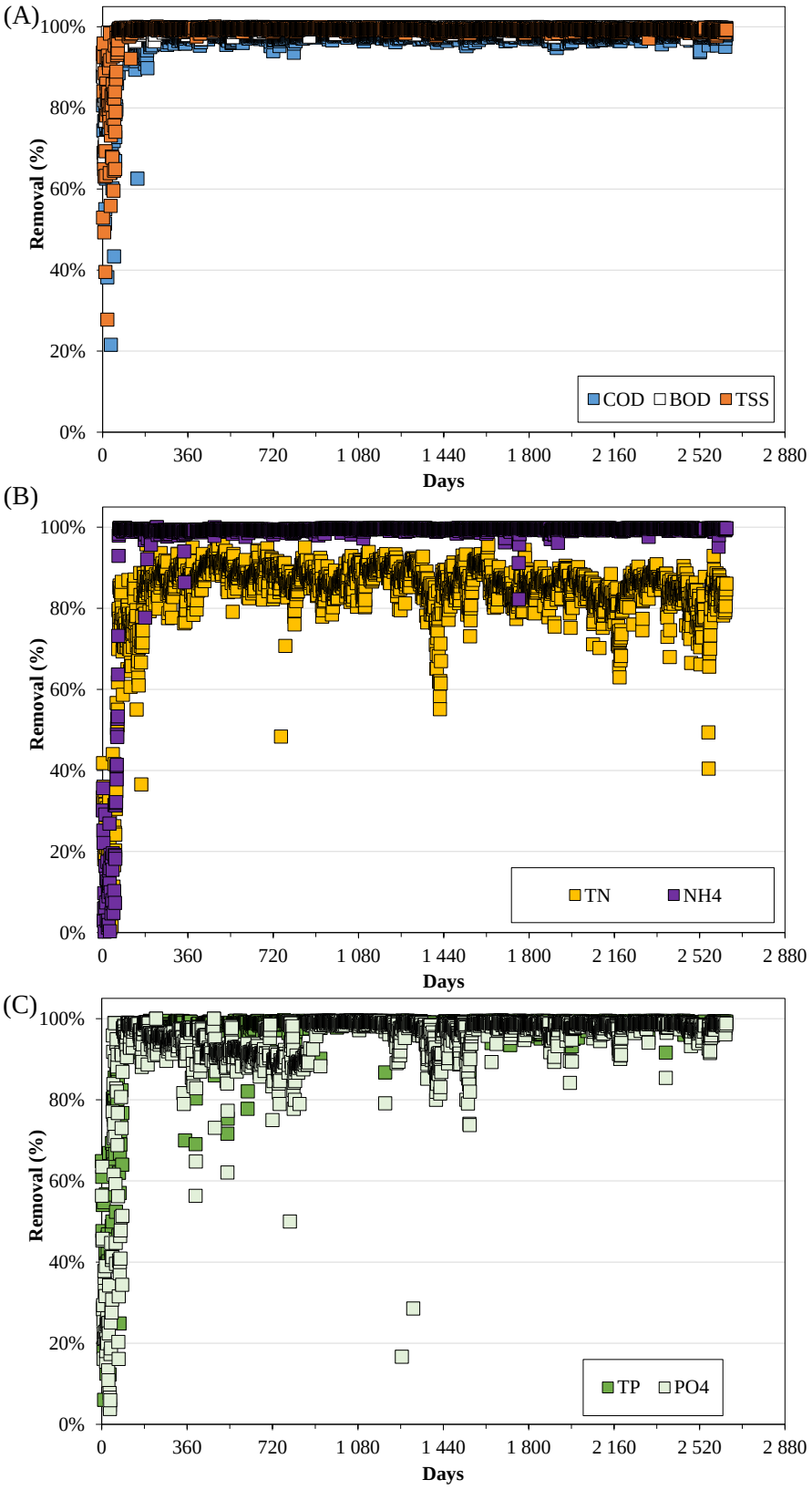

Figure 4.5 SEM-MBR removal in terms of COD, BOD and TSS (A), TN and NH_4 (B) and TP and PO_4 (C).

Table 4.3 Quality characteristics of effluents along with performances from SEM-MBR (data from May/2014 to January/2021) and SAV-MBR (data from November/2017 to June/2021).

		Characteristics of effluent		**Removal Efficiency (%)**	
Parameter	**Units**	**SEM-MBR**	**SAV-MBR**	**SEM-MBR**	**SAV-MBR**
TSS	(mg / L)	<2.0	<2.0	99 ± 4	98 ± 1
COD	(mg O_2 / L)	14 ± 3	14 ± 5	97 ± 4	85 ± 7
BOD_5	(mg O_2 / L)	1.1 ± 0.7	2.1 ± 0.9	99 ± 2	99.3 ± 0.4
Total Kjeldahl Nitrogen (TKN)	(mg N / L)	0.9 ± 0.5	1.6 ± 0.9	97 ± 11	96 ± 2
NH_4	(mg N / L)	0.3 ± 0.4	0.6 ± 0.5	98 ± 12	98 ± 3
Total Nitrogen (TN)	(mg N / L)	9.6 ± 3.0	14.1 ± 7.4	84 ± 11	70 ± 10
Total phosphorus (TP)	(mg P / L)	0.1 ± 0.2	1.1 ± 1.0	97 ± 9	76 ± 22
PO_4^{3-}	(mg P / L)	0.2 ± 0.2	1.0 ± 0.9	95 ± 11	68 ± 26
pH	-	7.7 ± 0.2	8.0 ± 2.5		
Temperature	(°C)	19.4 ± 3.4			
TAC	(mg CO3/L)		114.3 ± 23.2		

Permeate quality chronology

Zeeweed membranes present a pore size diameter of 0.04 µm, which enables the retention of particles, bacteria, protozoa, some viruses and colloidal matter. Following permeate quality is an indirect way to monitor membrane ageing, since increase in membranes pore size over time leads to the formation of defaults enable bigger particles to flow through the membranes. Figure 4.6 presents results of TSS concentration in permeate for both SAV-MBR (A) and SEM-MBR (B). Most of the time permeate was below the quantification limit of this analysis (2 mg/L), confirming membranes' integrity over time. Plant operators from SEM-MBR reported that this permeate presented slightly higher TSS concentrations in the beginning due to leaking in pipe connections. Moreover, plant operators from both MBR reported formation of biofilm in the

permeate collection tank when the MBRs presented long non-operating time, indicating the presence of microorganisms in permeate.

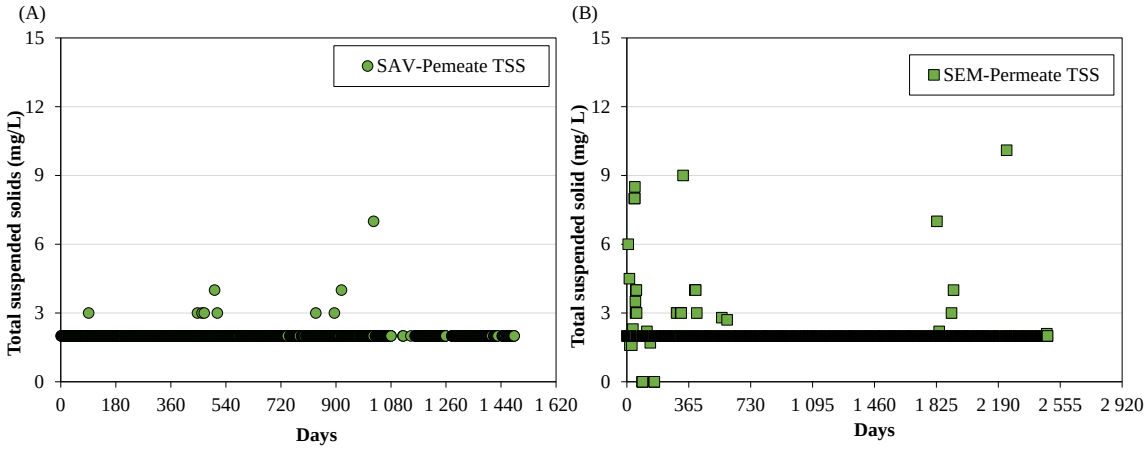

Figure 4.6 : Total suspended solids in permeate from SAV-MBR (A) and SEM-MBR (B).

2.4. OPERATING CONDITIONS OF MEMBRANE TANKS

Comparison of the operating conditions of the membrane tanks for the two studied WWTP

Regarding membrane tanks, chronology of supernatant COD measured in the recirculation channels (membrane tank to aerated zone) and MLSS in membrane tanks for both MBRs are presented in Figure 4.7 and Figure 4.8, respectively.

- SAV's supernatant COD may be separated into two periods with different trends (Figure 4.7.B): Period I, when supernatant COD presented high variability ranging between 20 and 90 mg O_2/L and period II, when this indicator decreased and was more stable around 20 mg O_2/L. The increase in COD from the period I is related to issues in the settling tanks between 2018 and 2019. The average value of the MLSS in the membrane tanks during the overall studied period is 6.4 $g.L^{-1}$.
- SEM's supernatant COD started to be measured from Jan/2019 and for this period, values varied between 20 and 60 mgO_2/L, with an average of 44 mg O_2/L. Regarding

MLSS in membrane tanks, SEM usually operated at higher concentrations (7.6 $g.L^{-1}$) than SAV (Figure 4.8).

Table 4.4 presents averages and standard deviations of the main operating data related to membrane tanks from both MBRs. SEM-MBR operates at MLSS concentrations and supernatant COD concentrations 19% and 40% greater than SAV-MBR, respectively. Moreover, both MBRs presented similar permeate instantaneous flux and SAD_m averages, but the daily filtration times of each MBR are highly different. Membrane tanks from SAV-MBR presented 20.7 h of filtration daily in average, whereas membrane tanks from SEM-MBR only filtered around 5.4 h per day, due to its operation under the nominal capacity (further described in chapter 2).

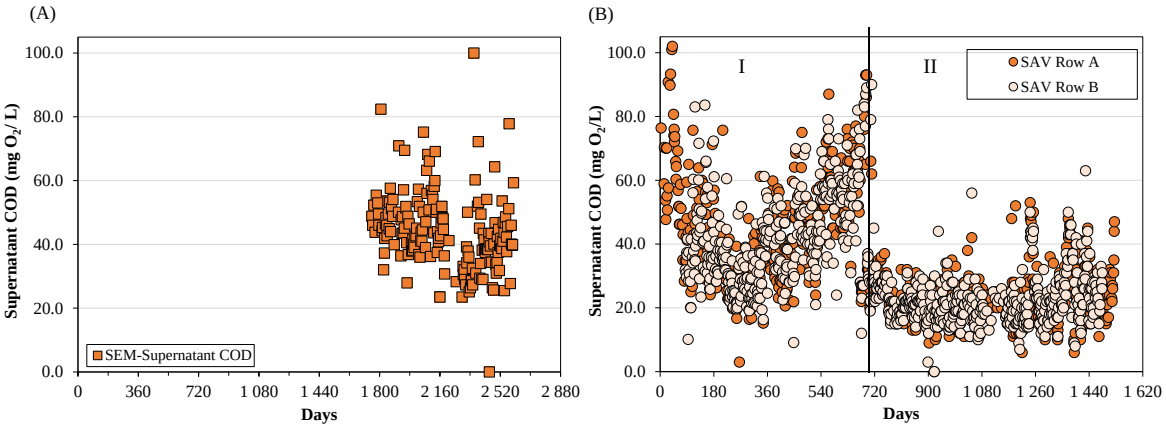

Figure 4.7 Supernatant COD in recirculation channel from membrane tanks to aerated zone for SEM-MBR (A) and SAV-MBR (B).

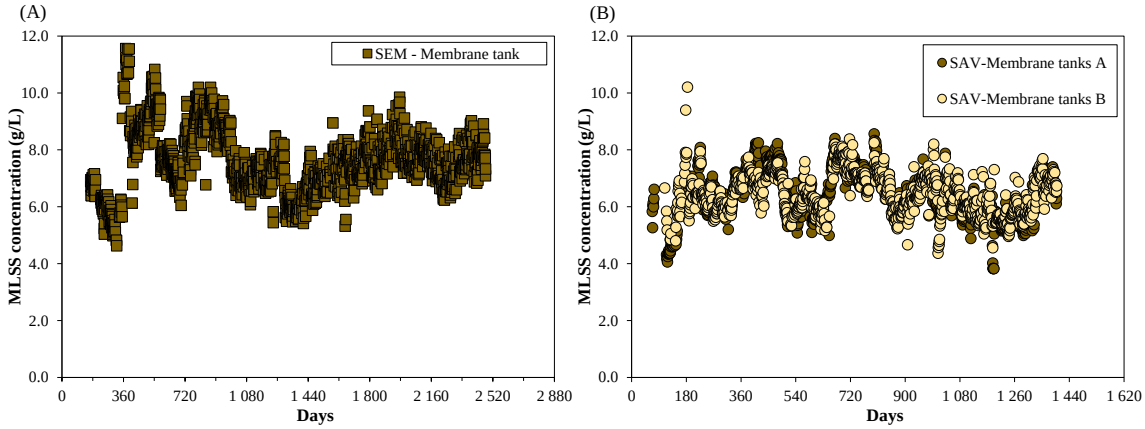

Figure 4.8 MLSS in membrane tanks for SEM-MBR (A) and SAV-MBR (B).

Table 4.4 Averages and standard deviations of operating conditions from SAV-MBR and SEM-MBR.

Operating conditions - Membranes					
Parameter	Unit	SAV-Period I	SAV-Period II	SAV	SEM
MLSS in membrane tank	(g / L)	6.6 ± 0.9	6.3 ± 0.8	6.4 ± 0.9	7.6 ± 1.1
Supernatant COD	(mg O2 / L)	44.9 ± 17.7	22.3 ± 7.6	31.3 ± 16.8	43.9 ± 11.5
Permeate instantaneous flux 20°C	(L / h / m^2)	26.6 ± 6.4	26.6 ± 6.6	26.6 ± 6.4	26.4 ± 6.0
SAD_m	(Nm^3 / m^2 membrane / h)	0.22 ± 0.05	0.20 ± 0.06	0.22 ± 0.05	0.21 ±0.09
Daily filtration hours	(h)	-	-	20.7 ± 1.7	5.4 ± 1.9

In addition, the permeate instantaneous flux at 20°C and the specific aeration demand with respect to membrane surface (SAD_m) for the 14 membrane tanks studied from SAV-MBR were statistically analyzed (see Appendix A). It was highlighted that all studied membrane tanks (selected according the methodology presented in Chapter 2 - § 2.3.2) are operated in a similar ranges in terms of aeration and permeate flux.

Analysis of the heterogeneity of operating conditions between the membrane tanks of SAV-MBR and SEM-MBR

The chronological behavior of permeate flux was assessed to compare the membrane tanks each other for both MBRs. Figure 4.9 presents chronological data of instantaneous permeate flux at 20°C for 14 membrane tanks from SAV-MBR and 8 from SEM-MBR over the studied period. For the first year, SEM's influent flowrate increased progressively and as a result, membrane tanks were initially operated with low permeate flux around 12 LMH, which has been progressively increased to reach between 20 and 30 LMH (Figure 4.9.A).

Regarding SAV's chronology (Figure 4.9.B), permeate flux is ranged from 17 to 50 LMH homogeneously throughout all membrane tanks. Since this MBR is operated at an influent flowrates during raining weather, permeate flowrate oscillated more throughout the years comparing to SEM-MBR. Therefore, MBRs were operated at a similar permeate flux in average (26.6 and 26.4 LMH for SAV-MBR and SEM-SBR respectively), but the main difference was found in the chronological behavior. SEM-MBR presented a stable flux along the period with a maximal value of permeate flux around 30 LMH, in comparison with the more dynamic evolution of the permeate flux for SAV-MBR in the range 17 to 50 LMH during the studied period, link to the seasonal variations.

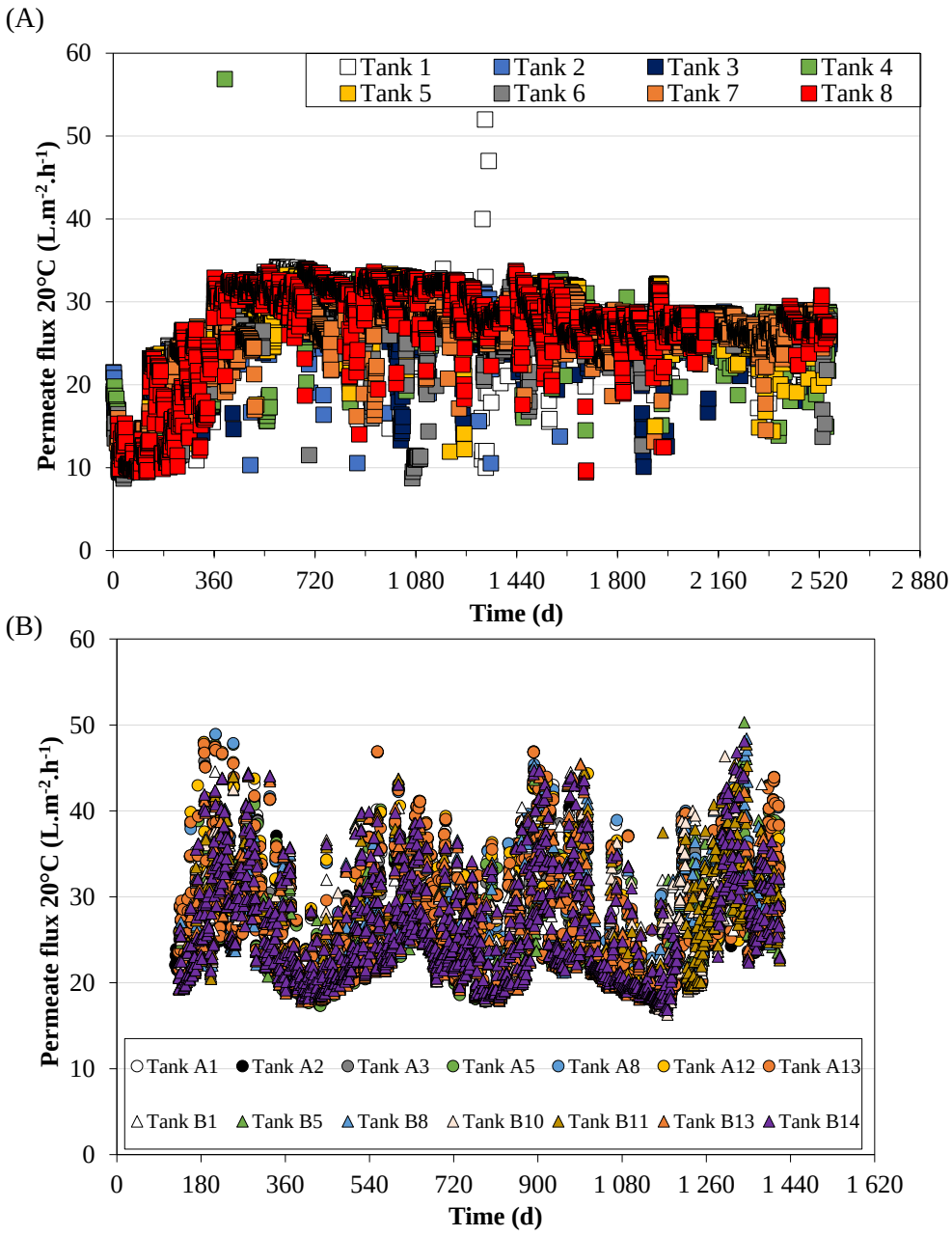

Figure 4.9: Permeate instantaneous flux at 20°C for SEM-MBR (A) and SAV-MBR (B).

To conclude, average values of permeate flux and SAD_m are similar for both MBRs, but some differences in membrane tank operation can be highlighted:

(i) Membrane tanks from SEM-MBR presented higher supernatant COD (43.9 and 31.3 $mg.L^{-1}$ respectively) and MLSS (7.6 and 6.4 $g.L^{-1}$ respectively) concentrations than the ones from SAV-MBR (Table 4.4 and Figure 4.*7* and Figure 4.8);

(ii) Permeate fluxes from SAV-MBR are more variable and reach highest peak values (up to 50 LMH) than the ones from SEM-MBR (with a relative stability over time and a highest value up to 30 LMH) (see Figure 4.9);

(iii) SEM-MBR only presented 5.4 ± 1.9 h of daily filtration hours, whereas SAV-MBR presented 20.7 ± 1.7 h due to the adaptation of flowrate to treat only 30% of its nominal capacity (further explained in Chapter 2).

2.5. CUMULATIVE PROCESS INDICATORS

MBR operating conditions cause changes in membrane properties and the mixed liquor filtration over time promotes the accumulation of residual fouling which ultimately affects membrane's filtration ability. In order to establish a historic of membranes based on factors that may impact its long-term performance, seven process indicators were continuously cumulated since the commission of both MBRs according to their availability and potential impact on the membrane lifetime. These indicators are selected in order to allow to distinguish the operation of each individual membrane tank.

According to the availability of the data for the two studied WWTP, the selected cumulative indicators were: operating days, exposure dose, specific permeate volume (V_p), specific aeration demand and filtered MLSS mass, filtered supernatant COD and ΔCOD. These cumulative indicators with respect to the time since the commissioning date are presented in Figure 4.10 to Figure 4.12. It is worth noting that Figure 4.10(A) represents the exposure doses related only to CIP protocols for SEM-MBR, whereas SAV-MBR's exposure doses are related to CIP and chemically enhanced backwashes.

Comparing these graphs, it is clear that:

1. Exposure dose: SAV's membranes are exposed to a slightly lower annual exposure doses than SEM's membranes. Some heterogeneities appears for the different membrane tanks of each MBR. SAV's membranes from tanks SAV-A5, SAV-B5 and SAV-B10 were the least exposed during the studied period (around 20 000 ppm.h after 1533 days). SEM's membranes from tank UF4 were the least exposed to chlorine remaining under 60 000 ppm.h after 2254 days. Membrane tanks SAV-B8 and SAV-B13 presented the highest annual exposure dose rate of 9 290 and 9 226 ppm.h/year, respectively, and for SEM's membranes, tank UF8 presented the highest annual exposure dose rate of 15 086 ppm.h/year;
2. Specific permeate volume: According to the difference in operation of the MBR in terms of filtration, SAV's membranes filtered more annually (130.8 - 171.5 m^3/m^2/year) than SEM's ones (39 – 57.6 m^3/m^2/year). Membrane tanks SAV-A2 and SAV-B10 filtered the least in SAV-MBR, mainly due to longer downtime periods. For SEM-MBR, UF2, UF6 and UF8 filtered the least, also due to longer downtime periods.
3. Specific aeration demand (SAD_m): The cumulated specific aeration demand is also highly different between the two WWTPs, with a mean value of 7,500, 6,500 and

1,500 $m^3/m_{membrane}^2$ for SAV-MBR-RowA, SAV-MBR-RowB and SEM-MBR respectively, after 1,440 days of operation. Moreover, important heterogeneities are observed between filtration zones for the SEM-MBR.

4. The other parameters (Figures presented in Appendix B) presented similar conclusions to the specific permeate volume as they are closely linked to this parameter, since they are mostly impacted by the downtime periods.

.

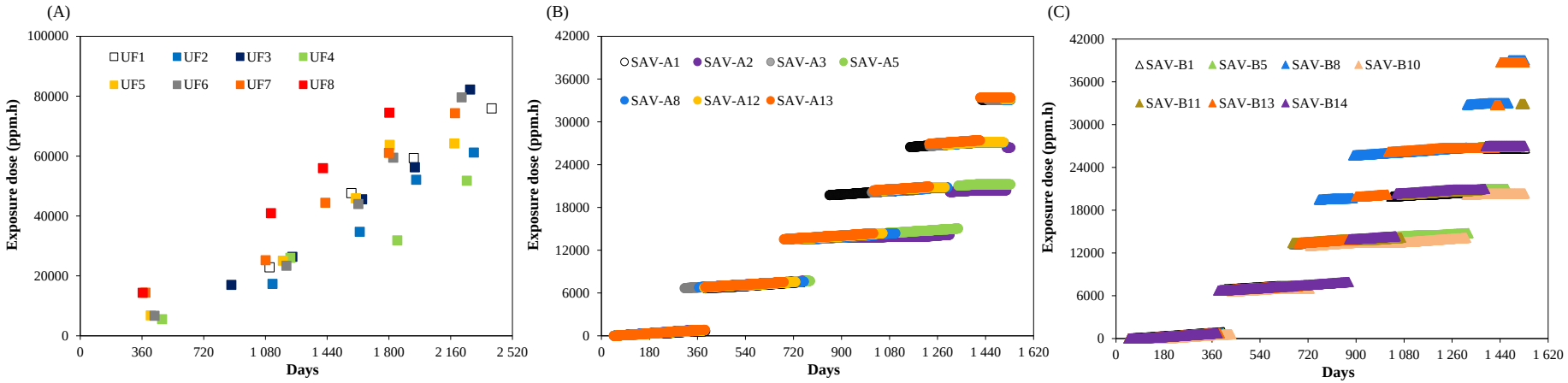

Figure 4.10 Cumulative exposure dose (C x t) for membranes tanks from SEM-MBR (A), SAV-MBR row A (B) and SAV-MBR row B (C).

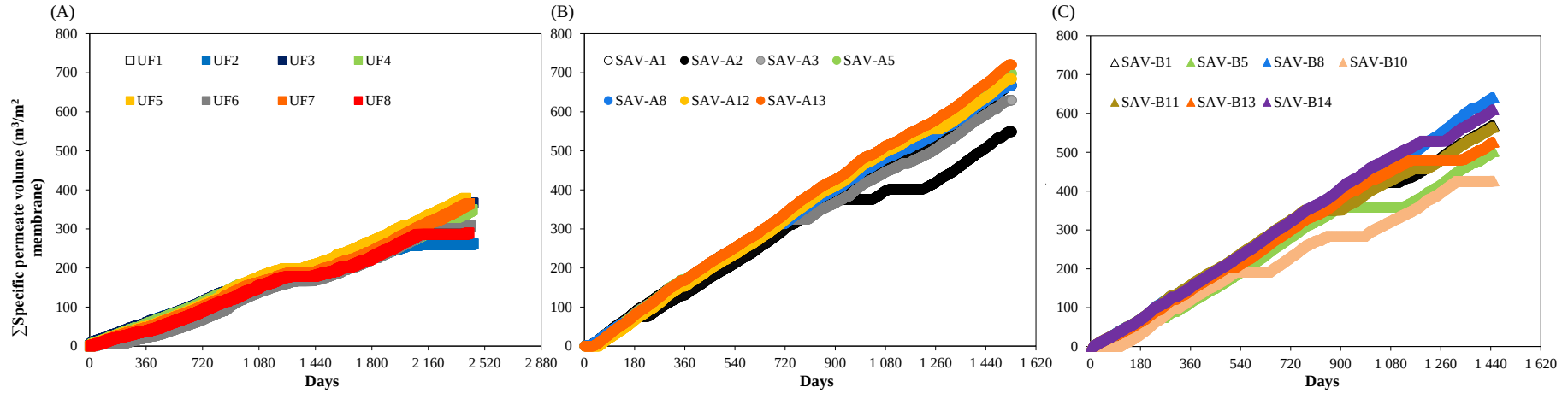

Figure 4.11 : Specific permeate volume evolutions for membranes tanks from SEM-MBR (A) SAV-MBR row A (B) and SAV-MBR row B (C).

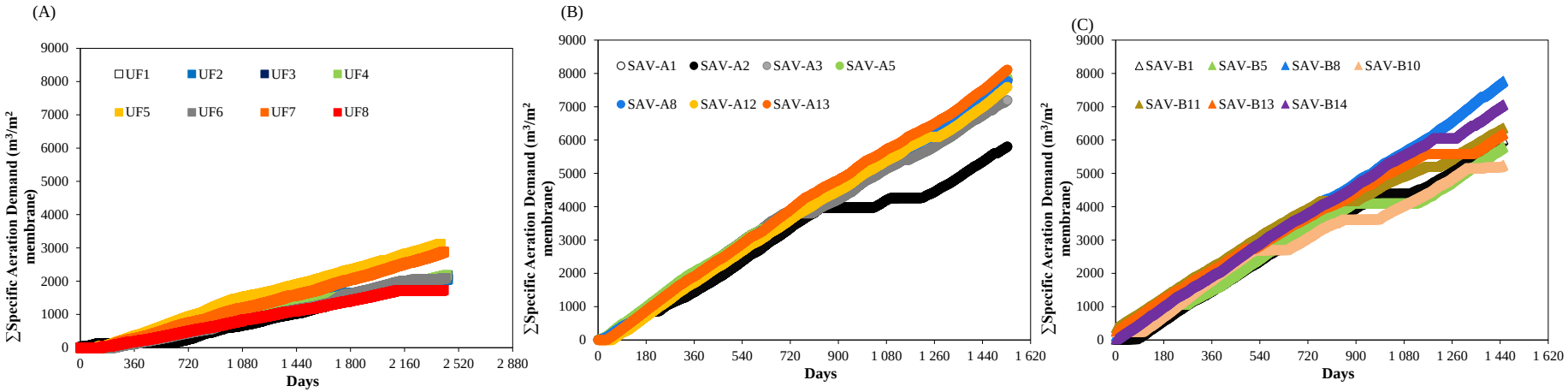

Figure 4.12: Specific aeration demand for membranes tanks from SEM-MBR (A), SAV-MBR row A (B) and SAV-MBR row B (C) with respect of days since commissioning date.

Membrane ageing is classically monitored either by the operating time or by the exposure dose C x t to chlorine. Membrane ageing in MBRs is presented in the following section in the traditional way and afterwards the other cumulative process indicators are integrated to this ageing monitoring.

3. MEMBRANE AGEING BASED ON AUTOPSIES CHARACTERIZATION

According to chapter 3, hollow-fibers became weaker as the chlorine exposure dose increased in full-scale operation. Additionally, intrinsic permeability and PVP content are important characteristics to monitor membrane ageing. An increase in intrinsic permeability was observed as a result of formation of bigger pores due to PVP removal for samples aged at full-scale MBR. Thus, samples harvested from SAV-MBR and SEM-MBR were characterized according to these properties and results are shown with respect to the exposure dose and the specific permeate volume hereby. The operating mode and its impacts on membrane properties for both MBRs are discussed as well.

3.1. MECHANICAL RESISTANCE

Regarding ultimate tensile strength (Figure 4.13), it seems that there are two different groups of membranes with different mechanical resistance:

- The first one presented higher ultimate tensile strength (H-UTS), over 300 MPa, namely, SAV-A1; SAV-A8; SAV-B1; SAV-B5; SAV-B8; SAV-B10; SAV-B11; SAV-B14, *SEM-UF1*;
- The other group with lower ultimate tensile strength (L-UTS), below 300 MPa, which are SAV-A5; *SEM-UF3; SEM-UF4; SEM-UF5; SEM-UF7; SEM-UF8*.

Considering membranes from tanks in the same group, ultimate tensile strength seemed to decrease homogeneously across the analyzed samples for both SAV-MBR and SEM-MBR. For instance, in the group of membranes with values comparable to the analyzed pristine membrane (396 ± 14 MPa), the ultimate tensile strength of the most aged sample (SEM-UF1 at 64,000 ppm.h) reached 315 ± 17 MPa, that is a decrease of 20%.

In order to understand the two distinct range of ultimate tensile strength found in Figure 4.13, the uniaxial stress-strain curves of a pristine membrane, two ages membranes, which present characteristic evolutions from each groups (H-UTS with higher ultimate tensile strength [SAV-A8 exposed to 24,740 ppm.h] L-UTS with lower ultimate tensile strength [SEM-UF3 exposed to 100,000 ppm.h]) are presented in Figure 4.14 to illustrate these differences. The stress-strain curves from all membrane tanks studied in this research are presented in Appendix C.

A difference in the shape of the curve in the highlighted region of low deformations is observed. The group of higher ultimate tensile strength presents a similar curve to the pristine membrane, indicating roughly the same rigidity. On the other side, the group of lower ultimate tensile strength presented a progressive deformation as tensile strength increased up to the break, which indicates progressive chain scission of the support polymer structure under tension until fissure and ultimately breakage. Nevertheless, since operators did not report fiber breakage, we may extrapolate the data from membrane tanks with low ultimate tensile strength and consider that even though ultimate tensile strength decayed to around 180 MPa, hollow-fibers would still be able to withstand stressed conditions in MBR conditions.

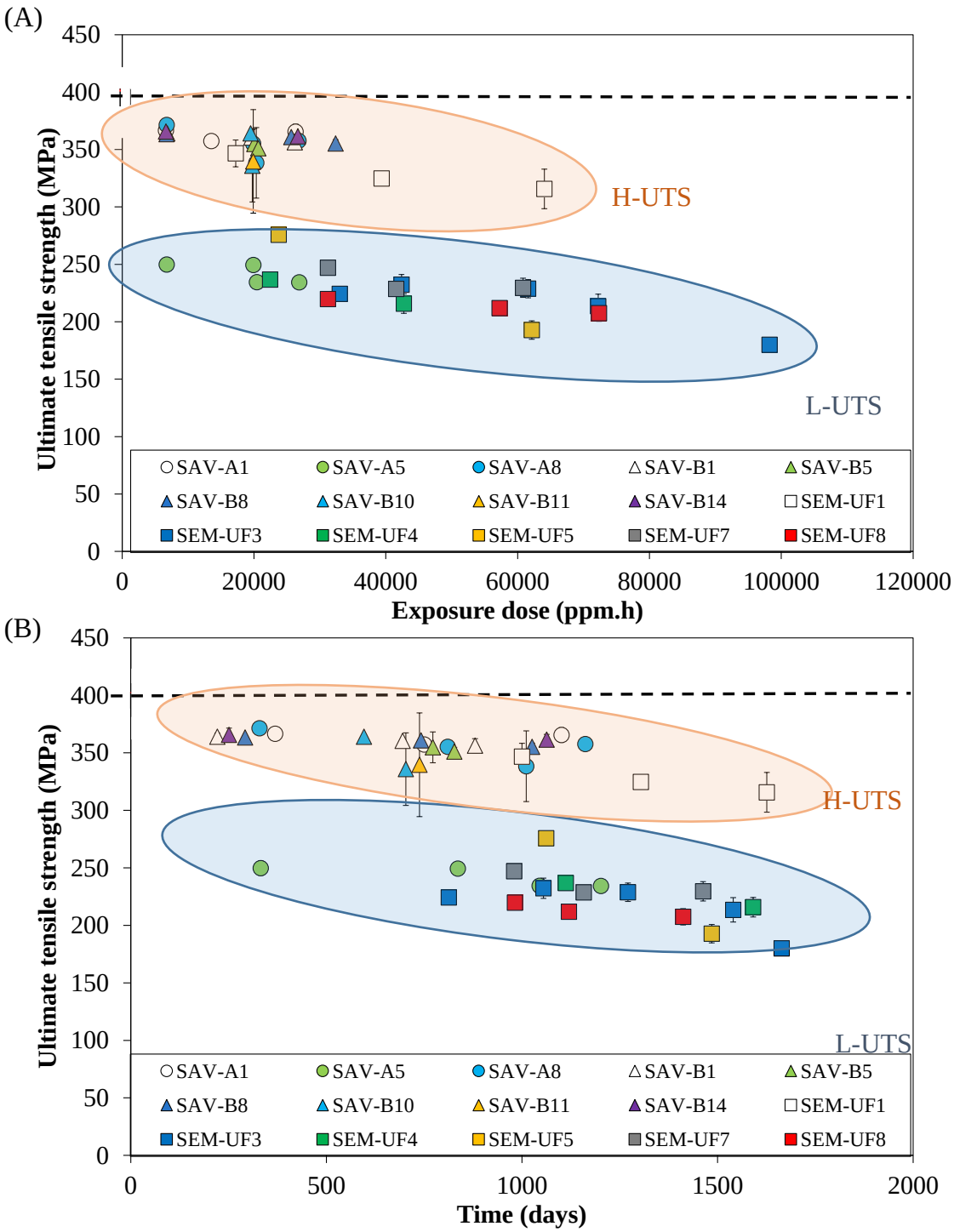

Figure 4.13 : Ultimate tensile strength of membranes harvested from both MBRs with respect to exposure dose (A) and operating days (B).

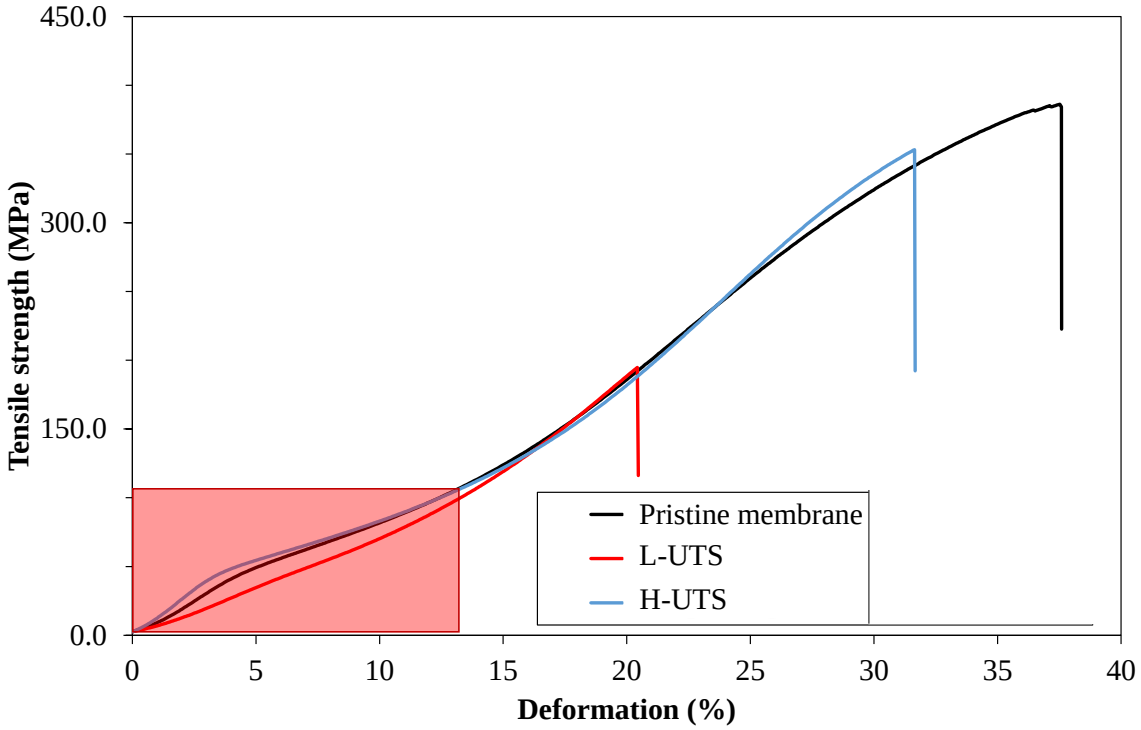

Figure 4.14: Uniaxial stress-strain curves for a pristine membrane (0 ppm.h), SAV-A8 at 24,740 ppm.h representing the higher ultimate tensile strength and SEM-UF3 at 100,000 ppm.h representing the lower ultimate tensile strength.

3.2. INTRINSIC PERMEABILITY

Modules of 18 cm of length were built with fibers harvested from both full-scale MBRs and intrinsic permeability was measured by water filtration after a cleaning of fibers in similar CIP conditions according to each MBR. These results are shown with respect to the exposure dose for the SAV-MBR group in Figure 4.15.A and SEM-MBR in Figure 4.15.C and with respect to the operating time for SAV-MBR in Figure 4.15.B and SEM-MBR in Figure 4.15.D.

Lp/Lp_0 SAV-MBR samples presented a higher variation, fluctuating mostly between 1.0 and 1.5. For SEM-MBR, Lp/Lp_0 values were higher and presented an increasing trend with both exposure dose and operating time. Since these membranes are weaker, they might be more

susceptible to pore enlargement than the SAV-MBR group. During CIP protocols in this MBR, membranes are soaked in 800 ppm of NaOCl for 20 h, whereas in SAV-MBR, CIP is performed for 6 h with a hypochlorite solution at 1000 ppm. Abdullah and Bérubé (2018) obtained an increase of 17% in intrinsic permeability when cleaning exposure time increased from 6 h to 24 h [9]. In an earlier study, the authors showed that for equivalent C x t, longer exposures are more detrimental to the membrane material than higher concentrations [10].Thus, we may expect that the cleaning protocol from SEM-MBR is more aggressive to the membrane material and effective in removing foulants than the one from SAV-MBR, resulting in higher Lp/Lp_0.

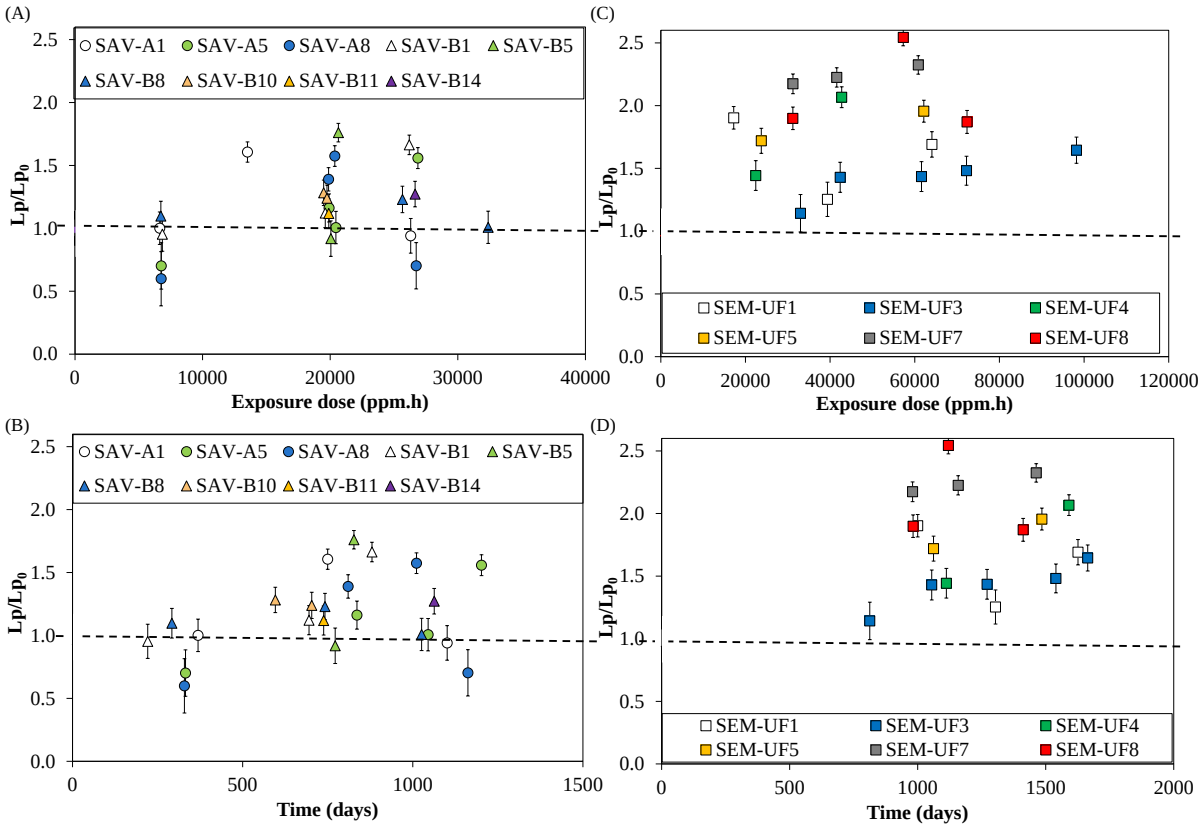

Figure 4.15 : Lp/Lp_0 with respect to the exposure dose for membrane tanks from SAV-MBR (A) and SEM-MBR (C) and with respect to the time of operation from SAV-MBR (B) and SEM-MBR (D).

3.3. PVP DEGRADATION

ATR-FTIR measurements were carried out to quantify the changes in PVP content in these samples. The ratio between the characteristic peak of PVP (1674 cm^{-1}) and the characteristic peak of PVDF (1403 cm^{-1}) was used as a percentage of the value from the pristine membrane. Thus, PVP content as a function of exposure dose is presented in Figure 4.16.A for membranes samples from SAV-MBR and in Figure 4.16.C for the ones from SEM-MBR. As expected, PVP is degraded as membranes aged in full-scale operation for both groups and the main differences are related to each MBR. Comparing the decline in PVP content between SAV-MBR and SEM-MBR samples, it seems that the decrease in PVP content highly depend on the studied MBR and is faster among SAV-MBR samples with respect to the operating time (Figure 4.16.B for SAV-MBR and Figure 4.16.D for SEM-MBR). This important observation highlights that, although the modifications of the membrane properties, in particular the PVP content, depend on the exposure dose (as discussed in Chapter 3), these properties also strongly depends on the operating conditions (different between the two sites). Despite the hypothesis of a more aggressive cleaning protocol applied on SEM-MBR, the operating conditions of the SAV-MBR site induce a significantly faster aging than for the SEM-MBR site (potentially linked to the higher daily filtration time, greater flow variability or a more regular exposure to sodium hypochlorite).

This difference in terms of operating conditions is highlighted by Figure 4.17 which presents the cumulated permeate volume as a function of the exposure dose for each individual samples. Two different zones, associated to the two MBR are clearly identified. The Zone 1, corresponding to the SAV-MBR samples, presents a high filtration intensity to exposure dose ratio, contrary to SAM-MBR samples which are submitted to a low filtration intensity to exposure dose ratio. Moreover, this diagram could be considered in order to interpret the preponderance of each individual ageing mechanisms (mechanical vs. chemical) on the global

ageing mechanism: although the chemical ageing mechanisms always plays an important role in the global ageing mechanism of the membrane properties, the global ageing mechanisms is clearly modulated and accentuated by the intensity of the mechanical stresses related to the filtration process (in terms of filtration time, flux and associated aeration).

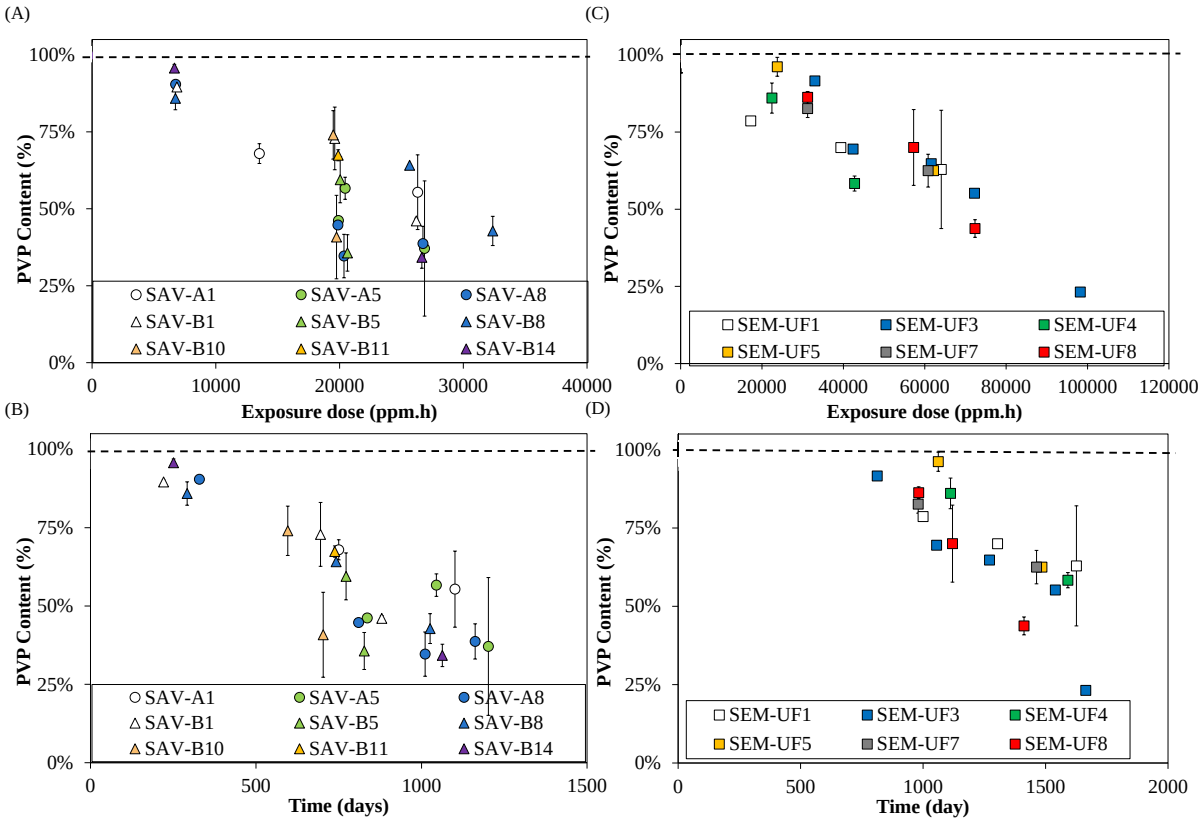

Figure 4.16: PVP content of membranes harvested from SAV-MBR with respect to exposure dose (A) and operating time (B) and from SEM-MBR with respect to the exposure dose (C) operating time (D).

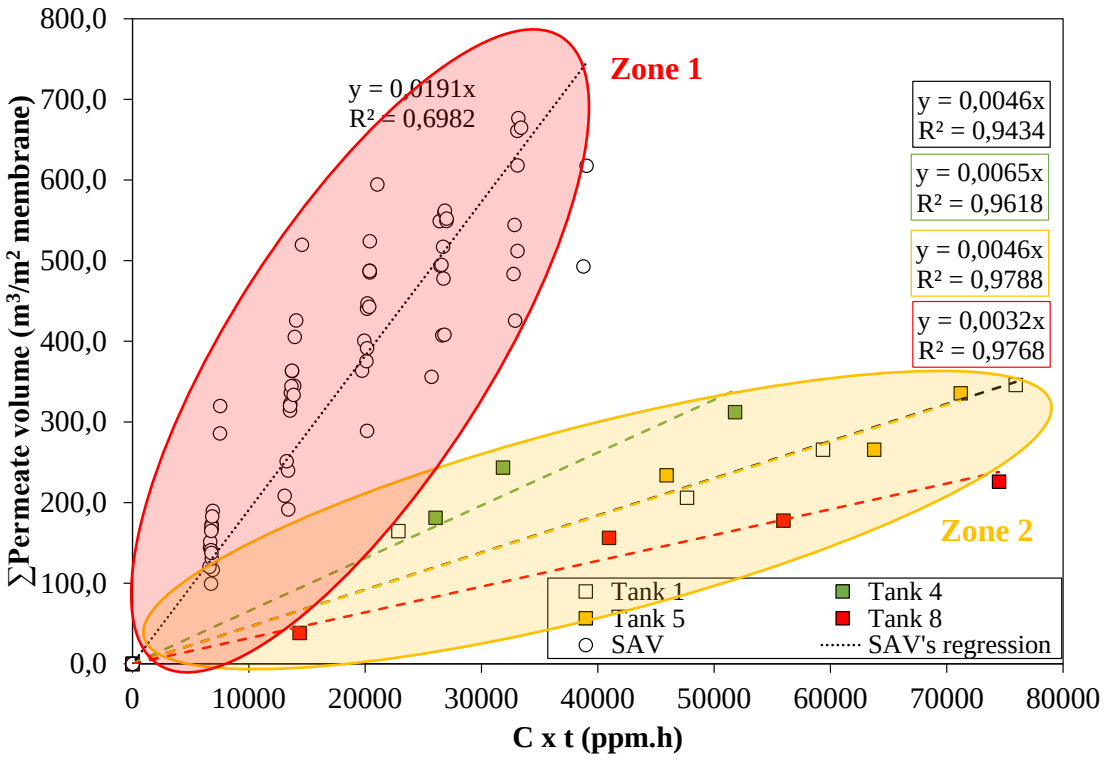

Figure 4.17 : Relationship between cumulated permeate volume and exposure dose for individual membrane tanks from SEM-MBR and overall tanks from SAV-MBR.

Since PVP degradation is highly dependent on the studied MBR and, among the studied MBR, there is a clear difference in operating settings regarding the rate of filtration (permeate volume) to C x t, membranes from zone 2 are closer to an ageing solely due to chlorine exposure as observed in chapter 3. Therefore, a comparison among the PVP contents from SAV-MBR (zone 1), SEM-MBR (zone 2) and results from bench-scale ageing by soaking in sodium hypochlorite is presented in Figure 4.18.A with respect to the C x t and Figure 4.18.B with respect to the specific permeate volume. It is clear that PVP content changes from SEM-MBR and bench-scale ageing are similar, whereas SAV-MBR promotes a faster PVP degradation, since for the same C x t, SAV-MBR usually presented less PVP than SEM-MBR (Figure 4.18.A). In addition, changes in PVP content for both MBRs presented closer correlations (Figure 4.18.B), illustrating the effects of filtration on this indicator.

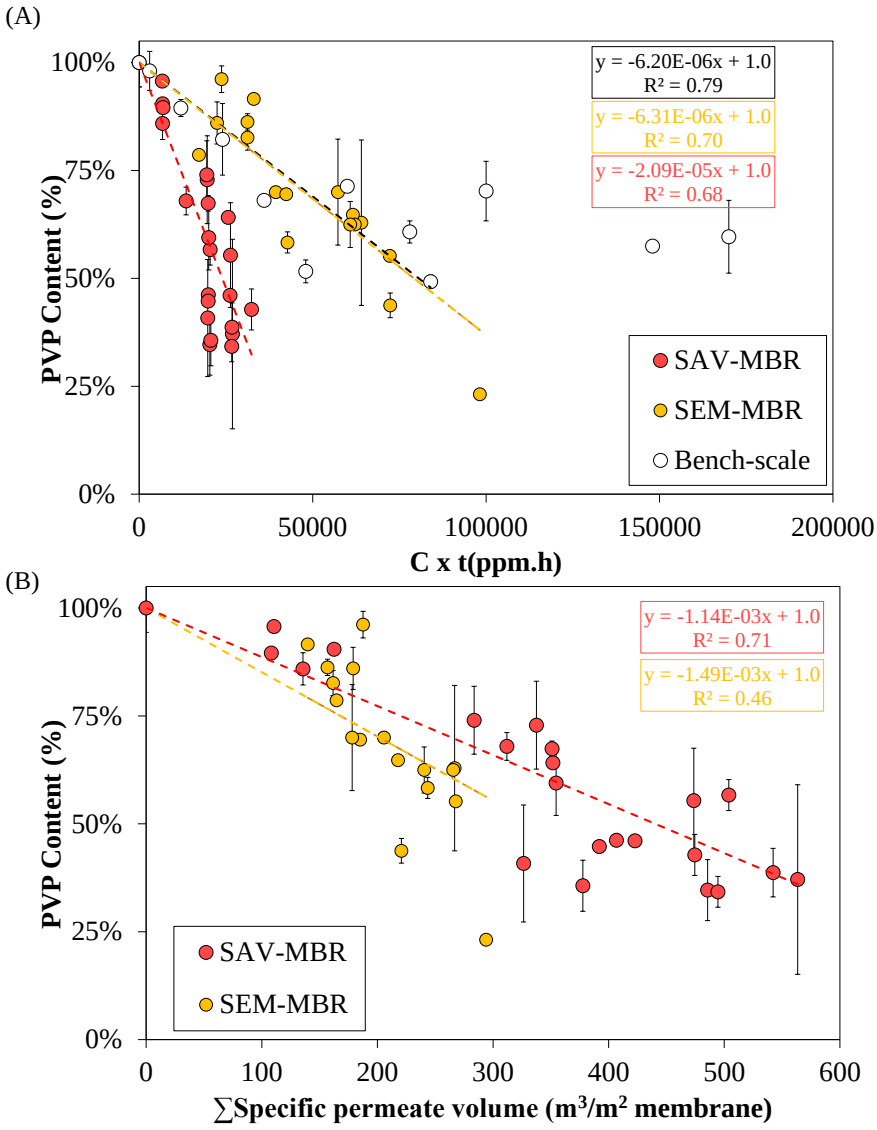

Figure 4.18: PVP content from membranes harvested from SAV-MBR, SEM-MBR and from bench-scale with respect to the C x t (A) and for SAV-MBR and SEM-MBR with respect to the specific permeate volume (B).

Therefore, PVP content seemed to be a key indicator to monitor ageing and to make operating choices, especially related to the control of permeate volume. Lp/Lp_0 presented great variability, because this measurement is sensible to the presence of residual fouling, changes in

hydrophobicity and pore size. In addition, mechanical resistance should not be a concern for these membranes at least for the 7 first years of operation, since fiber breakage was not reported. The membrane properties characterized in this study were also correlated to different cumulative indicators other than C x t and permeate volume and these results are presented in the Appendix D.

Since changes in membrane properties are expected to alter the MBR's filtration performance, the following section describes membrane ageing based on data generated directly from process sensors from both MBRs.

4. MEMBRANE AGEING BASED ON FULL SCALE INDICATORS

4.1. NORMALIZED PERMEABILITY INDEX

Using permeability index to describe membrane ageing in MBR was reported by Fenu et al. (2012) [6]. This parameter corresponds to the ratio between permeate flux and transmembrane pressure during the process after each cleaning-in-place protocol. It differs from intrinsic permeability as it combines the mechanisms related of the evolution membrane properties to its interaction with the activated sludge, since it is measured during a 7 day-period of mixed liquor filtration in the full membrane tank, whereas intrinsic permeability is measured by filtering pure water in lab modules built with membrane samples harvested. They observed that the residual fouling accumulation could be one of the main responsible for membrane replacement. Therefore, the normalized permeability index was calculated for SAV-MBR and SEM-MBR and is presented with respect to the C x t and the operating time in Figure 4.19. A global analysis of the evolution of this permeability index highlights a low but regular decrease of this parameter with time (and associated exposure dose) with a similar order of magnitude for the two MBRs.

For SAV-MBR, normalized permeability index correlated slightly better to the operating time with a correlation coefficient of -0.836 (p-value < 0.05, Spearman). Data decreased in a residual fouling rate of -1.91E-4 d^{-1}, leading the normalized permeability index to reach 0.73 after 1400 days of operation, which is a decline of 27% of permeability index after almost 4 years of treatment.

Regarding SEM-MBR, correlations with C x t and operating time were not statistically significant, but the C x t presented the higher correlation coefficient (-0.557). This MBR presented lower residual fouling rate than SAV-MBR, which might be related to the lower total filtration time, and associated total permeate volume. After the same 1400 operating days, SEM-MBR reached an average normalized permeability index of 0.84. However, this decline is not homogeneous between the different membrane tanks: as example, SEM-UF8 reached 0.75 after the same period.

A further analysis regarding all cumulative process indicators was performed in the following to determine the impacts of the other operating conditions in membrane ageing of each MBR and their membrane tanks.

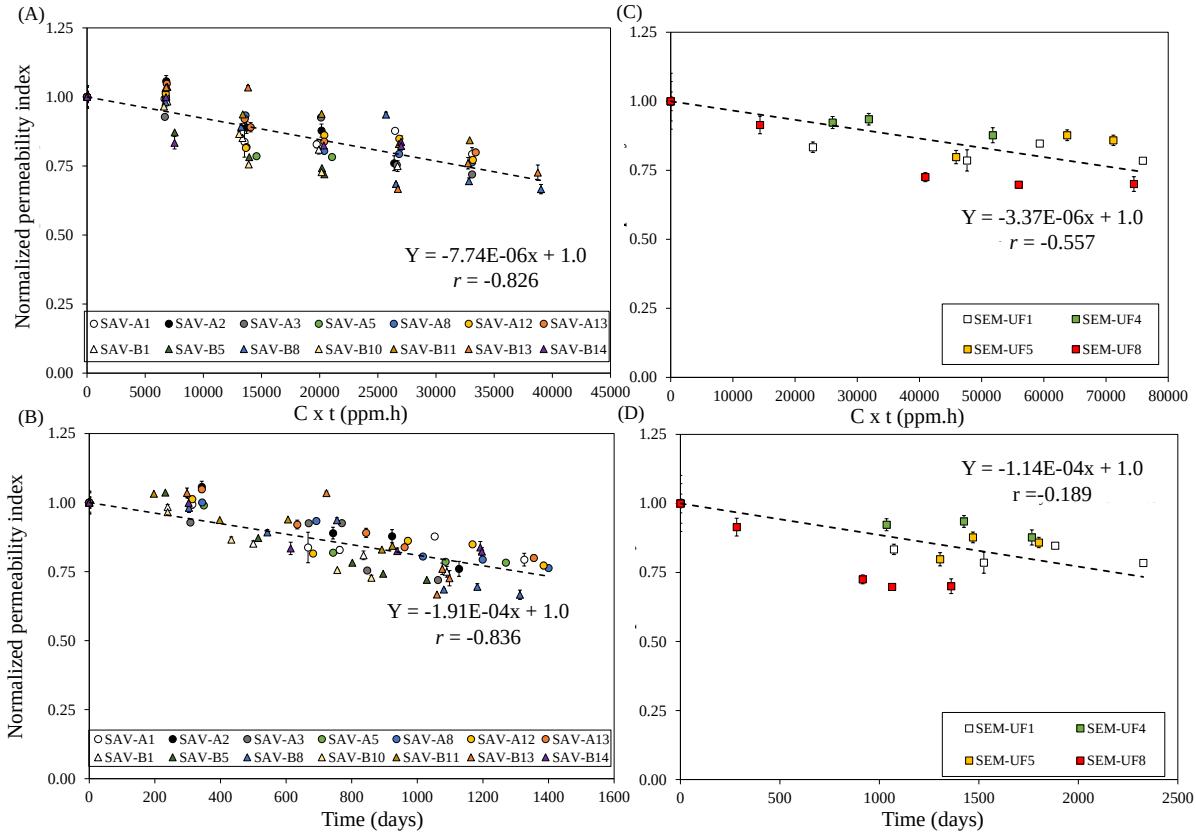

Figure 4.19: Normalized permeability index for SAV-MBR with respect to C x t (A) and to operating time (B) and similarly for SEM-MBR with respect to C x t (C) and to operating time (D).

4.2. CORRELATION BETWEEN PERMEABILITY INDEX AND PROCESS CUMULATIVE INDICATORS

The normalized permeability index was determined and correlated with the seven cumulative process indicators (Table 4.5). All indicators presented statistically significant correlations to the normalized permeability index for SAV (p-value< 0.05), but among those that are measured for each individual membrane tank, the operating days presented a slightly higher correlation coefficient. Regarding the sludge quality parameters, MLSS stood out over supernatant COD or ΔCOD. This higher correlation may indicate that sludge flocs and particulates may play a bigger role in membrane ageing than colloidal fractions. However, this slight difference may

be related to the frequency of each measurement. MLSS data is obtained every day and COD is only measured twice a week.

The higher correlation coefficient for SAV also suggested that normalized permeability index decreased linearly as a function of operating days and the cumulated specific filtered MLSS (closely linked to the cumulated permeate volume) with residual fouling rates of -1.905E-4 d^{-1} and -8.523E-5 (kg MLSS/m^2 membrane)$^{-1}$ (Figure 4.19.B and Figure 4.20.B, respectively). The graphs between normalized permeability index and the other indicators are presented in Appendix E.

For SEM-MBR, correlation coefficients are lower than the ones observed SAV-MBR, with non-significant correlations (Table 4.5). This dispersion can be observed in Figure 4.20. C and D with the plot of the normalized permeability index as a function of the cumulated specific permeate volume and the specific filtered MLSS. This higher variation in the behavior of each membrane tank might be associated to differences in chlorine exposure (Figure 4.10) and a lower rate of filtration (Figure 4.11).

Globally, SAV-MBR presented a slightly faster rate of decline in normalized permeability index than SEM-MBR with respect to operating days (slopes in Figure 4.19.B and D, respectively), which might be linked to the higher filtration rate observed in SAV-MBR (Figure 4.17).

Table 4.5 : Spearman correlation coefficients between each process indicator and the normalized permeability index (bold values are the highest correlation coefficients).

Process indicators	Normalized permeability index - SAV	Normalized permeability index - SEM
Operating time	**-0.836**	-0.189
Permeate volume	-0.823	-0.075
Exposure dose	-0.826	**-0.557**
SupernatantCOD	-0.763	-
ΔCOD	-0.667	-
Filtered MLSS	**-0.839**	-0.111
Aeration volume	-0.812	-0.129

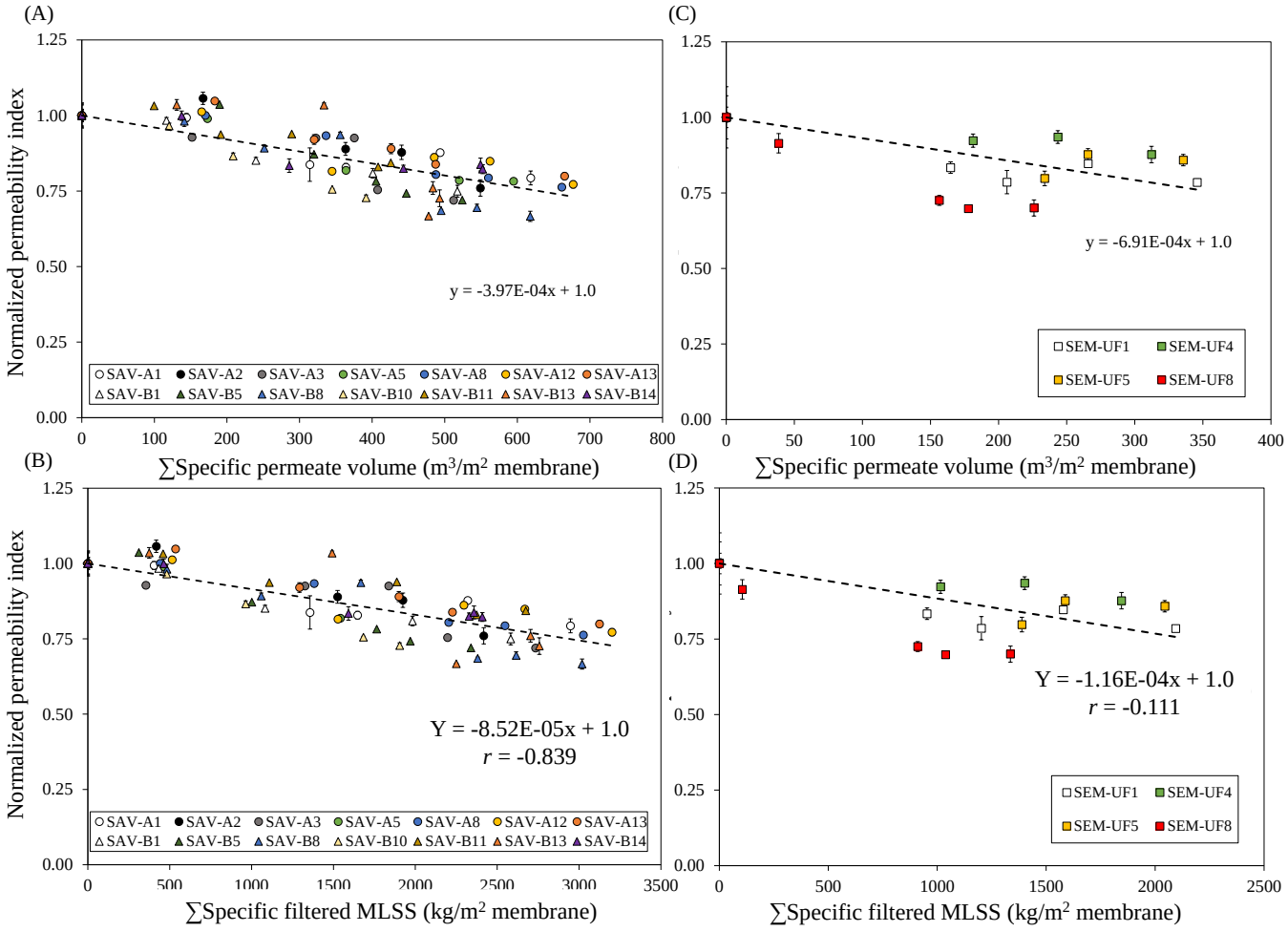

Figure 4.20: Normalized permeability index as a function of cumulated specific permeate volume (A), specific filtered MLSS (B) for SAV-MBR and specific permeate volume (C) and specific filtered MLSS (D) for SEM-MBR.

Additionally, SAV-MBR presented high variations of non-filtration time according to each membrane tank. A group of membrane tank with higher non-filtration time was compared to a group presenting lower non-filtration time and the differences in normalized permeability index were not statistically significant. These results are presented in Appendix F.

As a conclusion, it appears that the decline in permeability index at macro-scale may be linked to the residual fouling, related to the cumulated permeate volume, and these evolutions are equivalent in terms of order of magnitude between the two studied MBRs. However, it could be considered that the significant evolutions observed at micro scale do not affect at this stage the filtration performance at the industrial scale regarding the relative short period of time of the study compared to the membrane life-time expectations. The study of the evolution at full-scale, in parallel of the characterization of sampled membranes, must be continued in order to evaluate the consequences of these micro-scale observations on full-scale performances and the potential difference in impact between MBRs, linked to operating conditions.

4.3. CORRELATIONS BETWEEN MEMBRANE AUTOPSIES PROPERTIES AND NORMALIZED PERMEABILITY INDEX

Membrane properties is expected to affect their ability to filter organic matter. Since membrane were harvested just before each CIP protocol and characterized in the lab after cleaning at similar concentrations and soaking time from each MBR (see Chapter 2), results from samples characterization, i.e. intrinsic permeability (Figure 4.15) and PVP content (Figure 4.16), were correlated to the normalized permeability index (Figure 4.19) obtained from operating data. These correlations are presented in Figure 4.21.

PVP content and intrinsic permeability presented statistically significant correlations to the normalized permeability index. Moreover, hydrophilic agent content presented the highest

Spearman correlation coefficient (R = 0.598, p-value<0.001) compared to the intrinsic permeability (R= -0.476; p-value=0.006). Although it is still necessary to collect data in the later phases of membrane life to confirm these findings, these results showed a slight effect of the PVP content decrease on macroscopic indicators, such as the normalized permeability index.

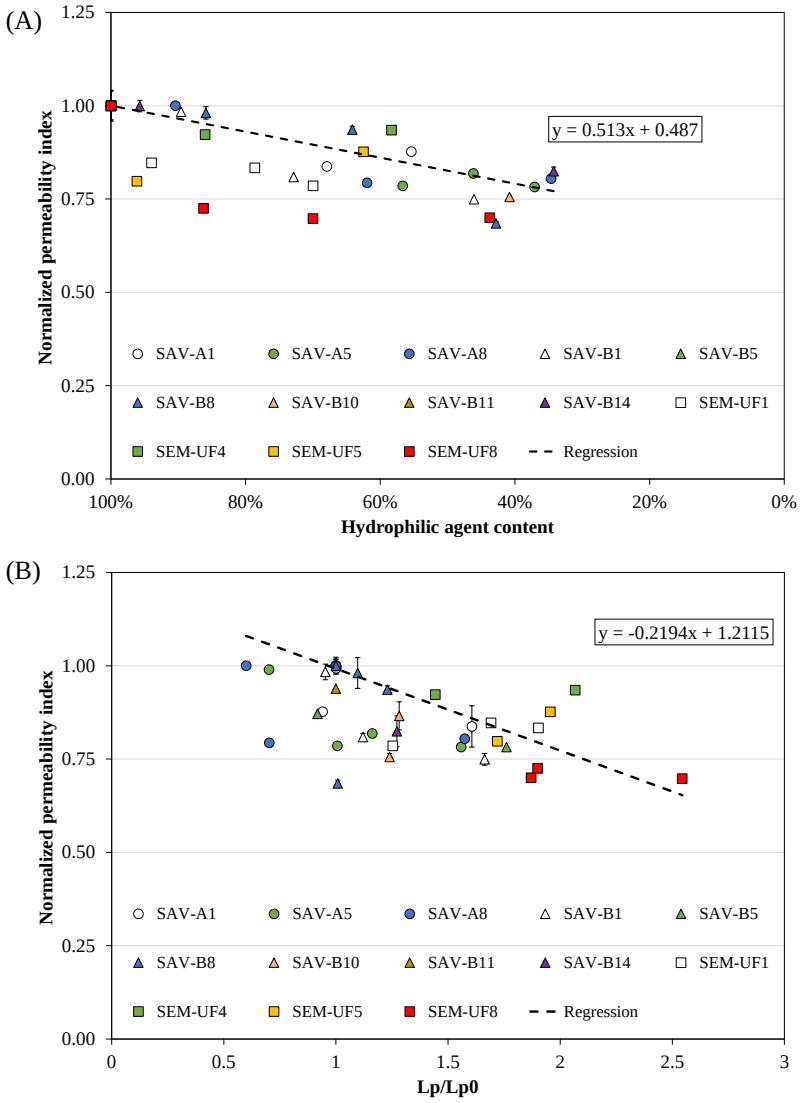

Figure 4.21: Normalized permeability index with respect to hydrophilic agent content and intrinsic permeability.

This decline in PVP content, affecting normalized permeability index to hamper filtration and favor fouling is in accordance with the findings of Robinson and Bérubé (2020) for the characterization of aged PVDF membranes harvested from drinking water facilities [26]. Authors measured fouling rate of harvested samples by filtration of a model solution and found higher fouling rates for membranes presenting lower hydrophilic agent contents.

Therefore, hydrophilic agent content and intrinsic permeability, in a minor precision, have proven to be key parameters to monitor membrane ageing and should be prioritized in the case of membrane autopsies.

These results also showed that efforts are needed into the conceptualization of more stable membrane compositions, especially, with stable hydrophilicity and pore size under MBR operating conditions.

5. CONCLUSIONS

Membrane autopsies

- Mechanical resistance is not a concern in full-scale MBR equipped with Zeeweed membranes, which are supported PVDF hollow-fibers. No signs of suspended solids are found in permeate over the duration of this research.
- Two MBRs with distinctive operating conditions were analyzed in long-term operation. Membranes from SEM-MBR are exposed to higher chlorine doses and less filtration, which contributed to higher intrinsic permeabilities than SAV-MBR. PVP content was lower for membranes from SAV-MBR at a same C x t, but equivalent for the same permeate volume produced. This indicates that not only chlorine exposure is responsible for the degradation of PVP, but also hydrodynamic conditions (linked to aeration and filtration dynamics) are likely to affect this degradation.

Process indicators

- For SAV-MBR, sludge flocs and particulates seemed to contribute more to the decline in permeability index than the colloidal fractions, since cumulated filtered MLSS presented higher correlation coefficient than cumulated filter COD or ΔCOD.
- SEM-MBR decline in permeability index correlated better with the exposure dose, probably due to higher chlorine exposure and less permeate filtration rates.
- SAV-MBR's strategy of conserving membranes in low chlorine levels (3 – 15 ppm) during non-filtration periods seemed to not affect permeability index decline.
- Decline in normalized permeability index for SAV-MBR and SEM-MBR were similar with respect to specific permeate volume.

Coupling process indicators and membrane autopsies

- Permeability index correlated well to the hydrophilic agent content and intrinsic permeability of harvested membranes. Thus, these measurements should be a priority when autopsies are carried out. In addition, efforts are needed into the conceptualization of more stable membrane compositions, especially, with stable hydrophilicity under chlorine exposure and hydraulic dynamics.
- The decline in permeability index at macro-scale is mainly linked to the residual fouling, related to the cumulated permeate volume, and these evolutions are equivalent in terms of order of magnitude for both MBRs studied. The significant evolutions observed at micro scale do not affect at this stage the filtration performance at the industrial scale regarding the relative short period of time of the study compared to the membrane life-time expectations. The study of the evolution at full-scale, in parallel of the characterization of sampled membranes, must be continued in order to evaluate the consequences of these micro-scale observations on full-scale performances and the potential difference in impact between MBRs, linked to operating conditions.

GENERAL CONCLUSIONS AND PERSPECTIVES

1. GENERAL CONCLUSIONS

Membrane ageing studies mainly focused on understanding changes of membrane properties in contact with sodium hypochlorite. A few others increased the complexity by including cycles of a model solution filtration and chemical cleaning in the ageing procedure. More recently, these two approaches were used and compared for the characterization of PVDF membranes aged in drinking water facilities. All these studies monitored ageing by membrane autopsies, which means harvesting fibers and characterizing them with different analytical techniques. Only one study monitored ageing of PVDF membranes in MBR considering rather data generated from sensors in the process. Therefore, this thesis focused on addressing the lack of knowledge regarding supported PVDF membrane ageing in MBR conditions treating urban wastewater.

Effect of chlorine exposure on supported PVDF membrane by single soaking in NaOCl at bench-scale

Supported PVDF membranes were single soaked in 1000 ppm NaOCl solutions at pH 9.0 for C x t ranging from 0 to 750 000 ppm.h. These samples were characterized according to a wide range of properties. Regarding mechanical resistance, chlorine exposure did not affect significantly ultimate tensile strength and elongation at the breaking point; however, hollow-fibers seemed to become slightly more rigid in their elastic zone (low deformation zones). These properties are related to the support polymer, which is likely to be based on PET, a highly chlorine resistant polymer.

Chlorine exposure highly influenced filtration properties of these membranes. Intrinsic permeability presented a three-phase behavior. At first, it increased up to 90% of initial intrinsic permeability for a C x t of 78,000 ppm.h, and then it decreased to the range of its initial value between 78,000 ppm.h and 150,000 ppm.h. After 150,000 ppm.h, intrinsic permeability

fluctuated around its initial value. It was demonstrated that the first increasing phase correlated well to the increasing membrane porosity with formation of small pores (< 20 nm), which is likely to be caused by the degradation of PVP into secondary products. The following decreasing phase might be related to changes in PVDF chains observed with the appearance of a band at 1650 cm^{-1} in FTIR spectra related to a carbonyl group, usually formed after defluorination. It seems that PVP should be eliminated up to a certain point, and then this restructuration of PVDF takes place. Further analysis are necessary to establish the exact mechanism behind this decreasing permeability.

Cleaning recovery increased from 56% to 65% after ageing membranes up to 125,000 ppm.h and should be related to a higher negatively charged surface, caused by the degradation of PVP into secondary products. After that, cleaning recovery decreased back to 51% probably due to topographic changes, with a potential increase in roughness contributing to foulant adsorption.

Representability of accelerated ageing protocols at bench-scale towards membrane ageing in full-scale MBR conditions

Contrarily to bench-scale ageing, membranes harvested from full-scale MBR presented a decline of 45% in ultimate tensile strength and relatively stable elongation at the breaking zone. At their elastic zone, membranes presented lower rigidity (Young's modulus decreased by 33%). However, fiber breakage was never reported by the operators of the studied WWTP.

Furthermore, intrinsic permeability increased during the studied period reaching 1.6 times the initial value at 98,000 ppm.h. This increasing trend in permeability is also linked to the PVP degradation and an increase in porosity with appearance of smaller (< 20 nm) and bigger (>40 nm) pores. PVP content reached lower levels for full-scale MBR ageing than at bench-scale (25% against 40%). Based on FTIR spectra, it seems that PVP is dislodged from membrane structure, creating bigger pores and contributing to the increase in permeability.

Cleaning recovery decreased from 56% for a pristine membrane to 32% for membranes harvested at 98,000 ppm.h. These results illustrate the stronger interactions between foulants and residual fouling from full-scale operation that remains in the membrane structure even after chemical cleanings.

Therefore, although accelerated ageing protocols by single soaking provide interesting information about membrane material sensitivity towards chlorine, the changes in membrane properties observed in this protocol did not fully represent results from membranes harvested at full-scale MBR. In both cases, PVP was oxidized, but different secondary products were found, besides different patterns in morphology, pore size, permeability and cleaning recovery.

Membrane ageing at full-scale MBR based on membrane properties and indicators of operation

Membrane ageing was studied in two full-scale MBR presenting slightly different conditions. Based on membrane properties, one group of membranes presented ultimate tensile strength higher than 300 MPa and another presented values lower than 300 MPa. Samples from both MBRs were in both groups, which suggests that the reason for membranes presenting lower ultimate tensile strength is more likely to be related to to operating conditions or sampling method. However, further analysis and sampling is been carried out to investigate the origin of such differences.

Intrinsic permeability seemed to be more sensible to ageing for the group of lower mechanical resistance, increasing up to 2.5 of initial values. Although the great dispersion, samples from both MBRs in the two groups presented similar trends.

PVP content was one of the most sensible membrane properties to ageing regarding operating conditions. Actually, membranes harvested from SAV-MBR presented a faster decline in PVP content reaching around 35% of the initial value at an exposure dose of 20,000 ppm.h (1000 days of operation), whereas samples from SEM-MBR were around 80% at the same dose.

However, when this parameter is plotted against filtration related indicators (cumulated specific permeate volume or specific MLSS mass), both MBRs presented the same rate of decline. This reinforces that operating conditions (filtration, aeration, biomass presence)other than chlorine exposure play an important role in membrane ageing.

Data generated directly from the process sensors were collected and filtration performance of MBRs was measured based on the permeability index, which is the ratio between permeate flux at 20°C and transmembrane pressure during filtration after CIP protocol. This indicator decreased faster for SAV-MBR than SEM-MBR in average with respect to the operating time (27% against 16% decline in 1400 days). However, the membrane tank SEM-UF8 decreased by 25% at the same period but this membrane tank presented a much higher chlorine exposure per permeate volume than all other membrane tanks due to accidentally prolonged CIP protocols. This data suggests that SEM-MBR choice to keep all membrane tanks filtering during a shorter period daily is efficient in maintaining permeability index at high levels over time, but special attention should be paid to control chlorine exposure.

Depending on the MBR operating conditions, some factors seemed to play bigger roles on the decline of permeability index. For SAV, the decline correlated well with cumulated filtered MLSS, whereas for SEM, chlorine exposure dose presented the best correlation. This might be related to the fact that SAV's membranes presented much higher cumulated permeate volume for the same exposure dose than SEM's membranes.

Whenever a membrane tank from SAV-MBR was not available for filtration for several days, membranes were kept in NaOCl solutions at low concentrations. This choice did not affect permeability index. Data in the later stages of membrane's life are needed to validate this operating choice.

Key indicators to monitor membrane ageing in full-scale MBR

To monitor membrane ageing, key indicators should provide information about filtration capacity and membrane properties. Permeability index presented statistically significant correlation to PVP content and intrinsic permeability. Therefore, these indicators are suitable to monitor membrane ageing, when PVP is degraded, intrinsic permeability is likely to increase and permeability index decreases.

Regarding cumulated process indicators, the C x t did not present the best correlations with membrane properties or permeability index. On the other hand, data related to filtration such as cumulated permeate volume, cumulated filtered MLSS mass and supernatant COD are promising to monitor membrane ageing and become new benchmarks for membrane lifespan.

2. PERSPECTIVES

Implications in terms of membrane lifespan

During the studied period, although bigger pores may be observed on the membrane surface, no signs of degradation in permeate quality were observed. Therefore, integrity issues did not promote membrane replacement over the 7 years considered in this research.

Based on the decline in permeability index with respect to the cumulated process indicators and assuming that the linear trends observed up to this date remain until membrane replacement, membrane end-life could be estimated considering average and peak filtration conditions. End-life was predicted for SAV-MBR and SEM-MBR in 11 – 13 and 18 – 22 operating years, respectively. However, membranes from SAV-MBR would have filtered around 1,900 – 2,300 m3/m2 (9,000 – 11,000 kg MLSS/m2) as opposed to 1,100 – 1,300 m3/m2 (6500 – 7800 kg MLSS/m2) for SEM-MBR. Further researches considering data from a full cycle of life for these membranes are still necessary to validate this approach.

Effect of chlorine exposure on supported PVDF membrane by single soaking in NaOCl at bench-scale

A further characterization of PVDF chains during chlorine exposure would provide useful information about the changes in membrane material and could help to validate the assumptions on the filtration properties evolution of these membranes over soaking in chlorine. Size exclusion chromatography might be able to determine crosslinking and chain scission. Crystallinity can be measured by differential scanning calorimetry and more information about functional groups may be obtained by nuclear magnetic resonance.

Representability of accelerated ageing protocols at bench-scale towards membrane ageing in full-scale MBR conditions

Based on the differences observed in membrane ageing by single soaking and in full-scale MBR, establishing an accelerated ageing protocol that takes into consideration filtration cycles, aeration and organic matter presence in addition to chlorine exposure would be an interesting tool to predict long-term performance. Different membranes could be tested, compared and these data could be taken into consideration when designing a full-scale MBR or replacing membranes in an already built one.

Preliminary tests were performed in a 2-m^3 membrane pilot installed in SAV WWTP (Figure GC.1). The pilot MBR was equipped with ZeeWeed® 500 D membrane modules operating in similar conditions to the full-scale SAV-MBR (permeate flux, aeration demand, cleaning cycles). The tank is fed by mixed liquor directly from the end of aerated zone from the same biological tank that fed membrane compartments in the full-scale SAV-MBR.

Figure GC.1: Pilot-scale membrane tank used in preliminary tests of accelerated ageing in on-site conditions.

The strategy used to accelerate ageing is to increase the frequency of CIP protocols. Thus, instead of doing each 6 to 12 months, CIP protocols in the pilot-scale MBR were performed every two months. Based on these tests performed over 18 months, a new project was granted by *Agence de l'Eau Seine Normandie* starting in January/2022 with the aim to characterize membrane ageing in operating conditions for two different PVDF membranes with different hydrophilic agents.

Membrane ageing at full-scale MBR based on membrane properties and operating indicators

Based on data presented in Chapter 4, it seems that the decline in permeability index correlated well with PVP content, thus strategies to avoid the elimination of PVP from membrane structure are necessary. These might be operating strategies, such as limiting chlorine exposure or

changing chemicals, or manufacturing strategies, such as developing chlorine resistant membrane materials.

Regarding chlorine exposure, a way to measure the optimal time for cleaning efficiency during CIP should be developed. During chemical cleaning, organic matter is oxidized from the membrane surface and solubilized in the cleaning solution. UV sensors that can measure this increase in organic matter in the solution until its stabilization and decrease might be useful to limit chlorine overexposure and increase membrane lifespan.

Key indicators to monitor membrane ageing in full-scale MBR

Permeability index after CIP protocols, PVP content and intrinsic permeability are promising indicators to monitor membrane ageing in full-scale MBR. PVP content and intrinsic permeability may be performed in-situ instead of harvesting membrane samples. Portable infrared devices are becoming available and intrinsic permeability may be performed by filtration of clean water after rinsing chemical cleaning solutions. Besides, cumulated process indicators related to the filtration conditions, such as permeate volume, filtered MLSS mass and supernatant COD, should be integrated in membrane ageing studies. Additionally, permeability index after CIP protocols characterize only the maximum value of flux that membranes can reach after cleaning. This indicator does not provide any information about the kinetics of flux decline between two CIP protocols. Therefore, a new indicator that provide this fouling rate during filtration between two CIP protocols would be useful to monitor membrane ageing.

BIBLIOGRAPHY

[1] The MBR site, (2021). https://www.thembrsite.com/ (accessed April 20, 2021).

[2] P. Krzeminski, L. Leverette, S. Malamis, E. Katsou, Membrane bioreactors – A review on recent developments in energy reduction, fouling control, novel configurations, LCA and market prospects, J. Membr. Sci. 527 (2017) 207–227. https://doi.org/10.1016/j.memsci.2016.12.010.

[3] G. Bertanza, M. Canato, G. Laera, M. Vaccari, M. Svanström, S. Heimersson, A comparison between two full-scale MBR and CAS municipal wastewater treatment plants: techno-economic-environmental assessment, Environ. Sci. Pollut. Res. 24 (2017) 17383–17393. https://doi.org/10.1007/s11356-017-9409-3.

[4] K. Xiao, S. Liang, X. Wang, C. Chen, X. Huang, Current state and challenges of full-scale membrane bioreactor applications: A critical review, Bioresour. Technol. 271 (2019) 473–481. https://doi.org/10.1016/j.biortech.2018.09.061.

[5] M. Bagheri, S.A. Mirbagheri, Critical review of fouling mitigation strategies in membrane bioreactors treating water and wastewater, Bioresour. Technol. 258 (2018) 318–334. https://doi.org/10.1016/j.biortech.2018.03.026.

[6] A. Fenu, W. De Wilde, M. Gaertner, M. Weemaes, G. de Gueldre, B. Van De Steene, Elaborating the membrane life concept in a full scale hollow-fibers MBR, J. Membr. Sci. 421–422 (2012) 349–354. https://doi.org/10.1016/j.memsci.2012.08.001.

[7] B. Verrecht, T. Maere, I. Nopens, C. Brepols, S. Judd, The cost of a large-scale hollow fibre MBR, Water Res. 44 (2010) 5274–5283. https://doi.org/10.1016/j.watres.2010.06.054.

[8] S. Robinson, S.Z. Abdullah, P. Bérubé, P. Le-Clech, Ageing of membranes for water treatment: Linking changes to performance, J. Membr. Sci. 503 (2016) 177–187. https://doi.org/10.1016/j.memsci.2015.12.033.

[9] S.Z. Abdullah, P.R. Bérubé, Filtration and cleaning performances of PVDF membranes aged with exposure to sodium hypochlorite, Sep. Purif. Technol. 195 (2018) 253–259. https://doi.org/10.1016/j.seppur.2017.12.004.

[10] S.Z. Abdullah, P.R. Bérubé, Assessing the effects of sodium hypochlorite exposure on the characteristics of PVDF based membranes, Water Res. 47 (2013) 5392–5399. https://doi.org/10.1016/j.watres.2013.06.018.

[11] F. Gao, J. Wang, H. Zhang, M.A. Hang, Z. Cui, G. Yang, Interaction energy and competitive adsorption evaluation of different NOM fractions on aged membrane surfaces, J. Membr. Sci. 542 (2017) 195–207. https://doi.org/10.1016/j.memsci.2017.08.020.

[12] I. Levitsky, A. Duek, E. Arkhangelsky, D. Pinchev, T. Kadoshian, H. Shetrit, R. Naim, V. Gitis, Understanding the oxidative cleaning of UF membranes, J. Membr. Sci. 377 (2011) 206–213. https://doi.org/10.1016/j.memsci.2011.04.046.

[13] K. Li, Q. Su, S. Li, G. Wen, T. Huang, Aging of PVDF and PES ultrafiltration membranes by sodium hypochlorite: Effect of solution pH, J. Environ. Sci. 104 (2021) 444–455. https://doi.org/10.1016/j.jes.2020.12.020.

[14] V. Puspitasari, A. Granville, P. Le-Clech, V. Chen, Cleaning and ageing effect of sodium hypochlorite on polyvinylidene fluoride (PVDF) membrane, Sep. Purif. Technol. 72 (2010) 301–308. https://doi.org/10.1016/j.seppur.2010.03.001.

[15] M.F. Rabuni, N.M.N. Sulaiman, N.A. Hashim, A systematic assessment method for the investigation of the PVDF membrane stability, Desalination Water Treat. 57 (2016) 1–12. https://doi.org/10.1080/19443994.2015.1012336.

[16] M.F. Rabuni, N.M. Nik Sulaiman, M.K. Aroua, C. Yern Chee, N. Awanis Hashim, Impact of in situ physical and chemical cleaning on PVDF membrane properties and performances, Chem. Eng. Sci. 122 (2015) 426–435. https://doi.org/10.1016/j.ces.2014.09.053.
[17] J. Ravereau, A. Fabre, A. Brehant, R. Bonnard, C. Sollogoub, J. Verdu, Ageing of polyvinylidene fluoride hollow fiber membranes in sodium hypochlorite solutions, J. Membr. Sci. 505 (2016) 174–184. https://doi.org/10.1016/j.memsci.2015.12.063.
[18] L. Ren, S. Yu, H. Yang, L. Li, L. Cai, Q. Xia, Z. Shi, G. Liu, Chemical cleaning reagent of sodium hypochlorite eroding polyvinylidene fluoride ultrafiltration membranes: Aging pathway, performance decay and molecular mechanism, J. Membr. Sci. 625 (2021) 119141. https://doi.org/10.1016/j.memsci.2021.119141.
[19] L. Vanysacker, R. Bernshtein, I.F.J. Vankelecom, Effect of chemical cleaning and membrane aging on membrane biofouling using model organisms with increasing complexity, J. Membr. Sci. 457 (2014) 19–28. https://doi.org/10.1016/j.memsci.2014.01.015.
[20] Q. Wang, H. Zeng, Z. Wu, J. Cao, Impact of sodium hypochlorite cleaning on the surface properties and performance of PVDF membranes, Appl. Surf. Sci. 428 (2018) 289–295. https://doi.org/10.1016/j.apsusc.2017.09.056.
[21] Q. Wu, X. Zhang, G. Cao, Impacts of sodium hydroxide and sodium hypochlorite aging on polyvinylidene fluoride membranes fabricated with different methods, J. Environ. Sci. 67 (2018) 294–308. https://doi.org/10.1016/j.jes.2017.07.014.
[22] Y. Zhang, J. Wang, F. Gao, Y. Chen, H. Zhang, A comparison study: The different impacts of sodium hypochlorite on PVDF and PSF ultrafiltration (UF) membranes, Water Res. 109 (2017) 227–236. https://doi.org/10.1016/j.watres.2016.11.022.
[23] S. Hajibabania, A. Antony, G. Leslie, P. Le-Clech, Relative impact of fouling and cleaning on PVDF membrane hydraulic performances, Sep. Purif. Technol. 90 (2012) 204–212. https://doi.org/10.1016/j.seppur.2012.03.001.
[24] F. Gao, J. Wang, H. Zhang, Y. Zhang, M.A. Hang, Effects of sodium hypochlorite on structural/surface characteristics, filtration performance and fouling behaviors of PVDF membranes, J. Membr. Sci. 519 (2016) 22–31. https://doi.org/10.1016/j.memsci.2016.07.024.
[25] S.J. Robinson, P.R. Bérubé, Seeking realistic membrane ageing at bench-scale, J. Membr. Sci. 618 (2021) 118606. https://doi.org/10.1016/j.memsci.2020.118606.
[26] S. Robinson, P.R. Bérubé, Membrane ageing in full-scale water treatment plants, Water Res. 169 (2020) 115212. https://doi.org/10.1016/j.watres.2019.115212.
[27] H. Yu, X. Li, H. Chang, Z. Zhou, T. Zhang, Y. Yang, G. Li, H. Ji, C. Cai, H. Liang, Performance of hollow fiber ultrafiltration membrane in a full-scale drinking water treatment plant in China: A systematic evaluation during 7-year operation, J. Membr. Sci. 613 (2020) 118469. https://doi.org/10.1016/j.memsci.2020.118469.
[28] R. Mailler, J. Pouillaude, Y. Fayolle, M. Oliveira Filho, C. Causserand, V. Rocher, Long-term performances and membrane lifespan of full-scale MBR treating filtrate from sludge ultra-dewatering, Environ. Technol. (2021) 1–29. https://doi.org/10.1080/09593330.2021.2010809.
[29] M. Oliveira Filho, R. Mailler, V. Rocher, Y. Fayolle, C. Causserand, Comprehensive study of supported PVDF membrane ageing in MBR: A direct comparison between changes at bench scale and full scale, Sep. Purif. Technol. 279 (2021) 119695. https://doi.org/10.1016/j.seppur.2021.119695.
[30] J.C. Martins, 2017 Annual Report: Scaling Up for Impact – 2030 Water Resources Group – World Bank Group, (n.d.). https://www.2030wrg.org/2017-annual-report-scaling-up-for-impact/ (accessed April 15, 2019).

[31] WHO | WHO water, sanitation and hygiene strategy 2018-2025, World Health Organization, Geneva, 2018.
[32] M. Salgot, M. Folch, Wastewater treatment and water reuse, Curr. Opin. Environ. Sci. Health. 2 (2018) 64–74. https://doi.org/10.1016/j.coesh.2018.03.005.
[33] I.V. Muralikrishna, V. Manickam, Chapter Twelve - Wastewater Treatment Technologies, in: I.V. Muralikrishna, V. Manickam (Eds.), Environ. Manage., Butterworth-Heinemann, 2017: pp. 249–293. https://doi.org/10.1016/B978-0-12-811989-1.00012-9.
[34] J. Reungoat, B.I. Escher, M. Macova, J. Keller, Biofiltration of wastewater treatment plant effluent: Effective removal of pharmaceuticals and personal care products and reduction of toxicity, Water Res. 45 (2011) 2751–2762. https://doi.org/10.1016/j.watres.2011.02.013.
[35] A.G.N. van Bentem, N. Nijman, P.F.T. Schyns, C.P. Petri, MBR Varsseveld: 5 years of operational experience, Water Pract. Technol. 5 (2010). https://doi.org/10.2166/wpt.2010.013.
[36] B. Seyhi, P. Droguil, G. Buelna, J.-F. Blais, M. Heran, État actuel des connaissances des procédés de bioréacteur à membrane pour le traitement et la réutilisation des eaux usées industrielles et urbaines, Rev. Sci. L'eau J. Water Sci. 24 (2011) 283–310. https://doi.org/10.7202/1006478ar.
[37] M. Scholz, Chapter 15 - Activated Sludge Processes, in: M. Scholz (Ed.), Wetl. Water Pollut. Control Second Ed., Elsevier, 2016: pp. 91–105. https://doi.org/10.1016/B978-0-444-63607-2.00015-0.
[38] P. Le-Clech, V. Chen, T.A.G. Fane, Fouling in membrane bioreactors used in wastewater treatment, J. Membr. Sci. 284 (2006) 17–53. https://doi.org/10.1016/j.memsci.2006.08.019.
[39] M. Stricot, Bioréacteurs à membranes à configuration externe : influence de la configuration du procédé sur la structuration des matrices biologiques et le colmatage des membranes, thesis, Toulouse, INSA, 2008. http://www.theses.fr/2008ISAT0015 (accessed March 19, 2019).
[40] P. Le-Clech, Membrane bioreactors and their uses in wastewater treatments, Appl. Microbiol. Biotechnol. 88 (2010) 1253–1260. https://doi.org/10.1007/s00253-010-2885-8.
[41] A. Drews, Membrane fouling in membrane bioreactors—Characterisation, contradictions, cause and cures, J. Membr. Sci. 363 (2010) 1–28. https://doi.org/10.1016/j.memsci.2010.06.046.
[42] T. Fenchel, G.M. King, T.H. Blackburn, Chapter 1 - Bacterial Metabolism, in: T. Fenchel, G.M. King, T.H. Blackburn (Eds.), Bact. Biogeochem. Third Ed., Academic Press, Boston, 2012: pp. 1–34. https://doi.org/10.1016/B978-0-12-415836-8.00001-3.
[43] S.M.K. Sadr, D.P. Saroj, 14 - Membrane technologies for municipal wastewater treatment, in: A. Basile, A. Cassano, N.K. Rastogi (Eds.), Adv. Membr. Technol. Water Treat., Woodhead Publishing, Oxford, 2015: pp. 443–463. https://doi.org/10.1016/B978-1-78242-121-4.00014-9.
[44] S.A. Deowan, S.I. Bouhadjar, J. Hoinkis, 5 - Membrane bioreactors for water treatment, in: A. Basile, A. Cassano, N.K. Rastogi (Eds.), Adv. Membr. Technol. Water Treat., Woodhead Publishing, Oxford, 2015: pp. 155–184. https://doi.org/10.1016/B978-1-78242-121-4.00005-8.
[45] L. Benavente, Low fouling membranes for water and bio tech applications, thesis, Toulouse 3, 2016. http://www.theses.fr/2016TOU30213 (accessed March 19, 2019).
[46] C. Liu, L. Wu, C. Zhang, W. Chen, S. Luo, Surface hydrophilic modification of PVDF membranes by trace amounts of tannin and polyethyleneimine, Appl. Surf. Sci. 457 (2018) 695–704. https://doi.org/10.1016/j.apsusc.2018.06.131.

[47] J. Lv, G. Zhang, H. Zhang, C. Zhao, F. Yang, Improvement of antifouling performances for modified PVDF ultrafiltration membrane with hydrophilic cellulose nanocrystal, Appl. Surf. Sci. 440 (2018) 1091–1100. https://doi.org/10.1016/j.apsusc.2018.01.256.
[48] H. Lin, M. Zhang, F. Wang, F. Meng, B.-Q. Liao, H. Hong, J. Chen, W. Gao, A critical review of extracellular polymeric substances (EPSs) in membrane bioreactors: Characteristics, roles in membrane fouling and control strategies, J. Membr. Sci. 460 (2014) 110–125. https://doi.org/10.1016/j.memsci.2014.02.034.
[49] W. Zhang, J. Luo, L. Ding, M.Y. Jaffrin, A Review on Flux Decline Control Strategies in Pressure-Driven Membrane Processes, Ind. Eng. Chem. Res. 54 (2015) 2843–2861. https://doi.org/10.1021/ie504848m.
[50] W. Guo, H.-H. Ngo, J. Li, A mini-review on membrane fouling, Bioresour. Technol. 122 (2012) 27–34. https://doi.org/10.1016/j.biortech.2012.04.089.
[51] F. Wang, V.V. Tarabara, Pore blocking mechanisms during early stages of membrane fouling by colloids, J. Colloid Interface Sci. 328 (2008) 464–469. https://doi.org/10.1016/j.jcis.2008.09.028.
[52] M.E. Hernandez Rojas, Bioréacteur à membranes immergées pour le traitement d'eaux usées domestiques : influence des conditions biologiques sur les performances du procédé, thesis, Toulouse, INPT, 2006. http://www.theses.fr/2006INPT004G (accessed March 19, 2019).
[53] K. Lee, H. Yu, X. Zhang, K.-H. Choo, Quorum sensing and quenching in membrane bioreactors: Opportunities and challenges for biofouling control, Bioresour. Technol. 270 (2018) 656–668. https://doi.org/10.1016/j.biortech.2018.09.019.
[54] C. Kunacheva, D.C. Stuckey, Analytical methods for soluble microbial products (SMP) and extracellular polymers (ECP) in wastewater treatment systems: A review, Water Res. 61 (2014) 1–18. https://doi.org/10.1016/j.watres.2014.04.044.
[55] F. Meng, S. Zhang, Y. Oh, Z. Zhou, H.-S. Shin, S.-R. Chae, Fouling in membrane bioreactors: An updated review, Water Res. 114 (2017) 151–180. https://doi.org/10.1016/j.watres.2017.02.006.
[56] Y. Shen, K. Xiao, P. Liang, J. Sun, S. Sai, X. Huang, Characterization of soluble microbial products in 10 large-scale membrane bioreactors for municipal wastewater treatment in China, J. Membr. Sci. 415–416 (2012) 336–345. https://doi.org/10.1016/j.memsci.2012.05.017.
[57] C.S. Laspidou, B.E. Rittmann, A unified theory for extracellular polymeric substances, soluble microbial products, and active and inert biomass, Water Res. 36 (2002) 2711–2720.
[58] P.K. Gkotsis, D.C. Banti, E.N. Peleka, A.I. Zouboulis, P.E. Samaras, Fouling Issues in Membrane Bioreactors (MBRs) for Wastewater Treatment: Major Mechanisms, Prevention and Control Strategies, Processes. 2 (2014) 795–866. https://doi.org/10.3390/pr2040795.
[59] R. Habib, M.B. Asif, S. Iftekhar, Z. Khan, K. Gurung, V. Srivastava, M. Sillanpää, Influence of relaxation modes on membrane fouling in submerged membrane bioreactor for domestic wastewater treatment, Chemosphere. 181 (2017) 19–25. https://doi.org/10.1016/j.chemosphere.2017.04.048.
[60] A. Robles, M.V. Ruano, J. Ribes, J. Ferrer, Factors that affect the permeability of commercial hollow-fibre membranes in a submerged anaerobic MBR (HF-SAnMBR) system, Water Res. 47 (2013) 1277–1288. https://doi.org/10.1016/j.watres.2012.11.055.
[61] T. Zsirai, P. Buzatu, P. Aerts, S. Judd, Efficacy of relaxation, backflushing, chemical cleaning and clogging removal for an immersed hollow fibre membrane bioreactor, Water Res. 46 (2012) 4499–4507. https://doi.org/10.1016/j.watres.2012.05.004.

[62] L. He, J. Zhang, Z. Wang, Z. Wu, Chemical Cleaning of Membranes in a Long-Term Operated Full-Scale MBR for Restaurant Wastewater Treatment, Sep. Sci. Technol. 46 (2011) 2481–2488. https://doi.org/10.1080/01496395.2011.598206.
[63] I. Levitsky, A. Duek, R. Naim, E. Arkhangelsky, V. Gitis, Cleaning UF membranes with simple and formulated solutions, Chem. Eng. Sci. 69 (2012) 679–683. https://doi.org/10.1016/j.ces.2011.10.060.
[64] C. Brepols, K. Drensla, A. Janot, M. Trimborn, N. Engelhardt, Strategies for chemical cleaning in large scale membrane bioreactors, Water Sci. Technol. J. Int. Assoc. Water Pollut. Res. 57 (2008) 457–463. https://doi.org/10.2166/wst.2008.112.
[65] Z. Wang, J. Ma, C.Y. Tang, K. Kimura, Q. Wang, X. Han, Membrane cleaning in membrane bioreactors: A review, J. Membr. Sci. 468 (2014) 276–307. https://doi.org/10.1016/j.memsci.2014.05.060.
[66] C. Regula, E. Carretier, Y. Wyart, G. Gésan-Guiziou, A. Vincent, D. Boudot, P. Moulin, Chemical cleaning/disinfection and ageing of organic UF membranes: A review, Water Res. 56 (2014) 325–365. https://doi.org/10.1016/j.watres.2014.02.050.
[67] K.H. Tng, A. Antony, Y. Wang, G.L. Leslie, 11 - Membrane ageing during water treatment: Mechanisms, monitoring, and control, in: A. Basile, A. Cassano, N.K. Rastogi (Eds.), Adv. Membr. Technol. Water Treat., Woodhead Publishing, Oxford, 2015: pp. 349–378. https://doi.org/10.1016/B978-1-78242-121-4.00011-3.
[68] E. Akhondi, F. Zamani, K.H. Tng, G. Leslie, W.B. Krantz, A.G. Fane, J.W. Chew, The Performance and Fouling Control of Submerged Hollow Fiber (HF) Systems: A Review, Appl. Sci. 7 (2017) 765. https://doi.org/10.3390/app7080765.
[69] S.Z. Abdullah, P.R. Bérubé, D.J. Horne, SEM imaging of membranes: Importance of sample preparation and imaging parameters, J. Membr. Sci. 463 (2014) 113–125. https://doi.org/10.1016/j.memsci.2014.03.048.
[70] C. Causserand, B. Pellegrin, J.-C. Rouch, Effects of sodium hypochlorite exposure mode on PES/PVP ultrafiltration membrane degradation, Water Res. 85 (2015) 316–326. https://doi.org/10.1016/j.watres.2015.08.028.
[71] B. Pellegrin, F. Mezzari, Y. Hanafi, A. Szymczyk, J.-C. Remigy, C. Causserand, Filtration performance and pore size distribution of hypochlorite aged PES/PVP ultrafiltration membranes, J. Membr. Sci. 474 (2015) 175–186. https://doi.org/10.1016/j.memsci.2014.09.028.
[72] S. Rouaix, C. Causserand, P. Aimar, Experimental study of the effects of hypochlorite on polysulfone membrane properties, J. Membr. Sci. 277 (2006) 137–147. https://doi.org/10.1016/j.memsci.2005.10.040.
[73] C. Regula, E. Carretier, Y. Wyart, M. Sergent, G. Gésan-Guiziou, D. Ferry, A. Vincent, D. Boudot, P. Moulin, Ageing of ultrafiltration membranes in contact with sodium hypochlorite and commercial oxidant: Experimental designs as a new ageing protocol, Sep. Purif. Technol. 103 (2013) 119–138. https://doi.org/10.1016/j.seppur.2012.10.010.
[74] M.T. Tsehaye, S. Velizarov, B. Van der Bruggen, Stability of polyethersulfone membranes to oxidative agents: A review, Polym. Degrad. Stab. 157 (2018) 15–33. https://doi.org/10.1016/j.polymdegradstab.2018.09.004.
[75] Y. Hanafi, P. Loulergue, S. Ababou-Girard, C. Meriadec, M. Rabiller-Baudry, K. Baddari, A. Szymczyk, Electrokinetic analysis of PES/PVP membranes aged by sodium hypochlorite solutions at different pH, J. Membr. Sci. 501 (2016) 24–32. https://doi.org/10.1016/j.memsci.2015.11.041.
[76] L. Marbelia, M.R. Bilad, I.F.J. Vankelecom, Gradual PVP leaching from PVDF/PVP blend membranes and its effects on membrane fouling in membrane bioreactors, Sep. Purif. Technol. 213 (2019) 276–282. https://doi.org/10.1016/j.seppur.2018.12.045.

[77] J. Delattre, B. Rabaud, A. Bréhant, K. Glucina, C. Sollogoub, F. Thominette, Ageing of Hollow Fiber Membranes in Polyvinylidene Fluoride (PVDF) used in Water Treatment, Procedia Eng. 44 (2012) 764–767. https://doi.org/10.1016/j.proeng.2012.08.562.
[78] M.F. Rabuni, The contrastive study of chemical treatment on the properties of hydrophobic PVDF membrane, in: J. Appl. Sci. Process Eng., 2015.
[79] P. Cote, Z. Alam, J. Penny, Hollow fiber membrane life in membrane bioreactors (MBR), Desalination. 288 (2012) 145–151. https://doi.org/10.1016/j.desal.2011.12.026.
[80] S. Menon, K. Bansode, S. Nandi, V. Kalyanraman, Impact of cleaning agents on properties of tubular polyvinylidene fluoride (PVDF) membrane, Mater. Today Proc. 47 (2021) 1466–1471. https://doi.org/10.1016/j.matpr.2021.03.722.
[81] B. Pellegrin, R. Prulho, A. Rivaton, S. Thérias, J.-L. Gardette, E. Gaudichet-Maurin, C. Causserand, Multi-scale analysis of hypochlorite induced PES/PVP ultrafiltration membranes degradation, J. Membr. Sci. 447 (2013) 287–296. https://doi.org/10.1016/j.memsci.2013.07.026.
[82] R. Prulho, S. Therias, A. Rivaton, J.-L. Gardette, Ageing of polyethersulfone/polyvinylpyrrolidone blends in contact with bleach water, Polym. Degrad. Stab. 98 (2013) 1164–1172. https://doi.org/10.1016/j.polymdegradstab.2013.03.011.
[83] R.W. Field, D. Wu, J.A. Howell, B.B. Gupta, Critical flux concept for microfiltration fouling, J. Membr. Sci. 100 (1995) 259–272. https://doi.org/10.1016/0376-7388(94)00265-Z.
[84] A. Robles, M.V. Ruano, F. García-Usach, J. Ferrer, Sub-critical filtration conditions of commercial hollow-fibre membranes in a submerged anaerobic MBR (HF-SAnMBR) system: The effect of gas sparging intensity, Bioresour. Technol. 114 (2012) 247–254. https://doi.org/10.1016/j.biortech.2012.03.085.
[85] A.E. Childress, P. Le-Clech, J.L. Daugherty, C. Chen, G.L. Leslie, Mechanical analysis of hollow fiber membrane integrity in water reuse applications, Desalination. 180 (2005) 5–14. https://doi.org/10.1016/j.desal.2004.12.026.
[86] S. Rosenberger, C. Laabs, B. Lesjean, R. Gnirss, G. Amy, M. Jekel, J.-C. Schrotter, Impact of colloidal and soluble organic material on membrane performance in membrane bioreactors for municipal wastewater treatment, Water Res. 40 (2006) 710–720. https://doi.org/10.1016/j.watres.2005.11.028.
[87] N. Philippe, Analyse statistique et modélisation multivariée de l'évolution long terme de la perméabilité dans un bioréacteur à membranes à échelle réelle, Institut National des Sciences Appliquées de Toulouse, 2014.
[88] E.P. Barrett, L.G. Joyner, P.P. Halenda, The Determination of Pore Volume and Area Distributions in Porous Substances. I. Computations from Nitrogen Isotherms, J. Am. Chem. Soc. 73 (1951) 373–380. https://doi.org/10.1021/ja01145a126.
[89] R Core Team, R: A Language and Environment for Statistical Computing, R Foundation for Statistical Computing, Vienna, Austria, 2019.
[90] B.A. Pulido, O.S. Habboub, S.L. Aristizabal, G. Szekely, S.P. Nunes, Recycled Poly(ethylene terephthalate) for High Temperature Solvent Resistant Membranes, ACS Appl. Polym. Mater. 1 (2019) 2379–2387. https://doi.org/10.1021/acsapm.9b00493.
[91] G. Matar, G. Gonzalez-Gil, H. Maab, S. Nunes, P. Le-Clech, J. Vrouwenvelder, P.E. Saikaly, Temporal changes in extracellular polymeric substances on hydrophobic and hydrophilic membrane surfaces in a submerged membrane bioreactor, Water Res. 95 (2016) 27–38. https://doi.org/10.1016/j.watres.2016.02.064.
[92] E. Akhondi, F. Zamani, A.W.K. Law, W.B. Krantz, A.G. Fane, J.W. Chew, Influence of backwashing on the pore size of hollow fiber ultrafiltration membranes, J. Membr. Sci. 521 (2017) 33–42. https://doi.org/10.1016/j.memsci.2016.08.070.

Appendix A:

Specific aeration demand with respect to membrane surface (SAD_m) for the 14 membrane tanks studied from SAV-MBR

Table A.1: Statistical summary of SADm for membrane tanks in row A from SAV-MBR.

	SADm ($m^3/m^2/h$)							
Membrane tanks	**A1**	**A2**	**A3**	**A5**	**A5**	**A8**	**A12**	**A13**
Average	0.22	0.21	0.22	0.22	0.22	0.22	0.22	0.22
SD	0.06	0.05	0.06	0.05	0.05	0.06	0.05	0.05
1Q	0.18	0.17	0.18	0.18	0.18	0.18	0.18	0.19
2Q	0.24	0.22	0.23	0.23	0.23	0.24	0.23	0.24
3Q	0.27	0.25	0.26	0.26	0.26	0.27	0.26	0.27
Min	0.04	0.04	0.04	0.04	0.04	0.04	0.04	0.04
Max	0.32	0.28	0.31	0.31	0.31	0.31	0.30	0.32
5th Percentile	0.11	0.11	0.11	0.12	0.12	0.10	0.13	0.14
10th Percentile	0.15	0.14	0.14	0.14	0.14	0.14	0.15	0.15
90th Percentile	0.29	0.26	0.28	0.28	0.28	0.28	0.27	0.28
95th Percentile	0.30	0.27	0.29	0.28	0.28	0.29	0.28	0.28
N	1357	1074	1298	1400	1400	1375	1340	1390

Table A.2: Statistical summary of SADm for membrane tanks in row B from SAV-MBR.

	SAD ($m^3/m^2/h$)						
Membrane tanks	**B1**	**B5**	**B8**	**B10**	**B11**	**B13**	**B14**
Average	0.20	0.21	0.23	0.22	0.20	0.20	0.22
SD	0.05	0.05	0.05	0.05	0.05	0.05	0.05
1Q	0.16	0.17	0.19	0.17	0.17	0.17	0.18
2Q	0.21	0.22	0.24	0.23	0.21	0.21	0.23
3Q	0.24	0.25	0.27	0.26	0.24	0.24	0.26
Min	0.04	0.04	0.04	0.04	0.04	0.04	0.04
Max	0.29	0.30	0.31	0.30	0.29	0.29	0.31
5th Percentile	0.09	0.12	0.13	0.12	0.12	0.11	0.12
10th Percentile	0.13	0.14	0.16	0.14	0.14	0.14	0.14
90th Percentile	0.25	0.27	0.28	0.27	0.25	0.26	0.27
95th Percentile	0.26	0.28	0.29	0.28	0.26	0.27	0.29
N	1153	1044	1341	994	1224	1169	1265

Appendix B:

Cumulative process indicators

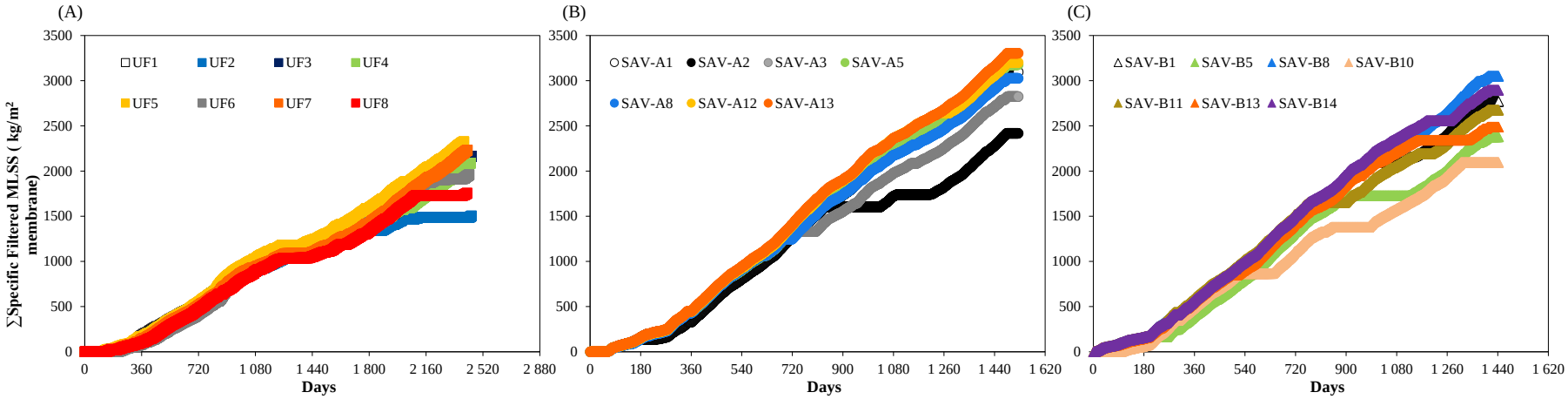

Figure B.1: Specific filtered MLSS for membranes tanks from SEM-MBR (A) row A (B) and row B (C) in SAV-MBR with respect of days since commissioning date.

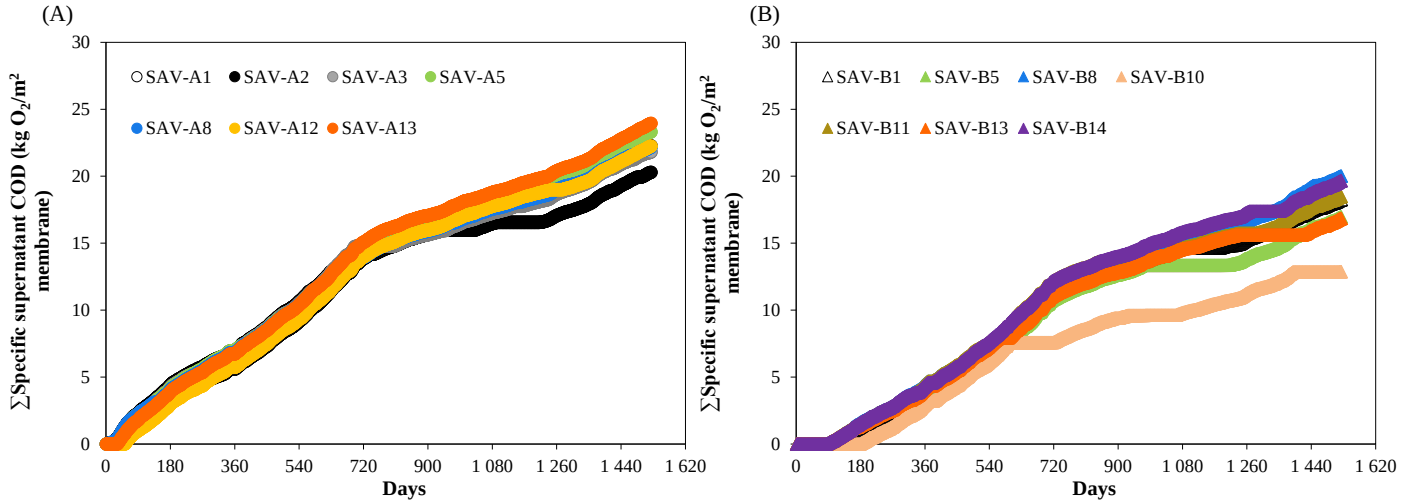

Figure B. 2: Specific filtered supernatant COD for membrane tanks in row A (A) and B (B) from SAV-MBR.

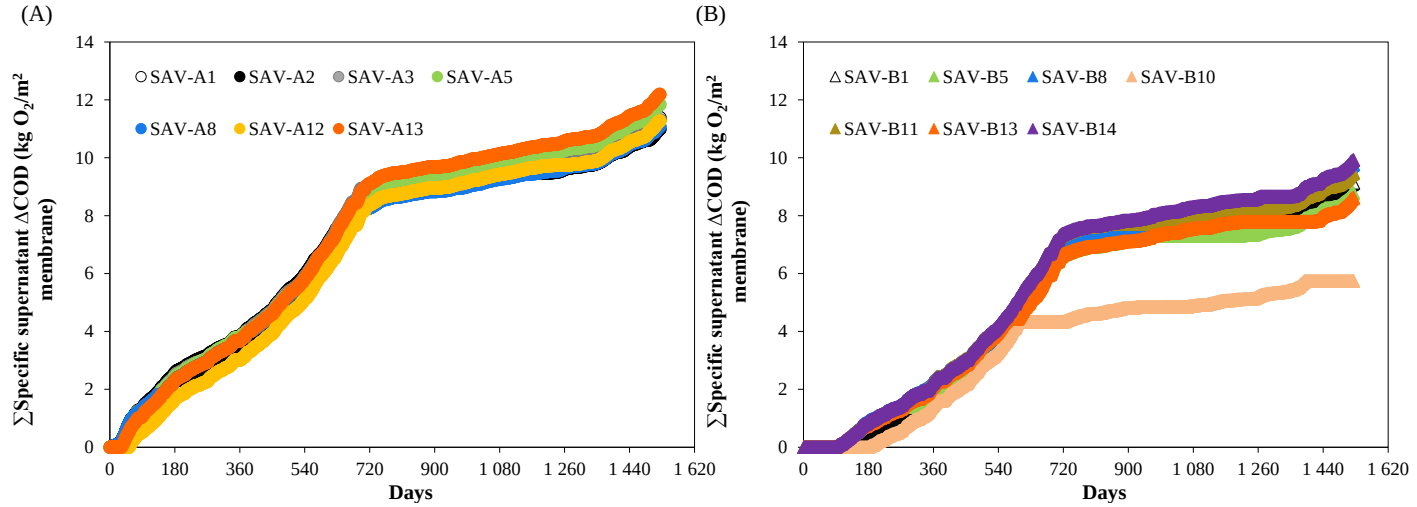

Figure B. 3: Specific filtered supernatant ΔCOD for membrane tanks in row A (A) and B (B) from SAV-MBR.

Appendix C:

Stress-strain curves from samples harvested from each MBR studied.

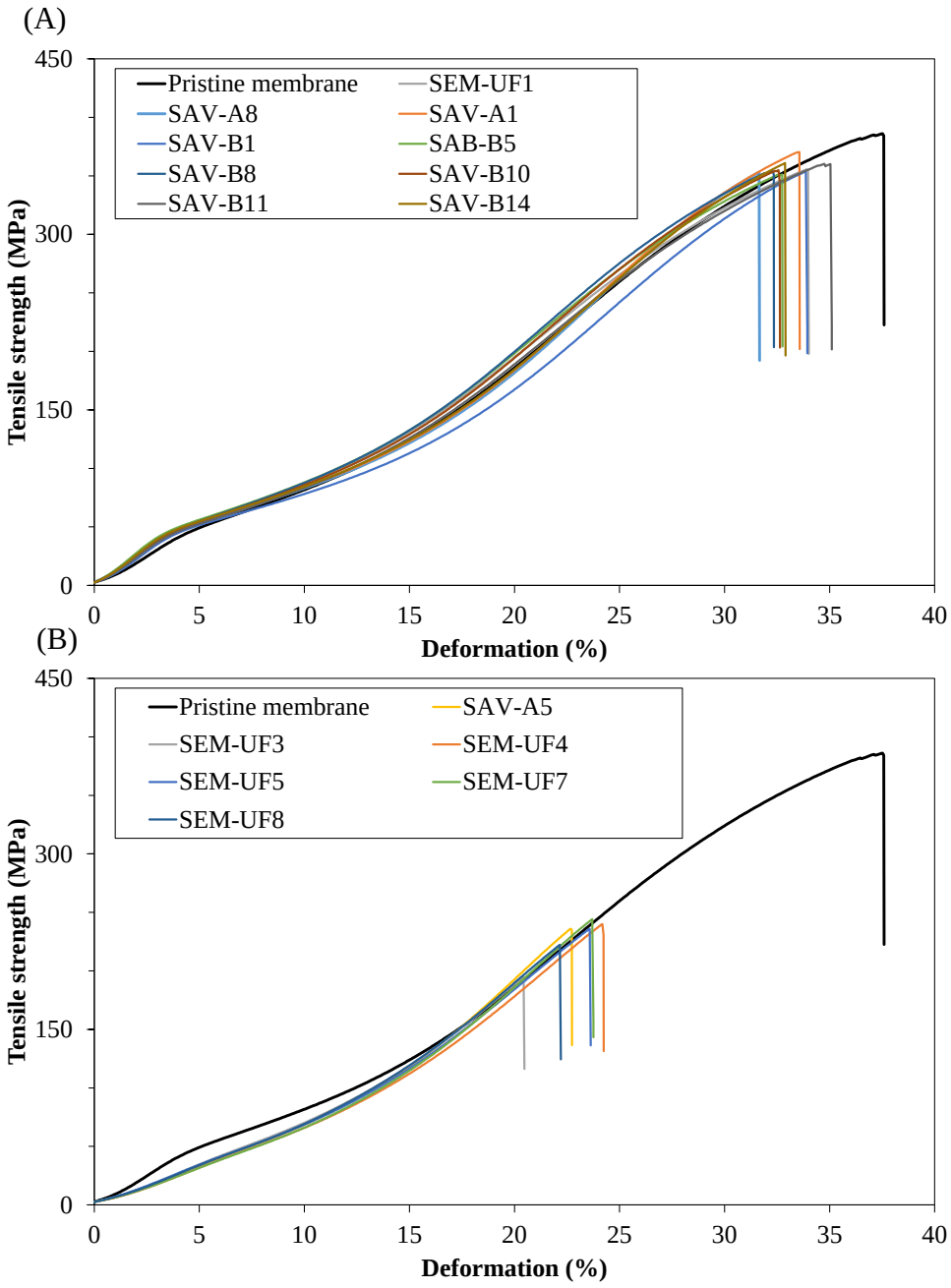

Figure C.1: Uniaxial stress-strain curves from samples harvested from each membrane tank studied from SAV-MBR and SEM-MBR. Samples were separated according to group H-UTS (A) and L-UTS (B).

Appendix D:

Correlation between membrane autopsies properties and cumulative process indicators

Results of the characterization of harvested membranes were correlated to the cumulative process indicators determined in this study, namely, operating time, specific permeate volume, C x t, supernatant COD, supernatant ΔCOD, filtered MLSS and aeration volume. Correlation coefficients and p-values for SAV-MBR samples are presented in Table D.1. Lp/Lp_0 did not correlated well with any of the indicators likely due to its high dispersion (Figure D.1.B). Ultimate tensile strength presented statistically significant correlations with all indicators, except for the C x t, supporting results from Chapter 3. In chapter 3, these membranes presented relatively stable mechanical properties regardless the C x t by ageing at bench-scale with only the chlorine action. The highest coefficient correlation (-0.575) was found with filtered supernatant ΔCOD, which is related to the filtration cycles and the colloidal organic matter faced by membranes (Figure D.1.A). Aeration volume also presented a statistically significant coefficient correlation (-0.515) with the ultimate tensile strength, but this value was below all filtration-related indicators (permeate volume, filtered MLSS, supernatant COD and ΔCOD).

Regarding PVP content for SAV-MBR, all indicators presented statistically significant correlations, with the highest correlation coefficient of -0.759 being the filtered MLSS (Figure D.1.C). Chapter 3 described the differences between PVP degradation at bench-scale only by the chlorine action and at a full-scale MBR. Chapter 4 highlighted the effects of different rates of filtration/chlorine exposure, demonstrating the effects of the filtration. The fact that the decline in PVP content correlated well with filtered MLSS confirm that the presence of organic matter and filtration dynamics also have an effect on PVP degradation and not only chlorine exposure.

Table D.1: Spearman correlation coefficient and (p-value) between membrane autopsies properties and cumulative process indicators for membrane tanks in from SAV-MBR.

	Ultimate tensile strength (MPa)	PVP content (%)	Lp/Lp_0
Operating time (d)	-0.507 (0.034)	-0.701 (0.002)	0.302 (0.222)
C x t (ppm.h)	-0.263 (0.290)	-0.647 (0.005)	0.286 (0.249)
Specific permeate volume (m^3/m^2)	-0.527 (0.026)	-0.682 (0.002)	0.271 (0.275)
Filtered MLSS (kg MLSS/m^2)	-0.490 (0.041)	**-0.759 (0.000)**	**0.387 (0.114)**
SupernatantCOD (kg O_2/m^2)	-0.538 (0.023)	-0.670 (0.003)	0.276 (0.267)
ΔCOD (kg O_2/m^2)	**-0.575 (0.014)**	-0.645 (0.005)	0.257 (0.302)
Aeration volume (m^3 air/m^2)	-0.515 (0.031)	-0.740 (0.001)	0.245 (0.327)

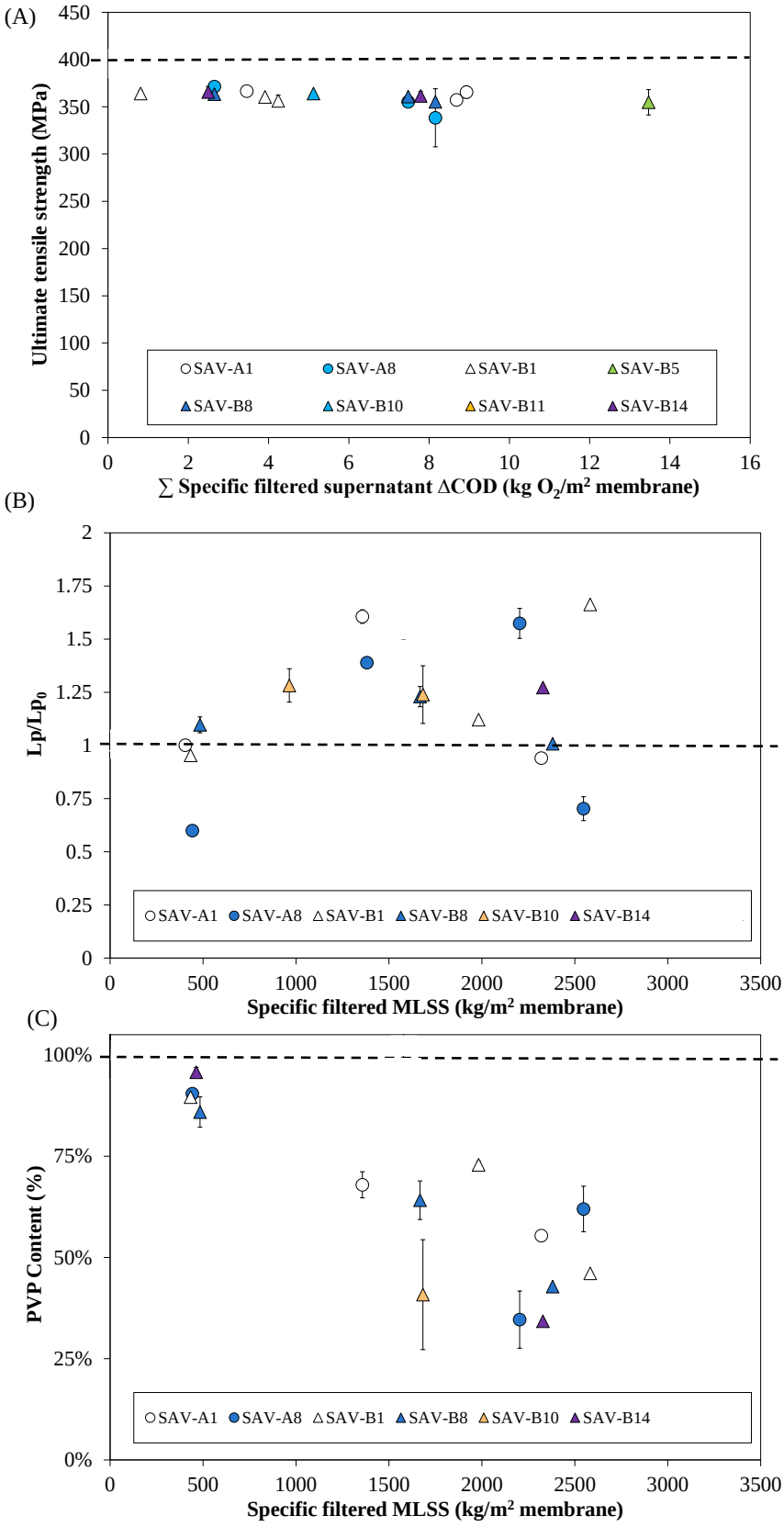

Figure D.1: Ultimate tensile strength with respect to specific ΔCOD (A), Lp/Lp0 (B) and PVP content (C) with respect to specific filtered MLSS.

Table D.2 presents correlation coefficients and p-values between membrane properties and cumulative process indicators for membrane tanks from SEM-MBR. Ultimate tensile strength correlated well with operating time (r = -0.815). PVP content and specific permeate volume presented the highest correlation coefficient of -0.878, followed by filtered MLSS (r = -0.862), also suggesting that filtration dynamics can have an impact on PVP degradation (Chapter 4 – Figure 4.18). In addition, Lp/Lp_0 correlated well to the C x t (r = 0.609).

Table D.2: Spearman correlation coefficient and (p-value) between membrane autopsies properties and cumulative process indicators for membrane tanks from SEM-MBR. Bold values are the highest correlation coefficients.

	Ultimate tensile strength	**PVP content**	**Lp/Lp_0**
Operating time (d)	**-0.815 (0.001)**	-0.345 (0.227)	0.459 (0.101)
C x t (ppm.h)	-0.648 (0.015)	-0.106 (0.721)	**0.609 (0.024)**
Specific permeate volume (m^3/m^2)	-0.323 (0.260)	**-0.878 (<0.001)**	0.213 (0.464)
Filtered MLSS (kg MLSS/m^2)	-0.648 (0.141)	-0.862 (<0.001)	0.081 (0.785)
Aeration volume (m^3 air/m^2)	-0.152 (0.605)	-0.427 (0.130)	-0.327 (0.253)

Based on these results, it seems that the specific filtered MLSS might be a promising indicator for monitoring membrane ageing. This indicator provides information about filtration and organic matter that membranes face over time. As a perspective of this research, the filtered MLSS will continue to be followed during this membrane life cycle for both MBRs.

Appendix E:

Correlation between membrane properties and normalized permeability index

The normalized permeability index with respect to specific aeration demand for both MBRs and with respect to the filtered supernant COD and ΔCOD, specifically for SAV, are presented in the Figure E.1.

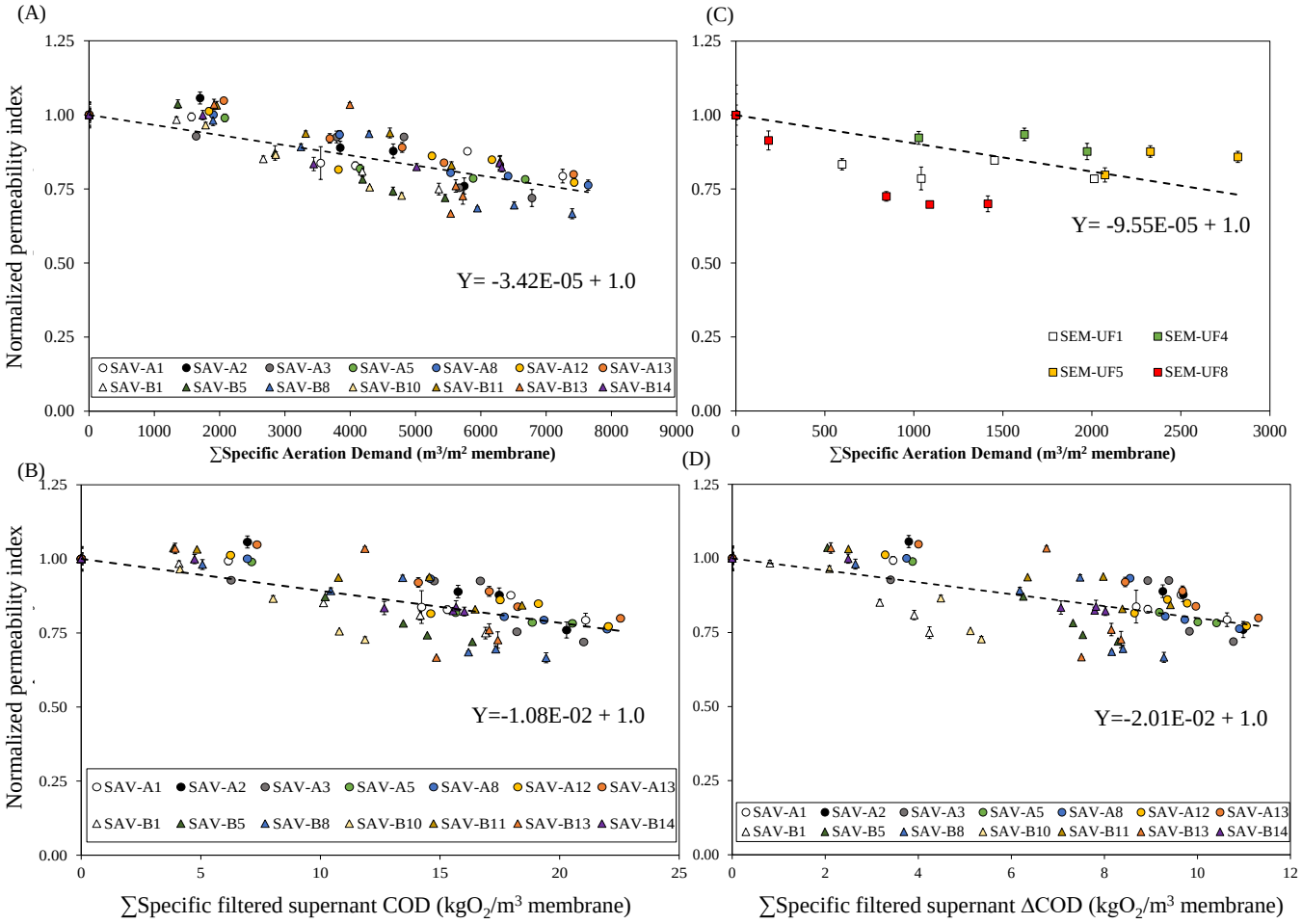

Figure E.1: Normalized permeability index with respect to specific aeration demand for SAV-MBR (A) and SEM-MBR (B) and with respect to the filtered supernatant COD (C) and ΔCOD (D), specifically for SAV-MBR.

Appendix F:

Effects of non-operating periods on normalized permeability index of membrane tanks of SEM-MBR

Regarding some particularities among membrane tanks from SAV-MBR, whenever these membrane tanks were shut down due to different reasons, e.g. unavailability of cleaning-in-place line, pump issues, etc, these membrane tanks were stocked in low NaOCl concentration solutions (3 – 15 ppm). Some of these membrane tanks were stocked more often than others, thus the ratio of these non-operating days since the commissioning date (November/2017 to June/2021) were calculated and presented in Table F.1. Membrane tanks were divided into group 1 for the ones that presented a ratio below 10% and group 2 for the ones above this value.

Table F.1: Ratio of non-operating days since the commissioning date (in %) for each membrane tank from SAV.

Membrane tank	**Operating days**	**Non-operating days**	**%Non-operating days since commissioning date**
Group 1			
A13	1451	41	3%
A5	1457	68	4%
A12	1399	70	5%
B8	1362	80	6%
B13	1166	72	6%
A8	1400	112	7%
A1	1410	115	8%
B14	1316	126	9%
Group 2			
B1	1201	250	17%
B5	1083	367	25%
A2	1127	398	26%
A3	1127	398	26%
B10	928	423	31%
B11	928	514	36%

The effect of these operating modes in membrane ageing are analyzed and presented hereby. Each membrane tank presented highly different conditions over time due to operating issues, e.g. cleaning reagents lines unavailability, dry weather (lower inflow) and equipment related issues. When a membrane tank is unavailable for long periods, membranes are submerged in a diluted chlorine solution (3 – 15 ppm) with 5 min aeration cycles every 60 min for SAV-MBR. Thus, regarding the ratio between days that each membrane tank did not properly function since commissioning, membrane tanks can be separated into two groups (Table F.1). Group 1 for the membrane tanks with the most important time in operation, ranging from 3 to 9% of non-operating days and group 2 with non-operation days ranging from 18 to 36% of the total days since November/2017.

A statistical analysis was carried out with these two separated groups in order to evaluate the effects of these conditions onto membrane ability to filter mixed liquor over time. The differences between group 1 and 2 are not statistically significant (p-value=0.786; Mann-Whitney test). This is also visible when normalized permeability indexes are plotted against filtered volume, the number of days since commissioning days and cumulated exposure dose in Figure F.1. The decline in this indicator is roughly the same for both groups, and variations are within statistical errors.

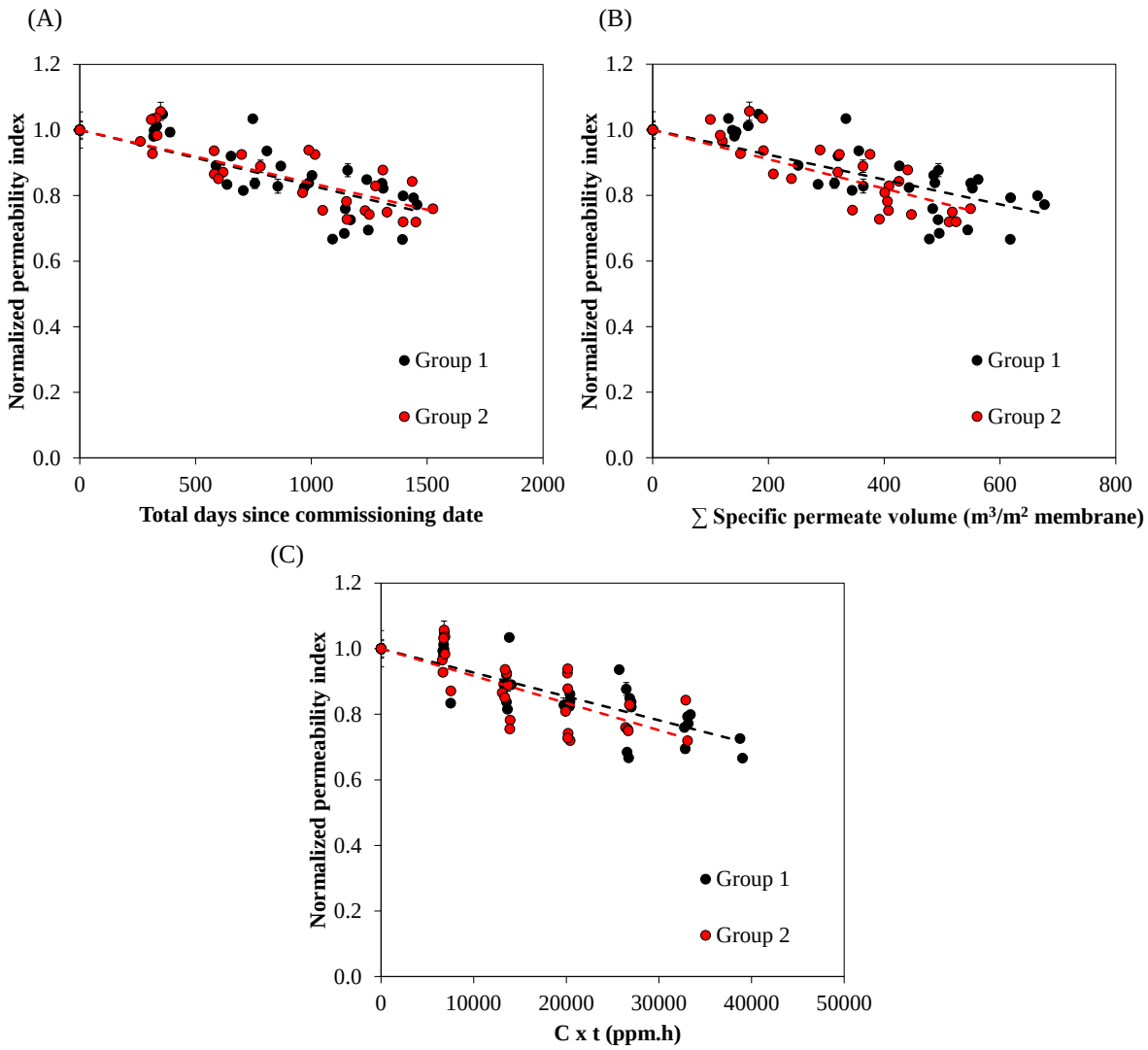

Figure F.1: Normalized permeability index with respect to the number of days since commissioning date (A) and specific permeate volume (B) and exposure dose (C) from SAV-MBR.

Similarly, normalized permeability indexes were calculated to SEM-MBR from 2015 to 2020. As already observed, the main difference between these two MBRs is the daily filtration time. The average filtration duration per day (with standard deviations) for each membrane tank from SEM-MBR between 2015 and 2020 are presented in Table F.2. This shows that each membrane tank operate roughly the same way daily.

Table F.2: Daily filtration time for membrane tanks from SEM.

Membrane tanks	Tank 1	Tank 2	Tank 3	Tank 4	Tank 5	Tank 6	Tank 7	Tank 8
Daily filtration duration (h)	5.4±1.9	5.2±2.3	5.6±1.9	5.4±1.9	5.6±1.9	5.4±1.8	5.4±1.8	5.2±1.9

Roughly, each tank filtered for 5.4 h per day, which means that these tanks undergo long periods of relaxation or non-filtration. On the other hand, membrane tanks from SAV-MBR operate in their designed flux, usually presenting between 19 and 22.3 h of filtration per day in normal conditions. Comparing the changes of normalized permeability index between the SAV and SEM provided us valuable information whether this operating mode is harmful or protective towards the membrane material. Normalized permeability indexes from SEM and SAV with respect to the specific permeate volume are plotted in Figure F.2.

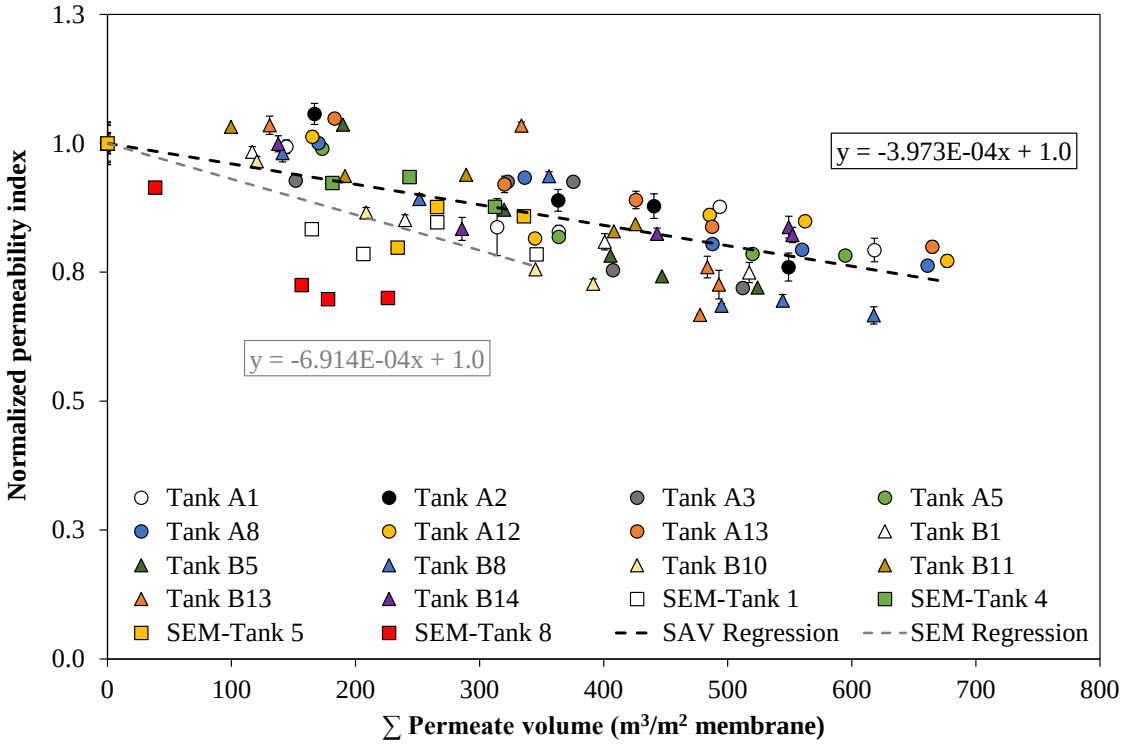

Figure F.2: Normalized permeability index as a function of the cumulated specific permeate volume produced for membrane tanks from SAV-MBR and SEM-MBR.

Although Figure F.2 shows a variation in the regression's slopes, statistical analysis presented no significant differences between these MBRs (p-value = 0.0504). Actually, SEM-MBR's stronger decline in normalized permeability index was highly influenced by data from SEM-UF8, without considering this tank, SEM-MBR's slope would be closer to SAV-MBR (-5.565E-04) and p-value of the statistical analysis between these two MBRs would increase to 0.198, reinforcing their similarity. Therefore, long non-filtration periods may also be efficient to limit the residual fouling accumulation, reinforcing that dynamics of filtration play a major role on membrane ageing.